

Biobased pyrazines

Citation for published version (APA):

Würdemann, M. A. (2022). *Biobased pyrazines: from amino acids to polyesters*. [Doctoral Thesis, Maastricht University]. Maastricht University. <https://doi.org/10.26481/dis.20220411mw>

Document status and date:

Published: 01/01/2022

DOI:

[10.26481/dis.20220411mw](https://doi.org/10.26481/dis.20220411mw)

Document Version:

Publisher's PDF, also known as Version of record

Please check the document version of this publication:

- A submitted manuscript is the version of the article upon submission and before peer-review. There can be important differences between the submitted version and the official published version of record. People interested in the research are advised to contact the author for the final version of the publication, or visit the DOI to the publisher's website.
- The final author version and the galley proof are versions of the publication after peer review.
- The final published version features the final layout of the paper including the volume, issue and page numbers.

[Link to publication](#)

General rights

Copyright and moral rights for the publications made accessible in the public portal are retained by the authors and/or other copyright owners and it is a condition of accessing publications that users recognise and abide by the legal requirements associated with these rights.

- Users may download and print one copy of any publication from the public portal for the purpose of private study or research.
- You may not further distribute the material or use it for any profit-making activity or commercial gain
- You may freely distribute the URL identifying the publication in the public portal.

If the publication is distributed under the terms of Article 25fa of the Dutch Copyright Act, indicated by the "Taverne" license above, please follow below link for the End User Agreement:

www.umlib.nl/taverne-license

Take down policy

If you believe that this document breaches copyright please contact us at:

repository@maastrichtuniversity.nl

providing details and we will investigate your claim.

Biobased Pyrazines

From amino acids to polyesters

Martien Adriaan Würdemann

Voor mijn ouders

Biobased pyrazines: from amino acids to polyesters

© *M.A. Würdemann* | Maastricht University, 2022

All rights reserved

ISBN: 978-94-6423-716-0

Gedrukt door ProefschriftMaken

Cover door Merel Witteman

Layout door Martien Würdemann

Dit onderzoek is financieel mogelijk gemaakt door de Provincie Limburg.

Biobased pyrazines

From amino acids to polyesters

PROEFSCHRIFT

ter verkrijgen van de graad van doctor aan de Universiteit Maastricht, op
gezag van de Rector Magnificus, Prof. dr. Pamela Habibovic volgens het
besluit van het College van Decanen, in het openbaar te verdedigen op
maandag 11 april 2022 om 16:00 uur

door

Martien Adriaan Würdemann

Geboren te Wageningen op 1 juni 1989

Promotoren

Prof. Dr. Romano V.A. Orrù

Prof. Dr. Andrij Pich

Copromotor

Dr. Katrien V. Bernaerts

Beoordelingscommissie

Prof. Dr. Maarten Honing (Chair) (Maastricht University)

Dr. Matthew B. Baker (Maastricht University)

Prof. Dr. Gert-Jan M. Gruter (Universiteit van Amsterdam)

Prof. Dr. Thomas J.J. Mueller (Heinrich-Heine-Universität Düsseldorf)

Table of contents

INTRODUCTION	1
AIM AND SCOPE	9
OUTLINE	10
REFERENCES	11
CHAPTER 1 - THE FORGOTTEN PYRAZINES: EXPLORING THE DAKIN-WEST REACTION	13
ABSTRACT	13
INTRODUCTION	14
EXPERIMENTAL	17
RESULTS AND DISCUSSION	21
CONCLUSIONS	33
REFERENCES	34
APPENDIX	36
CHAPTER 2 - BIOBASED (DIMETHYL)-PYRAZINE DIPROPIONIC ACID BASED POLYESTERS	45
ABSTRACT	45
INTRODUCTION	46
EXPERIMENTAL	48
RESULTS AND DISCUSSION	50
CONCLUSIONS	59
REFERENCES	60
APPENDIX	61
CHAPTER 3 - MECHANICAL PROPERTIES OF POLY(HEXAMETHYLENE DIMETHYLDIPROPIONIC ACID PYRAZINE)	81
ABSTRACT	81
INTRODUCTION	82
EXPERIMENTAL	84
RESULTS AND DISCUSSION	88
CONCLUSIONS	103
REFERENCES	104
APPENDIX	105

CHAPTER 4 - POST-MODIFICATION OF BIOBASED PYRAZINES AND THEIR POLYESTERS	107
ABSTRACT	107
INTRODUCTION	108
EXPERIMENTAL	110
RESULTS AND DISCUSSION	113
CONCLUSIONS	127
REFERENCES	128
APPENDIX	130
CHAPTER 5 - CRYSTAL STRUCTURE AND POLYMORPHISM OF BIOBASED AROMATIC POLYESTERS: ELUCIDATION OF MELTING TEMPERATURE DIFFERENCES	151
ABSTRACT	151
INTRODUCTION	152
EXPERIMENTAL	154
RESULTS AND DISCUSSION	157
CONCLUSIONS	172
REFERENCES	173
APPENDIX	174
CONCLUSIONS & OUTLOOK	183
IMPACT PARAGRAPH	187
SAMENVATTING	189
ACKNOWLEDGEMENTS	193
CURRICULUM VITAE	197
PUBLICATION LIST	199

Introduction

Curiosity

Since the beginning of time mankind has tried to get a grip on how the world works and explain natural phenomena. Humans are naturally curious, almost childlike, constantly asking questions: How? Why? What? When? Who? The search for answers initially resulted in deities and religions; natural events were explained by means of supernatural powers.^[1] This provided answers but there were always people who wanted to know more, for whom the provided answers were not enough. The pursuit of knowledge, of explaining the world continues to this day. In a large number of modern societies deities have been replaced by theories and supernatural powers have become natural forces, electromagnetism, gravity and the strong and weak atomic forces.

This Thesis is the result of a long tradition of curious people in search of knowledge. From the Greek philosophers who critically thought about the world and started with empirical research,^[2] via the alchemists who sought to explain god's creation and find eternal life by experimenting with the elements^[3], to those we now call scientists. This latter group has taken a systematic approach to the pursuit of knowledge since the renaissance. While scientists initially also wanted to gain deeper understanding of god's creation this slowly changed to just understanding the world.

There has always been a balance between fundamental research and applied research, for instance the work of alchemists in pursuit of eternal life had a large influence on metallurgy and enabled better alloys. As the benefits of the scientific approach became more evident, applied research gained prominence compared to fundamental work. This shift has resulted in an enormous improvement in the standard of living over the last century. The focus on such applied research has to some extent, compromised research simply out of curiosity. Since taxes fund most current research society wants to know what their money is used for, what the benefit is. Research funding, in for instance the Netherlands, has become increasingly application tied with accompanying deliverables. Such deliverables limit the freedom to fully pursue interesting phenomena or results.^[4] The research described in this Thesis does not correspond to such applied investigation lines. Here, I present my work, which is more related to genuine curiosity but still considers the eventual applicability.

Sustainability

Curiosity driven research without immediate applicability, practical need or set goal does not mean that there is no problem at the basis of this work. Answering questions like how can we live better, have more food and keep warm has provided mankind with a tremendous increase in standards of living.^[5] It has provided sturdy houses, electricity to provide light, warmth and power for our electronic devices, cars and planes that show us different parts of the world, and artificial fertilizers to give us food. Answers however generate new questions; Is our new way of life sustainable? What is the effect on our planet and the other inhabitants? The answer to these new questions, unfortunately, is negative in most cases.

Although some pollution related problems such as acid rain have been dealt with since the 70's and 80's, we have been seeing the effects of unsustainable economic behavior more and more in recent years. Resources such as fresh water^[6], forests^[7] and arable land are in decline due to our economic activity.^[8] Several non-renewable natural resources are also getting scarce, especially (rare earth) metals.^[9-10] Another major problem arises from our use of fossil oil, coal and gas reserves for our electricity, heating, chemical and transportation needs. These resources are not only non-renewable but also were formed millions of years ago when the earth's atmosphere had a completely different composition, they represent captured carbon from that moment in earth's history. Their use now, mostly by burning, results in the production of so-called greenhouse gasses. These gasses are causing global temperatures to rise, in turn causing storms to get more severe, ice caps to melt, sea levels to rise and biodiversity to decline. This climate change is the major crisis of our time.^[11]

The possible effect of gasses in the atmosphere on the temperature of the planet was realized in the 19th century and the effect of carbon dioxide was put forward first by Arrhenius already in 1896.^[12] With regard to use of other non-renewable resources, we also received warnings, such as the report "Limits to Growth" by the Club of Rome in 1972.^[13] Unfortunately, action to mitigate the effects of unsustainable economic practices has only gained traction on a global scale in the past 20 to 30 years. The introduction of concepts such as "green chemistry" and "life cycle assessment" have influenced the development of new chemical processes and the optimization of established ones.^[14-15] A process is no longer only judged on its economic merits but the effects of the process on the environment and human life are taken into account.

As such, waste production should be minimized, the toxicity should be taken into account, as should the end of life of the produced product and finally the energy need of a process needs to be limited.^[14] This latter factor can be expressed as a process's

carbon footprint or global warming potential.^[1] This can be decreased by making a process more energy efficient or by using so-called biogenic carbon. This is carbon taken from plants and other biological sources, not fossil ones. Replacing current fossil building blocks by drop-in but biogenic replacements is one option to lower a process's carbon footprint. Another approach might consist of developing an entirely new process and product all together, starting from biomass. Use of biogenic carbon is per definition sustainable. Carbon taken from the atmosphere is released back in the atmosphere as the material is burned or degraded. No fossil carbon was used, thus no extra carbon is introduced to the atmosphere that was not there before, in other words the carbon cycle is complete. The remainder of the process might however not be sustainable, due to larger heat requirements, massive land use or highly toxic intermediates for instance. Not to mention the effect on other elemental cycles such as the nitrogen and phosphorus cycles. Determination of the sustainability of a process/product is the subject of the field of "life cycle assessment".^[16-17]

Considering the end of life, products should ideally, either be designed to be fully and easily recycled or a product should be biodegradable. Historically the end of life was not really a consideration for a product, only its use. Plastics for instance are great materials with good properties and they have replaced a large number of older materials such as glass, paper and wood. For the older materials end of life was never really an issue since they were mostly degradable or innocuous. This cannot be said for plastics, they were not designed or developed with an end of life in mind and are usually not degradable. This can be seen from the great garbage patches in the oceans and the large amount of plastic pollution.^[18-19] Any new product that enters the market should thus have an end of life in mind, be that degradation or recycling. Even when end of life is taken in to consideration care is necessary, a product might degrade in nature but not fully and then may leave behind harmful or toxic compounds or the molecular building blocks left-over after degradation. Adhering to the principles of "green chemistry" will prevent such products from entering the market.

Aromatic polymers

The term plastic technically refers to the mechanical behavior of a material. In common usage however, plastic usually refers to thermoplastic polymers. Polymers are macromolecules that consist of long chains or networks of repeating molecular building blocks, called monomers. Polymers can be divided in categories based on the chemical structure of the monomer, the resulting physical properties, the application niche or by polymerization technique.^[20] Based on physical properties the categories of so-called high performance and engineering polymers are defined as materials that show improved mechanical properties compared commodity plastics such as

poly(ethylene), poly(propylene) and poly(styrene).^[21] A convenient rule of thumb for engineering polymers is that they will maintain their dimensional stability and mechanical properties, above 100 °C or below 0 °C. Engineering polymers are considered high performance polymers when they excel further at one single aspect. This might be extremely high thermal stability, chemical inertness or special melting behavior, such as liquid crystalline polymers.

Polymers in either the engineering and high-performance category include, polyethylene terephthalate (PET) used for beverage packaging, polycarbonate (PC) used as lightweight glass replacements, polyaramids (Kevlar and Twaron) used in bullet-proof vests and different polyamides (nylons) used in the automotive industry (**Figure 1**). The first three of these examples have one structural feature in common, namely they contain aromatic rings in the repeating units.

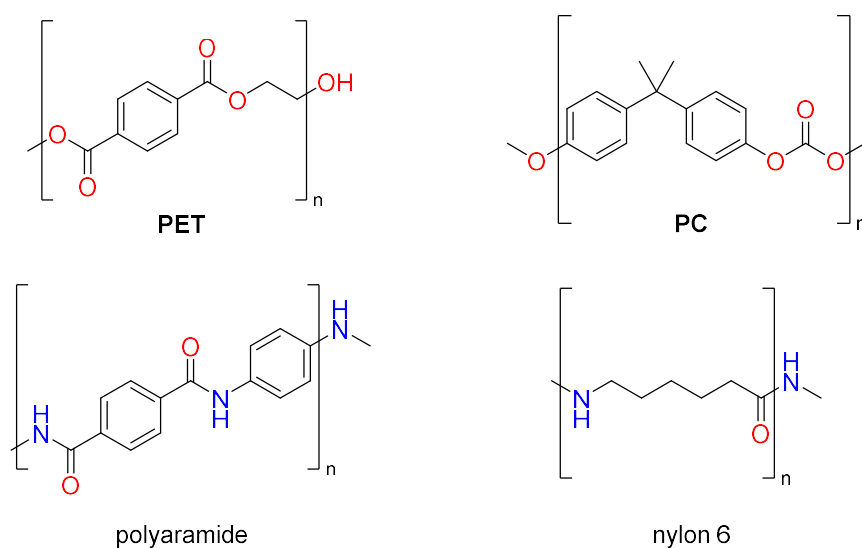


Figure 1: The structures of PET, PC, polyaramide and nylon 6.

Aromatic rings integrated into the main chain of macromolecules provide enhanced backbone stiffness originating from the rigidity and chemical stability of the aromatic rings and enable interchain π - π interactions often combined with hydrogen bonds. These molecular features result in stronger, higher melting crystals and lead to high melting points, high glass transition temperatures and increased thermal and chemical stability of polymers, which are perfect candidates for materials with advanced properties and functions. Most of the monomers that contain aromatic rings are currently obtained from fossil sources, which makes the corresponding materials not sustainable. Drop-in replacement aromatics from biomass are being developed but no commercial production has been started yet.^[22] These drop-in

molecules will also not solve any end-of-life issues associated with these materials. Novel aromatic monomers are also being developed and some have entered pre-commercial production, such as furandicarboxylic acid, which is used to make the PET replacement polyethylene furanoate (PEF) (**Figure 2**).^[23-24]

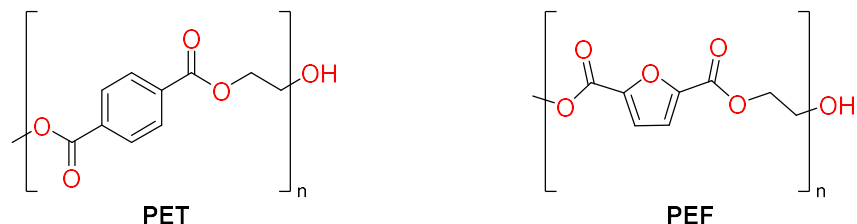


Figure 2: The structure of PET versus the structure of PEF.

Novel monomers/polymers usually have great difficulty entering the market, commonly there are problems with scale and cost.^[25] Besides this, the polymer user-base is usually conservative and not willing to shift to new materials. On only the premise of a “green” or sustainable solution market entrance efforts usually fail. This is changing however; consumers are more aware of their environmental impact and are willing to adopt new materials, if the cost is not too great. Besides consumer pressure, another important factor for companies to make the move to biobased feedstock is superior properties. For instance, the gas barrier for PEF is higher than for PET allowing longer shelf life of soft drinks. This added benefit is the major reason that PEF is even considered as a replacement for PET.^[23, 26] Other superior properties or added benefits of a biobased alternative are what is going to ensure phase-out of fossil-based polymers.^[27] The search for other aromatic biobased monomers thus has to take into consideration this added benefit factor, any new monomer needs to bring something extra to the table. Considering the wide range of different aromatic systems known, a lot of room to find new monomers is left.

Pyrazines

One of the possible aromatic cores that might provide added functionality to a polymer is the pyrazine core (**Figure 3**). The pyrazine is one of the diazines (see **Figure 3** top), a six-membered ring containing two nitrogen atoms. In case of pyrazine these nitrogens are on opposite sides of the ring, which typically results in highly symmetric cores. This arrangement partially negates the electron withdrawing nature of a single nitrogen atom, as such a pyrazine is a far weaker base than a pyridine which contains only one nitrogen (the first pK_a of pyrazine is around 1, that of pyridine around 5).^[28-29] The two, opposing nitrogen's in a pyrazine also result in the ring being highly aromatic at 89% the aromaticity of benzene.^[30] Besides this the presence of nitrogen atoms in the ring also results in two available free electron pairs, a feature phenyl rings do not have. These free electron pairs can undergo different types of reactions and thus form a handle for added functionality (see **Figure 3** bottom).

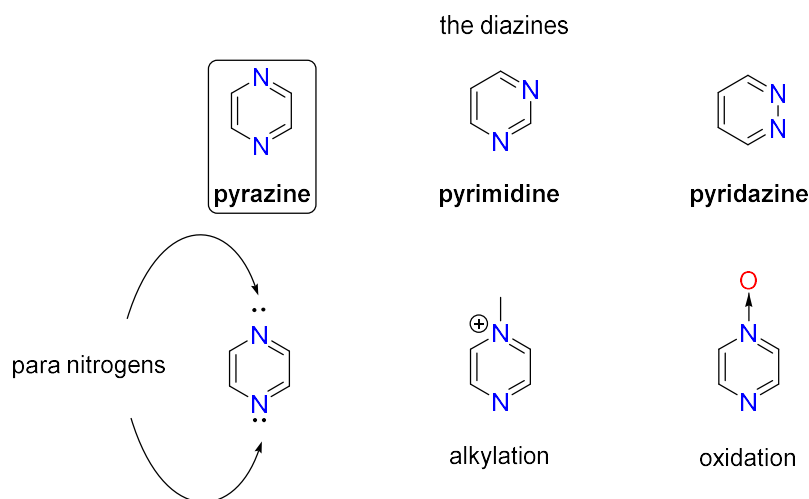


Figure 3: The structure of pyrazine (top left) compared to the other diazines and the reactions of the nitrogen lone electron pairs in pyrazine (bottom).

Although pyrazines have very interesting properties, they are uncommon in polymers. Pyrazines are mostly reported in semi-conducting polymers (**Figure 4A**), but almost no polyesters or polyamides have been reported containing pyrazines.^[31-34] This presents an interesting knowledge gap, especially when combined with the ability to make pyrazines from biomass. It makes one curious, which pyrazines to make and how? And can they be used in polymers?

Pyrazines from biomass

Pyrazine applicable in polymers could be sustainably sourced from biomass. The pyrazine core is found in naturally occurring molecules such as mycotoxins, which are compounds made by fungi as antimicrobials (**Figure 4B**)^[35-38], as glandular compounds produced by ants (**Figure 4C**)^[39] and as flavor compounds (**Figure 4D**).^[40] These pyrazines are usually formed in low quantities and are difficult to isolate, hampering the use of these naturally occurring pyrazines as monomers. How then to make pyrazines from biomass? Pyrazines have been studied for well over a hundred and fifty years, with A. Laurent giving the first report on the synthesis of tetraphenylpyrazine.^[41] Since then various ways of making pyrazines have been explored^[42-43] although none specifically mention using biomass as the starting material.

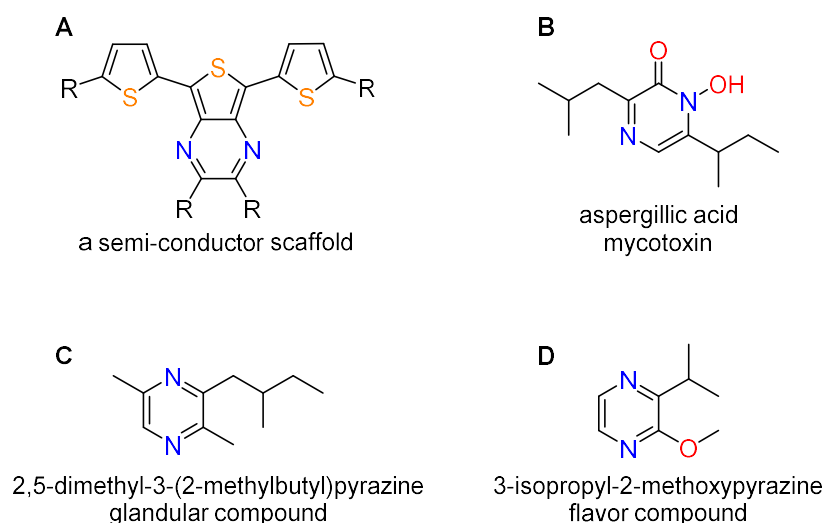


Figure 4: An example of a polymeric pyrazine containing semi-conductor (**A**) and several pyrazine containing natural products (**B,C and D**).

Taking a retrosynthetic approach to the pyrazine core, several disconnections are possible (**Figure 5**). A single disconnection requires a relatively complex synthon, for which the equally complex synthetic equivalent would limit the scalability of the synthesis. Triple and higher disconnections result in small synthons, for which the synthetic equivalent would be difficult to obtain from biomass. The most interesting approach therefore is the double disconnection next to the nitrogens, which results in two synthons each having one nitrogen. These synthons allow for an easy and often exploited synthesis route by using α -amino carbonyls as the synthetic equivalent.^[42-43] Such α -amino carbonyls can cyclize into a six-membered double imine, that auto-oxidizes towards the pyrazine. The approach via α -amino carbonyl compounds

was therefore selected as the route of choice to access pyrazine monomers from biomass.

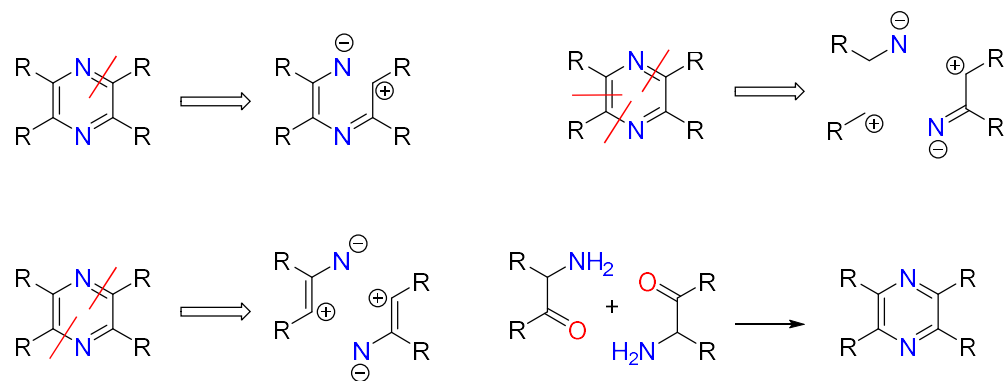


Figure 5: Single disconnection (top left), triple disconnection (top right), double disconnection (bottom left) and synthesis from α -amino carbonyls (bottom right).

Aim and scope

Coming back to the beginning of this introduction, this Thesis can be seen mostly as an exercise in curiosity. The work presented does not attempt to solve any of the major problems in society, the goal was not to develop the most energy efficient, most benign, most recyclable process or material. The goal was to try and fill the knowledge gap regarding pyrazines in polymers. Not because this provides an immediate benefit or with an application in mind but to explore a new direction, out of curiosity. This direction might lead to new, better and more sustainable materials in the future, therefore some factors which will influence the applicability will already be taken in to account. Considering the knowledge gap regarding pyrazines in polymers the main objective of the research described in this Thesis was to answer the following questions:

- can we synthesize pyrazine monomers from biomass and which ones?
- can these pyrazine monomers successfully be used to synthesize polymers?
- what are the properties of pyrazine containing polymers?

The chemical and reactivity space wherein these questions can be answered is enormous. To limit this, several factors were considered at an early stage. At the start of the project different sources of biomass were considered and several test reactions conducted. Although not a pressing issue at the beginning any interesting pyrazine monomer should be applicable in a real-world setting. Therefore, monomer synthesis should be safe, straightforward and scalable, column chromatography was only considered as a last resort.

Regarding the type of polymers, condensation polymers were considered the best candidates to explore. For one polyesters and polyamides are theoretically always biodegradable, although not always in practice. Next to this no natural amino acids exist which contain an alkene for use in radical addition reactions. Finally, the synthesis of polyesters and polyamides is usually conducted in the melt, a more sustainable process than polymerizations conducted in solution.

Outline

This Thesis presents the search for answers on biobased pyrazines in polymers in the following chapters:

Having already identified α -amino carbonyls as the most promising starting materials for pyrazines, their synthesis from amino acids via the Dakin-West reaction and subsequent pyrazine formation is reported in **Chapter 1**. The Chapter is a reinvestigation of this more than 90-year-old reaction focusing on natural amino acids as input. The reaction scope, scalability, pyrazine synthesis, side-reactions and mechanistic details are explored.

Two of the pyrazine monomers obtained via the Dakin-West reaction are polymerized into polyesters with co-monomers as reported in **Chapter 2**. These two pyrazine monomers, dimethyl dipropionic acid pyrazine and dipropionic acid pyrazine, provide a rare opportunity to study both the effects of the pyrazine ring as well as the effect of methyl-groups on aromatic systems in polymers. Highly interesting melting point effects are found the semi-crystalline materials, with one polymer having a melting point up to 80 °C higher than its close structural analog.

To be able to place these new materials in a wider framework the investigation of mechanical properties from one of the polyesters from Chapter 2 is reported in **Chapter 3**. Although the results were inconclusive, the selected polyester seems to possess decent mechanical properties similar to other current commodity polymers.

Since pyrazine rings have electron lone pairs, which undergo reactions under different conditions. The post-modification of the polyesters reported in Chapter 2 by use of this lone pair reactivity is explored in **Chapter 4**. This post-modification by either alkylation or oxidation was found to result in major changes in thermal properties with both loss of crystallinity and large increases in melting point depending on the polymer. This latter effect was attributed by infra-red studies to hydrogen bonding between polymer chains. Surface modification of the polymers was also found possible, enabling tunable surface properties.

The structural and physio-chemical basis for the melting point differences found in Chapter 2 are explored in **Chapter 5**, by fiber x-ray diffraction, powder diffraction and infrared measurements. The polymer was found to possess a textbook case of orientation polymorphism. Thermal and mechanical induction of these polymorphs was found possible.

References

- [1] Y. N. Harari, *Sapiens : a brief history of humankind*, Penguin Random House, London, **2014**.
- [2] E. Grant, *A History of Natural Philosophy: From the Ancient World to the Nineteenth Century*, Cambridge University Press, Cambridge, **2007**.
- [3] L. Principe, *The Secrets of Alchemy*, University of Chicago Press, **2013**.
- [4] KNAW, Koninklijke Nederlandse Academie van Wetenschappen (KNAW), Amsterdam, **2019**.
- [5] H. de Jong, in *Global Handbook of Quality of Life: Exploration of Well-Being of Nations and Continents* (Eds.: W. Glatzer, L. Camfield, V. Møller, M. Rojas), Springer Netherlands, Dordrecht, **2015**, pp. 45-74.
- [6] M. M. Mekonnen, A. Y. Hoekstra, *Science Advances* **2016**, 2, e1500323
- [7] FAO & UNEP, *The State of the World's Forests 2020. In brief. Forests, biodiversity and people.*, UN, Rome, **2020**.
- [8] J. Bruinsma, *FAO report* **2009**
- [9] L. D. Meinert, G. R. Robinson, N. T. Nassar, *Resources* **2016**, 5, 14
- [10] S. M. Jowitt, G. M. Mudd, J. F. H. Thompson, *Communications Earth & Environment* **2020**, 1, 13
- [11] P. R. Shukla, J. Skea, E. C. Buendia, V. Masson-Delmotte, H.-O. Pörtner, D. C. Roberts, R. S. P. Zhai, S. Connors, R. v. Diemen, M. Ferrat, E. Haughey, S. Luz, S. Neogi, M. Pathak, J. Petzold, J. P. Pereira, P. Vyas, E. Huntley, K. Kissick, M. Belkacemi, e. J. Malley, *IPCC report* **2019**
- [12] S. Arrhenius, *The London, Edinburgh, and Dublin Philosophical Magazine and Journal of Science* **1896**, 41, 237-276
- [13] D. H. Meadows, D. L. Meadows, J. Randers, W. W. B. III, *The limits to growth : a report for club of Rome's project on the predicament of mankind*, Universe Books, New York, **1972**.
- [14] P. T. Anastas, J. C. Warner, *Green Chemistry: Theory and Practice*, Oxford University Press, Oxford, **1998**.
- [15] M. Owsianiak, A. Bjørn, A. Laurent, C. Molin, M. W. Ryberg, in *Life Cycle Assessment: Theory and Practice* (Eds.: M. Z. Hauschild, R. K. Rosenbaum, S. I. Olsen), Springer International Publishing, Cham, **2018**, pp. 31-41.
- [16] A. Bjørn, M. Owsianiak, C. Molin, A. Laurent, in *Life Cycle Assessment: Theory and Practice* (Eds.: M. Z. Hauschild, R. K. Rosenbaum, S. I. Olsen), Springer International Publishing, Cham, **2018**, pp. 9-16.
- [17] A. Moltesen, A. Bjørn, in *Life Cycle Assessment: Theory and Practice* (Eds.: M. Z. Hauschild, R. K. Rosenbaum, S. I. Olsen), Springer International Publishing, Cham, **2018**, pp. 43-55.
- [18] in *The New Plastics Economy*, Ellen MacArthur Foundation, **2017**.
- [19] R. Geyer, J. R. Jambeck, K. L. Law, *Science Advances* **2017**, 3, e1700782
- [20] R. J. Young, P. A. Lovell, *Introduction to Polymers, Third Edition*, Third Edition ed., CRC Press Boca Raton, **2011**.
- [21] H.-G. Elias, in *Macromolecules Volume 4: Applications of polymers*, Wiley-VCH, Weinheim, **2009**, pp. 303-370.
- [22] D. I. Collias, A. M. Harris, V. Nagpal, I. W. Cottrell, M. W. Schultheis, *Industrial Biotechnology* **2014**, 10, 91-105
- [23] A. J. J. E. Eerhart, A. P. C. Faaij, M. K. Patel, *Energy & Environmental Science* **2012**, 5, 6407-6422
- [24] Avantium, **2021**.
- [25] E. de Jong, H. Stichnothe, G. Bell, H. Jørgensen, in *Bio-based Chemicals: A 2020 Update*, IEA Bioenergy, **2020**.
- [26] S. K. Burgess, J. E. Leisen, B. E. Kraftschik, C. R. Mubarak, R. M. Kriegel, W. J. Koros, *Macromolecules* **2014**, 47, 1383-1391
- [27] A. Partanen, M. Carus, S. Piotrowski, L. Dammer, M. Küppers, in *Bio-based products: Green premium prices and consumer perception of different biomass feedstocks*, nova Insitute, **2020**.
- [28] A. S. Chia, R. F. Trimble, *The Journal of Physical Chemistry* **1961**, 65, 863-866
- [29] A. Albert, R. Goldacre, J. Phillips, *Journal of the Chemical Society (Resumed)* **1948**, 2240-2249
- [30] C. W. Bird, *Tetrahedron* **1986**, 42, 89-92
- [31] N. Ogata, K. Shimamura, *Polym. J.* **1975**, 7, 72-78
- [32] N. Ogata, *J. Macromol. Sci., Part A: Pure Appl. Chem.* **1979**, 13, 477-501
- [33] S. Ueta, Y. Fukuda, K. Koga, M. Takayanagi, *Polym. J.* **1992**, 24, 1429-1436
- [34] R. H. Wiley, *J. Polym. Sci., Part A: Polym. Chem.* **1987**, 25, 735-737

- [35] J. D. Dutcher, *J. Biol. Chem.* **1958**, 232, 785-795
- [36] J. J. Gallagher, G. T. Newbold, W. Sharp, F. S. Spring, *Journal of the Chemical Society (Resumed)* **1952**, 4870-4874
- [37] G. Dunn, G. T. Newbold, F. S. Spring, *Journal of the Chemical Society (Resumed)* **1949**, 2586-2587
- [38] R. G. Micetich, J. C. MacDonald, *Journal of the Chemical Society (Resumed)* **1964**, 1507-1510
- [39] E. D. Morgan, R. R. Do Nascimento, S. J. Keegans, J. Billen, *J. Chem. Ecol.* **1999**, 25, 1395-1409
- [40] E. Leete, J. A. Bjorklund, G. A. Reineccius, T. B. Cheng, *Spec. Publ. - R. Soc. Chem.* **1992**, 95, 75-95
- [41] A. Laurent, *Justus Liebigs Ann. Chem.* **1844**, 52, 348-358
- [42] G. B. Barlin, *The Pyrazines*, Wiley, New York, **1982**.
- [43] D. J. Brown, *The Pyrazines: Supplement I*, Wiley, New York, **2003**.

Chapter 1

The Forgotten Pyrazines: Exploring the Dakin-West Reaction

Published as:

Martien A. Würdemann, Cristina Nițu, Dr. Stefaan M.A. De Wildeman, Dr. Katrien V. Bernaerts, Prof. Dr. Romano V.A. Orru, *Chemistry: A European Journal*, **2020**, *26*, 8090-8100

Abstract

Pyrazines are an underreported class of N-heterocycles available from nitrogen-rich biomass presenting an interesting functional alternative for current aromatics. In this work, we explore access to pyrazines obtained from amino acids using the 90-year-old Dakin-West reaction. After a qualitative screening, several functional proteinogenic amino acids proved good substrates for this reaction, which were successfully scaled to multigram scale synthesis of the corresponding intermediate α -acetamido ketones. Subsequently, we optimized the conditions towards pyrazine formation using δ -amino-levulinic acid, these were employed to synthesize a relevant set of five functional dimethylpyrazines in high purity. These pyrazines can be considered a versatile toolbox of aromatic building blocks for a wide range of applications such as in the synthesis of polymers or metal-organic frameworks.

Introduction

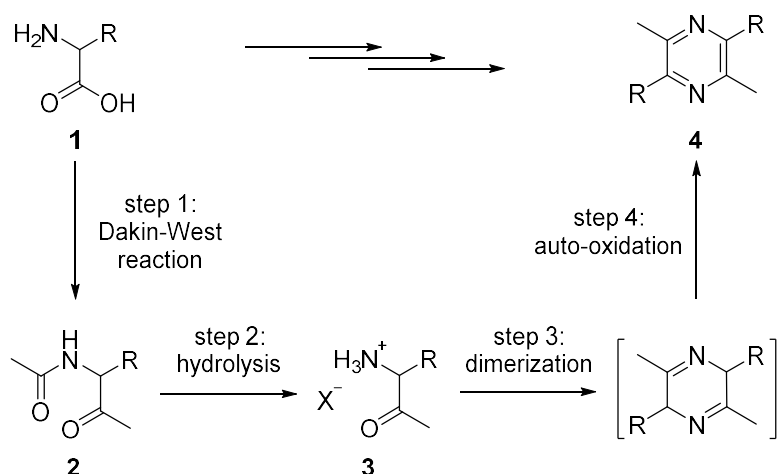
Petrochemicals are widely used, either as an energy source or as a source of functional aromatic building blocks for the chemical production of valued materials. However, the notable environmental impact associated with petrochemical resources makes their use inherently not sustainable. Current chemical research therefore focuses on more sustainable alternatives to access industrially important aromatic monomers. In this respect, the use of lignocellulosic biomass has received considerable interest.^[1-5] On the other hand, nitrogen-rich biomass based on proteins or amino acids is rather underutilized.^[6] This type of biomass is either available from waste streams or can be generated by fermentative production and holds great promise for sustainable use in new or existing materials. Especially since access to a wide range of N-heterocyclic aromatic monomers from amino acids can be achieved via numerous highly established routes.^[6]

The 1,4-diazines (pyrazines) attracted our attention as the most aromatic N-heterocycle known (89% aromaticity compared to benzene).^[7] We anticipate that this property combined with their high degree of symmetry should result in similar thermal and mechanical properties for pyrazine containing monomers compared to those containing benzene. Furthermore, the reactivity of both nitrogen atoms in pyrazines provides opportunities for post-polymerization functionalization.^[8-9] Despite these properties, pyrazines have barely been reported in polymer compositions nor as additives for polymers or advanced materials. A lack of precedent offering great potential for further development. We envisioned that pyrazines should be accessible from certain nitrogen-rich biomass streams, but to the best of our knowledge however, no methodology for the transformation of such biomass to pyrazines has recently been reported.

Although underreported in a polymer context, pyrazines are a well-studied class of compounds.^[8-9] The pyrazine core is found in pharmaceuticals and dyes as well as in many flavors.^[8-14] The synthesis of para-symmetric pyrazines is most easily achieved via the auto-condensation of α -amino-carbonyl compounds. These are moderately stable as their salts or under air free conditions. When the basic nitrogen in α -amino carbonyls is liberated, cyclic diimines (see step 3 in **Scheme 1**) are formed which spontaneously oxidize to pyrazines in the presence of oxygen (air) or other oxidants (see step 4 in **Scheme 1**).^[8] All synthesis methods to form pyrazines via the α -amino carbonyl compounds are inherently atom efficient, with only the release of water.

Synthesis of the required α -amino carbonyl compounds can be achieved via various approaches from different starting materials.^[8-9] In our opinion the use of

commercially available proteinogenic amino acids as starting materials would be highly interesting as they constitute a chemically pure source of nitrogen-rich biomass, which potentially could be obtained from waste streams. The Dakin-West reaction, reported already in 1928, is a most interesting means to obtain the desired α -amino carbonyls directly from amino acid starting materials. In this reaction, an α -amino acid (**1**) is converted to an α -amino methyl ketone with acetic anhydride (see step 1 in **Scheme 1**).^[15-17] The initial product obtained is an α -acetamido ketone (**2**) formed after loss of carbon dioxide. Subsequent hydrolysis of **2** to an α -amino ketone hydrochloride (**3**) (see step 2 in **Scheme 1**) followed by dimerization and auto-oxidation provides direct access to pyrazines (**4**).



Scheme 1: Dimethylpyrazine synthesis via the Dakin-West reaction on amino acids.

The Dakin-West reaction proceeds under relatively mild reaction conditions, which tolerate for example carboxylic anhydrides and functionalized α -H carboxylic acids as starting materials.^[18] This is highlighted by the fact that the reaction was already used by Woodward *et al.* in his famous first total synthesis of strychnine reported in 1963.^[19] Dakin and West already showed that proteinogenic amino acids could be transformed to pyrazines by their procedure. However, a comprehensive overview of which amino acids may be employed as effective substrates in the Dakin-West reaction has never been composed.^[18, 20-21] Also, in a more recent review that discusses the mechanism in more detail, no general substrate scope of the Dakin-West reaction is presented.^[22] In addition, analytical records for both α -acetamido ketones (**2**) synthesized via the reaction as well as for the corresponding pyrazines (**4**) obtained in this way are sparse or based on derivatives, especially since most of these reactions were performed before 1980.

Based on the above considerations we decided to explore the potential of the Dakin-West reaction to access dimethylpyrazines (**4**) from amino acids. We focused on the use of proteinogenic amino acids with a non-aliphatic side chain, leading directly to a dimethylpyrazine product with a reactive functionality for further development into functionalized bio-based materials or metal organic frameworks.

In this Chapter we discuss the results of our studies, including optimization, scope and scale-up towards functional dimethylpyrazines.

Experimental

General information

Acetic anhydride, hydrogen peroxide solution (35 wt%), formic acid, dimethylaminopyridine, glutamic acid, lysine, tryptophan, sodium bicarbonate, threonine, cysteine, arginine, glutamine and asparagine were obtained at Sigma-Aldrich at >95% purity and used as received. Triethylamine, sodium hydroxide and potassium hydroxide were obtained from Fischer/Acros chemical at 99% purity and used as received. Glacial acetic acid, methanol, acetone, isopropyl alcohol, acetonitrile, hydrochloric acid, dichloromethane and chloroform were obtained from Biosolve as analytical reagent grade or higher and used as received. Histidine, methionine, tyrosine and serine were obtained from Bachem at >95% purity and used as received. Δ -amino-levulinic acid hydrochloride (DALA) was obtained from Ark-Pharm in 95% purity and used as received. Fumed silica microcolloidal powder was obtained from Plasmachem and had an average particle size of 7-14 nm. Deuterated solvents were obtained from Cambridge Isotope Labs.

Preparative chromatography was performed on a Grace Davison Reveleris X2 system using Büchi FlashPure EcoFlex silica columns.

Liquid Chromatography – Mass Spectrometry (LC-MS) analysis was performed on a Shimadzu Nexera 2 UHPLC system equipped with a Shimadzu LC-30AD pump, a SPD-M30A photodiode array detector and LCMS-2020 single quadrupole detector. The system was run on MilliQ water and LC-MS grade acetonitrile both modified with 0.1% formic acid. A Waters XSelect CSH C18 column (3.0 mm x 75 mm with a particle size of 3.5 μ m) was used operating at 30 °C. The method was set up with a gradient of 5% acetonitrile in water for 2 min, an increase to 95% acetonitrile over 6 min, 1 min at 95% followed by flushing back to 5% acetonitrile. Samples were prepared by dissolving the reaction mixture in methanol at \pm 1 mg/mL.

$^1\text{H-NMR}$ (300 MHz) and $^{13}\text{C-NMR}$ (75 MHz) analysis were recorded on a Bruker AVANCE 300 MHz apparatus at room temperature. $^1\text{H-NMR}$ experiments were carried out with 16 scans, using approximately 5 mg of material in 0.5 mL deuterated solvent. Both CDCl_3 and DMSO-d_6 were used as solvents. $^{13}\text{C-NMR}$ attached proton test (APT) experiments were carried out with 1024 scans, using approximately 50 mg of material. The chemical shifts are reported in ppm referenced against either the residual solvent peak or TMS standard (0 ppm).

FTIR analysis spectra were recorded on a Shimadzu IRAffinity-1 system fitted with a MIRacle 10 ATR at room temperature. Background corrected measurements were conducted at 2 cm^{-1} resolution from 4000 to 600 cm^{-1} using 32 scans.

Melting points were recorded in triplicate on a Mettler-Toledo MP90 melting point system using open capillaries and are uncorrected.

Elemental analyses were recorded on an Elementar varioEL at the Institut für Organische Chemie of the RWTH Aachen, Germany.

All characterization details can be found in the appendix.

General procedure for qualitative screening on amino acids (1a-1m) (1 mmol scale)

A 25 mL 2-necked flask fitted with a cooler and bubble-counter was loaded with triethylamine (0.49 mL, 3.5 mmol), acetic anhydride (0.32 mL, 3.3 mmol), acetic acid (29 μ L, 0.5 mmol) and dimethylaminopyridine (1.2 mg, 0.01 mmol). The resulting reaction mixture was heated to 65 °C. Upon reaching the desired temperature, the amino acid (1 mmol) was added as a solid and the addition neck stoppered. The reaction was sampled several times in intervals of 1 hour to check progress and left to stir overnight (\pm 17h). After concentration *in vacuo* (10 mBar, 85 °C) the crude reaction mixture was analyzed by LC-MS. Amino acids that showed selective reactions were selected for scale-up.

Procedure Dakin-West reaction for acetamido-ketone 2g

A 3-necked flask fitted with a reflux condenser, bubble-counter and thermometer was loaded with triethylamine (34 mL, 245 mmol 3.6 equiv.), acetic anhydride (34 mL, 360 mmol, 5.3 equiv.), acetic acid (2 mL, 34 mmol, 0.5 equiv.) and dimethylaminopyridine (83 mg, 0.01 mol%). The resulting reaction mixture was heated to 65 °C. Upon reaching the desired temperature, glutamic acid (10 g, 68 mmol) was added step-wise. The reaction was monitored by gas formation and amino acid was added whenever gas formation was slow. Upon complete addition, the reaction left to stir overnight (± 19 h). The crude reaction mixture was quenched by the addition of water and concentrated *in vacuo* (10 mBar, 85 °C) followed by short path vacuum distillation. The first fraction, a clear oil, consisted of triethylammonium acetate (pass-over 30-60 °C at 0.5 mBar). The second fraction consisting of the desired ketone **2g** was collected as a yellow oil (pass-over 100-120 °C at 0.3 mbar), which solidified in the setup and on standing. The desired acetamido ketone **2g** was isolated as a low melting waxy solid still containing some triethylammonium acetate (8.85 g, corrected: 50.9 mmol, 74%). Ten-fold scale-up of this reaction was easily achieved in an automated setup using a Lambda solid doser by adding microcolloidal silica as a flowing agent. At this scale, the material was isolated in 79.5 g yield (corrected: 459 mmol, 67%). The material can be recrystallized from hexane to yield yellow to colorless needles that cluster into a solid.

General procedure Dakin-West reaction, formation of ketones 2h-2l

A 3-necked flask fitted with a reflux condenser, bubble-counter and thermometer was loaded with triethylamine (3.5 equiv.), acetic anhydride (3.3 equiv.), acetic acid (0.5 equiv.) and dimethylaminopyridine (0.01 mol%). The resulting reaction mixture was heated to 65 °C. Upon reaching the desired temperature, 10 grams of the amino acid (between 49-68 mmol) was added step-wise. The reaction was monitored by gas formation and amino acid was added whenever gas formation was slow. Upon complete addition, the reaction left to stir until gas formation had seized completely or overnight (between 5 and 19 hours). Each substrate required a slightly different work-up details for which are listed in the appendix.

General procedure hydrolysis of ketones to synthesize hydrochloride salts 3g-3k

A round-bottom flask was filled with the respective acetamido ketone and taken up in 3 equiv. of 6M hydrochloric acid. The resulting solution was heated to reflux until complete hydrolysis was achieved according to LC-MS. The crude was concentrated to dryness *in vacuo* and the obtained solid triturated with either acetone (ketones **3g-I** & **3k**) or IPA (ketone **3j**). The resulting solids were isolated by filtration, washed on the filter with an equal volume of either acetone (ketones **3h**, **3i** & **3k**) or IPA (ketones **3g** & **3j**) and subsequently dried *in vacuo* (40 °C). The obtained material was pure enough for the next reaction step. Further details on the work-up and analytical data are listed in the appendix.

General condensation procedure of hydrochloride salts (DALA, 3g, 3i-k) to form pyrazines 11, 4g, 4i-4k

Each hydrochloride salt was dissolved in methanol in a round-bottom flask to form a 0.2 M solution. The solution was cooled on ice. Once reaching 0 °C, a solution of hydrogen peroxide (2 equiv.) was added followed by slow addition of TEA (1 equiv.). The resulting solution was allowed to come to room temperature and left to stir overnight followed by further work-up.

2,5-bis(2-carboxyethyl)-pyrazine (**11**)

Δ -aminolevulinic acid hydrochloride (**DALA**) (5.03 g, 30.0 mmol) was dissolved in methanol (150 mL) and cooled on ice. Upon reaching 0 °C, a 35wt% solution of hydrogen peroxide was added slowly (5.2 mL, 59.7 mmol) followed by slow addition of TEA (4.1 mL, 30.0 mmol). The formed yellow solution was allowed

to come to room temperature and left to stir overnight (± 18 h). The resulting suspension was concentrated *in vacuo*, resulting in a yellow solid. The material was dissolved in 10 mL of water and the pH adjusted to 4 using 1M HCl. A yellow solid precipitated which was isolated by filtration, washed with 3x 10 mL water and dried *in vacuo* (40 °C) overnight to yield the desired pyrazine (2.14 g, 9.56 mmol, 63%). The material could be recrystallized from water to give yellow crystals.

mp 221-223 °C (decomp.)(lit. 219-221 °C)^[48]; ¹H NMR (300 MHz, DMSO-*d*₆) δ (ppm) = 12.16 (s, 2H), 8.46 (s, 2H), 2.97 (t, *J*=7.2 Hz, 4H), 2.68 (t, *J*=7.2 Hz, 4H); ¹³C NMR (75 MHz, DMSO-*d*₆) δ (ppm) = 174.1, 153.4, 143.7, 32.6, 29.5; IR (ATR) $\tilde{\nu}$ = 2863 (br), 2498 (br), 1702 (vs), 1493 (m), 1382 (m), 1229 (s), 1189 (vs), 1060 (s), 894 (m), 820 (m) cm⁻¹; elemental analysis calcd (%) for C₁₀H₁₂N₂O₄: C 57.57, H 5.39, N 12.49; found: C 53.37, H 5.24, N 12.48

2,5-bis(2-carboxyethyl)-3,6-dimethylpyrazine (4g)

Keto hydrochloride **3g** (4.99 g, 27.5 mmol) was dissolved in methanol (135 mL) and cooled on ice. Upon reaching 0 °C, a 35wt% solution of hydrogen peroxide was added slowly (4.8 mL, 55.5 mmol) followed by slow addition of TEA (3.8 mL, 27.5 mmol). The formed yellow solution was allowed to come to room temperature and left to stir overnight (± 18 h). The resulting suspension was concentrated *in vacuo*, resulting in a colorless solid. The material was suspended in 10 mL of water. The precipitate was isolated by filtration, washed with 3x 10 mL water and dried *in vacuo* (40 °C) overnight to yield the desired pyrazine (3.03 g, 12.0 mmol, 87%). The material could be recrystallized from water giving colorless needles or methanol giving colorless stout prisms.

mp 211-213 °C (decomp.)(lit. 211-213 °C)^[15]; ¹H NMR (300 MHz, DMSO-*d*₆) δ (ppm) = 12.09 (s, 2H), 2.91 (t, *J*=7.1 Hz, 4H), 2.66 (t, *J*=7.1 Hz, 4H), 2.43 (s, 6H); ¹³C NMR (75 MHz, DMSO-*d*₆) δ (ppm) = 174.5, 149.9, 148.0, 31.6, 28.5, 21.2; IR (ATR) $\tilde{\nu}$ = 2901 (br), 2513 (br), 1928 (w), 1706 (s), 1419 (m), 1300 (m), 1189 (vs), 1128 (s), 1035 (m), 647 (m) cm⁻¹; elemental analysis calcd (%) for C₁₂H₁₆N₂O₄: C 57.13, H 6.39, N 11.10; found: C 56.90, H 6.12, N 11.06

2,5-dimethyl-3,6-bis(2-(methylthio)ethyl)pyrazine (4i)

Keto hydrochloride **3i** (4.50 g, 24.50 mmol) was dissolved in methanol (120 mL) and cooled on ice. Upon reaching 0 °C, TEA (3.4 mL, 24.5 mmol) was added. The formed yellow solution was allowed to come to room temperature and left to stir overnight (± 18 h). The resulting suspension was concentrated *in vacuo*, resulting in a brown solid. The material was suspended in 50 mL EtOAc, isolated by filtration over a silica plug and washed with 50 mL of EtOAc. The filtrate was concentrated and the resulting brown solid was recrystallized twice from EtOAc, to yield the desired pyrazine (1.46 g, 5.71 mmol, 66% corrected for 30% oxidation) as beige platelets.

mp 87-88 °C; ¹H NMR (300 MHz, DMSO-*d*₆) δ (ppm) = 3.01 - 2.93 (m, 4H), 2.85 - 2.76 (m, 4H), 2.46 (s, 5H), 2.10 (s, 6H); ¹³C NMR (75 MHz, DMSO-*d*₆) δ (ppm) = 150.3, 148.4, 33.8, 32.2, 21.2, 15.3; IR (ATR) $\tilde{\nu}$ = 2920 (m), 2909 (m), 1416 (vs), 1390 (s), 1221 (m), 1104 (s), 981 (m), 961 (m), 711 (m), 683 (m) cm⁻¹; elemental analysis calcd (%) for C₁₂H₂₀N₂S₂: C 56.20, H 7.86, N 10.92; found: C 56.39, H 7.94, N 11.02

2,5-bis(imidazol-5-yl)methyl)-3,6-dimethylpyrazine (4j)

Keto dihydrochloride **3j** (5.65 g, 25.00 mmol) was dissolved in methanol (125 mL) and cooled on ice. Upon reaching 0 °C, a 35wt% solution of hydrogen peroxide was added slowly (4.4 mL, 50.0 mmol) followed by slow addition of TEA (3.5 mL, 25.0 mmol). The resulting suspension was concentrated *in vacuo*, resulting in an orange solid. The material was suspended in 50 mL of 2M NaOH accompanied by a color change from orange to colorless. The suspension was left overnight to release triethylamine, the remainder of which was liberated *in vacuo*. The resulting colorless solid was isolated by filtration and recrystallized from 250 mL of boiling water. The crystals were isolated by filtration, washed with 3x 50 mL water and dried *in vacuo* (60 °C) overnight to yield the desired pyrazine (2.81 g, 10.5 mmol, 84%) as very fine colorless needles.

no mp (decomp.); $^1\text{H NMR}$ (300 MHz, DMSO-d_6) δ = 7.31 (s, 2H), 6.54 (s, 2H), 3.93 (s, 4H), 2.43 (s, 6H); $^{13}\text{C NMR}$ (75 MHz, DMSO-d_6) δ (ppm) = 150.6, 148.4, 135.9, 135.2, 117.1, 33.7, 21.3; IR (ATR) $\tilde{\nu}$ = 2800 (br), 2619 (br), 1415 (m), 1232 (m), 1110 (m), 999 (vs), 839 (vs), 745 (vs), 696 (s), 626 (vs) cm^{-1} ; elemental analysis calcd (%) for $\text{C}_{14}\text{H}_{16}\text{N}_6$: C 62.67, H 6.01, N 31.32; found: C 62.51, H 5.91, N 31.86

2,5-bis(4-hydroxybenzyl)-3,6-dimethylpyrazine (4k)

Keto hydrochloride **3k** (5.50 g, 25.50 mmol) was dissolved in methanol (125 mL) and cooled on ice. Upon reaching 0 °C, a 35wt% solution of hydrogen peroxide was added slowly (4.5 mL, 51.00 mmol) followed by slow addition of TEA (3.5 mL, 25.50 mmol). The formed yellow solution was allowed to come to room temperature and left to stir overnight (± 18 h). The material was isolated by filtration, washed with methanol (3x 20 mL) and dried *in vacuo* (40 °C) to yield the desired pyrazine (3.76 g, 11.7 mmol, 92%) as a colorless solid.

no mp (decomp.); $^1\text{H NMR}$ (300 MHz, DMSO-d_6) δ (ppm) = 9.22 (s, 2H), 6.96 (d, $J=8.2$ Hz, 4H), 6.72 - 6.58 (m, 4H), 3.96 (s, 4H), 2.38 (s, 6H); $^{13}\text{C NMR}$ (75 MHz, DMSO-d_6) δ (ppm) = 156.1, 151.3, 148.5, 129.9, 129.0, 115.7, 21.4; IR (ATR) $\tilde{\nu}$ = 3100 (br), 1612 (m), 1595 (m), 1517 (vs), 1417 (s), 1237 (s), 1174 (s), 1124 (s), 993 (m), 808 (vs) cm^{-1} ; elemental analysis calcd (%) for $\text{C}_{20}\text{H}_{20}\text{N}_2\text{O}_2$: C 74.98, H 6.29, N 8.74; found: C 74.09, H 6.12, N 8.74

2,5-bis(4-aminobutyl)-3,6-dimethylpyrazine (4h) (adapted from J. Scholl)^[31]

Dihydrochloride salt **4h** (8.08 g, 37.2 mmol) was dissolved in water (8 mL) and cooled on ice. A 45% solution of NaOH (29 mL) was added slowly resulting in the formation of a yellow to brown solution. The reaction was allowed to warm to room temperature resulting in a biphasic system. After stirring at room temperature for 2h the mixture was extracted with 5x 50 mL toluene and the organic phase dried over K_2CO_3 . After removal of the solvent *in vacuo*, the resulting yellow oil was subjected to vacuum distillation in a Kugelrohr at 205 °C and 1 mBar. The desired material was collected as a yellow oil boiling at 170-175 °C. If sufficiently pure, the oil will crystallize into a yellow waxy solid (2.45 g, 9.78 mmol, 52%). Thermal degradation takes place during distillation lowering yield and purity.

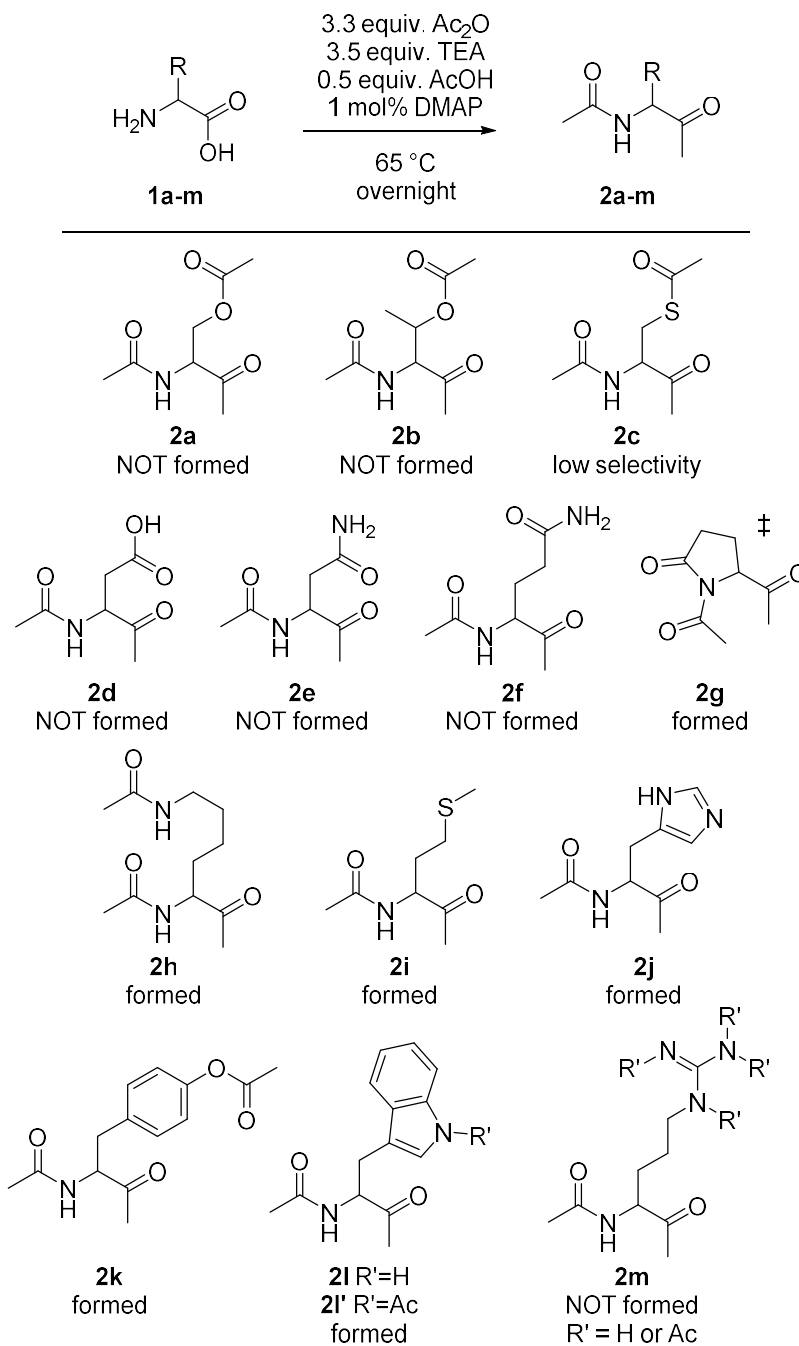
mp 54-55 °C; $^1\text{H NMR}$ (300 MHz, DMSO-d_6) δ (ppm) = 2.71 - 2.62 (t, $J=6.9$ Hz, 4H), 2.55 (t, $J=6.9$ Hz, 4H), 2.42 (s, 6H), 1.71 - 1.51 (m, 4H), 1.49 - 1.28 (m, 4H); $^{13}\text{C NMR}$ (75 MHz, DMSO-d_6) δ (ppm) = 151.6, 147.8, 42.0, 34.0, 33.8, 25.9, 21.2; IR (ATR) $\tilde{\nu}$ = 3353 (m), 3256 (br), 3180 (br), 2917 (vs), 2860 (s), 1610 (m), 1414 (vs), 1396 (s), 1027 (vs), 879 (s) cm^{-1} ; elemental analysis calcd (%) for $\text{C}_{14}\text{H}_{26}\text{N}_4$: C 67.16, H 10.47, N 22.38; found: C 64.94, H 9.75, N 20.94

Results and discussion

Qualitative screening of proteinogenic amino acids and selection of targets.

We first set out to identify which non-aliphatic proteinogenic amino acids (**1a-m**) indeed can be transformed into dimethylpyrazines (**4**) using the Dakin-West reaction. By keeping currently accepted principles of green chemistry in mind and taking potential scalability into consideration,^[23] the Steglich and Höfle reaction conditions using triethylamine (TEA) as base and dimethylaminopyridine (DMAP) as catalyst seemed a most relevant starting point for optimization.^[24-25] These conditions allow for reduced reaction temperatures while increasing the yield of the α -acetamido ketone (**2**) pyrazine precursors considerably. However, autocatalytic carbon dioxide evolution, which accompanies the formation of the desired α -acetamido ketones (**2**), is quite sudden and violent presenting a significant safety hazard potentially hampering scale-up. In a modification, Fischer and Misun reported the use of reduced ratios of both acetic anhydride and TEA and they safely scaled the reaction using 0.5 kmol alanine producing the corresponding α -acetamido ketone (**2**, R = Me) in excellent yields.^[26]

Thus, these conditions were selected and adapted for our screening of the amino acids (**1a-m**) of interest in the Dakin-West approach towards different functionalized α -acetamido ketones (**2a-m**). Since the selected amino acids contain possibly reactive functional groups, an extra equivalent of both acetic anhydride and TEA were added compared to the Fischer conditions. The screening was set up at one mmol scale with the reactions being qualitatively analyzed by LC-MS to select possible candidates for scale-up later on. The results of this screening are summarized in **Scheme 2**.



Scheme 2: Qualitative screening conditions and results. (‡ 1g = glutamic acid)

Dakin and West already reported that the formation of α -acetamido ketone **2a**, from serine (**1a**) proceeds in poor yields.^[15] Also, under our conditions no identifiable products were observed using serine as the starting material. On the other hand, the reaction with threonine showed the clear formation of the side product **5b** (see frame A in **Figure 1**). Acetylation of the hydroxyl group in threonine generates, under the reaction conditions, a relatively good leaving group and elimination results in alkene **5b**. A similar elimination most likely also occurs using serine and gives **5a**, in this case. The formed alkene is not stabilized by a methyl group resulting in further side-reactions. Dakin and West reported that with phenylserine, indeed elimination followed by ring closure to cinnamic acid azlactone **6** (see frame A in **Figure 1**) took place, an observation that further supports our findings.^[15] For the above reasons, the use of serine (**1a**) and threonine (**1b**) in our further scale-up studies was discarded.

Under the conditions applied in this study using TEA as base, cysteine (**1c**) showed the formation of the desired α -acetamido ketone (**2c**) with low selectivity. This observation is in line with earlier reports using more classical conditions that also provided ketone **2c**, in mediocre yields.^[20, 27] The selectivity for α -acetamido ketone (**2c**) formation using cysteine (**1c**) was too low to merit further research.

Aspartic acid (**2d**) was not included in this study since it was shown by others that double intramolecular ring closures of different kinds preclude any selective formation of the desired acetamido-ketone product.^[20, 24]

To the best of our knowledge, the Dakin-West reaction has never been performed with asparagine (**1e**) or glutamine (**1f**). Under our conditions complex product mixtures were obtained using these starting materials. Most notable were dehydrated, acetylated amino acids byproducts according to the MS spectra. The desired products (**2e** & **2f**) were, however, not observed and no further efforts were made with asparagine and glutamine as starting materials.

Glutamic acid (**1g**) was already reported as a substrate by Dakin and West in 1928, however the corresponding ketone product was not isolated by them and ultimate evidence of its synthesis was provided by the synthesis of the corresponding pyrazine.^[15] The intermediate α -acetamido ketone product, 1,5-diacetyl-2-pyrrolidone **2g** was later identified in combination with the major side-product, acetyl-pyroglutamic acid **7** (see frame B in **Figure 1**).^[28] The synthesis of **2g** is well reported and was smoothly formed under our conditions. Glutamic acid (**1g**) was therefore selected for scale-up towards pyrazines (see below).^[29-30]

The use of lysine (**1h**) in the Dakin-West reaction has only been reported in a family of patents by Bayer.^[31-35] The original Steglich conditions were used herein to synthesize the corresponding ketone **2h**. Subsequent acid hydrolysis and ring formation affords the desired pyrazine. In the screening using our modified conditions the α -acetamido ketone (**2h**) was indeed formed smoothly. We therefore selected lysine as starting material for scale-up towards the corresponding pyrazines.

Methionine (**1i**) is reported to act as a selective substrate in the Dakin-West reaction under classical conditions^[20, 36-38] as well as under the Steglich conditions.^[39] Under our screening conditions the desired ketone **2i** was indeed formed selectively in good yield and methionine was thus selected for scale-up towards pyrazines.

The α -acetamido ketone (**2j**) derived from histidine (**1j**) was originally reported by Dakin and West. This compound received quite some attention as a histidine decarboxylase inhibitor.^[15, 21, 40-41] The dimethylpyrazine derived from **2j** has also been reported for the same application although no synthetic details were enclosed.^[42] Under our conditions the desired product was found to be formed with high selectivity and we thus selected **1j** for our scale-up studies discussed below.

Tyrosine (**1k**) was one of the first substrates for the Dakin-West reaction, with α -acetamido ketone **2k** being formed in high yield and the corresponding pyrazine was synthesized effectively.^[16-17, 37] The α -acetamido ketone **2k** was also synthesized in high yields under Steglich-like conditions.^[39] Under our screening conditions, tyrosine (**1k**) reacted smoothly and since the pyrazine was already reported tyrosine was selected as starting material for scale-up as well.

Similarly, the tryptophan-derived acetamido-ketone **2l** has been synthesized before in good yields.^[15, 37-38, 43-44] In our study the desired product **2l** was formed together with the acetylated indole ketone **2l'**. The combined selectivity towards these two products proved very high and tryptophan was selected for scale-up towards the corresponding pyrazines.

Formation of α -acetamido ketone (**2m**) using arginine (**1m**) in the Dakin-West reaction proved not successful in earlier studies with both the free arginine as well as N-benzoyl-arginine.^[45] Under the conditions applied in our study a range of different ketones, different extents of acetylation on the guanidine system as well as ring closed ornithine **8** (see frame C in **Figure 1**) could be detected. Consequently, pursuit of arginine as starting material for pyrazine synthesis was not further explored.

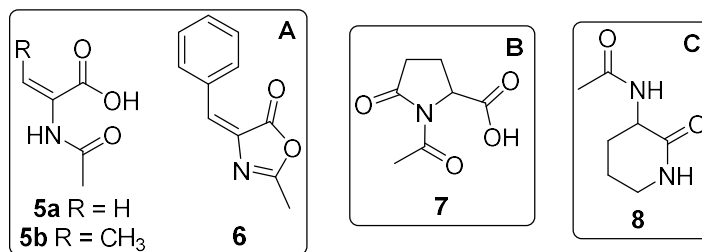


Figure 1: Side-products observed during qualitative screening of the Dakin-West reaction.

Scale-up of α -acetamido ketone (*2g-2l*) synthesis

The qualitative screening described above identified Glu (**1g**), Lys (**1h**), Met (**1i**), His (**1j**), Tyr (**1k**), and Trp (**1l**) as successful amino acid starting materials in the Dakin-West synthesis of the corresponding α -acetamido ketones (**2g-2l**). We now turned our attention to explore suitable work-up conditions and therefore performed these Dakin-West reactions at 10 mmol scale using our initial conditions described above in **Scheme 2**. Further, in order to assess safety hazards, gas formation and exotherms the reactions were scaled further to 49-68 mmol (≈ 10 grams).

Except for the reaction with Glu (**1g**), all reactions provided the desired ketones in good yields (73% - 84%). For glutamic acid it was found that competition with pyroglutamic acid formation inhibited the formation of the desired ketone (**2g**). Reactions at the same scale using conditions with more equivalents of acetic anhydride and triethylamine provided yields of **2g** similar to those reported by Lepschy *et al.*^[24]

Work-up and purification of all reaction mixtures was performed by concentration *in vacuo* followed by a distinct procedure depending on the nature of each α -acetamido ketone (**2g-2l**) that was formed. Column chromatography was considered a last resort option for purification, as it has limited scalability and is inherently not “green”. Concentration of the reaction mixtures was conducted at high temperature and low pressure to minimize product loss.^[26] Triethylammonium acetate is formed during the reaction and after complexation it acts as an ionic liquid with a high boiling azeotrope of 160 °C.^[46] This complex was removed by distillation.

In the case of ketone **2l**, derived from Trp (**1l**), the indole-moiety was partially acetylated under our screening conditions. However, easy deacetylation by stirring in a potassium hydroxide solution at room temperature gave the desired **2l** selectively after simple filtration. Unfortunately, in case of the methionine-derived product **2i**, column chromatography proved necessary to obtain the desired material. Finally,

isolation of the ketone derived from histidine (**2j**) was not possible because traces of the above reported ionic liquid even persisted after prolonged concentration and the reaction was therefore hydrolyzed to the dihydrochloride salt **3j** without isolation.

As mentioned before, safety and scalability aspects were further tested performing our modified Dakin-West procedure at 10 gram scale (49-68 mmol). After stepwise addition of the solid amino acid starting material, control over gas formation was satisfactory. On the other hand, reversed addition, adding the acetic anhydride to a stirred suspension of amino acid in TEA gave no appreciable yield of the corresponding α -acetamido ketones. During addition of the amino acid substrates in the Dakin-West process no large exotherms were observed except when lysine was used. Also noteworthy is that scale-up of our Dakin-West procedure using glutamic acid at 100 gram scale conducted in an automated setup with a Lambda solid doser, proceeds with full control of gas formation no active cooling of the reaction mixture was necessary affording the desired ketone product in excellent yield. The only adjustment to the 10 grams procedure was that we applied micro-colloidal silica as a flowing agent.

The observations during these scale-up experiments indicate that our conditions provide a high level of control for the Dakin-West reaction towards α -acetamido ketones (**2g-2l**), which is comparable to the Fischer and Misun conditions developed for Ala. This, together with the fact that the reaction with Ala as starting material was scaled to 0.5 kmol (50 kg)^[26], led us to conclude that these conditions allow for safe scale-up of the Dakin-West reaction to kilogram scale regardless of the amino acid substrate chosen. The work-up conditions and yields for each substrate after further scale-up to 49-68 mmol (10 g) are listed in **Table 1**.

Table 1: Results and work-up/purification conditions for the α -acetamido ketone products 2g-2l obtained from the Dakin-West reaction using the amino acids 1g-1l.

#	Substrate	Work-up	Product	Isolated yield [mol%]
1g	Glutamic acid	Vacuum distillation	2g	74 ^[a]
1h	Lysine	Trituration in EtOAc	2h	77
1i	Methionine	Extraction and column ^[b]	2i	73
1j	Histidine	Continued to diHCl 3j	x	x
1k	Tyrosine	Trituration in Et ₂ O	2k	84
1l	Tryptophan	Trituration 0.7M KOH	2l	78

[a] Yield corrected for co-distilled ionic liquid of triethylammonium acetate. [b] See experimental for details.

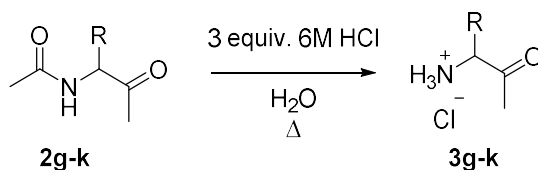
Hydrolysis of α -acetamido ketones 2g-2l

Next we turned our attention to the deprotection of the α -acetamido ketones (**2g-2l**) formed during the Dakin-West reaction (step 2 in **Scheme 1**), which is necessary before the final ring-closure to the desired dimethylpyrazine building blocks (**4**) can

occur. Except for tryptophan-based ketone **2l**, the removal of the acetyl-group was easily achieved in good yields by refluxing in 3 equiv. of 6M hydrochloric acid (see **Table 2**). Reaction progress was monitored by LC-MS and the hydrolysis was stopped after complete consumption of the starting ketone. In case of **2l** hydrolysis was unsuccessful with numerous side-products being formed. Based on earlier mechanistic studies, side-reactions are likely to involve a chlorine-induced oxidation, which could be suppressed by running the reaction under anaerobic conditions or by using a different acid such as sulfuric acid.^[47] However, hydrolysis of ketone **2l** in sulfuric acid or under anaerobic conditions was not successful in our hands. The use of other protective groups that could be removed under milder conditions was outside the scope of this work and no further efforts to synthesize a dimethylpyrazine derived from tryptophan were pursued.

The other hydrochloride salts (**3g-k**) formed during hydrolysis could be easily isolated as solids by concentration to dryness *in vacuo* followed by either trituration in acetone for salts **3g-i** & **3k** or isopropyl alcohol (IPA) for salt **3j**. After filtration and washing with either IPA (salts **3g** & **3j**) or acetone (salts **3h-i** & **3k**), the obtained solids were dried overnight and could be used without further purification in the formation of pyrazines.

Table 2: Results for the removal of the acetyl group of ketones 2g-2k.



#	Work-up	Product	Isolated yield [mol%]
2g	Trituration acetone, wash IPA	3g	82
2h	Trituration acetone	3h ^[a]	84
2i	Trituration acetone	3i	69
2j	Trituration IPA	3j ^[a]	76 ^[b]
2k	Trituration acetone	3k	86

[a] Isolated as double HCl salts, [b] Over two steps

Pyrazine formation

The formation of pyrazines via auto-condensation of α -amino-carbonyl compounds is well known.^[8-9] The reaction proceeds via a double imine formation that gives a dihydropyrazine intermediate which is subsequently oxidized to the pyrazine (see **Scheme 3**). Various mild oxidizing agents such as air, hydrogen peroxide, bromine water and cupric, ferric or mercuric ions can promote the final oxidation. The pyrazine

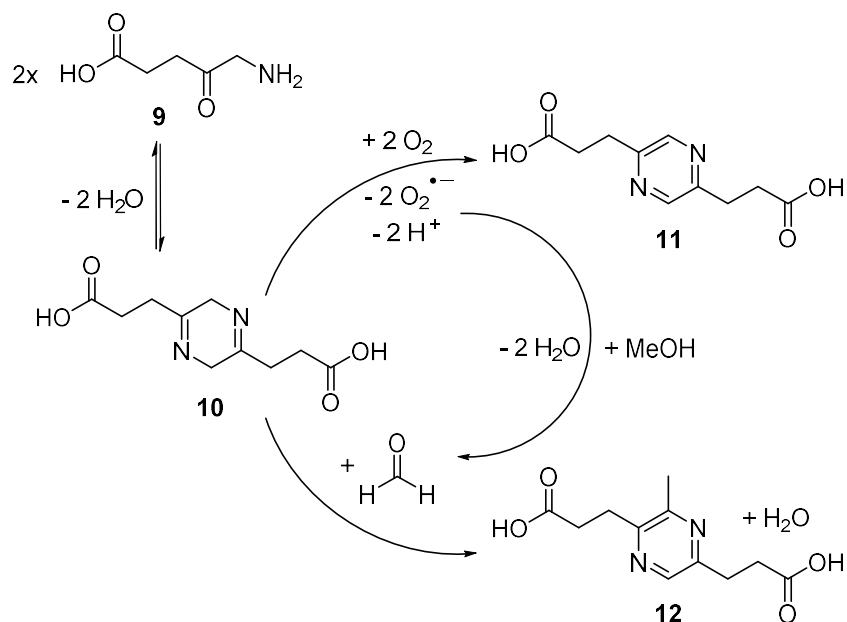
formation from the α -amino-ketone δ -amino-levulinic acid (DALA) **9** is particularly well studied. The mechanism has been fully elucidated including all involved intermediates and side products.^[48-51] Since **9** is commercially available and its pyrazine formation is well studied we selected it as model compound to establish optimal and scalable conditions to form ultimately our pyrazines of type **4**.

The reported mechanistic studies on **9** have all been performed in dilute aqueous solution and high conversions towards the pyrazine end-product were observed.^[49-51] During scale-up using such conditions (water at pH 6-8) the formation of the pyrazino dicarboxylic acid **11** proved, however, rather slow at increasing concentrations of DALA. To the extent that, at higher concentrations, which would allow facile isolation (> 0.1 mol/L), the reaction was not complete after stirring for 1 week under an air atmosphere. Although the reaction rate increases at higher pH, an increase in pH is accompanied by discoloration of the reaction mixture.^[51] This discoloration indicates side-reactions, thus preventing exploitation of this variable as a driver for the scale-up of the dimerization reaction. Dimerization towards the pyrazine scaffold is most likely rather slow in water due to the limited solubility of oxygen in water as well as the fact that water has to eliminate to form the intermediate non-aromatic dihydropyrazine **10**. The equilibrium towards **10** is more towards the starting material **9** due to the presence of water. Pyrazine condensation in aqueous solution was therefore not considered a viable scalable synthesis method.

Several solvents tolerating higher oxygen solubility were tested as alternatives, using triethylamine as an organic base at 100 mg scale. Methanol proved optimal because it allows complete dissolution of the free base. In methanol the reaction proceeds rapidly, with a suspension of the desired product forming within several hours. The dimerization reaction towards **11** was complete upon stirring at room temperature overnight.

Two major impurities were detected in the MS-spectra of the reaction mixture both with a mass of $M+15$. At first we believed *in-situ* esterification after initial formation of **11** occurred. Further scale-up was accompanied with strong discoloration of the reaction from yellow to brown and MS-analysis showed that only one of major impurities persisted in the reaction mixture. Since the formation of **11** results in the formation of superoxide radical anions according to the mechanistic studies discussed in **Scheme 3**, we believed that these reactive species account for the formation of the observed impurity and *in-situ* esterification is not a major issue.^[51] Especially since at increased scale limited oxygen diffusion into the reaction gives the formed superoxide radical anions enough time to oxidize methanol to formaldehyde, instead of decomposing with molecular oxygen. Methanol oxidation to formaldehyde would

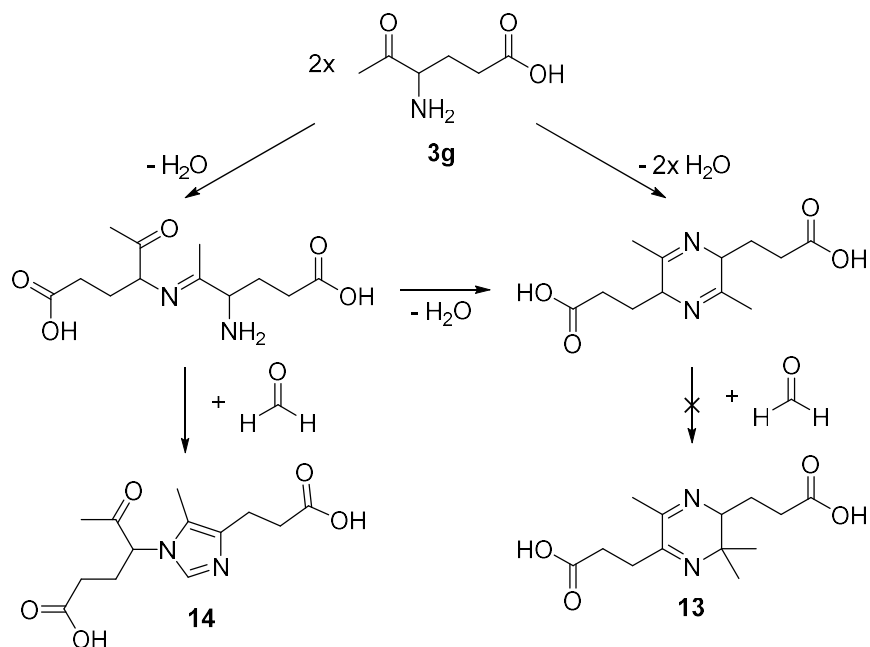
then result in methylation of the aromatic pyrazine ring to form **12**. Aldehydes have been reported to react with dihydropyrazines, forming alkyl substituted pyrazines. Acetaldehyde specifically, has been reported to react with DALA forming the ethyl substituted pyrazine, which further corroborates our idea.^[52] A cross-over experiment with formaldehyde, resulted in the formation of a product with the same retention time and molecular ion on LC-MS as the major impurity confirming the hypothesis that the methylated pyrazino product **12** is the observed impurity. Methanol oxidation by superoxide has been reported to take place electrochemically.^[53] Formation of large amounts of the side-product could be prevented by the addition extra oxidant to the reaction in the form of hydrogen peroxide.



Scheme 3: Model reaction of pyrazine formation using DALA (top) and the side-reaction involving methanol (bottom).

Since the dimerization of hydrochloride salts (**3g-k**) proceeds via similar mechanism as that of salt **9**, we suspect that formaldehyde formation by oxidation of methanol may also occur with these substrates. Any formaldehyde formed would then frustrate regioselective formation of the desired functional pyrazines **4**. To test this, a condensation reaction using the keto-hydrochloride obtained from glutamic acid **3g**, which is DALA's (**9**) closest structural isomer, was performed. Formaldehyde was added to a methanol mixture of ketone **3g** followed by addition of TEA. Upon addition a deep orange to brown reaction mixture immediately formed, indicating that a side reaction indeed occurs.

Attack of formaldehyde on the diimine formed from **3g**, however, would not result in an aromatic compound (**13**) and is unlikely to take place (see **Scheme 4**). On the other hand, a stabilized aromatic product can be formed upon formaldehyde induced aldol reaction with the linear mono-imine, which is a plausible intermediate. This reaction results in imidazole **14**, (see **Scheme 4**) and indeed an ion corresponding to this product was detected after LC-MS analysis (see appendix A18). This imidazole could unfortunately not be isolated; however, since discoloration was observed for the reaction of **3g** with formaldehyde, hydrogen peroxide was added to all further pyrazine condensation reactions.

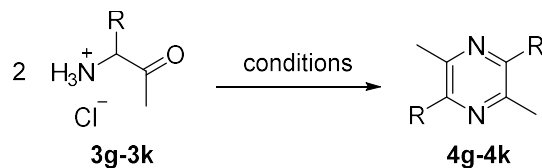


Scheme 4: Side reactions with formaldehyde in the pyrazine formation starting from **3g**.

After we identified the optimal conditions for pyrazine formation from DALA (**9**) these conditions were employed to dimerize the hydrochloride salts of the amino acid ketones **3g-3k** to form the corresponding pyrazines **4g-4k** (**Table 3**). Each hydrochloride salt was suspended in methanol and cooled on ice after which first hydrogen peroxide was added slowly (2 equiv.) followed by addition of TEA (1 equiv.). In most cases this resulted in condensation towards the desired pyrazines, however, the relatively high pKa of the lysine-based double hydrochloride salt **3h** prevented deprotonation by TEA and the desired reaction did not proceed in this case. Deprotonation of **3h** proceeds smoothly using strong lye upon which the desired reaction took place and **4h** was indeed formed in reasonable yields. For the

methionine-based hydrochloride **3i**, the formation of superoxide radical anions results in oxidation of the sulfide to the sulfoxide, which was exacerbated by addition of peroxide. When the dimerization reaction of **3i** was performed excluding peroxide 30% mono-sulfoxide formation was observed. This sulfoxidation could not be prevented by a radical scavenger such as butylated hydroxytoluene (BHT).

Table 3: Conditions and yields for the formation of pyrazines 4g-4k.



#	Conditions ^[a]	Product	Isolated yield [mol%]	Overall yield ^[b] [mol%]	Appearance	Lit. yield [mol%] ^[d]
3g	A	4g	87	52	Colorless needles	3 ^[15]
3h	B	4h	52	33	Yellow wax	87 ^[31]
3i	C	4i	66 ^[c]	33	Beige platelets	n.a.
3j	A	4j	84	64	Colorless needles	n.a.
3k	A	4k	92	63	Colorless powder	87 ^[17]

[a] A) 1 equiv. TEA, 2 equiv. H₂O₂ in MeOH from 0 °C to RT overnight; B) 10M NaOH in water; C) conditions A - H₂O₂. For work-up see experimental. [b] Over three steps. [c] Corrected for oxidation. [d] Over one step

Upon completion of the dimerization to afford the functionalized pyrazines **4g-4k** the crude reaction mixtures were allowed to come to room temperature and left to stir overnight. After testing for residual peroxide and concentration *in vacuo*, the resulting suspensions were diluted with water. The pH was adjusted if necessary to ensure the side-groups were not present as salts. Most of the resulting pyrazines are not soluble in water at appropriate pH and could easily be isolated via filtration except for lysine-based pyrazine **4h**. Pyrazine **4h** was therefore extracted in portions with toluene from the lye solution in which it was formed and subjected to vacuum distillation to obtain the product. This vacuum distillation proved difficult due to thermal degradation of the material. Scholl in his patents reports the use of thin film distillation, hinting at this thermal instability, which is not explicitly mentioned.^[31] Scholl isolated the material as a yellow oil, in our hands it solidified into a waxy low melting solid. The other pyrazines (**4g** and **4i-k**) could be further purified by recrystallization in an appropriate solvent (see experimental) and were obtained in good overall yield. The yield for the already reported pyrazine **4g** was significantly increased from 3%^[15] over 3 steps to 52% following our procedures. For the other substrates, the procedure for the pyrazine formation results in good to excellent yields.

All but one (**4i**) of these dimethylpyrazines are known compounds (see **Figure 2**), however, no physical or spectroscopic data of them have been reported before.

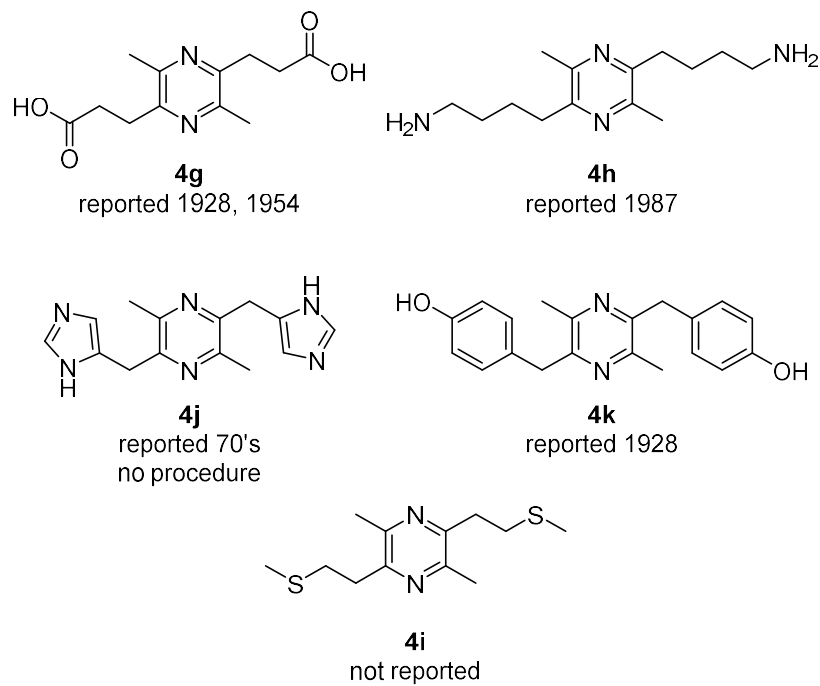


Figure 2: Toolbox of amino acid derived dimethylpyrazine building blocks.

Conclusions

A comprehensive set of functionalized proteinogenic amino acids proved good substrates in the Dakin-West reaction for the synthesis of α -amino-ketones. A safe and scalable method was developed for the transformation of six of these amino acids (**1g-l**), to their corresponding α -amino-ketones (**2g-l**). Five of these could be successfully hydrolyzed to the corresponding hydrochloride salts (**3g-k**), which were dimerized to form the desired pyrazine products **4g-k** (see **Figure 2**). We found, based on a model study with δ -amino-levulinic acid as the substrate, that the superoxide radical anions formed during the final dimerization/auto-oxidation step reaction oxidize methanol, forming formaldehyde. This formaldehyde causes side-reactions, in case of δ -amino-levulinic acid as methylation of the pyrazine and in case of the other salts (**3g-k**) most likely imidazole formation. Addition of hydrogen peroxide to the reaction mixture minimizes oxidation of methanol. This enabled us to develop a scalable synthesis that yielded the desired dimethylpyrazines in good yields. Thus, the five successfully hydrolyzed amino-ketones were condensed into their respective dimethyl pyrazines. The dimethylpyrazines **4g-k** are formed with our scalable and safe Dakin-West-based process in three steps starting from renewable amino acids that can be obtained via fermentation. Several of these functionalized pyrazines have not been reported for more than 90 years, they have been rediscovered and can be considered a toolbox for application towards added functionality materials. We are currently investigating these pyrazines as bio-based aromatic building blocks for polyesters and polyamides or as additives for such polymers.

References

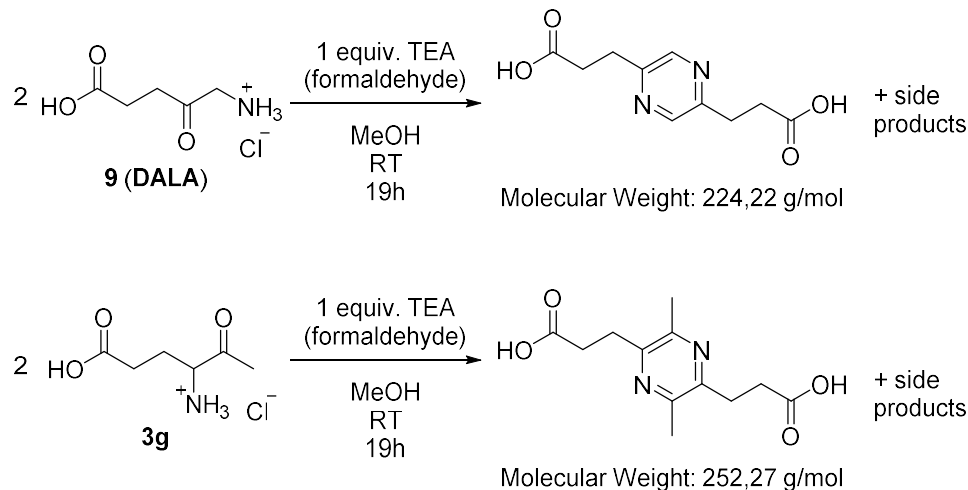
- [1] F. H. Isikgor, C. R. Becer, *Polym. Chem.* **2015**, *6*, 4497-4559
- [2] I. Delidovich, P. J. C. Hausoul, L. Deng, R. Pfütznerreuter, M. Rose, R. Palkovits, *Chem. Rev.* **2016**, *116*, 1540-1599
- [3] J. N. Chheda, G. W. Huber, J. A. Dumesic, *Angew. Chem. Int. Ed.* **2007**, *46*, 7164-7183; *Angew. Chem.* **2007**, *119*, 7298-7318.
- [4] R.-J. van Putten, J. C. van der Waal, E. de Jong, C. B. Rasrendra, H. J. Heeres, J. G. de Vries, *Chem. Rev.* **2013**, *113*, 1499-1597
- [5] A. Gandini, T. M. Lacerda, A. J. F. Carvalho, E. Trovatti, *Chem. Rev.* **2016**, *116*, 1637-1669
- [6] F. De Schouwer, L. Claes, A. Vandekerckhove, J. Verduyck, D. E. De Vos, *ChemSusChem* **2019**, *12*, 1272-1303
- [7] C. W. Bird, *Tetrahedron* **1986**, *42*, 89-92
- [8] G. B. Barlin, *The Pyrazines*, Wiley, New York, **1982**.
- [9] D. J. Brown, *The Pyrazines: Supplement I*, Wiley, New York, **2003**.
- [10] T. B. Adams, J. Doull, V. J. Feron, J. I. Goodman, L. J. Marnett, I. C. Munro, P. M. Newberne, P. S. Portoghese, R. L. Smith, W. J. Waddell, B. M. Wagner, *Food Chem. Toxicol.* **2002**, *40*, 429-451
- [11] H. Berneth, in *Ullmann's Encyclopedia of Industrial Chemistry*, Wiley-VCH Verlag GmbH & Co. KGaA, **2008**.
- [12] L. G. Palmer, T. R. Kleyman, in *Diuretics* (Eds.: R. F. Greger, H. Knauf, E. Mutschler), Springer Berlin Heidelberg, Berlin, Heidelberg, **1995**, pp. 363-394.
- [13] J. Adams, M. Kauffman, *Cancer Investigation* **2004**, *22*, 304-311
- [14] O. Zimhony, J. S. Cox, J. T. Welch, C. Vilchèze, W. R. Jacobs, *Nature Medicine* **2000**, *6*, 1043-1047
- [15] H. D. Dakin, R. West, *J. Biol. Chem.* **1928**, *78*, 745-756
- [16] H. D. Dakin, R. West, *J. Biol. Chem.* **1928**, *78*, 91-104
- [17] P. A. Levene, R. E. Steiger, *J. Biol. Chem.* **1928**, *79*, 95-103
- [18] G. L. Buchanan, *Chem. Soc. Rev.* **1988**, *17*, 91-109; *Chem. Soc. Rev.*
- [19] R. B. Woodward, M. P. Cava, W. D. Ollis, A. Hunger, H. U. Daeniker, K. Schenker, *Tetrahedron* **1963**, *19*, 247-288
- [20] Z. H. Israili, E. E. Smismán, *J. Chem. Eng. Data.* **1977**, *22*, 357-359
- [21] E. E. Smismán, J. A. Weis, *J. Med. Chem.* **1971**, *14*, 945-947
- [22] L. Dalla Vecchia, R. O. M. A. de Souza, L. S. de Mariz e Miranda, *Tetrahedron* **2018**, *74*, 4359-4371
- [23] P. T. Anastas, J. C. Warner, *Green Chemistry: Theory and Practice*, Oxford University Press, Oxford, **1998**.
- [24] J. Lepschy, G. Höfle, L. Wilschowitz, W. Steglich, *Justus Liebigs Ann. Chem.* **1974**, *1974*, 1753-1762
- [25] W. Steglich, G. Höfle, *Angew. Chem. Int. Ed.* **1969**, *8*, 981-981; *Angew. Chem.* **1969**, *81*, 1001-1001.
- [26] R. W. Fischer, M. Misun, *Org. Process. Res. Dev.* **2001**, *5*, 581-586
- [27] S. I. Zav'yalov, T. K. Budkova, *Bull. Acad. Sci. USSR, Div. Chem. Sci. (Engl. Transl.)* **1977**, *26*, 1530-1531
- [28] J. A. King, F. H. McMillan, *J. Am. Chem. Soc.* **1952**, *74*, 2859-2864
- [29] A. Morere, C. Menut, Y. Z. Gunata, A. Agrebi, (Centre National de la Recherche Scientifique), WO2010/149744, **2012**
- [30] E. P. Woo, M. J. Mullins, (Dow Chemical Co.), US4943640A, **1990**
- [31] H. J. Scholl, (Bayer AG), US4665178, **1987**
- [32] H. J. Scholl, (Bayer AG), DE3425814A1, **1986**
- [33] H. J. Scholl, (Bayer AG), DE3427400A1, **1986**
- [34] H. J. Scholl, (Bayer AG), DE3429962A1, **1986**
- [35] H. J. Scholl, J. Pedain, (Bayer AG), EP302338A1, **1989**
- [36] F. E. Lehmann, A. Bretscher, H. Kühne, E. Sorkin, M. Erne, H. Erlenmeyer, *Helv. Chim. Acta* **1950**, *33*, 1217-1226
- [37] T. N. Ghosh, S. Dutta, *J. Indian Chem. Soc.* **1956**, *33*, 296-298
- [38] R. W. Johnson, R. J. Matison, J. W. Sowell Sr., *J. Heterocycl. Chem.* **1977**, *14*, 383-385
- [39] R. C. Wende, A. Seitz, D. Niedek, S. M. M. Schuler, C. Hofmann, J. Becker, P. R. Schreiner, *Angew. Chem. Int. Ed.* **2016**, *55*, 2719-2723; *Angew. Chem.* **2016**, *128*, 2769-2773.

- [40] R. E. Boyd, J. B. Press, C. R. Rasmussen, R. B. Raffa, E. E. Codd, C. D. Connelly, D. J. Bennett, A. L. Kirifides, J. F. Gardocki, B. Reynolds, J. T. Hortenstein, A. B. Reitz, *J. Med. Chem.* **1999**, *42*, 5064-5071
- [41] Z. Lin, M. D. Smith, G. P. Concepcion, M. G. Haygood, B. M. Olivera, A. Light, E. W. Schmidt, *J. Nat. Prod.* **2017**, *80*, 2360-2370
- [42] R. J. Taylor, *Biochem. Pharmacol.* **1978**, *27*, 2653-2654
- [43] R. V. Heinzelman, W. C. Anthony, D. A. Lyttle, J. Szmuszkovicz, *J. Org. Chem.* **1960**, *25*, 1548-1558
- [44] N. Engel, W. Steglich, *Justus Liebigs Ann. Chem.* **1978**, 1916-1927
- [45] R. Kikumoto, K. Okubo, (Mitsubishi Chemical Industries), JP52083609A, **1977**
- [46] P. Berton, S. P. Kelley, H. Wang, R. D. Rogers, *J. Mol. Liq.* **2018**, *269*, 126-131
- [47] T. Ohta, S. Suzuki, M. Todo, T. Kurechi, *Chem. Pharm. Bull.* **1981**, *29*, 1767-1771
- [48] B. Franck, H. Stratmann, *Heterocycles* **1981**, *15*, 919-923
- [49] A. R. Butler, S. George, *Tetrahedron* **1992**, *48*, 7879-7886; *Tetrahedron*.
- [50] M. Novo, G. Hüttmann, H. Diddens, *J. Photochem. Photobiol. B.* **1996**, *34*, 143-148
- [51] G. A. Hunter, E. Rivera, G. C. Ferreira, *Arch. Biochem. Biophys.* **2005**, *437*, 128-137
- [52] T. Suzuki, N. Yasuhara, T. Ueda, M. Inukai, M. Mio, *Chem. Pharm. Bull.* **2015**, *63*, 126-129
- [53] M. Singh, K. N. Singh, S. Dwivedi, R. A. Misra, *Synthesis* **1991**, *1991*, 291-293
- [54] R. A. F. Bullerwell, A. Lawson, H. V. Morley, *Journal of the Chemical Society (Resumed)* **1954**, 3283-3287
- [55] G. J. Durant, J. C. Emmett, C. R. Ganellin, P. D. Miles, M. E. Parsons, H. D. Prain, G. R. White, *J. Med. Chem.* **1977**, *20*, 901-906

Appendix

LC-MS data for pyrazine formation cross-over experiment

To prove formaldehyde formation during pyrazine auto-oxidation a cross-over experiment was run using both DALA as well as hydrochloride **3g**.



Procedure for the cross-over experiment

Four parallel reactions were setup A: DALA control, B: DALA formaldehyde, C: **3g** control, D: **3g** formaldehyde. Snapcap vials (5 mL) with magnetic stirrers were loaded with 0.597 mmol of hydrochloride salt (100-110 mg) which was dissolved in 3 mL of methanol. Upon complete dissolution, TEA (83 μ L, 0.597 mmol, 1 equiv.) was added to all reactions, immediately followed by addition of a formaldehyde solution in water to reactions B and D (44 μ L, 37 wt%, 0.597 mmol, 1 equiv.). The reaction were sampled periodically by diluting 50 μ L of the reaction mixture in 1 mL of methanol. To these samples was added 50 μ L of acetic acid to quench the reaction and 100 μ L of DMSO to ensure full dissolution of the reaction mixture. Only the last time point after stirring overnight (19h) was found relevant. For reaction B the product between DALA and formaldehyde was isolated after a preparative TLC in 100% EtOAc.

The reactions were analyzed using the standard LC-MS protocol but with a twice as long gradient to ensure resolution in the reaction with DALA. PDA data was analysed at 250 – 290 nm since the pyrazine core was found to absorb best at around 270 nm.

Liquid Chromatography – Mass Spectrometry (LC-MS) analysis was performed on a Shimadzu Nexera 2 UHPLC system equipped with a Shimadzu LC-30AD pump, a SPD-M30A photodiode array detector and LCMS-2020 single quadrupole detector. The system was run on MilliQ water and LC-MS grade acetonitrile both modified with 0.1% formic acid. A Waters XSelect CSH C18 column (3.0 mm x 75 mm with a particle size of 3.5 μ m) was used operating at 30 $^{\circ}$ C. The method was setup with a gradient of 5% acetonitrile in water for 2 min, an increase to 95% acetonitrile over 12 min, 1 min at 95% followed by flushing back to 5% acetonitrile.

LC-MS results for cross-over reaction

Reaction A

Reaction with DALA and TEA.

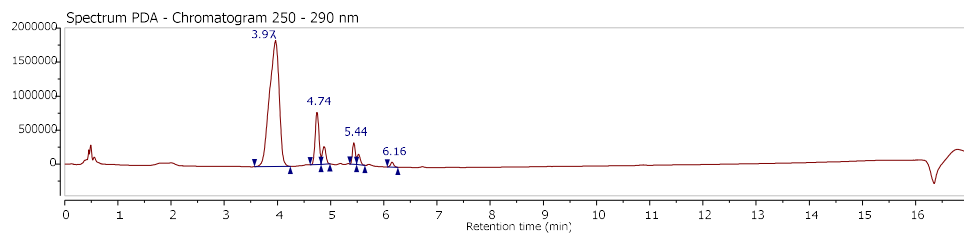


Figure A1: Cross-over reaction A PDA trace (250-290 nm). Clearly showing two peaks around 4.75 min, indicating multiple compounds.

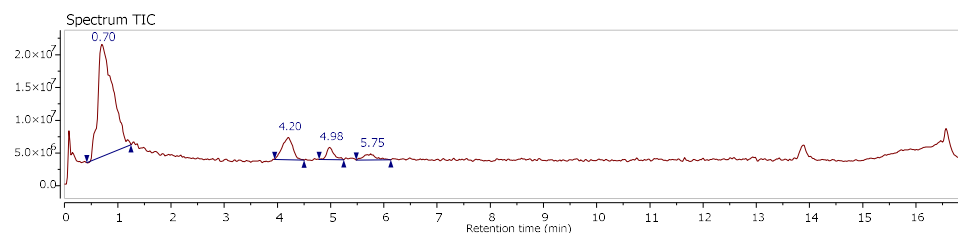


Figure A2: Cross-over reaction A Total Ion Count trace.

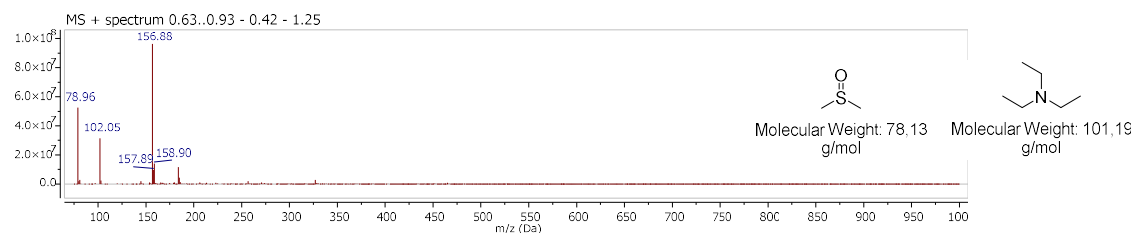


Figure A3: Reaction A MS at 0.70 min; contains TEA and DMSO.

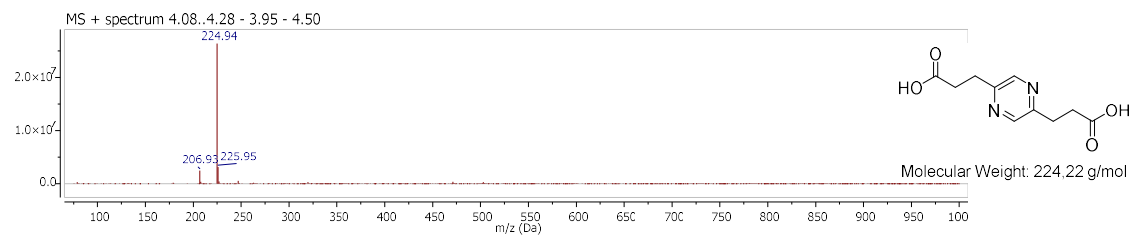


Figure A4: Reaction A MS at 4.20 min; mass of the desired pyrazine.

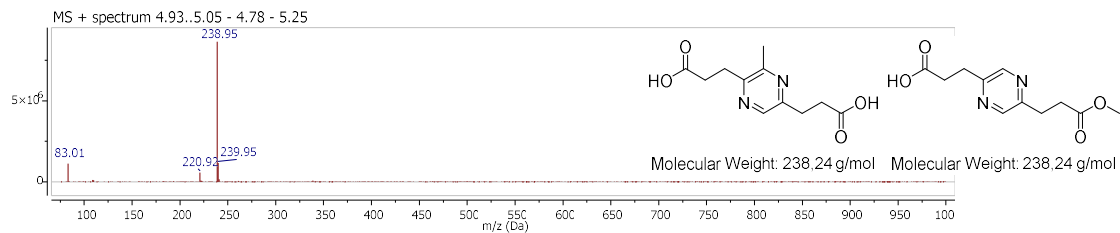


Figure A5: Reaction A MS at 4.98 min; mass of methyl ester or methyl pyrazine. The ions corresponding to the peak at 4.75 are not resolved but no other ion then 239 m/z is found in significant amounts.

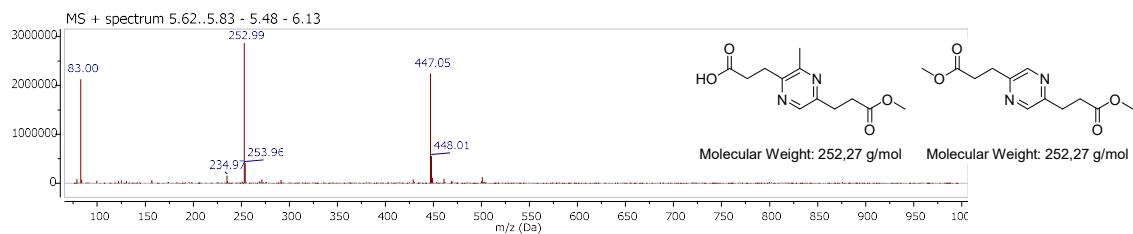


Figure A6: Reaction A MS at 5.75 min; mass of dimethyl ester or mono ester methyl pyrazine and a dimer.

Reaction B

Reaction with DALA, formaldehyde and TEA.

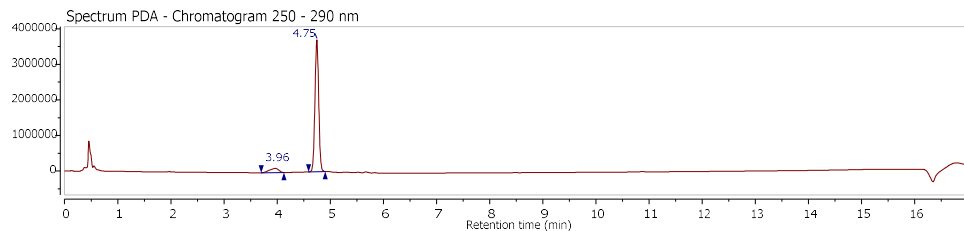


Figure A7: Cross-over reaction B PDA trace (250-290 nm). Clearly showing only one peak around 4.75 min.

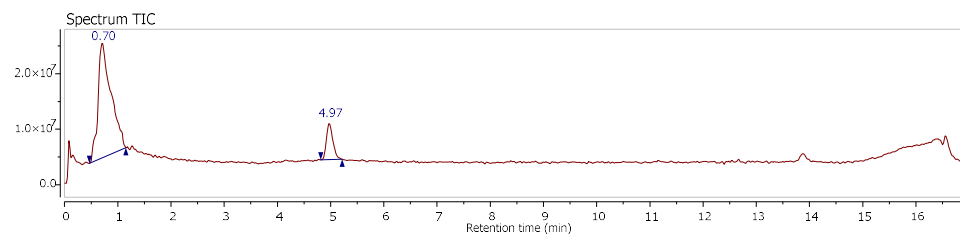


Figure A8: Cross-over reaction B Total Ion Count trace.

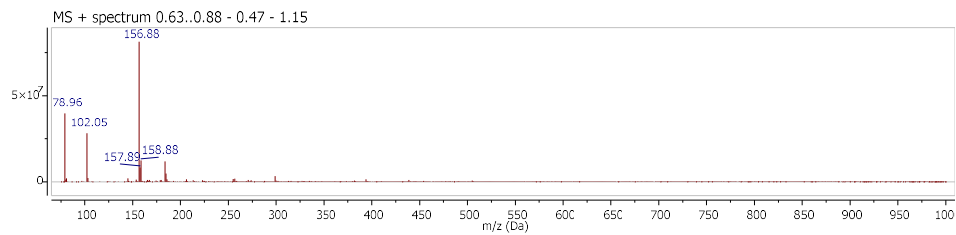


Figure A9: Reaction B MS at 0.70 min; contains TEA and DMSO.

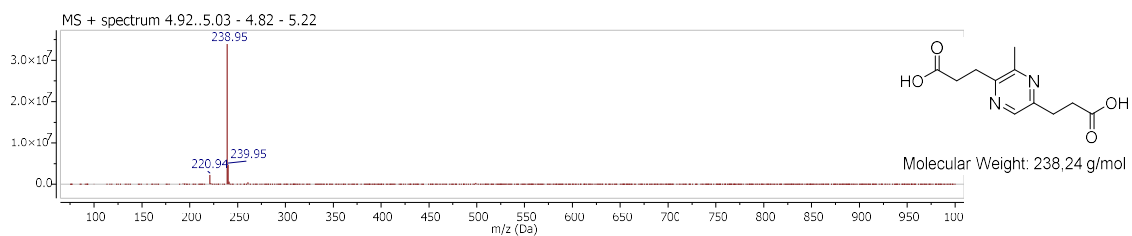
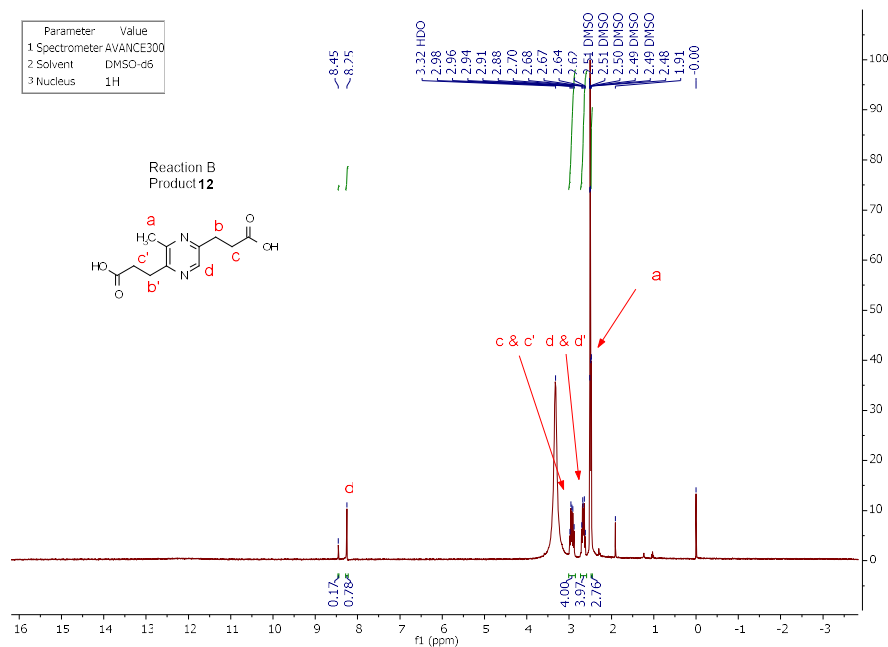


Figure A10: Reaction B MS at 4.97 min; mass of methyl pyrazine.

Figure A11: ¹H NMR of DALA-formaldehyde product 12.

Reaction C

Reaction with **3g** and TEA.

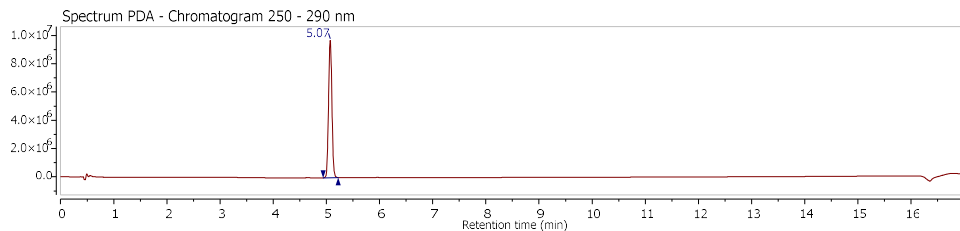


Figure A12: Cross-over reaction C PDA trace (250-290 nm).

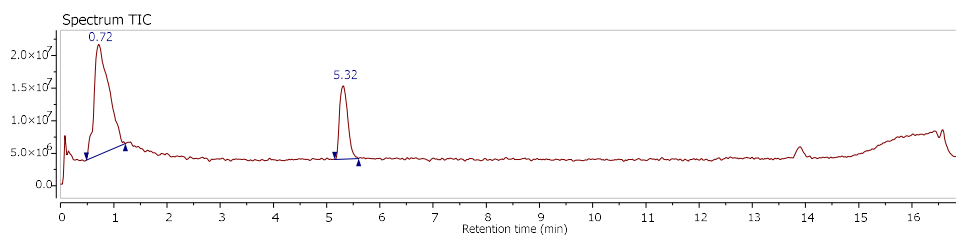


Figure A13: Cross-over reaction C Total Ion Count trace.

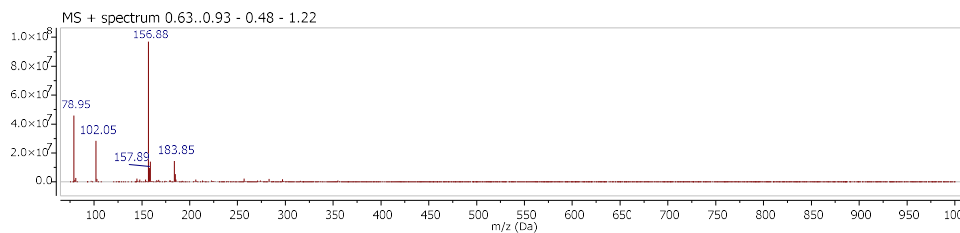


Figure A14: Reaction C MS at 0.72 min; contains TEA and DMSO.

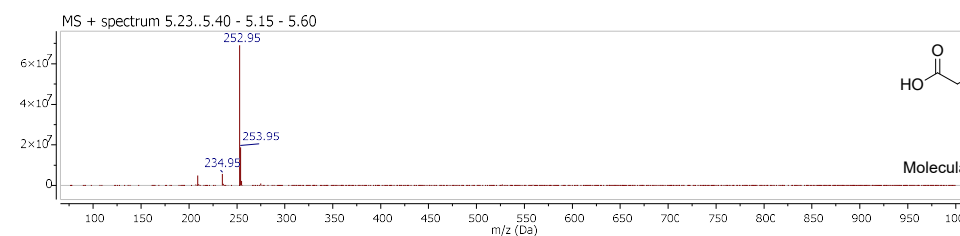
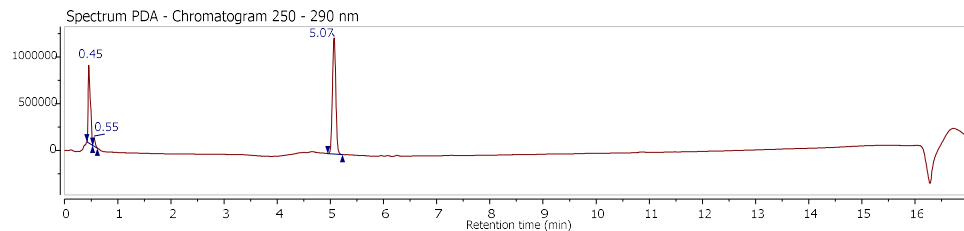
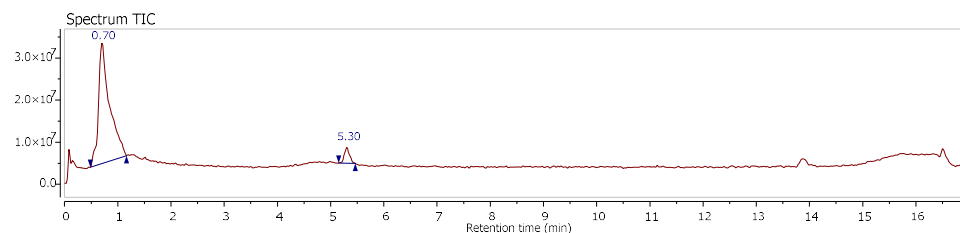
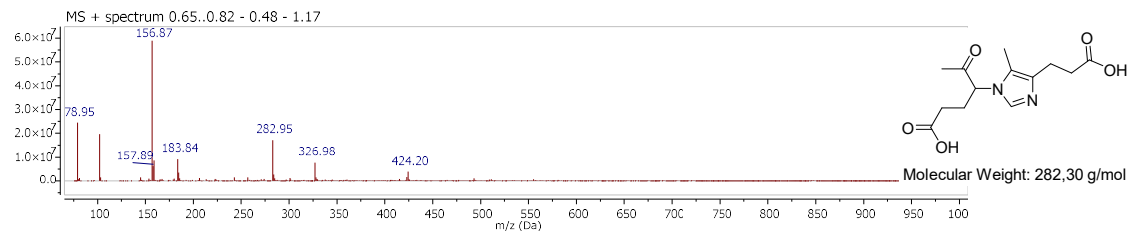
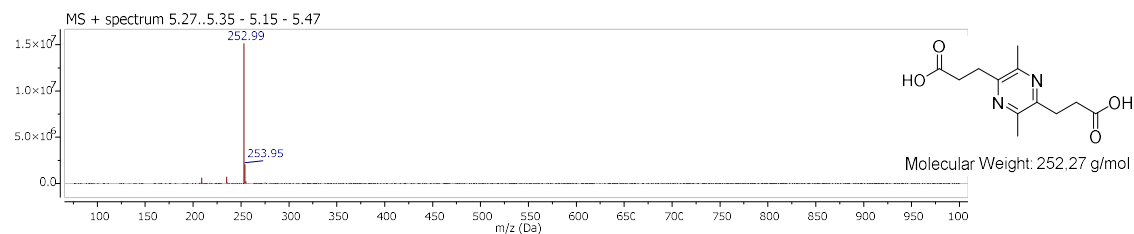


Figure A15: Reaction B MS at 5.32 min; contains the desired dimethylpyrazine

Reaction DReaction with **3g**, formaldehyde and TEA.**Figure A16: Cross-over reaction D PDA trace (250-290 nm); UV active injection peak when compared to reaction C.****Figure A17: Cross-over reaction D Total Ion Count trace.****Figure A18: Reaction D MS at 0.70 min; containing TEA, DMSO and possibly pyrrole.****Figure A19: Reaction D MS at 5.30 min; contains the desired dimethylpyrazine.**

*Experimental details & compound analysis*N-acetyl-5-acetylpyrrolidin-2-one (2g)

m.p. 71-72 °C (lit. 68-69)^[28]; ¹H NMR (300 MHz, CDCl₃) δ (ppm) = 4.87 (dd, *J*=9.7, 2.9 Hz, 1H), 2.80 – 2.54 (m, 2H), 2.52 (s, 3H), 2.29 (s, 3H), 2.39 – 2.14 (m, 1H), 2.01 – 1.84 (m, 1H); ¹³C NMR (75 MHz, CDCl₃) δ (ppm) = 204.4, 174.5, 171.0, 63.1, 31.7, 26.9, 24.5, 19.8; IR (neat) $\tilde{\nu}$ = 2970 (w), 1734 (vs), 1714 (s), 1691 (vs), 1367 (vs), 1281 (vs), 1174 (vs), 1030 (m), 964 (m), 854 (m) cm⁻¹; elemental analysis calcd (%) for C₈H₁₁NO₃: C 56.80, H 6.55, N 8.28; found: C 56.50, H 6.31, N 8.13.

Work-up procedure for acetamido-ketone 2h

The crude of the reaction with lysine (9.99 g, 68.4 mmol) was quenched by addition of 5 mL of water and concentrated *in vacuo* (10 mBar, 85 °C) followed by trituration by stirring in EtOAc (120 mL). The resulting solid was isolated by filtration, washed with EtOAc (3x 40 mL) and dried *in vacuo* (40 °C). The desired acetamido-ketone **2h** (12.06 g, 52.8 mmol, 77%) was isolated as an off-white solid.

N-N'-diacetyl-3,7-diaminoheptan-2-one (2h)

mp 112-114 °C (lit. 111-113 °C)^[31]; ¹H NMR (300 MHz, CDCl₃) δ (ppm) = 6.56 (d, *J*=7.2 Hz, 1H), 5.94 (s, 1H), 4.58 (td, *J*=7.8, 4.0 Hz, 1H), 3.35 – 3.11 (m, *J*=6.9 Hz, 2H), 2.22 (s, 3H), 2.04 (s, 3H), 1.98 (s, 3H), 1.94 – 1.80 (m, 1H), 1.68 – 1.44 (m, 3H), 1.44 – 1.22 (m, 2H); ¹³C NMR (75 MHz, CDCl₃) δ (ppm) = 206.9, 170.5, 170.3, 58.4, 38.7, 30.6, 28.9, 27.1, 23.2, 23.1, 22.0; IR (neat) $\tilde{\nu}$ = 3296 (s), 3069 (w), 2950 (w), 1707 (vs), 1636 (vs), 1541 (vs), 1370 (s), 1289 (s), 701 (s), 610 (s) cm⁻¹; elemental analysis calcd (%) for C₁₁H₂₀N₂O₃: C 57.87, H 8.83, N 12.27; found: C 57.61, H 8.69, N 12.03

Work-up procedure for acetamido-ketone 2i (adapted from Wende et al.)^[39]

The crude of the reaction with methionine (9.99 g, 67.0 mmol) was quenched by addition of 5 mL of water and concentrated *in vacuo* (10 mBar, 85 °C). The crude was diluted with satd. NaHCO₃ (300 mL) and extracted using CHCl₃ (4x 100 mL), the combined organic layers were washed with 1M HCl (3x 100 mL) and brine (1x 100 mL). The organic phase was dried over Na₂SO₄, concentrated and purified by chromatography on silica using 100% EtOAc as eluent (*R*_f=0.25). The desired acetamido-ketone **2i** (9.26 g, 48.9 mmol, 73%) was isolated as a yellow oil.

3-acetamido-5-(methylthio)pentan-2-one (2i)

¹H NMR (300 MHz, CDCl₃) δ (ppm) = 6.34 (d, *J*=7.3 Hz, 1H), 4.76 (td, *J*=7.3, 4.4 Hz, 1H), 2.62 – 2.39 (m, 2H), 2.27 (s, 3H), 2.34 – 2.17 (m, 1H), 2.12 (s, 3H), 2.05 (s, 3H), 1.96 – 1.78 (m, 1H); ¹³C NMR (75 MHz, CDCl₃) δ (ppm) = 206.4, 170.2, 58.1, 30.6, 30.0, 27.2, 23.0, 15.6; IR (neat) $\tilde{\nu}$ = 3286 (br), 2917 (m), 1718 (s), 1650 (vs), 1535 (s), 1432 (m), 1372 (s), 1289 (m), 1043 (m), 604 (m) cm⁻¹; elemental analysis calcd (%) for C₈H₁₅NO₂S: C 50.76, H 7.99, N 7.40; found: C 49.78, H 8.13, N 7.58

Work-up procedure for acetamido-ketone 2j

The crude of the reaction with histidine (10.01 g, 64.5 mmol) was quenched by addition of 5 mL of water followed by concentration *in vacuo* (10 mBar, 85 °C). The resulting crude was continued to dihydrochloride salt **3j** without further purification.

Work-up procedure for acetamido-ketone 2k (adapted from Wende et al.)^[39]

The crude of the reaction with tyrosine (11.75 g, 64.8 mmol) was quenched by addition of 5 mL of water and concentrated *in vacuo* (10 mBar, 85 °C). The material was subsequently trituated by stirring in Et₂O (30 mL). The resulting solid was isolated by filtration, washed with Et₂O (3x 10 mL) and dried *in vacuo* (40 °C). The desired acetamido ketone **2k** (14.47 g, 54.9 mmol, 84%) was isolated as an off-white solid.

3-acetamido-4-(4-acetoxyphenyl)butan-2-one (2k)

mp 129-130 °C (lit. 123-123.5 °C)^[39]; ¹H NMR (300 MHz, CDCl₃) δ (ppm) = 7.19 – 7.10 (m, 2H), 7.09 – 7.00 (m, 2H), 6.09 (d, *J*=7.2 Hz, 1H), 4.88 (q, *J*=6.8 Hz, 1H), 3.23 – 3.00 (m, 2H), 2.31 (s, 3H), 2.19 (s, 3H), 2.01 (s, 3H); ¹³C NMR (75 MHz, CDCl₃) δ (ppm) = 206.1, 169.7, 169.4, 149.8, 133.4, 130.2, 121.8, 59.4, 36.4, 28.1, 23.1, 21.1; IR (neat) $\tilde{\nu}$ = 3373 (s), 1746 (s), 1708 (s), 1668 (vs), 1525 (s), 1373 (m), 1278 (m), 1190 (vs), 1013 (m), 911 (s) cm⁻¹; elemental analysis calcd (%) for C₁₄H₁₇NO₄: C 63.87, H 6.51, N 5.32; found: C 63.61, H 6.32, N 5.22

Work-up procedure for acetamido-ketone 2l (adapted from Engel et al.)^[44]

The crude of the reaction with tryptophan (10.33 g, 50.5 mmol) was quenched by addition of 30 mL of methanol while cooling on ice. The quenched crude was poured into 650 mL of ice water followed by addition of potassium hydroxide (24 g, 0.43 mol) and left to stir overnight. The resulting brown suspension was filtered, washed with water and dried *in vacuo* (40 °C). The desired acetamido ketone **2l** (9.67 g, 39.6 mmol, 78 %) was isolated as a brownish solid. The material could be recrystallized from methanol/water to give light brown needles.

3-acetylamino-4-(3-indolyl)butan-2-one (2l)

mp 138-140 °C (lit. 134-135 °C)^[44]; ¹H NMR (300 MHz, CDCl₃) δ (ppm) = 8.36 (s, 1H), 7.59 (d, *J*=7.8 Hz, 1H), 7.35 (d, *J*=7.9 Hz, 1H), 7.16 (dt, *J*=22.4, 7.3 Hz, 2H), 6.96 (d, *J*=2.4 Hz, 1H), 6.24 (d, *J*=7.3 Hz, 1H), 4.96 (q, *J*=6.4 Hz, 1H), 3.39 – 3.17 (m, 2H), 2.15 (s, 3H), 1.95 (s, 3H); ¹³C NMR (75 MHz, CDCl₃) δ (ppm) = 207.0, 170.0, 136.1, 127.6, 122.6, 122.3, 119.8, 118.6, 111.4, 110.0, 59.2, 28.0, 27.0, 23.2; IR (neat) $\tilde{\nu}$ = 3345 (s), 3246 (br), 1704 (vs), 1654 (vs), 1539 (vs), 1356 (s), 1221 (m), 1104 (m), 739 (vs), 657 (m) cm⁻¹; elemental analysis calcd (%) for C₁₄H₁₆N₂O₂: C 68.83, H 6.60, N 11.47; found: C 68.43, H 6.41, N 11.31

Hydrochloride salt 3g

Acetamido ketone **2g** (8.00 g, 47.3 mmol) was hydrolyzed (6M HCl, 24 mL, 144 mmol). The resulting crude was concentrated to dryness. The obtained orange solid crushed, triturated in acetone (10 mL) isolated by filtration and washed with IPA (3x 5 mL) resulting in hydrochloride salt **3g** (7.14 g, 39.3 mmol, 82% yield) as colorless cubic crystals.

4-amino-5-oxohexanoic acid hydrochloride (3g)

mp 166-168 °C (decomp.)(lit. 162 °C)^[54]; ¹H NMR (300 MHz, DMSO-d₆) δ (ppm) = 12.36 (s, 1H), 8.45 (s, 3H), 4.13 (t, *J*=6 Hz, 1H), 2.57 – 2.27 (m, 2H), 2.26 (s, 3H), 2.24 – 2.06 (m, 1H), 2.03 – 1.85 (m, 1H); ¹³C NMR (75 MHz, DMSO-d₆) δ (ppm) = 204.6, 173.8, 58.0, 29.4, 27.3, 24.6; IR (ATR) $\tilde{\nu}$ = 2976 (br), 2479 (w), 1719 (s), 1606 (m), 1475 (m), 1409 (m), 1256 (m), 1172 (s), 1084 (s), 812 (m) cm⁻¹; elemental analysis calcd (%) for C₆H₁₂ClNO₃: C 39.68, H 6.66, N 7.71; found: C 39.65, H 6.77, N 7.78

Dihydrochloride salt 3h

Acetamido ketone **2h** (12.00 g, 52.6 mmol) was hydrolyzed (6M HCl, 27 mL, 162 mmol). The resulting crude was concentrated to dryness. The obtained brown solid was triturated in acetone (10 mL), isolated by filtration and washed with acetone (3x 10 mL) resulting in dihydrochloride salt **3h** (9.59 g, 44.2 mmol, 84% yield) as a grey solid.

3,7-diaminoheptan-2-one dihydrochloride (3h)

mp 166-170 °C (decomp.)(lit. 160-166 °C)^[55]; ¹H NMR (300 MHz, DMSO-d₆) δ (ppm) = 8.38 (s, 3H), 8.10 (s, 3H), 4.11 (s, 1H), 2.76 (s, 2H), 2.26 (s, 3H), 1.99 – 1.85 (m, 1H), 1.85 – 1.70 (m, 1H), 1.67 – 1.53 (m, 2H), 1.53 – 1.28 (m, 2H); ¹³C NMR (75 MHz, DMSO-d₆) δ (ppm) = 204.8, 58.5, 38.5, 28.5, 27.4, 26.7, 21.4; IR (ATR) $\tilde{\nu}$ = 2869 (br), 1998 (br), 1714 (vs), 1586 (m), 1527 (s), 1370 (m), 1207 (m), 1148 (m), 949 (w), 739 (w) cm⁻¹; elemental analysis calcd (%) for C₇H₁₈Cl₂N₂O: C 38.72, H 8.36, N 12.90; found: C 37.90, H 8.26, N 13.05

Hydrochloride salt **3i**

Acetamido ketone **2i** (8.00 g, 42.3 mmol) was hydrolyzed (6M HCl, 21 mL, 127 mmol). The resulting crude was concentrated to dryness. The obtained brown solid was triturated in acetone (20 mL), isolated by filtration and washed with acetone (2x 5 mL) resulting in hydrochloride salt **3i** (5.41 g, 29.4 mmol, 69% yield) as an off-white solid.

3-amino-5-(methylthio)pentan-2-one hydrochloride (**3i**)

mp 141-143 °C (decomp.)(lit. 133-135 °C)^[36]; ¹H NMR (300 MHz, DMSO-d₆) δ (ppm) = 8.53 (s, 3H), 4.16 (s, 1H), 2.70 – 2.53 (m, 2H), 2.27 (s, 3H), 2.24 – 2.11 (m, 1H), 2.08 (s, 3H), 2.11 – 1.94 (m, 1H); ¹³C NMR (75 MHz, DMSO-d₆) δ (ppm) = 204.4, 58.0, 29.0, 28.8, 27.3, 14.8; IR (ATR) $\tilde{\nu}$ = 2980 (br), 2879 (br), 1980 (w), 1718 (vs), 1473 (vs), 1362 (m), 1174 (s), 1146 (m), 1019 (m), 779 (w) cm⁻¹; elemental analysis calcd (%) for C₆H₁₄ClNOS: C 39.23, H 7.68, N 7.63; found: C 39.57, H 7.83, N 7.65

Dihydrochloride salt **3j**

The crude of the Dakin-West reaction with histidine (**1j**) (10.01 g, 64.5 mmol) was hydrolyzed (6M HCl, 32 mL, 194 mmol). The resulting crude was concentrated to dryness. The obtained brown solid was triturated in IPA (60 mL), isolated by filtration and washed with IPA (2x 30 mL) resulting in dihydrochloride salt **3j** (11.16 g, 49.3 mmol, 76%) as a yellow solid.

4-(4-imidazolyl)-3-amino-butan-2-one dihydrochloride (**3j**)

mp 207-208 °C (decomp.)(recryst. MeOH/IPA)(lit. 212-215 °C)^[21]; ¹H NMR (300 MHz, DMSO-d₆) δ (ppm) = 14.74 (s, 2H), 9.09 (s, 1H), 8.57 (s, 3H), 7.50 (s, 1H), 4.56 (dd, *J*=8.7, 4.8 Hz, 1H), 3.47 (dd, *J*=15.5, 4.8 Hz, 1H), 3.17 (dd, *J*=15.5, 9.1 Hz, 1H), 2.35 (s, 3H); ¹³C NMR (75 MHz, DMSO-d₆) δ (ppm) = 203.4, 127.1, 118.7, 57.9, 27.6, 24.5; IR (ATR) $\tilde{\nu}$ = 3319 (br), 2859 (br), 2597 (br), 1723 (vs), 1521 (s), 1419 (s), 1068 (vs), 810 (vs), 719 (s), 624 (s) cm⁻¹; elemental analysis calcd (%) for C₇H₁₃Cl₂N₃O: C 37.18, H 5.80, N 18.59; found: C 37.20, H 5.88, N 18.79

Hydrochloride salt **3k**

Acetamido ketone **2k** (11.50 g, 43.7 mmol) was hydrolyzed (6M HCl, 22 mL, 132 mmol). The resulting crude was concentrated to dryness. The obtained black solid was triturated in acetone (20 mL), isolated by filtration and washed with acetone (4x 10 mL) resulting in hydrochloride salt **3k** (8.12 g, 37.7 mmol, 86% yield) as an off-white solid.

3-amino-4-(4-hydroxyphenyl)butan-2-one hydrochloride (**3k**)

mp 170-172 °C (decomp.)(lit. 165-166 °C)^[17]; ¹H NMR (300 MHz, DMSO-d₆) δ (ppm) = 9.56 (s, 1H), 8.40 (s, 3H), 7.09 (d, *J*=8.3 Hz, 2H), 6.75 (d, *J*=8.2 Hz, 2H), 4.29 (d, *J*=7.9 Hz, 1H), 3.14 – 2.91 (m, 2H), 2.12 (s, 3H); ¹³C NMR (75 MHz, DMSO-d₆) δ (ppm) = 204.7, 157.2, 130.9, 125.1, 116.0, 59.9, 34.7, 28.4; IR (ATR) $\tilde{\nu}$ = 3145 (br), 2859 (br), 1725 (vs), 1614 (m), 1513 (vs), 1495 (m), 1362 (s), 1245 (vs), 836 (m), 687 (w) cm⁻¹; elemental analysis calcd (%) for C₁₀H₁₄ClNO₂: C 55.69, H 6.54, N 6.49; found: C 55.73, H 6.81, N 6.

Chapter 2

Biobased (dimethyl)-pyrazine dipropionic acid based polyesters

Published as:

Martien A. Würdemann, Dr. Katrien V. Bernaerts, *ACS Sustainable Chemistry & Engineering*, 2020, 8, 12045-12052

Abstract

A set of twelve, first in class, biobased pyrazine containing polyesters was synthesized based on (dimethyl)-pyrazine dipropionic acid. These new diacid monomers were obtained from underutilized nitrogen-rich biomass. The polyester materials were synthesized via a two-step melt transesterification-polycondensation procedure in molecular weights between 12300-47500 g/mol and dispersities between 1,9 and 2,3. Six of the obtained polymers were amorphous and six were semi-crystalline. The thermal properties of the materials were studied; thermal degradation was found to take place at the monomer degradation temperature. The effect of methyl groups on the glass transition temperature was investigated and the materials were found to behave mostly as aliphatic polyesters in this regard. The melting points of the methyl substituted polyesters were found to be high and within the range of current high performance polyesters. These materials are thus a welcome addition to current biobased polyesters.

Introduction

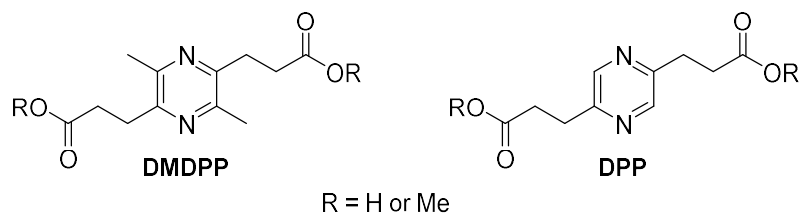
One of the most important classes of chemicals are the aromatic compounds. These compounds are currently being produced mostly from unsustainable fossil feedstocks. Research efforts into sustainable and “green” production processes for aromatic compounds are being undertaken, mainly due to higher awareness regarding the limits of fossil feedstocks and concerns about environmental impact. These efforts focus on the conversion of biomass streams into either drop-in replacements or into novel compounds. The biomass used in these efforts is predominantly lingo-cellulosic in origin, nitrogen-rich biomass such as proteins and amino acids receive far less attention.^[1]

Our research group recently developed a scalable synthesis for biobased pyrazine building blocks starting from nitrogen-rich biomass in the form of proteinogenic amino acids.^[2] Pyrazines hold a special place within the heterocyclic aromatic systems as one of the most benzene-like structures known, possessing a degree of aromaticity 89% of that of benzene. As opposed to benzene, pyrazines also possess two electron lone pairs which might be exploited as handles for added functionality. Since pyrazines are a class of compounds which have been sparsely reported as monomers, the study of pyrazine incorporation in polymers and its effects on chemical and material properties of these polymers is of significant interest. To the best of our knowledge, mentions in two patent families and four academic papers comprise the entire literature regarding pyrazine containing condensation polymers.^[3-10] As such, the incorporation of pyrazine monomers in polyesters has not been reported thoroughly or investigated systematically. Our recent work on the synthesis of biobased pyrazines, which provided access to two pyrazine diacids, combined with this lack of precedent, prompted investigation into the synthesis of pyrazine containing polyesters.

To investigate the incorporation of pyrazines in polyesters, we set out to determine an initial structure-thermal property relationship with the aim of providing a direction for the applications of these new aromatic building blocks. To systematically explore the effect of pyrazine incorporation in polyesters two different biobased pyrazine diacids were selected as monomers to synthesize a range of polyester homopolymers. The first diacid, dimethyl dipropionic acid pyrazine (DMDPP) can be obtained from glutamic acid via the Dakin-West reaction and has a biogenic atom content of 88 wt%. The second diacid, diproinic acid pyrazine (DPP), the unsubstituted analogue of DMDPP, is also available from biomass in the form of levulinic acid resulting in a biogenic atom content of 87 wt% (see **Figure 1**). Both starting materials for the synthesis of the monomers are naturally occurring molecules but can be produced

from sugars. In case of glutamic acid by fermentation and in case of levulinic acid by catalytic dehydration. Besides a chance to study the properties of pyrazines in polyesters, the selected diacids also provide an opportunity to study the effect of methyl substitution on aromatic rings in polyesters. This effect is underreported with only two studies investigating methyl substitution on terephthalic acid.^[11-12] We herein report our findings on the thermal properties of these two new biobased pyrazine diacids in polyesters and the effects of methyl substitution.

Diacids & diesters studied



Diols studied

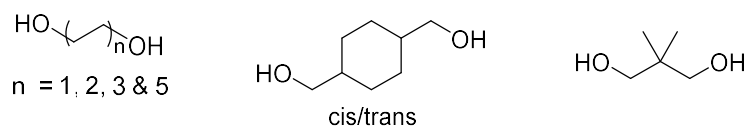


Figure 1: Dimethyl dipropionic acid pyrazine (DMDPP), dipropionic acid pyrazine (DPP) and the diols used as monomers in this study.

Experimental

Materials

Dimethyldipropionic acid pyrazine (DMDPP) and dipropionic acid pyrazine (DPP) were synthesized according to the procedure in Chapter 1.^[2] The dimethyl esters of these compounds were synthesized by Fischer esterification in methanol and used after work-up (see appendix). 1,4-Butanediol, 1,6-hexanediol, 1,10-decanediol, neopentylglycol and m-xylene were supplied by Sigma-Aldrich in >97% purity and used as received. Cyclohexanedimethanol was supplied as mixture of cis and trans isomers (30%/70%) and used as received. Ethyleneglycol was supplied by TCI in 99% purity and used as received. Tin(II) 2-ethylhexanoate was supplied by Sigma-Aldrich in 95% purity and used as received. Methanol, chloroform, diethylether and ethylacetate were supplied by Biosolve in at least analytical reagent grade purity and used as received. Deuterated chloroform (CDCl₃) was supplied by Cambridge isotopes and kept over 4Å molecular sieves obtained from Sigma-Aldrich.

Polymer synthesis

Small scale polymerization reactions were used for the synthesis of reported polyesters. The chosen scale was 1 gram of diester per reaction with the amount of diol varying depending on its boiling point (see **Table 1**). The syntheses were performed in a 20 mL cylindrical three-necked flask fitted with a nitrogen inlet, an overhead stirrer, and a vigreux connected to a distillation bridge. The flask was first loaded with diol and diester and heated to 130 °C forming a melt, to this step was added m-xylene (2 mL) to remove water by azeotropic drying. The synthesis was subsequently performed in a two-step procedure in the presence of 0.5 mol% tin(II) 2-ethylhexanoate (Sn(II)Oct₂) as catalyst. The first step consisted of a transesterification reaction at 160-180 °C until the methyl ester peak on ¹H-NMR was less than 5%. The second reaction step consisted of polycondensation *in vacuo* at 180-200 °C until the ratio between both monomers was within 1% of 1:1 on ¹H-NMR. If the ratio between the unreacted diol and the diester dropped lower than 1:1, more of the starting diol was added to the reaction mixture (see **Table 1**). A series of polyesters was synthesized under these conditions using the following diols; ethylene glycol (C₂), butanediol (C₄), hexanediol (C₆), decanediol (C₁₀), cyclohexanedimethanol (CHDM) and neopentyl glycol (Neo). For the reactions with DPP, the dimethyl ester (synthesis, see appendix) was subjected to the same polymerization conditions with the same diols as for DMDPP. All obtained polymers were analyzed as nascent polymer from the melt, except for those synthesized with ethylene glycol. These polymers were purified via dissolution in chloroform (3 mL) and subsequent precipitation in cold diethyl ether (60 mL or 75 mL, -20 °C). The precipitated polymer was dried *in vacuo* overnight (40 °C). A representative example of the procedure is presented below.

Example polymerization: DMDPP-C6 (see **Table 1**, entry 5)

A 20 mL cylindrical three-necked flask was loaded with Me₂DMDPP (991 mg, 3.54 mmol), 1,6-hexanediol (463 mg, 3.92 mmol) and 2 mL m-xylene. The resulting suspension was heated to 130 °C under open nitrogen flow. A clear melt soon formed and after 15 min an aliquot of a 1M Sn(II)Oct₂ solution in m-xylene (18 µL, 0.5 mol%, 18 µmol) was added to the reaction, the nitrogen flow was closed and the reaction heated to 160 °C. After 1.5h nitrogen flow over the reaction was opened allowing the removal of condensate. After 1h the reaction was heated to 180 °C, another hour later the reaction was sampled and analyzed by NMR. The methyl ester peak was still more than 5% and the reaction was heated for another 2 hours. Another sample indicated the methyl ester peak had dropped below 5%, the vigreux was removed from the setup and vacuum was applied (3*10⁻¹ mBar). The reaction was kept under vacuum and analyzed by NMR until the last sample showed the monomer ratio to be close to 1:1 (5h). The resulting melt was removed while hot and crystalized into a cream colored solid.

DMDPP-C6

^1H NMR (300 MHz, CDCl_3) δ (ppm) = 4.00 (t, J = 6.7 Hz, 4H), 2.96 (t, J = 7.3 Hz, 4H), 2.71 (t, J = 7.3 Hz, 4H), 2.41 (s, 6H), 1.63 – 1.48 (m, 4H), 1.36 – 1.24 (m, 4H); ^{13}C NMR (75 MHz, CDCl_3) δ (ppm) = 173.4, 149.4, 148.0, 64.4, 31.7, 28.5, 25.6, 20.9. IR (ATR) $\tilde{\nu}$ (cm^{-1}) = 2939, (w), 1730 (vs), 1420 (m), 1364 (m), 1297, (m) 1176 (s), 1132 (s), 970 (vs), 785 (m), 672 (w).

Characterization

Since the polymers showed no appreciable water uptake no special sample preparation was conducted and the polymers were analyzed as obtained from the melt.

Gel permeation chromatography (GPC) was conducted on a Shimadzu Prominence-i LC-2030 HPLC system fitted with a Shimadzu RID-20A detector. The measurements were run with isocratic elution of chloroform at 1 mL/min on a Shodex KF-805L column (10 mm by 300 mm, 10 μm pore size) operating at 40 $^\circ\text{C}$. Samples were prepared by making 1 mg/mL solutions in chloroform and filtered over a 0.2 μm PTFE filter. GPC was used to determine the molecular weight distribution of the obtained polymers as compared to polystyrene standards.

Nuclear magnetic resonance (NMR) was conducted on a Bruker AVANCE 300 MHz apparatus. Measurements were run in d-chloroform using 5-10 mg of polymer. The ^1H -NMR (300 MHz) spectra were recorded with 16 scans and the ^{13}C -NMR (75 MHz) APT spectra were recorded at 1024 scans. The obtained NMR data was used to determine the conversion of the end-groups and the degree of polymerization. This data was also used to determine the ratio of the constituents of the chains by comparing the normalized integrals of the monomeric units in the polymer chain.

Thermal stability of the polymers was determined by use of thermal gravimetric analysis (TGA) by heating 3 to 10 mg samples at 10 $^\circ\text{C}/\text{min}$ up to 700 $^\circ\text{C}$ under a nitrogen atmosphere on a TA instruments TGA 500 machine. The degradation temperature (T_d) was set as 5% weight loss.

Differential scanning calorimetry (DSC) thermograms were recorded on 2 to 7 mg samples in pierced lid pans on a Netzsch Polyma 14 machine at heating and cooling rates of 10 $^\circ\text{C}/\text{min}$ from -40 $^\circ\text{C}$ to 200 $^\circ\text{C}$ with 3 min isothermals at those temperatures. Two temperature cycles were measured with the melting (T_m) and crystallization temperatures (T_c) of the second cycle being reported. Glass transition temperatures (T_g) are reported as the inflection point of the first observed change in enthalpy in the second cycle.

Dynamic Mechanical Analysis (DMA) was conducted on an Anton Paar MCR 702 twin drive rheometer with plate-plate geometry. A 5 mm and 50 mm spindle with a 1 mm gap were used at a frequency of 10 rad/s while cooling from 30 $^\circ\text{C}$ above the melting point to -50 $^\circ\text{C}$ for semi-crystalline polymers and from 80 $^\circ\text{C}$ to -50 $^\circ\text{C}$ for amorphous polymers at 5 $^\circ\text{C}/\text{min}$. The T_g was determined as the temperature at the peak maximum of $\tan \delta$.

Results and discussion

Polymer synthesis

Since a melt polycondensation generally is a green reaction with a high atom efficiency, the possibility to polymerize DMDPP was initially tested in such a reaction using 1,6-hexanediol. Under such conditions however, a stoichiometric amount of diol was found to be too small for dissolution of the diacid upon melting of the diol. Since DMDPP does not show a melting point and degrades at 211-213 °C^[13-14] further heating of the reaction until the diacid would melt was not a viable synthesis approach. This limitation was circumvented by synthesis of the dimethyl ester of DMDPP which has a stable melt at 96-98 °C, allowing polymerization via transesterification. This approach was deemed most in line with the principles of green chemistry compared to other options such as solution polymerization. Especially since a relatively atom efficient and green Fischer esterification, of which the methanol can be recycled, was developed (see appendix) for the formation of the dimethyl esters of both diacids (Me₂DMDPP and Me₂DPP). These diesters allowed successful polymerization via transesterification. All polymers so obtained could be analyzed directly from the melt except for those based on ethylene glycol (**Table 1**, entries 1 and 2). The amount of remaining ethylene glycol in the melt of these polymers acted as a plasticizer and was therefore removed by dissolving the melt in chloroform and precipitation in cold diethyl ether.

A series of polyesters was synthesized under these conditions using the following diols; ethylene glycol (C2), 1,4-butanediol (C4), 1,6-hexanediol (C6), 1,10-decanediol (C10), cyclohexanedimethanol (CHDM) and neopentyl glycol (Neo). The applied protocol resulted polyesters with number average molecular weights (M_n) of between 13700 and 34700 g/mol for DMDPP and between 12300 and 47500 g/mol for DPP as determined by chloroform GPC against polystyrene standards (see **Table 1**). The dispersity (\bar{D}) of the obtained polymers was between 1.9 and 2.3, the absence of a high molecular weight shoulder indicated polycondensation had occurred without significant crosslinking or side-reactions both of which could occur during thermal degradation as discussed in the next section. These results show that the effect of the methyl groups on the pyrazine ring between both diacids has a negligible effect on the polymerization behavior of the monomers. NMR analysis confirmed that high conversion was reached and that the polymerization took place without significant side-reactions (see **Figure A1-A12**). End-group analysis in NMR suggested degrees of polymerization (DP) of between 18 and 62 indicating lower M_n than obtained by GPC (see **Table A1**). Using the DP the NMR M_n was calculated with the molecular weights of the repeating units and end-groups (see **Table 1** and **Table A1** for the calculations).

The polymers were considered of sufficient molecular weight to have stable thermal properties and thus suitable for fair comparison.

Table 1: Overview of results for the obtained polymers.

#	Diacid	Diol ^[a]	M_n (GPC) (g/mol)	\bar{D}	T_d (°C) [5 wt%]	T_m (°C)	T_c (°C)	T_g (°C) DSC	T_g (°C) DMA ^[b]	NMR ratio ^[c] (mol %)	M_n (NMR) ^[d] (g/mol)	Feed diol (equiv)
1	DMDPP	C2	13700	2,2	331	amorp.	n.a.	14	20	49,6/50,4	6400	3
2	DPP	C2	12300	2,1	318	amorp.	n.a.	-5	-1	50,3/49,7	4800	3
3	DMDPP	C4	26700	2,1	287	165	125	n.a.	18	49,7/50,3	14700	1,2
4	DPP	C4	34200	2,0	308	85	34	-22	-20	49,6/50,4	13800	1,2
5	DMDPP	C6	26500	1,9	324	143	107	n.a.	4	49,6/50,4	15700	1,1
6	DPP	C6	32000	2,1	321	64	5	-33	-26	49,8/50,2	15600	1,1 ^[e]
7	DMDPP	C10	34700	1,9	320	114	74	n.a.	-7	49,7/50,3	18800	1
8	DPP	C10	47500	2,2	342	70	30	n.a.	-30	49,6/50,4	22900	1
9	DMDPP	CHDM	25800	2,0	333	amorp.	n.a.	25	33	48,8/51,2	12800	1,05
10	DPP	CHDM	29500	2,3	329	amorp.	n.a.	8	13	50,1/49,9	12500	1,05
11	DMDPP	Neo	31800	1,9	327	amorp.	n.a.	13	18	50,0/50,0	14300	1,1 ^[e]
12	DPP	Neo	29000	2,1	323	amorp.	n.a.	-6	-2	49,7/50,3	14500	1,2

[a] C2 = ethylene glycol, C4 = 1,4-butanediol, C6 = 1,6-hexanediol, C10 = 1,10-decanediol, CHDM = cyclohexanedimethanol, Neo = neopentylglycol

[b] Determined by DMA at the loss factor peak, $\tan \delta$

[c] Diester/diol ratio in polymer, calculated from ^1H NMR based on the diester peaks labeled a, b & c and all the diol peaks (labeled d to h) (Figure A1-A12), all corrected for their respective number of protons.

[d] See appendix for calculations

[e] Addition diol as added during the reaction to ensure high conversion 0.2 equiv, for DPP-C6 and 1,1 equiv, due to sublimation for DMDPP-Neo

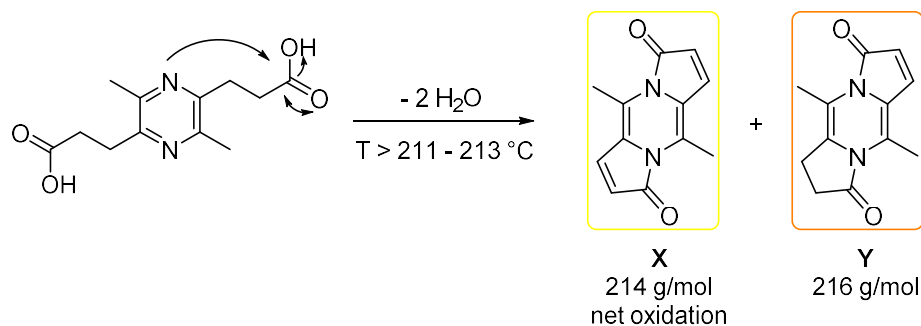
Thermal stability

All polymers were analyzed by TGA to determine their thermal degradation temperature (T_d). The T_d for all materials was found between 287 °C and 342 °C (see **Table 1**). Within this range no trends or significant differences were observed in the T_d between DMDPP and DPP based polymers composed of the same diols. However, since the diacid monomers do not show a stable melt but degrade above 211-213 °C and 221-223 °C respectively, the thermal stability for one of each of the polymers above this temperature was assessed.

A sample of both DMDPP-C6 and DPP-C6 (entries 5 and 6 in **Table 1**) was subjected to isothermal degradation at 180, 200 and 220 °C for 90 min in the TGA. After this time the material showed no color change at 180 °C; at 200 °C the material had turned slightly orange or brown respectively indicating some degradation, while at 220 °C the material was deep orange or dark brown. The weight loss measured for these processes was <0.2% for 180 °C, around 1% for 200 °C and 2% for 220 °C. Sample preparation for GPC resulted in full dissolution after 180 °C, slight gel formation after 200 °C and a large amount of colorless gel after thermal treatment at 220 °C. The formation of gel at these last two temperatures clearly indicated crosslinking and degradation of the

material. GPC of the soluble fractions of each reaction revealed an increase in M_w and \bar{D} in the degraded cases as compared to the nascent material (see **Figure A13**). Based on these results it can be concluded that both DMDPP and DPP are not stable above their degradation temperature even when incorporated into a polymer.

To gain more insight in the degradation mechanism and its implication for processability, the free acid DMDPP was subjected to temperatures above the degradation temperature (211-213 °C). Upon reaching this temperature, vapor evolved and a yellow to orange solid formed. The solid was subjected to column chromatography and one yellow and one orange fraction were isolated (see appendix). LC-MS analysis of the yellow fraction provided ions indicating the loss of two molecules of water and two hydrogens (net oxidation) and for the orange fraction the loss of two molecules of water (see **Figures A14-A15**). Subsequent NMR analysis of the orange material showed that degradation takes place via intra-molecular attack of the pyrazine nitrogens on the acid end-groups (see **Figures A16-A17**). This intra-molecular attack would result in tri-cyclic aromatic compounds **X** and **Y**, which correspond with the observed masses (see Scheme 1). Since degradation was also observed for polymers containing DPP and considering its similarity to the DMDPP structure, it is reasonable to assume DPP degradation takes place via a similar mechanism. The fact that this intra-molecular attack can take place indicates that, even though the pyrazine is very aromatic in character, its thermal stability is limited by its structure. The implication of this is that thermal processing of these materials will be limited to around 180-190 °C. Besides this it also indicates that the nitrogens can be reactive, providing handles for future post-modification of this class of polymers. Modifications that have been reported on pyrazines include oxidation, alkylation and complexation to metal ions.^[15-16] The possibility of post-modification is explored in Chapter 4.



Scheme 1: Proposed degradation mechanism and observed degradation products for DMDPP.

Glass transition

To assess a possible application window for the synthesized polymers and determine the effect of methyl groups on the glass transition (T_g), we first turned to DSC. For the semi-crystalline polymers (entries 3-8 in **Table 1**), DSC did not provide a clear T_g (**Figures A19-A21**) indicating a very high degree of crystallinity. Attempts to melt quench these polymers were unsuccessful due to very high rates of crystallization. Therefore, all polymers were analyzed by DMA (**Figure A24-A25**) and the T_g was determined by the maximum of the loss factor ($\tan \delta$).

Comparison with literature T_g values is complicated by the second order transition nature of the T_g which results in the transition being highly dependent on measurement conditions such as scan rate and direction. Some generalizations can be made and typical ranges are known, aliphatic polyesters such as polybutylene adipate or polycaprolactone for instance, have a T_g significantly below room temperature.^[17] Contrary to this, aromatic polyesters of ethylene glycol with either terephthalic acid or furandicarboxylic acid possess a higher T_g at around 70 resp. 90 °C.^[18] There is however, a very large dependency on spacer length with for instance decanediol based materials having a T_g below room temperature.^[19-21]

Both pyrazine monomers studied possess some aromatic, as well as some aliphatic character. The range of observed glass transitions reflects this, being higher than those of pure aliphatic polyesters but lower than short spacer aromatic ones (see **Figure 6**). The increase in steric bulk between the methyl substituted DMDPP and the unsubstituted DPP clearly explains the differences between the two monomers. The same clear trend for the semi-crystalline polymers is also found where T_g drops with increasing aliphatic spacer length. This effect can be attributed to an increase in chain flexibility and thus rotational freedom with increasing spacer length resulting in a decrease in T_g . In terephthalates the difference in T_g between C2 and C4 is about 10 °C, the small difference in T_g between the C2 and C4 polymers of DMDPP compared to terephthalates can be explained by the crystalline nature of the C4 polymer as opposed to the amorphous C2 polymer in our case. Since the T_g is a property of the amorphous phase and this its movement is highly restricted with high crystallinity this can result in a rigid amorphous phase. The T_g associated with a rigid amorphous phase is increased compared to the mobile amorphous phase.^[22] Another factor resulting in the observed difference between C2 and C4 might be their difference in molecular weight. In case of the cycloaliphatic CHDM and substituted Neo monomers the T_g difference compared to the C2 polymers is comparable to the difference observed in terephthalates, with Neo being similar to C2 and CHDM being about 15 °C higher.^[23] The size of the effect of the introduction of methyl groups on the

pyrazine can most clearly be seen for the amorphous polymers (entries 1 and 2, 9-12 in **Table 1**, **Figure A24**). Here the difference between the higher T_g DMDPP polymers and the lower T_g DPP polymers was found to be around 20 °C in all cases. Summarizing, the T_g follows known steric and spacer length arguments between the glycol monomers, and the semi-aromatic nature of both pyrazine monomers is clearly reflected in the range of the observed T_g 's.

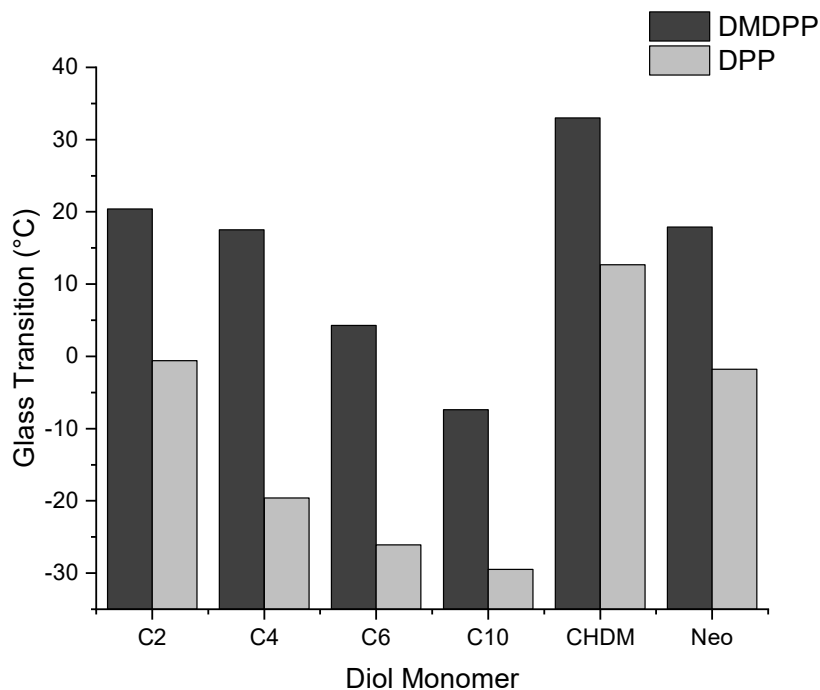


Figure 6: Glass transition comparison between polyesters based on DMDPP (black) and DPP (grey).

Melting point

Next to the assessment of monomer structure and the effect of methyl groups on T_g , we assessed their effect on the melting behavior of the synthesized polymers. This property was compared to the averaged literature values of the terephthalate, sebacate and furandicarboxylate polyesters of the same diols (see **Table A2**).^[17, 24] Terephthalate polyesters were chosen to represent the aromatic character and sebacic acid to represent the aliphatic character of each monomer. Furandicarboxylate polyesters were selected for comparison as a representative biobased aromatic diacid. For the linear diols reference data were also available for phenylene diacetate based polyesters.^[25] This compound possesses both aromatic and aliphatic character and can thus serve as a good representation of these properties. The melting points for phenylene diacetate polyesters were found to be significantly lower than for terephthalic acid, which is attributed to the lack of conjugation between the ester

carbonyl and the aromatic ring. The comparison between all literature melting point values and the melting points for the reported polymers is summarized in **Figure 3**.

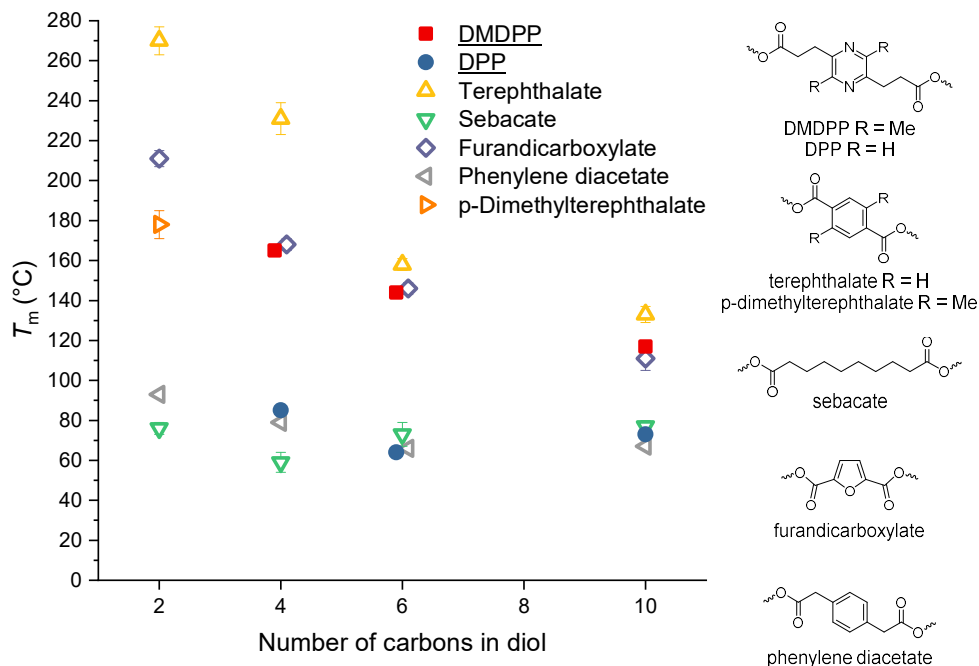


Figure 3: Melting point comparison using literature data.

The linear aliphatic polymers of both DMDPP and DPP were found to be semi-crystalline materials if the chain length of the diol was longer than 2 methylene units. The synthesized polymers with C₂, CHDM and Neo were not semi-crystalline (**Table 1**), this in contrast to the polyesters of reference diacids.^[17, 26] For the EG-based materials (entries 1 and 2) a melting peak was found in the first heating cycle on DSC but not on the second cycle, since the material was purified by precipitation this melting peak is attributed to solution crystallization. The DPP-C₂ material did crystallize after two weeks, as did the DMDPP-C₂ material on even longer time scales. The materials with CHDM (entries 9 and 10) did not form semi-crystalline solids straight from the melt. These materials also crystallized very slowly on standing (multiple weeks) and showed three melting enthalpies in the first heating cycle. The polyesters of DMDPP and DPP with Neo (entries 11 and 12) were both found to be completely amorphous. This in contrast to both terephthalate and furandicarboxylate polyesters of Neo which are both reported to be semi-crystalline.^[27-28]

For higher linear diols the melting point of the DPP-based polyesters (entries 4, 6 and 8 in **Table 1**) were very close to those of phenylene diacetate and sebacate polyesters

(see blue circles in **Figure 3**). The DPP polyesters lack conjugation between the aromatic ring and the ester carbonyl similarly to phenylene diacetate polyesters for which the lower melting point compared to terephthalic acid containing polymers was attributed to this lack.^[25] After breaking conjugation, addition of one extra methylene spacer on each side should not greatly influence the melting point as can be determined from the melting points of the sebacate polyesters. The breaking of conjugation thus results in DPP-based polyesters behaving as linear aliphatic polyesters. Having determined that loss of conjugation between the aromatic ring and the acid for these monomers results in significant aliphatic character, the question arose if this lack of conjugation also has an effect on reactivity. This was assessed by determining transesterification kinetics using a model reaction. This kinetics study showed that both pyrazine monomers react faster than terephthalate and furanoate and have a similar reactivity to sebacate (see **Figure A26**). This confirms that loss of conjugation between the acid and the aromatic ring results in significant aliphatic character of a monomer.

In contrast DMDPP-based polyesters with linear diols, (entries 3, 4 and 7 in **Table 1**) exhibit melting points significantly higher than those of the DPP, sebacate and phenylene diacetate polyesters (red squares in **Figure 3**). Semi-crystalline DMDPP polyesters exhibited the same trend as observed for terephthalic acid, that increasing spacer length of the diol lowers the melting point of the obtained materials due to increasing aliphatic character. Interestingly, the melting points observed for these materials are similar to those observed for furandicarboxylic acid, a monomer in which the acid groups are in conjugation with the aromatic ring.^[24]

These significantly higher melting points for DMDPP polyesters however, are not in line with the observation that addition of methyl groups in the 2 and 5 positions on the terephthalate in poly(ethylene terephthalate) (PET) lowers the melting point by 87 °C.^[11] Nor is it in line with the melting points observed for DPP, for which the low melting point is attributed to the lack of conjugation with the ester groups. The esters in DMDPP-based polyesters also lack conjugation with the aromatic ring. Besides this, the addition of the methyl groups should not affect the character of the pyrazine to an extent that such a significant effect on melting point is observed. For instance, the reported pK_a for 2,5-dimethyl pyrazinium is 2.0 and for tetramethyl pyrazinium 3.6, about a 40-fold decrease in acidity.^[15] A large increase but most likely not enough to explain an 80 degree increase in melting point. Especially since there are no hydrogen bond donors present which might form stronger bonds with a more basic system. It is hypothesized a different physical phenomenon is at the basis for this increase in melting point. These phenomena might include more efficient crystal packing, some

kind of inter- or intra molecular hydrogen bonding or an as of yet unreported phenomenon. These hypotheses were explored as reported in Chapter 5.

Expected performance & application niche

Having determined the T_g and T_m , the expected performance and application niche for these polymers can be determined with help of the DMA data measured in shear. For the amorphous polymers (entries 1-2 and 9-12 in **Table 1**) a plot of the storage modulus versus temperature (**Figure 4A**) shows that within each glycol monomer pair similar glassy moduli are obtained. The entire range of glassy moduli is also similar, between 450 – 900 MPa. There is thus no effect of the methyl groups on the mechanical properties of these amorphous polyesters. These materials will behave rubbery at room temperature which will dictate any potential application.

For the semi-crystalline materials (entries 3-8 in **Table 1**) a more interesting picture emerges. The difference in T_c between DMDPP and DPP is clearly seen in **Figure 4B**, as well as the fast crystallization of the DMDPP-based polymers. For the DPP-based polymers overall lower plateau moduli and a larger difference between this modulus and the glassy modulus indicate lower crystallinity. Especially for the C₄ monomer pair (blue) the difference is striking, the DPP-C₄ material crystallizes very slowly as can be seen by the lack of a true plateau modulus. This is also seen in the DSC data (**Figure A20**) where mostly cold crystallization in the heating cycle is observed. For all polymers the glassy moduli are in a similar range between 450 – 1150 MPa with the DMDPP polymers being higher. The plateau moduli for these DMDPP materials are also in the same range and are similar to those observed for other semi-crystalline polyesters based on terephthalate and furandicarboxylate when taking the difference between shear and compression in to account.^[29-32] The polymers based in DMDPP show high crystallinity from the small difference between the plateau modulus and the glassy modulus. DSC data confirms this, with non-isothermal crystallization enthalpies of 70-80 J/g (see **Figures A20-A22**). Assuming similar heats of fusion as for polybutylene terephthalate or furanoate this would be around 60% crystallinity.^[33] To what extent this assumption holds and the complex melting of the resultant crystals make further interpretation of the crystallinity beyond the scope of this study.

This initial examination of the overall properties in terms of thermal and mechanical behavior place the semi-crystalline DMDPP based polymers firmly in the high performance niche.

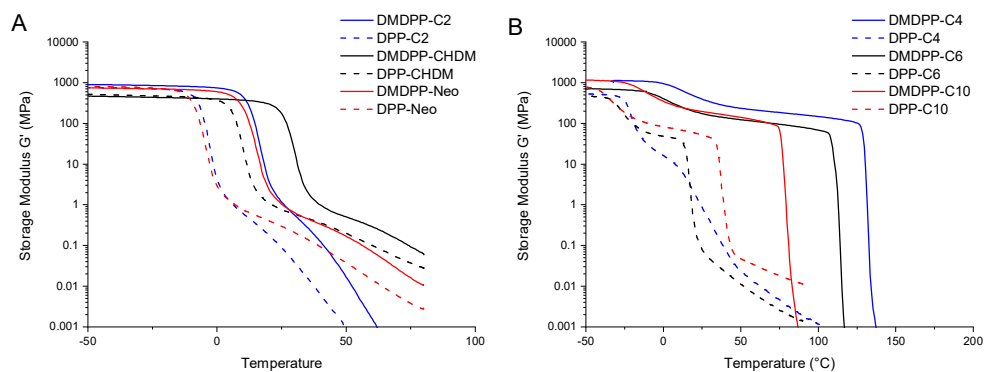


Figure 4: Storage modulus vs temperature for the amorphous polymers (A) and semi-crystalline polymers (B).

Conclusions

This work shows the first systematic study of pyrazine containing polyesters based on dimethyl dipropionic acid pyrazine and dipropionic acid pyrazine, two biobased pyrazine diacids obtained from nitrogen-rich biomass. The dimethyl esters of these monomers have been successfully polymerized via transesterification with six diols resulting in twelve polymers with GPC molecular weights between 12300 and 47500 and dispersities between 1,9 and 2,3. Six of the obtained polymers were amorphous and six were semi-crystalline. The thermal properties of pyrazines and the effect of methyl groups on the aromatics in the polymers were studied. The thermal stability of the polymers was found to be limited by the degradation temperature of the monomer, which was unstable even when incorporated in a polymer. The degradation mechanism was determined to take place via intra molecular attack of the pendant acid by the pyrazine nitrogens. Although this limits the processing temperature of the materials to 180-190 °C it does show that these nitrogens are reactive and might be exploited for post-modification. Further determination of the thermal properties showed that the effect of methyl groups on the glass transition temperature follows steric, chain length and free volume arguments. The presence of methyl groups was found to increase the T_g by approximately 20 °C in case of amorphous polymers. For the semi-crystalline polymers the following structure-property relationships could be determined. In case of the unsubstituted pyrazine monomers, the materials act mostly as a linear aliphatic polyesters. For the methyl substituted pyrazine however, melting points are elevated resulting in high melting polyesters. These melting points are very close to those of furandicarboxylate polyesters. Since the difference between the two pyrazines is not enough to explain the differences in melting point another interaction is hypothesized to cause this effect. Further work on the precise nature of the interaction causing difference in melting point is ongoing, as well as further determination of the mechanical properties of these new polyesters. Preliminary results in this work indicate that the polymers belong to the class of high performance polymers with storage moduli between 450 and 1150 MPa. These first in class biobased aromatic polyesters show that nitrogen-rich biomass can successfully be converted into high performance, high melting semi-crystalline polyesters.

References

- [1] F. De Schouwer, L. Claes, A. Vandekerckhove, J. Verduyck, D. E. De Vos, *ChemSusChem* **2019**, *12*, 1272-1303
- [2] M. A. Würdemann, C. Nitu, S. M. A. De Wildeman, K. V. Bernaerts, R. V. A. Orru, *Chem. Eur. J.* **2020**, *26*, 8090-8100
- [3] G. Kvakovszky, R. Vicari, O. S. Fruchey, A. M. Tafesh, C. B. Hilton, (Hoechst Celanese), US 5,393,860, **1995**
- [4] R. Vicari, G. Kvakovszky, O. S. Fruchey, H. J. Metz, (Hoechst Celanese), US 5,464,941, **1995**
- [5] H. J. Scholl, (Bayer AG), US 4,665,178, **1987**
- [6] H. J. Scholl, (Bayer AG), DE3427400A1, **1986**
- [7] N. Ogata, *J. Macromol. Sci., Part A: Pure Appl. Chem.* **1979**, *13*, 477-501
- [8] N. Ogata, K. Shimamura, *Polym. J.* **1975**, *7*, 72-78
- [9] S. Ueta, Y. Fukuda, K. Koga, M. Takayanagi, *Polym. J.* **1992**, *24*, 1429-1436
- [10] R. H. Wiley, *J. Polym. Sci., Part A: Polym. Chem.* **1987**, *25*, 735-737
- [11] M. Cachia, *Annales de chimie.* **1959**, *S13*, 5-41
- [12] L. P. Chen, A. F. Yee, J. M. Goetz, J. Schaefer, *Macromolecules* **1998**, *31*, 5371-5382
- [13] H. D. Dakin, R. West, *J. Biol. Chem.* **1928**, *78*, 745-756
- [14] J. A. King, F. H. McMillan, *J. Am. Chem. Soc.* **1952**, *74*, 2859-2864
- [15] G. B. Barlin, *The Pyrazines*, Wiley, New York, **1982**.
- [16] D. J. Brown, *The Pyrazines: Supplement I*, Wiley, New York, **2003**.
- [17] J. Brandrup, E. H. Immergut, E. A. Grulke, *Polymer handbook*, 4th edition, Wiley, New York; Chichester, **2004**.
- [18] S. K. Burgess, J. E. Leisen, B. E. Kraftschik, C. R. Mubarak, R. M. Kriegel, W. J. Koros, *Macromolecules* **2014**, *47*, 1383-1391
- [19] V. Tsanaktsis, D. N. Bikiaris, N. Guigo, S. Exarhopoulos, D. G. Papageorgiou, N. Sbirrazzuoli, G. Z. Papageorgiou, *RSC Advances* **2015**, *5*, 74592-74604
- [20] G. Farrow, J. McIntosh, I. M. Ward, *Die Makromolekulare Chemie* **1960**, *38*, 147-158
- [21] J. G. Smith, C. J. Kibler, B. J. Sublett, *Journal of Polymer Science Part A-1: Polymer Chemistry* **1966**, *4*, 1851-1859
- [22] B. Wunderlich, *Prog. Polym. Sci.* **2003**, *28*, 383-450
- [23] W. J. Jackson, T. F. Gray, J. R. Caldwell, *J. Appl. Polym. Sci.* **1970**, *14*, 685-698
- [24] G. Papamokos, T. Dimitriadis, D. N. Bikiaris, G. Z. Papageorgiou, G. Floudas, *Macromolecules* **2019**, *52*, 6533-6546
- [25] V. V. Korshak, S. V. Vinogradova, V. M. Belyakov, *Bull. Acad. Sci. USSR, Div. Chem. Sci. (Engl. Transl.)* **1957**, *6*, 1029-1031
- [26] C. J. Kibler, A. Bell, J. G. Smith, *J. Polym. Sci., Part A: Gen. Pap.* **1964**, *2*, 2115-2125
- [27] M. Soccio, N. Lotti, L. Finelli, M. Gazzano, A. Munari, *J. Polym. Sci., Part B: Polym. Phys.* **2008**, *46*, 170-181
- [28] V. Tsanaktsis, Z. Terzopoulou, S. Exarhopoulos, D. N. Bikiaris, D. S. Achilias, D. G. Papageorgiou, G. Z. Papageorgiou, *Polym. Chem.* **2015**, *6*, 8284-8296
- [29] K. Banik, G. Mennig, *Polym. Eng. Sci.* **2008**, *48*, 957-965
- [30] Y. G. Jeong, S. C. Lee, W. H. Jo, *Macromol Res* **2006**, *14*, 416-423
- [31] M. Kwiatkowska, I. Kowalczyk, K. Kwiatkowski, A. Zubkiewicz, *Polymers (Basel)* **2020**, *12*, 271
- [32] J. Zhu, J. Cai, W. Xie, P.-H. Chen, M. Gazzano, M. Scandola, R. A. Gross, *Macromolecules* **2013**, *46*, 796-804
- [33] G. Z. Papageorgiou, V. Tsanaktsis, D. G. Papageorgiou, S. Exarhopoulos, M. Papageorgiou, D. N. Bikiaris, *Polymer* **2014**, *55*, 3846-3858

Appendix

Fischer esterification

Dimethyldipropionic acid pyrazine dimethyl ester (Me₂DMDPP)

A 500 mL flask was loaded with 5.04 g (20.0 mmol) of 2,5-bis(2-carboxyethyl)-3,6-dimethylpyrazine (DMDPP) and methanol (200 mL) was added. To the resulting suspension was added 2 mol% para-toluenesulfonic acid (76 mg, 0.4 mmol). The mixture was heated to 65 °C for 48 hours. The resulting clear solution was concentrated to dryness *in vacuo* taken up in 50 mL of ethyl acetate and extracted twice with 25 mL of satd. NaHCO₃. The organic phase was filtered over silica and concentrated *in vacuo*, providing the desired product as a colorless solid (5.44 g, 19.4 mmol, 97%).

2,5-bis(2-carboxyethyl)-3,6-dimethylpyrazine dimethyl ester

mp 96-98 °C; ¹H NMR (300 MHz, CDCl₃) δ = 3.69 (s, 6H), 3.04 (t, *J*=7.3 Hz, 4H), 2.80 (t, *J*=7.3 Hz, 4H), 2.48 (s, 6H); ¹³C NMR (75 MHz, CDCl₃) δ = 173.8, 149.4, 147.9, 51.6, 31.6, 28.5, 20.9; IR (ATR) $\tilde{\nu}$ (cm⁻¹) = 2950, (w), 1722 (vs), 1425 (s), 1362 (m), 1218 (s), 1201 (s), 1163 (vs), 1133 (vs), 981 (m), 841 (s)

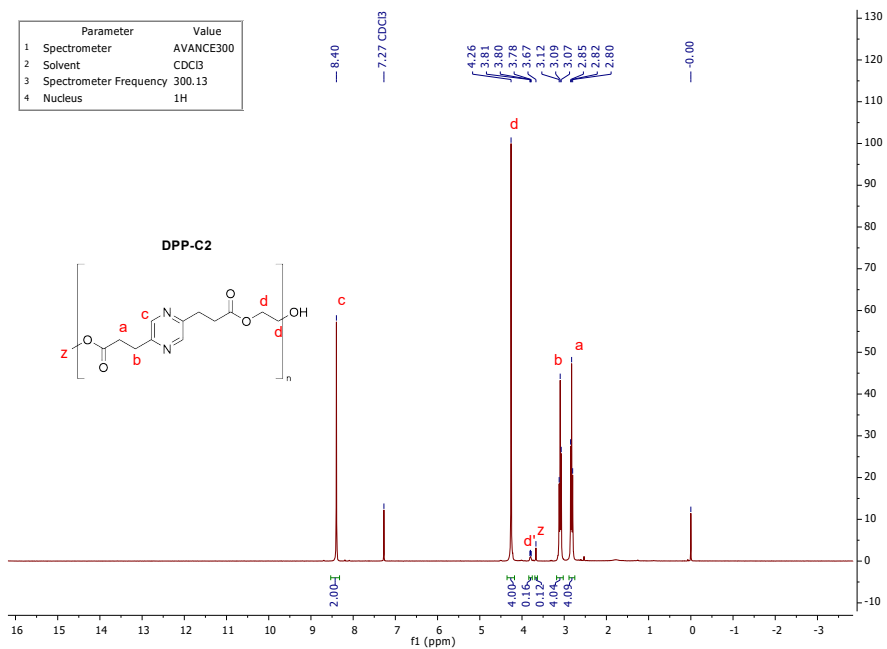
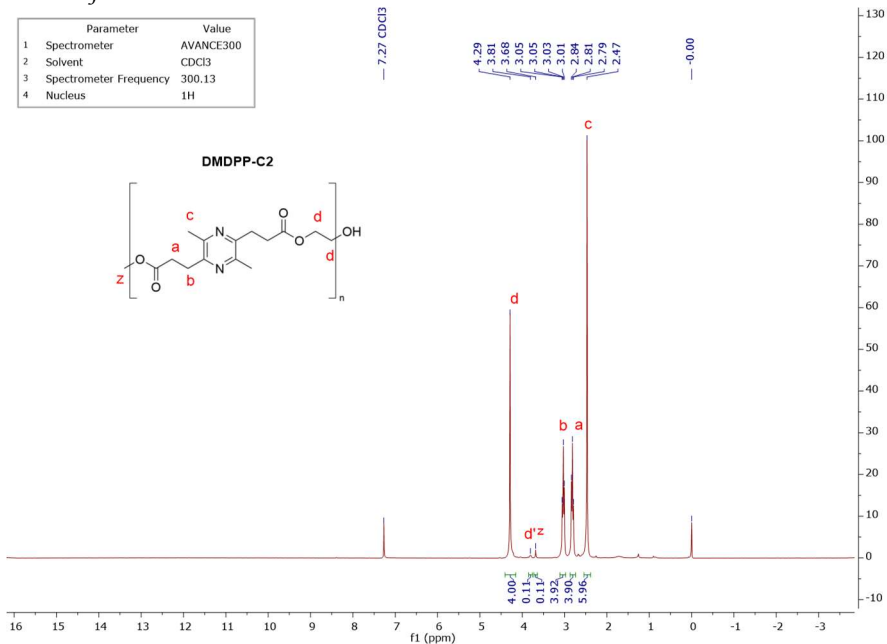
Dipropionic acid pyrazine dimethyl ester (Me₂DPP)

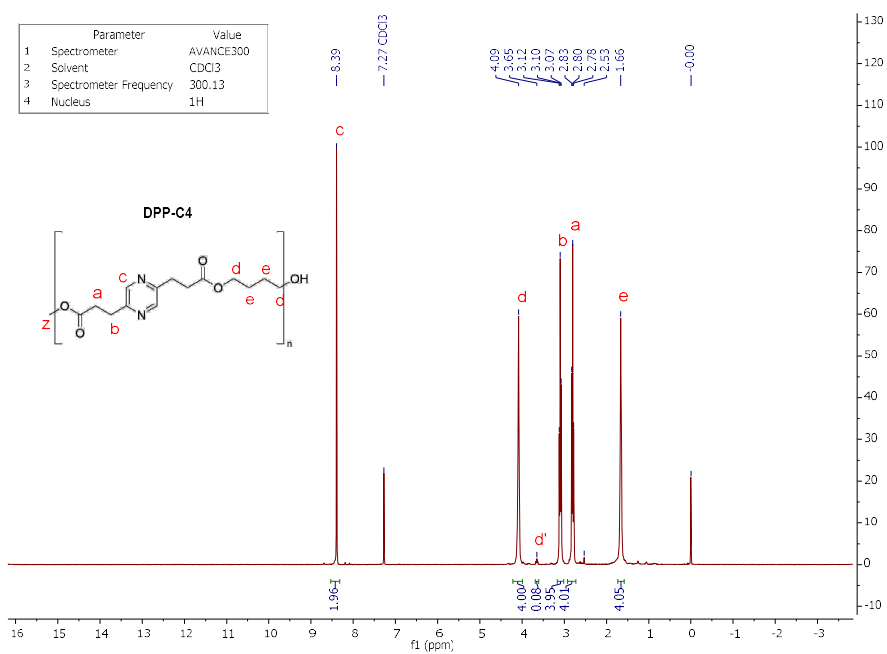
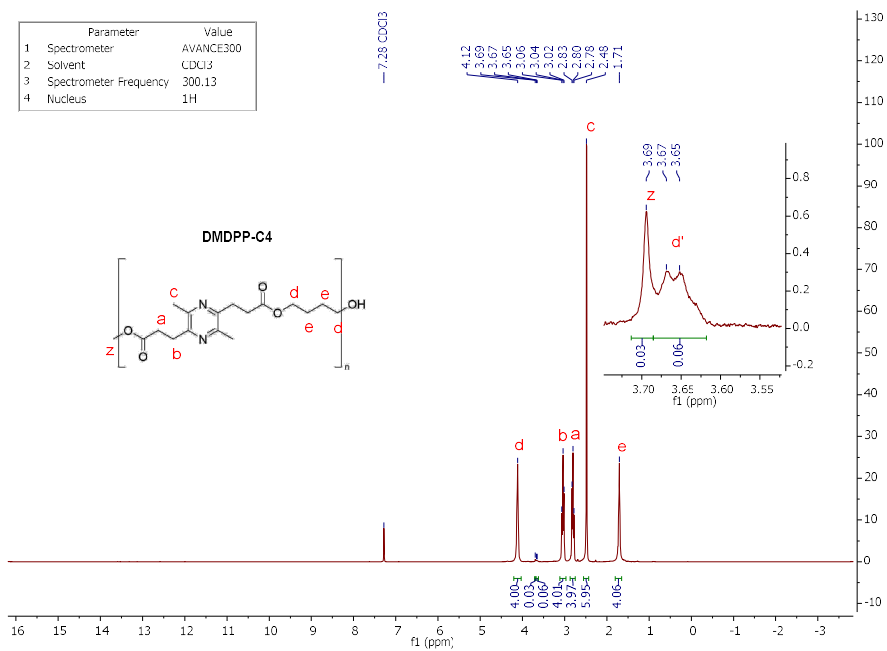
A 500 mL flask was loaded with 4.05 g (18.1 mmol) of 2,5-bis(2-carboxyethyl)-pyrazine (DPP) and methanol (180 mL) was added. To the resulting suspension was added 2 mol% para-toluenesulfonic acid (76 mg, 0.4 mmol). The mixture was heated to 65 °C for 48 hours. The resulting clear solution was concentrated to dryness *in vacuo*, taken up in 50 mL of ethyl acetate and extracted twice with 25 mL of satd. NaHCO₃. The organic phase was filtered over silica and concentrated *in vacuo*, providing the desired product as a colorless solid (4.13 g, 16.4 mmol, 91%).

2,5-bis(2-carboxyethyl)-pyrazine dimethyl ester

mp 69-70 °C; ¹H NMR (300 MHz, CDCl₃) δ (ppm) = 8.33 (s, 2H), 3.60 (s, 6H), 3.03 (t, *J*=7.3 Hz, 4H), 2.74 (t, *J*=7.3 Hz, 4H); ¹³C NMR (75 MHz, CDCl₃) δ (ppm) = 173.1, 152.9, 143.6, 51.7, 32.5, 29.5; IR (ATR) $\tilde{\nu}$ (cm⁻¹) = 2954 (w), 1725 (vs), 1435 (m), 1343 (s), 1280 (m), 1163 (vs), 1132 (vs), 1040 (m), 894 (s), 775 (m)

NMR data for entries 1 to 12





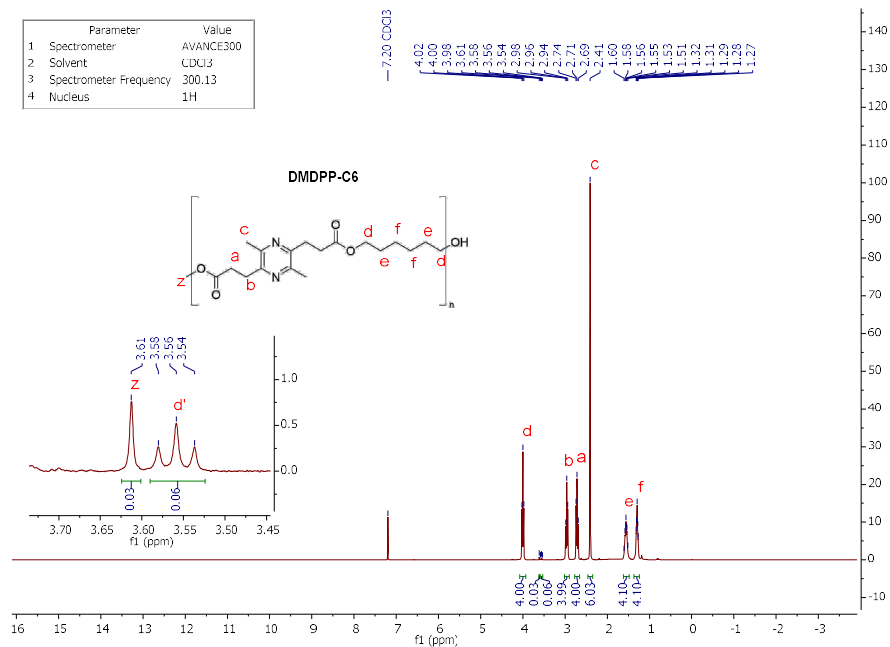


Figure A5: ¹H NMR data for entry 5, DMDPP-C6.

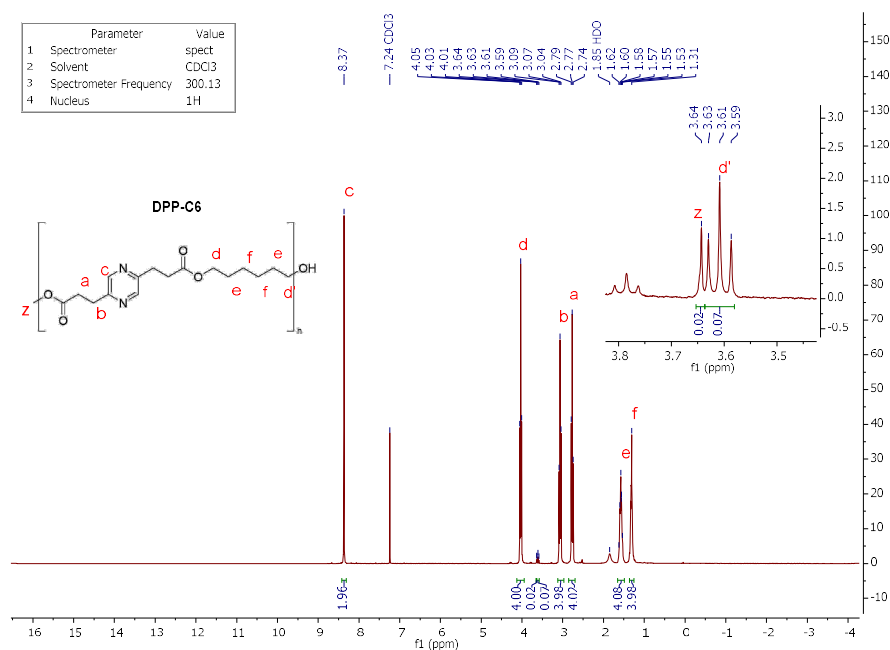


Figure A6: ¹H NMR data for entry 6, DPP-C6.

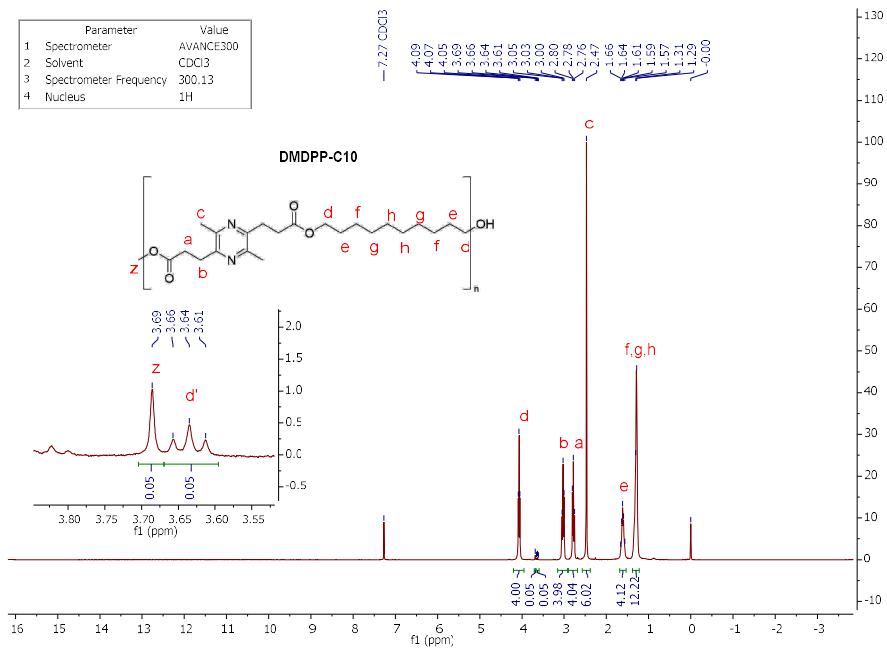


Figure A7: ¹H NMR data for entry 7, DMDPP-C10.

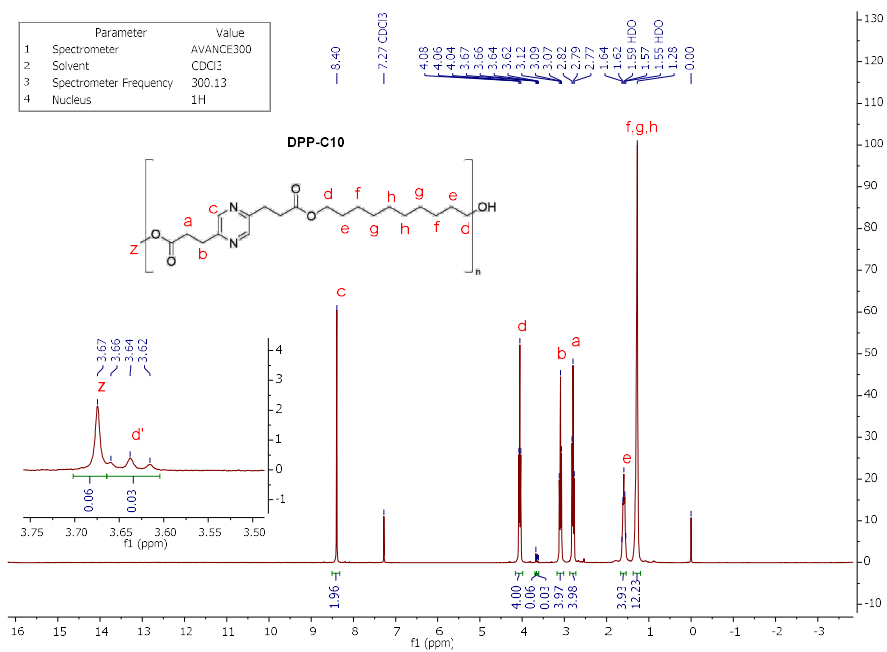


Figure A8: ¹H NMR data for entry 8, DPP-C10.

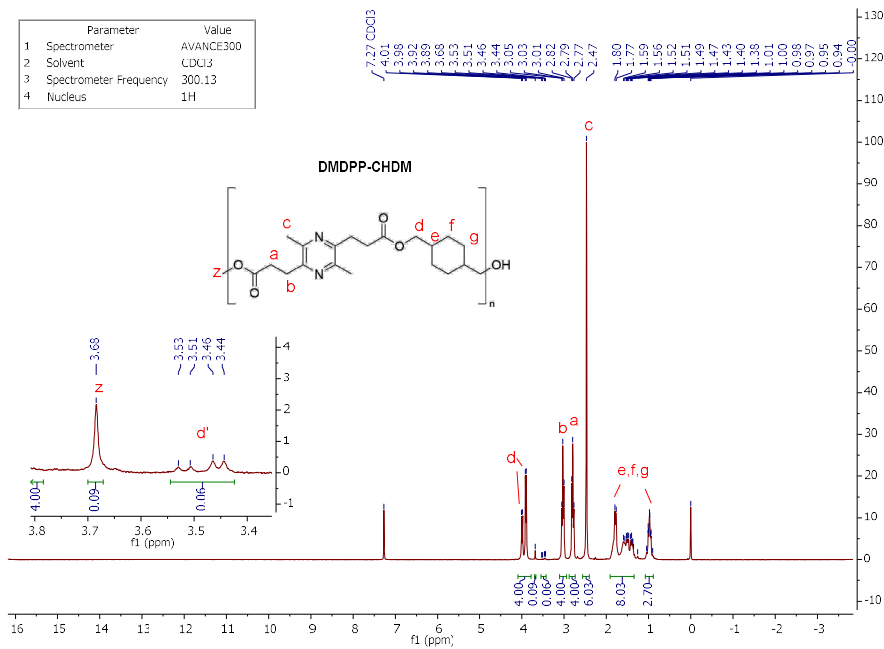


Figure A9: ¹H NMR data for entry 9, DMDPP-CHDM.

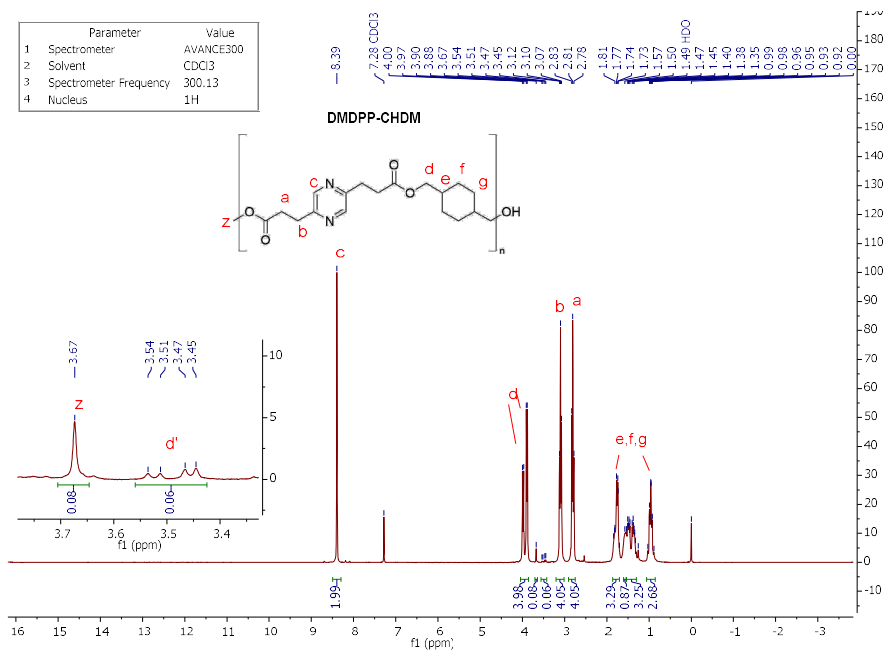
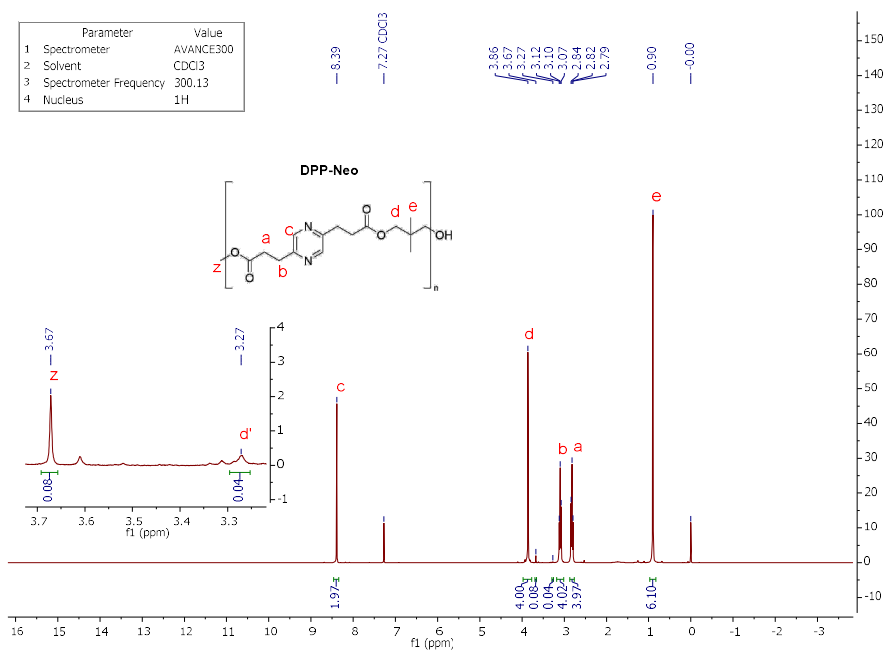
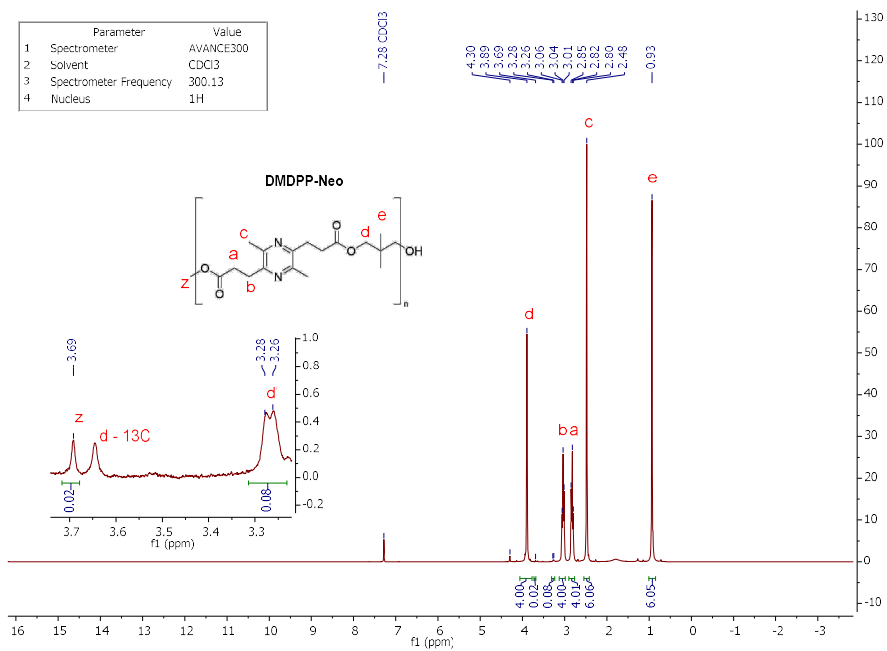


Figure A10: ¹H NMR data for entry 10, DPP-CHDM.



NMR calculations

The end-group distribution of the synthesized polymers can be calculated from the ratio between both end-groups corrected for the number of protons of each end-group. This ratio is then translated to a percentage based on 200% (since there are 2 end-groups per chain). **Equation 1** provides an example using the peak labeling above. Using this formula for all polymers provides the distributions in **Table A1**.

$$\text{Eq 1: } \text{End - group distribution} = \frac{d'}{2} / \left(\frac{d'}{2} + \frac{z}{3} \right) \times 200\%$$

The degree of polymerization (*DP*) can be calculated from NMR end-groups as long as these can be integrated properly and used in **equation 2**.^[1]

$$\text{Eq 2: } \overline{DP} = \frac{(I_{ru} \times m_{end} \times n_{end})}{(I_{end} \times m_{ru})}$$

In this equation I_{ru} is the integral of the repeating unit, m_{end} is the number of protons for the end-groups, n_{end} is the number of end-groups, I_{end} is the integral for the end groups and m_{ru} is the number of protons for the repeating unit.

Since most of the polymers synthesized still show both end-groups on NMR, the number of end-groups has to be corrected for the end-group distribution. Using this correction, either end-group can be used to calculate the *DP*. For these *DP* calculations, the repeating unit was defined as the glycol ester protons labeled **d** and being 4 protons. The end-group was defined as the alcohol end group peak **d'** being 2 protons and the number of end-groups corrected for the distribution. As an example of the calculations, the data for DMDPP-C2 was used.

Here I_{ru} is 4.00, m_{end} is 2, n_{end} is the fraction of alcohol end-groups and m_{ru} is 4. The end-group integral I_{end} is 0.108 in this case (peak **d'**). Filling these numbers in **equation 1** give the approximate *DP* of DMDPP-C2 (see **equation 3**).

$$\text{Eq 3: } \overline{DP} = \frac{(4.00 \times 2 \times 1.17)}{(0.108 \times 4)} = 22$$

These calculations were done for all polymers and the resulting *DP* values are found in **Table 1** of the main manuscript and **Table A1** below.

Using the approximate *DP* values calculated the M_n can be calculated by multiplying this number by the repeating unit weight and adding the end-group weights corrected for their distribution. The M_n values were rounded to the nearest 100 and are listed in **Table A1** below.

Table A1: NMR calculations overview

Polymer	End-group conv. ratio ^[a] (%)	Repeating unit molecular weight (g/mol)	Ester end-group weight (g/mol)	Alcohol end-group weight (g/mol)	End-group distribution (alcohol/ester) (%)	DP	$M_n - NMR$ (g/mol)
DMDPP-C2	96,2/94,9	278,31	265,29	61,06	117 / 83	22	6400
DPP-C2	95,1/94,4	250,25	237,24	61,06	106 / 94	18	4800
DMDPP-C4	98,9/94,1	306,36	265,29	89,11	148 / 52	47	14700
DPP-C4	99,9/96,1	278,31	237,24	89,11	200 / 0	49	13800
DMDPP-C6	98,9/96,9	334,42	265,29	117,17	149 / 51	46	15700
DPP-C6	99,4/96,7	306,36	237,24	117,17	169 / 31	50	15600
DMDPP-C10	98,5/97,5	390,52	265,29	173,28	126 / 74	47	18800
DPP-C10	98,2/98,7	362,47	237,24	173,28	84 / 116	62	22900
DMDPP-CHDM	97,1/97,1	374,48	265,29	143,21	102 / 98	33	12800
DPP-CHDM	97,3/97,2	346,43	237,24	143,21	103 / 97	35	12500
DMDPP-Neo	99,4/95,9	334,42	265,29	103,14	177 / 23	42	14300
DPP-Neo	97,5/98,2	306,36	237,24	103,14	82 / 118	46	14500

[a] Diester/diol end-groups, calculated from ¹H NMR. For the diester, peaks labeled a,b & c and the methyl end-groups labeled z were used. For the diol, peaks labeled d to h and the diol end group d' were used. All labels can be found in the supporting information and for the calculation all peaks were corrected for their respective number of protons.

Polymer degradation

The polymer degradation study was performed under a nitrogen atmosphere on a TA instruments TGA 500 machine. Samples of DMDPP-C6 and DPP-C6 were kept for 90 min isothermal at 180 °C, 200 °C and 220 °C. Above 200 °C crosslinking was found in both polymers and the soluble fractions were analyzed by GPC. Below are the combined GPC trace with dispersities for both sets of experiments.

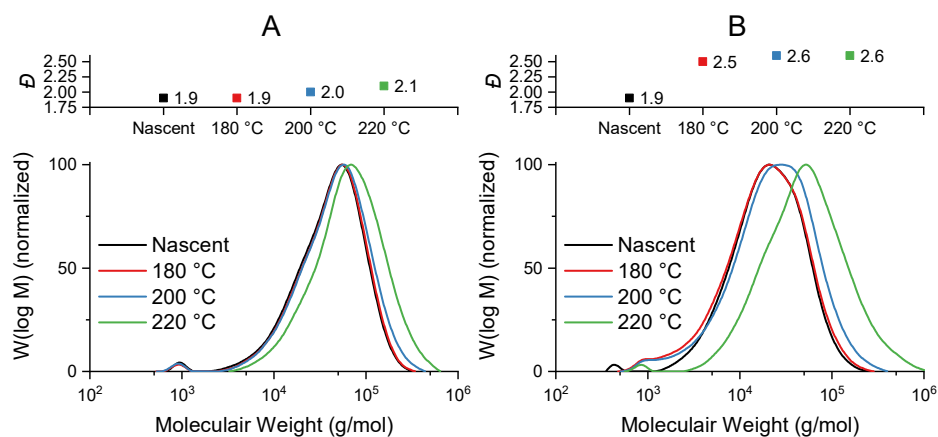


Figure A13: GPC trace overlay (bottom) of the thermal degradation study and the corresponding Đ values (top) of both DMDPP-C6 (panel A) and DPP-C6 (panel B)

Monomer degradation

Monomer degradation was studied by heating 200 mg of DMDPP diacid in a vial on a hotplate at 250 °C. A deep orange solid formed together with some liquid (most likely water), sublimation was also observed to some extent. The resulting orange solid was suspended in 15 mL CHCl₃ and sonicated for 1 hour after which it was filtered and washed with 2x 5 mL CHCl₃. The deep red organic extract was washed with 3x 10 mL satd. NaHCO₃. The organic phase was concentrated *in vacuo* to yield a small amount of orange solid (50 mg). The solid was subjected to column chromatography on silica using a gradient of 1:1 hexane and ethyl acetate to 100% ethyl acetate. A yellow first fraction was collected and an orange second fraction. An orange baseline remained which did not elute even with 10% methanol in dichloromethane. The yellow first fraction was analyzed by LC-MS and found to have an *m/z* 215 and an absorption maximum of 432 nm (see **Figure A14**). NMR of the fraction was unsuccessful due to the extremely small amount of material (<5 mg). The orange second fraction (± 20 mg) was analyzed by LC-MS and found to have an *m/z* 217 and an absorption maximum of 437 nm (see **Figure A15**). (2D)-NMR (**Figure A16&A17**) of this fraction indicated double ring closure of the pyrazine to a tricyclic system. Based on these observations structures X & Y have been assigned to these products.

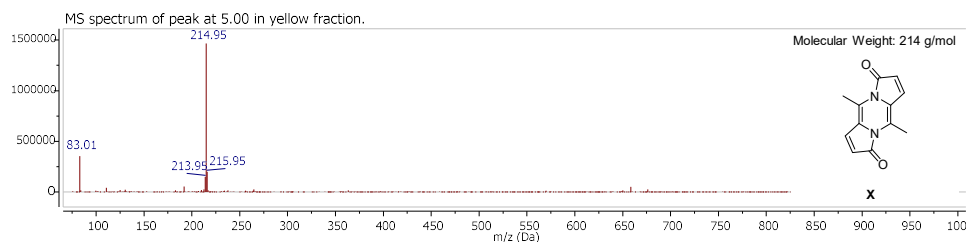


Figure A14: LC-MS results for yellow fraction of DMDPP monomer degradation experiment (structure X).

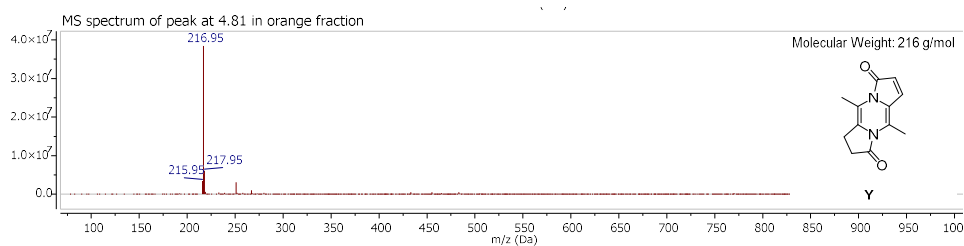
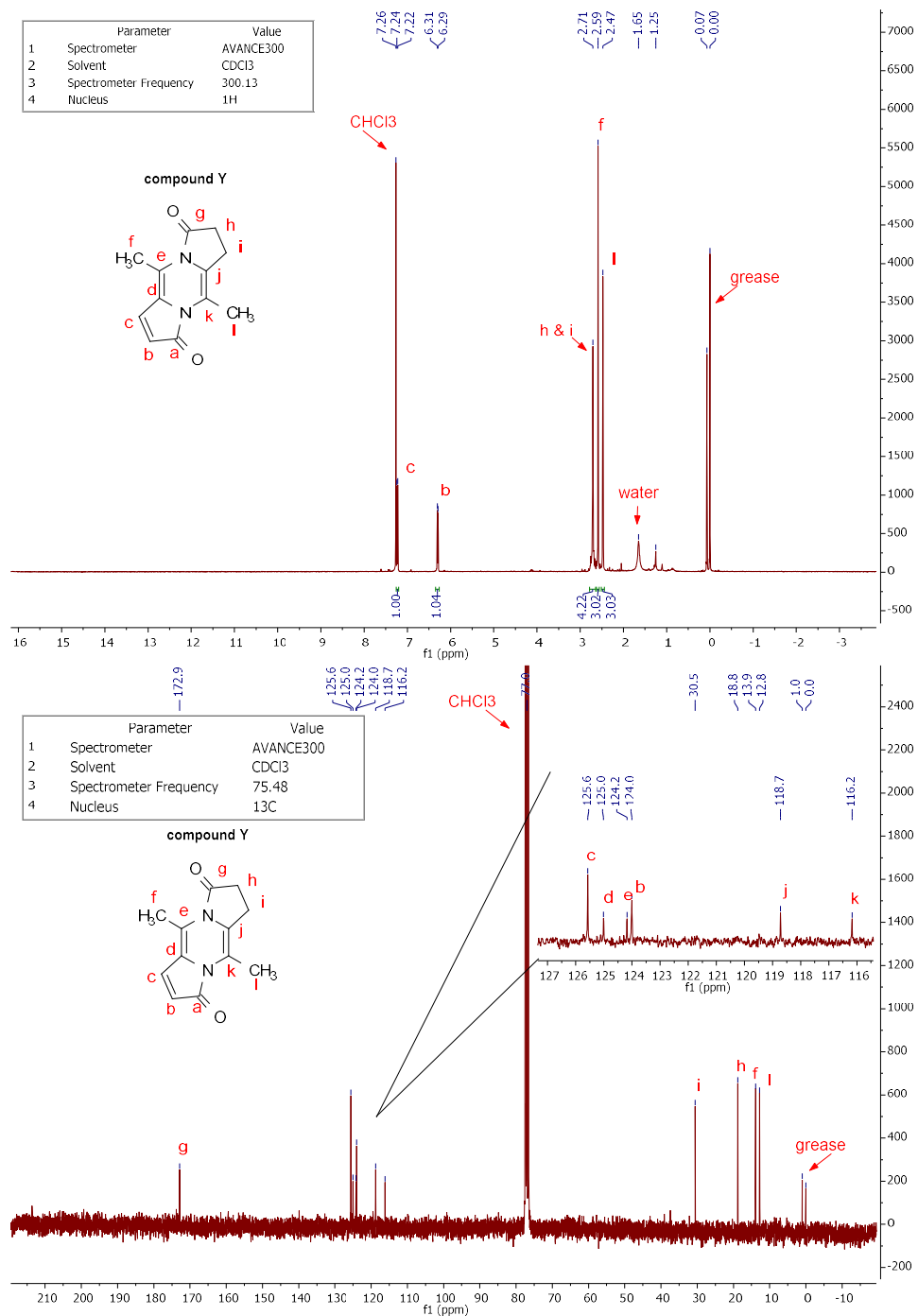


Figure A15: LC-MS results for orange fraction of DMDPP monomer degradation experiment (structure Y).

Figure A16: ¹H (top) and ¹³C (bottom) NMR data for compound Y.

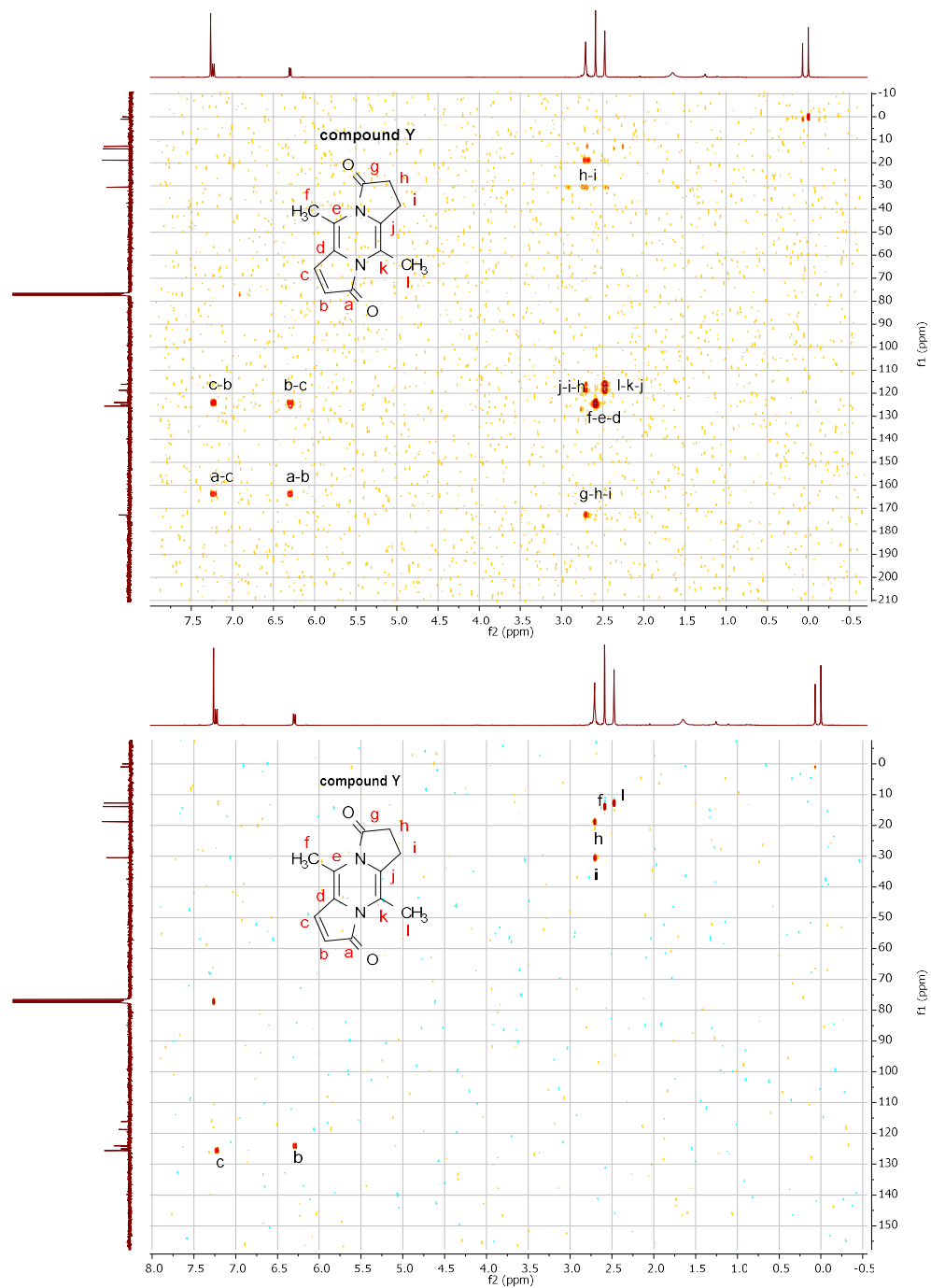


Figure A17: HMBC (top) and HSQC (bottom) NMR data for compound Y.

DSC data for entries 1 to 12

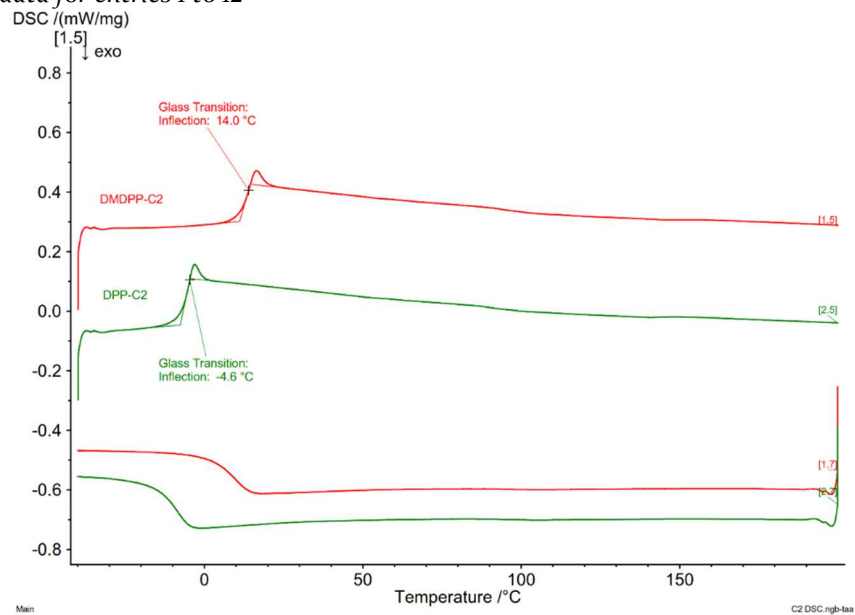


Figure A18: DSC second heating and cooling cycle for DMDPP-C2 (red) and DPP-C2 (green) (entries 1&2).

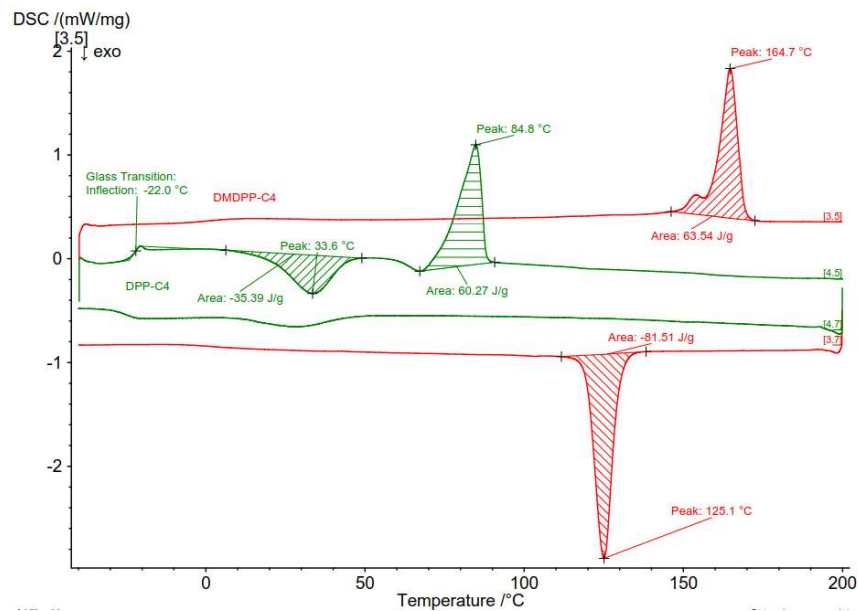


Figure A19: DSC second heating and cooling cycle for DMDPP-C4 (red) and DPP-C4 (green) (entries 3&4).

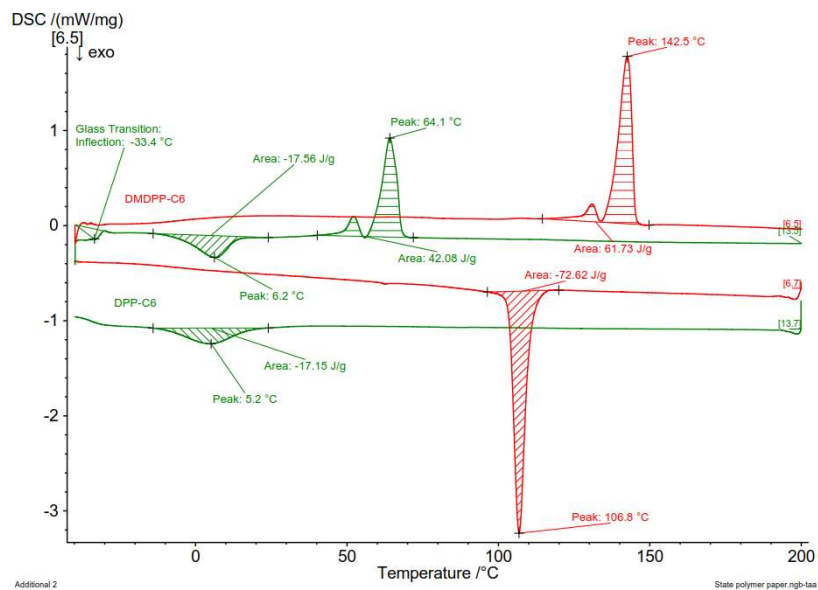


Figure A20: DSC second heating and cooling cycle for DMDPP-C6 (red) and DPP-C6 (green) (entries 5&6).

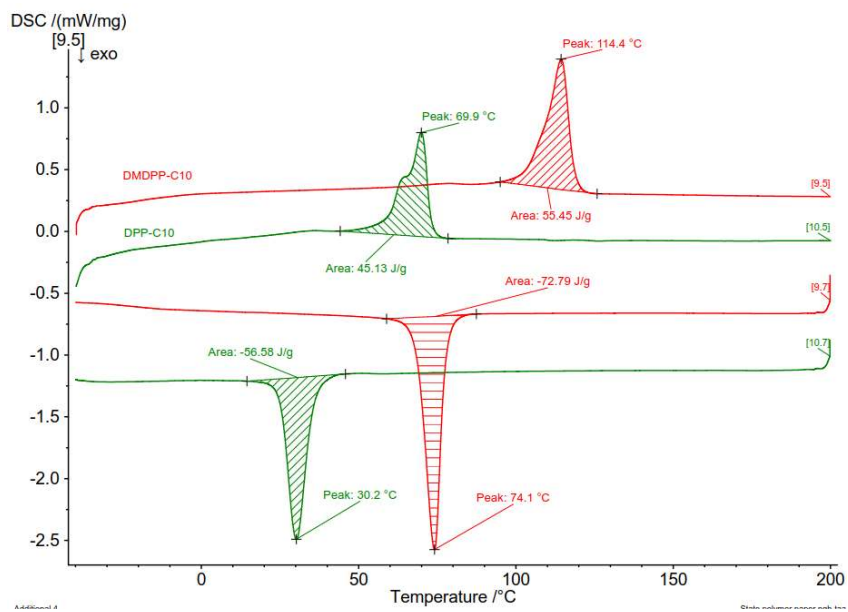


Figure A21: DSC second heating and cooling cycle for DMDPP-C10 (red) and DPP-C10 (green) (entries 7&8).

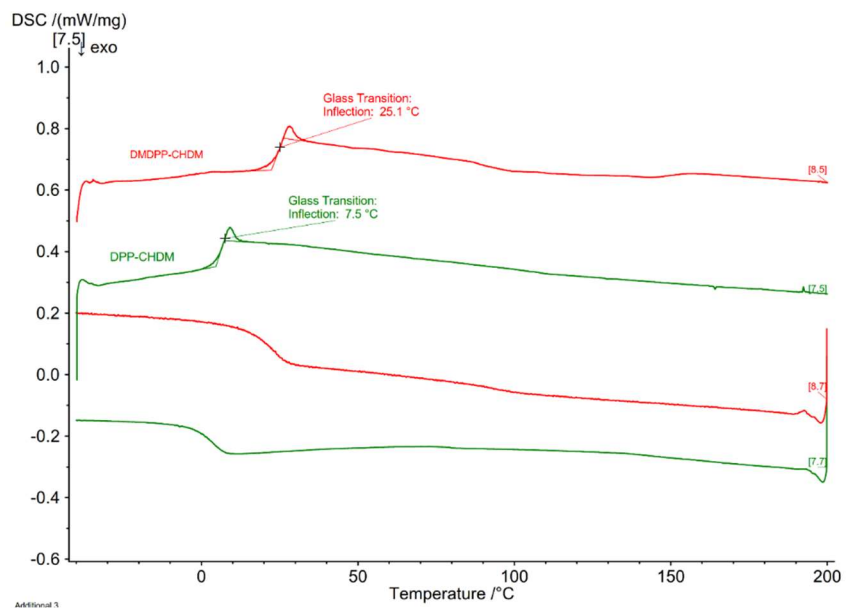


Figure A22: DSC second heating and cooling cycle for DMDPP-CHDM (red) and DPP-CHDM (green) (entries 9&10).

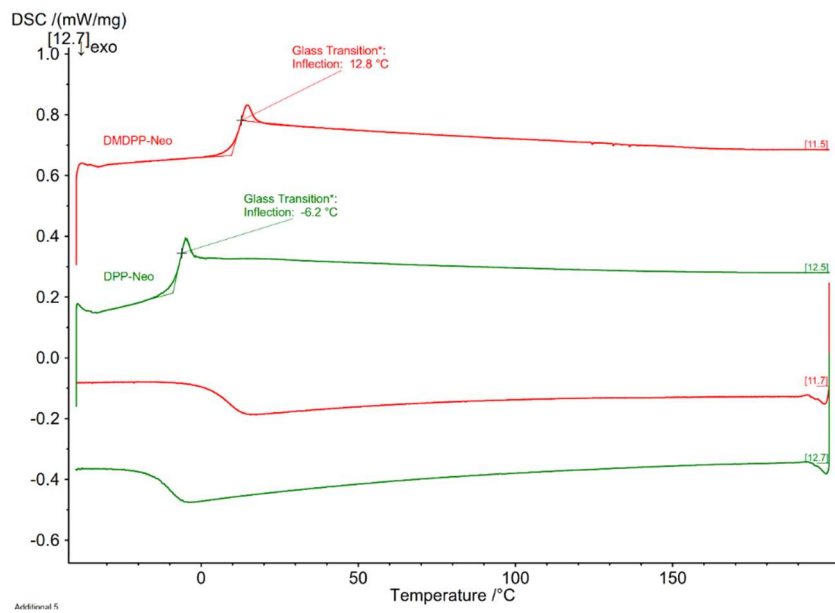


Figure A23: DSC second heating and cooling cycle for DMDPP-Neo (red) and DPP-Neo (green) (entries 11&12).

DMA data

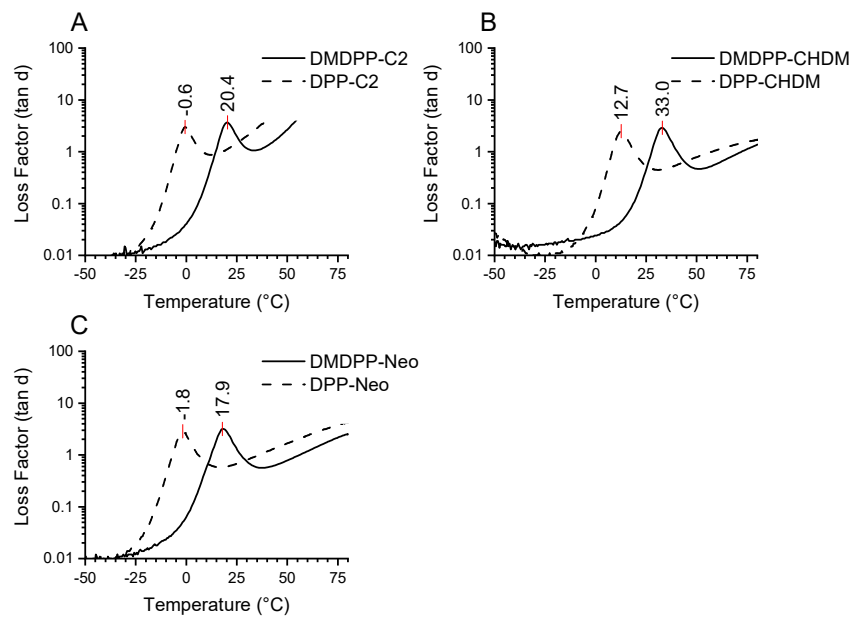


Figure A24: DMA data the amorphous entries in table 1 (A entries 1-2, B entries 9-10, C entries 11-12)

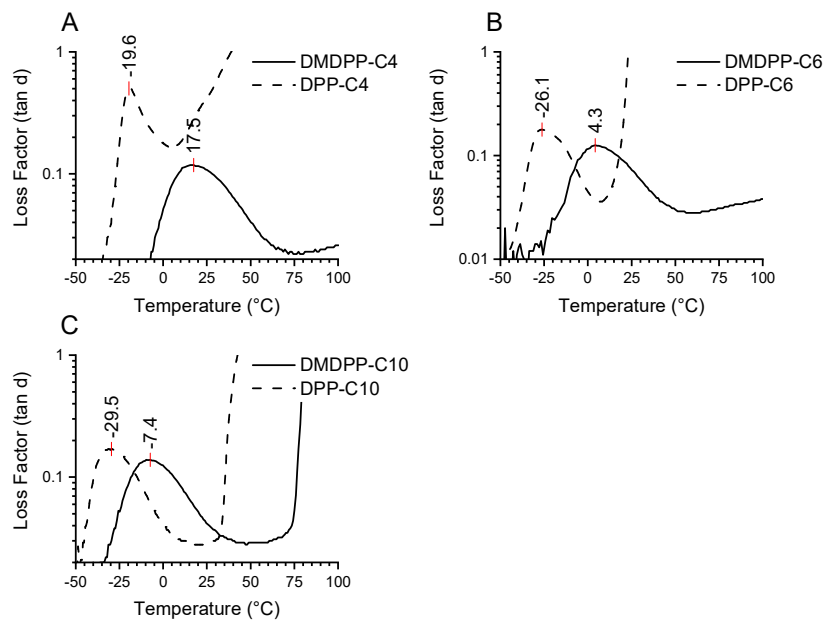


Figure A25: DMA data the semi-crystalline entries in table 1 (A entries 3-4, B entries 5-6, C entries 7-8)

Literature melting point data

The melting point data used in **Figure 4** of the main manuscript are summarized below in **Table A2** including references of the consulted literature.

Table A2: Literature melting point values for reference polyesters.

Diol	Terephthalic acid (°C) ^[2]	Sebacic acid (°C) ^[2]	Furandicarboxylic acid (°C) ^[3-17]	Phenylene diacetate (°C) ^[18]	p-Dimethylterephthalic acid (°C) ^[19]
C2	270 ± 7	76 ± 3	211 ± 4	93 ± 1	178 ± 7
C4	231 ± 8	59 ± 5	168 ± 3	79 ± 1	-
C6	158 ± 3	73 ± 6	146 ± 3	66 ± 1	-
C10	133 ± 4	77 ± 3	111 ± 6	67 ± 1	-

Kinetics of monomer transesterification

It was found that the reported pyrazine monomers behave largely similar to aliphatic monomers and not to aromatic monomers. The question arose whether these monomers also have reactivity similar to aliphatic monomers under polymerization conditions. Transesterification reactions for polycondensation have been studied extensively; however, the reaction mechanisms are not fully understood.^[20] These transesterification processes have been found mostly be third order being depended on the concentrations of both the starting diester and the diol as well as the catalyst.^[21-22] These kind of conditions make experimental determination of the reaction rate complicated, especially since the mechanisms involved for a terephthalate could be different then for an aliphatic diester for instance. Under pseudo-first order conditions determination of relative reaction rates is experimentally more feasible and would allow isolation of the transesterification step. The pseudo-first order reaction rate for a monomer can then be considered representative for that monomers reactivity under step-growth conditions.

Determination of pseudo-first order transesterification rates for dimethyl terephthalate, dimethyl furandicarboxylate, dimethyl sebacate, dimethyl DMDPP and dimethyl DPP would allow assessment of the reactivity of the pyrazine monomers. An experiment was setup to determine the pseudo-first order transesterification rates of these monomers at the same temperature as during the initial polymerization step.

A 25 mL two-necked flask fitted with a condenser was loaded with 1.0 mmol of monomer, 0.5 mmol of biphenyl as an internal standard and 19 mg (1 mol%) of p-toluene sulfonic acid as the catalyst. These solids were suspended in 10 mL of 1-octanol to form a 0.1 M solution of monomer. A 0.1 M concentration of monomer in 1-octanol equals around 30 equivalents of reagent per mole of monomer, more than enough to approach pseudo-first order conditions.^[23] After addition of the solvent/reactant the reaction was heated to 160 °C and a t = 0 min sample (50 µL in 1 mL of acetonitrile) taken as soon as all solids had dissolved. For that point time samples were taken at 5, 10, 15, 30, 45, 60, 75 etc. min (with maximum of 4 hours). For dimethyl sebacate more samples were taken in the beginning of the reaction since aliphatic esters have higher reactivity then aromatic ones.

The change in concentration of the starting dimethyl esters was determined by the photodiode array detector (PDA) of the LC-MS. Except for dimethyl sebacate, which was analyzed by GC since it does not contain a fluorophore. Calibration curves were made from a dilution series for each monomer and the biphenyl internal standard to determine a response factor. Using this response factor the concentration of monomer at each time point was determined, after correction for the biphenyl concentration. This to limit the effects of sampling error or evaporation. Plotting the natural logarithm of the concentration versus time allows for the determination of the pseudo-first order rate constant by taking the slope of the trendline connecting these points (where the rate constant has the units of 1/min). The plot of the performed reactions can be seen in **Figure A26**.

In **Figure A26** it can be clearly seen that both the aromatic diesters, terephthalate and furanoate, are significantly slower than sebacate. The rates of both pyrazine monomers are in a similar range as that of the sebacate monomer. The polymerization rates for the pyrazine monomers can thus be expected to be similar to any aliphatic monomers and faster than fully aromatic monomers. The pyrazine monomers act as aliphatic esters in terms of reactivity. The smaller number of samples for the pyrazines and lack of statistical power makes it difficult to say whether the observed differences in the rates between the pyrazines and the sebacate are due to the pyrazine catalyzing the reaction. To determine this, further work would be necessary.

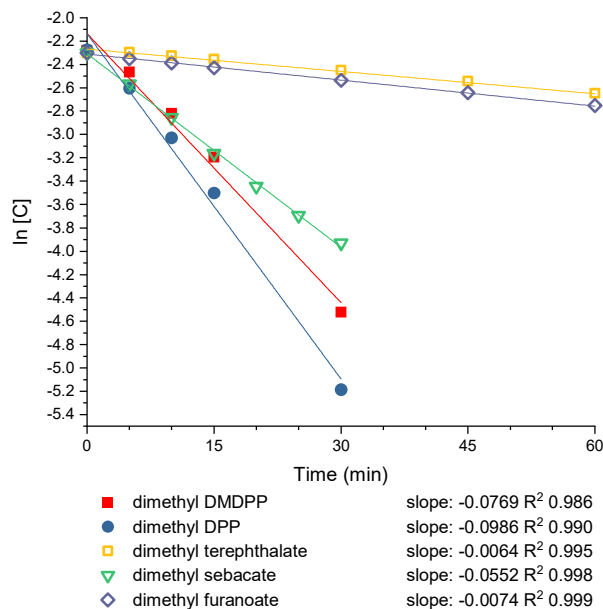


Figure A26: Pseudo-first order kinetics plot to determine relative reaction rates.

Analysis methods for kinetic study

Liquid Chromatography – Mass Spectrometry (LC-MS) analysis was performed on a Shimadzu Nexera 2 UHPLC system equipped with a Shimadzu LC-30AD pump, a SPD-M30A photodiode array detector and LCMS-2020 single quadrupole detector. The system runs on MilliQ water and LC-MS grade acetonitrile both modified with 0.1% formic acid. A Waters XSelect CSH C18 column (3.0 mm x 75 mm with a particle size of 3.5 μ m) was used operating at 30 °C. The method was set up with a gradient of 5% acetonitrile in water for 2 min, an increase to 95% acetonitrile over 6 min, 3 min at 95% followed by flushing back to 5% acetonitrile. Samples were prepared by dissolving 50 μ L the reaction mixture in 1 mL of acetonitrile.

Gas Chromatography (GC) analysis was performed on a Shimadzu GC-2010 system running on helium as the carrier gas and fitted with a Supelco SPB-1 column (3000 mm, 0.25 mm ID, 0.25 μ m film thickness). The sample was injected at an injection volume of 1 μ L using a split of 50 at 300 °C. The temperature program of the method was from 80 °C to 140 °C at 10 °C/min, a 1 min hold, a ramp to 300 °C at 20 °C/min with a final hold of 5 min.

Appendix references

- [1] J. U. Izunobi, C. L. Higginbotham, *J. Chem. Educ.* **2011**, *88*, 1098-1104
- [2] J. Brandrup, E. H. Immergut, E. A. Grulke, *Polymer handbook*, 4th edition, Wiley, New York; Chichester, **2004**.
- [3] G. Z. Papageorgiou, V. Tsanaktsis, D. G. Papageorgiou, K. Chrissafis, S. Exarhopoulos, D. N. Bikiaris, *Eur. Polym. J.* **2015**, *67*, 383-396
- [4] J. Zhu, J. Cai, W. Xie, P.-H. Chen, M. Gazzano, M. Scandola, R. A. Gross, *Macromolecules* **2013**, *46*, 796-804
- [5] G. Z. Papageorgiou, D. G. Papageorgiou, Z. Terzopoulou, D. N. Bikiaris, *Eur. Polym. J.* **2016**, *83*, 202-229
- [6] V. Tsanaktsis, G. Z. Papageorgiou, D. N. Bikiaris, *J. Polym. Sci., Part A: Polym. Chem.* **2015**, *53*, 2617-2632
- [7] V. Tsanaktsis, D. N. Bikiaris, N. Guigo, S. Exarhopoulos, D. G. Papageorgiou, N. Shirrazzuoli, G. Z. Papageorgiou, *RSC Advances* **2015**, *5*, 74592-74604
- [8] Y. Shen, B. Yao, G. Yu, Y. Fu, F. Liu, Z. Li, *Green Chemistry* **2017**, *19*, 4930-4938
- [9] J. Zhang, Q. Liang, W. Xie, L. Peng, L. He, Z. He, S. P. Chowdhury, R. Christensen, Y. Ni, *Polymers (Basel)* **2019**, *11*, 197
- [10] Y. Geng, Z. Wang, X. Hu, Y. Li, Q. Zhang, Y. Li, R. Wang, L. Zhang, *Eur. Polym. J.* **2019**, *114*, 476-484
- [11] P. Gopalakrishnan, S. Narayan-Sarathy, T. Ghosh, K. Mahajan, M. N. Belgacem, *J. Polym. Res.* **2013**, *21*, 340
- [12] M. Jiang, Q. Liu, Q. Zhang, C. Ye, G. Zhou, *J. Polym. Sci., Part A: Polym. Chem.* **2012**, *50*, 1026-1036
- [13] J. Ma, Y. Pang, M. Wang, J. Xu, H. Ma, X. Nie, *J. Mater. Chem.* **2012**, *22*, 3457-3461
- [14] G. Wang, M. Jiang, Q. Zhang, R. Wang, G. Zhou, *RSC Advances* **2017**, *7*, 13798-13807
- [15] M. Gomes, A. Gandini, A. J. D. Silvestre, B. Reis, *J. Polym. Sci., Part A: Polym. Chem.* **2011**, *49*, 3759-3768
- [16] A. Gandini, A. J. D. Silvestre, C. P. Neto, A. F. Sousa, M. Gomes, *J. Polym. Sci., Part A: Polym. Chem.* **2009**, *47*, 295-298
- [17] G. Papamokos, T. Dimitriadis, D. N. Bikiaris, G. Z. Papageorgiou, G. Floudas, *Macromolecules* **2019**, *52*, 6533-6546
- [18] V. V. Korshak, S. V. Vinogradova, V. M. Belyakov, *Bull. Acad. Sci. USSR, Div. Chem. Sci. (Engl. Transl.)* **1957**, *6*, 1029-1031
- [19] M. Cachia, *Annales de chimie.* **1959**, *S13*, 5-41
- [20] M. E. Rogers, T. E. Long, *Synthetic Methods in Step-Growth Polymers*, Wiley, **2003**.
- [21] J. Yamanis, M. Adelman, *Journal of Polymer Science: Polymer Chemistry Edition* **1976**, *14*, 1945-1959
- [22] S. S. Park, S. S. Im, D. K. Kim, *J. Polym. Sci., Part A: Polym. Chem.* **1994**, *32*, 2873-2881
- [23] F. Sicilio, M. D. Peterson, *J. Chem. Educ.* **1961**, *38*, 576

Chapter 3

Mechanical properties of poly(hexamethylene dimethyldipropionic acid pyrazine)

Based on the Master Thesis of Antonis Vasileiadis

Abstract

In this Chapter the mechanical properties of the polyester of 1,6-hexanediol with dimethyldipropionic acid pyrazine are explored. The synthesis of this polyester as well as rheology studies to determine the molecular weight between entanglements are described. All synthesized samples were below the entanglement molecular weight. Nevertheless, mechanical testing in both compression, tensile and impact provided insight on the expected Young's modulus, yield stress and impact strength at higher molecular weights. The material shows low to medium strength with a Young's modulus between 0.6-0.8 GPa and a yield stress between 20-30 MPa, similar to isotactic poly(propylene) and poly(hexamethylene furanoate). Increasing the molecular weight of the polymer using solid-state post-condensation is feasible but scaling was unsuccessful.

Introduction

The first Chapter of this Thesis describes the synthesis of new pyrazine building blocks. Since these were not necessarily designed with an application in mind, we felt that their specific properties relevant for potential applications in materials need more detailed study. Initially the thermal properties of the pyrazine building blocks were explored by synthesizing a range of polyesters, as reported in the second chapter. Depending on the composition, different thermal properties were found and the polyesters of dimethyldipropionic acid pyrazine (DMDPP) with linear diols longer than two carbons were considered the most interesting to focus our attention. These materials are semi-crystalline and relatively high melting, which opens up potential application as engineering or high-performance plastics. Detailed insight of the mechanical properties was considered necessary to further narrow-down the potential application of DMDPP-containing polyesters.

The mechanical properties of polymers are important to predict their performance under applied stress and thus for their application in materials. Most polymers show the following typical behavior when subjected to stress. At low strain ($\leq 1\%$), most polymeric materials behave elastic, the deformation is homogenous and after removal of the load the material returns to its original shape and size.^[1] In this regime, the stress (σ) is directly proportional to the strain (ϵ) and the material obeys Hooke's law (Equation (1)). Where E is the Young's modulus, a measure for the materials stiffness.

$$\text{Equation (1)} \quad \sigma = E \times \epsilon$$

At higher strain a material does not return to its original shape and size, the behavior is no longer elastic. The amount of stress needed to reach this point is known as the yield stress. Exceeding the yield stress initially results in permanent deformation while maintaining material integrity. This behavior regime continues until material failure is observed, the amount of stress needed for failure is known as the ultimate yield strength. Material failure can be either brittle or ductile. In the first case, the material breaks suddenly. In the latter case, plastic deformation is observed whereby the material flows. Ductile failure thus results in a much higher strain being reached at lower stress before the material finally breaks.

The typical elastic and plastic behavior of polymers is largely due to entanglements between polymer chains. Such entanglements play a major role in several polymer properties.^[2] They influence both thermal properties and crystallinity but more importantly are responsible for the specific mechanical properties of a material.

Without entanglements, chains can move freely and a polymer has low strength. With a sufficient number of entanglements, a physical network between the chains forms which provides resistance against deformation. On the other hand, when the level of entanglements becomes too high this results in difficulties with processing due to increased viscosity.^[3] Therefore, when a polymer shows low strength under mechanical testing this can be attributed to two factors. Either the intrinsic strength of the polymer is low or the level of entanglements is too low to form a physical network. This latter case is in turn dependent on the overall molecular weight of the polymer (its chain length) and the chain flexibility. A flexible chain has more entanglements per chain length than a stiff chain and thus forms a network more easily. In other words, a stiff chain needs to be longer to form the same network. Chain flexibility is usually expressed as the average molecular weight between entanglements (M_e).

Since entanglements play such an important role, it is crucial to determine the M_e before mechanical testing of the new materials is undertaken. Entanglements not only have a large effect on polymer properties in the solid state but also cause the viscoelastic behavior of the polymer melt. This provides a means to determine the M_e via melt rheology. A common approach to determine M_e via rheology is to perform a frequency sweep of the melt and find the rubber plateau modulus, this modulus is proportional to the M_e .^[4]

It would be most interesting to compare the mechanical properties of DMDPP-based polyesters directly with well-studied and commercial terephthalate-based polyesters such as poly(butylene terephthalate). However, the degradation temperature of DMDPP is around 190 °C, regardless of whether it has been incorporated in a polyester.^[5] The polyester with 1,4-butanediol with a melting point of around 160 °C thus has a very small processing window before degradation. Therefore, the polyester of DMDPP with 1,6-hexanediol (DMDPP-C6) was selected for our studies to determine mechanical properties. This material has a melting point of 143 °C, leaving a suitable processing window. Next to this, this melting point is close to that of the polyesters of both furandicarboxylate and terephthalate with 1,6-hexanediol allowing for comparison with these materials.^[6-8] The DMDPP-C6 polyester was thus considered the most interesting candidate to explore of mechanical properties of pyrazine containing polyesters.

This Chapter summarizes various synthetic strategies towards high molecular weight DMDPP-C6 polyester and our efforts to determine the M_e as well as the mechanical properties.

Experimental

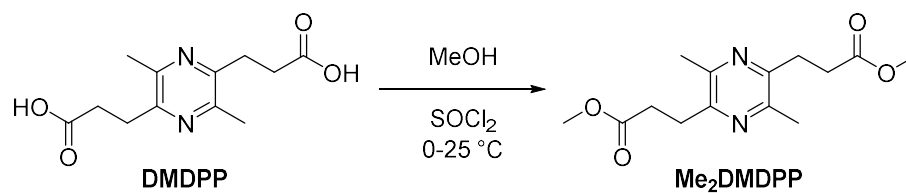
Materials

Thionyl chloride (Acros Organics, 99.7%), 4-toluenesulfonic acid monohydrate (Sigma-Aldrich, 98%), sodium bicarbonate (Acros Organics, >98%), sodium hydroxide (VWR, >98%), 1,6-hexandiol (Sigma-Aldrich, >97%) dibutyltin(IV) oxide (Sigma-Aldrich, 98%), tin(II) 2-ethylhexanoate (Sigma-Aldrich, 98%), titanium(IV) tert-butoxide (Sigma-Aldrich 99%), and m-xylene (Sigma-Aldrich, 99%) were used as received. All solvents were provided from Biosolve at least analytical reagent grade (A.R.). Deuterated CDCl_3 was provided by Cambridge Isotope Laboratories Inc.

DMDPP was synthesized according to the procedure reported in Chapter 1.

Methylation of DMDPP

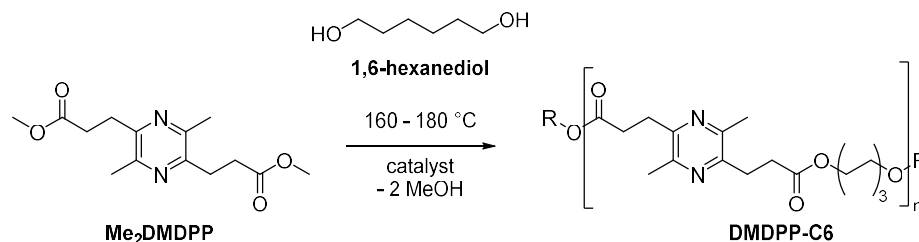
Me_2DMDPP was synthesized via two different methods. Method 1: A thionyl chloride activated esterification and Method 2: a 4-toluenesulfonic acid catalysed Fischer esterification, the latter of which is described in Chapter 2. The first is described below.



Scheme 1: Methylation of DMDPP.

A single-necked 250 mL flask equipped with a magnetic stirrer was loaded with DMDPP (4.79 g, 18.97 mmol) which was suspended in methanol (75 mL). The resulting slightly pink suspension was placed on an ice bath. Upon cooling down to 0 °C, thionyl chloride (1.53 mL, 48 mmol, 2.5 eqv.) was added dropwise, forming a cream-colored suspension. Upon complete addition, a brown solution had formed which was heated to reflux overnight. After the reaction was complete, the mixture was concentrated *in vacuo* to yield a brown oil. While on an ice bath, first a small amount of deionized water was added to the oil followed by adjustment of the pH value to 4 by addition of 80 mL 2M NaOH under vigorous stirring. While warming back to room temperature the volume was made up to 120 mL. The mixture was extracted three times with 120 mL of ethyl acetate and the organic phase was filtered over silica to remove unesterified material. The desired product Me_2DMDPP (4.78 g, 17.07 mmol, 90%) was isolated as an off-white solid after concentration *in vacuo*.

General procedure for the synthesis of DMDPP-C6



Scheme 2: Step-growth polymerization of DMDPP and 1,6-hexanediol.

A 25-100 mL three-necked tube-like or round-bottom flask was equipped with a magnetically coupled overhead mechanical stirrer, a distillation bridge with vigreux and a nitrogen inlet. This setup was placed in a heating mantle with an external temperature control. The setup was loaded with 1 eq. of Me_2DMDPP , 1.1 eq. of 1,6-hexanediol and 2 mL of xylene. The resulting suspension was initially heated to 130 °C, under open nitrogen flow without stirring. Upon reaching the set temperature and complete melting, the reaction mixture was heated up further to 160 °C and stirring started. Having reached 160 °C, the nitrogen flow was closed and either 0.005 eq. of tin(II) 2-ethylhexanoate (1 M in m-xylene), dibutyltin(IV) oxide or 400 ppm of titanium butoxide ($\text{Ti}(\text{BuO})_4$, 0.1 M in m-xylene) was added as a catalyst. The reaction was allowed to proceed for two hours at 160 °C while stirring with 90 rpm. After this time, nitrogen flow over the reaction was opened. After 1h under open N_2 flow, the temperature was increased to 180 °C and kept there for another 2h. The reaction mixture was left to cool overnight. The following day, the mixture was heated to 160 °C for 1h under open N_2 flow and for at least another 1h at 180 °C while stirring with 90 rpm. Periodic samples were taken to determine conversion and ratios of the monomers by NMR. If necessary, the reaction's stoichiometry was corrected by addition of diol or diester. When a conversion was $\geq 95\%$ was reached, the vigreux was removed and vacuum was slowly applied at $< 2 \times 10^{-2}$ mbar. The reaction was kept under vacuum with periodic sampling either until GPC or NMR confirmed that the targeted M_n was achieved or conversion was stagnant.

Isolation and purification of the polymer

When either the targeted molecular weight was achieved or the polycondensation reaction had stopped, the reaction mixture was cooled to room temperature. Afterwards between 20 mL and 80 mL of CHCl_3 was introduced to the reaction flask depending on the scale of the reaction. Upon complete dissolution, the contents of the flask were precipitated in 500 ml to 1 L of cold MeOH under vigorous stirring (600 rpm). The resulting colorless threads were filtered over a glass filter (pore size 4) and dried *in vacuo* at 40 °C for at least 18h.

Preparation of cylinders

A 12 mm diameter mold of 15 mm high was filled with the precipitated strands of DMDPP-C6 and placed between the plates of the Collin Laboratory Platen Press P200E at 175 °C without any pressure. After 3 min in the melt, the mold was removed and more material was added, until the height of 1 cm was reached. At this point, an instant load of 7 bar was applied and released. This was repeated three to four times in order to remove any bubbles from the cylinders' surface. Subsequently the press was left to cool to room temperature and the cylinders were removed from the mold. The cylinders were dried *in vacuo* at 40 °C overnight before testing under uniaxial compression.

Preparation of tensile bars

The deformed cylinders that were used in the compression tests were dissolved in 50 mL of CHCl_3 . The resulting mixture were first filtered over a Buchner filter with an additional 25 mL of CHCl_3 , some solid impurities and dust remained. These were removed by filtration over a coffee filter. The filtrate was cast on a Teflon petri dish, covered with perforated aluminum foil and left to evaporate. The resulting films were of low quality due to rapid evaporation. The cast films were dried *in vacuo* at 40 °C overnight and broken in small pieces. These subsequently placed in a homemade rectangular mold (7.5 cm x 10 cm), sandwiched between Kapton film coated steel plates and compressed in a Collin Laboratory Platen Press P200E. A 5 bar load was applied at 175 °C for 2 minutes after which the pressure was increased at 40 bar for 1 minute. The mold was left to cool down to 20 °C in approximately 10 minutes, maintaining pressure. Finally, the pressure was released and the film was removed from the mold. From the resulting films, mini-tensile bars were punched into 13 x 2 x 0.3 mm (gage length x width x thickness) dogbones.

Preparation of impact bars

For the preparation of impact bars, a batch of polyester (batch 5) was synthesized and purified by the general procedure. The resulting material was processed in a DSM Xplore twin-screw micro-extruder with a barrel size of 5 mm operating at 100 rpm for 1 minute at 180 °C and immediately injected into a pre-heated (180 °C), rectangular mold with dimensions 10 cm x 1.0 cm x 4 mm (length x width x height).

Characterization

Nuclear Magnetic Resonance (NMR) spectra were recorded on a Bruker Avance III 300 MHz apparatus at room temperature. ^1H -NMR experiments were carried out with 16 scans, using 5 mg of material. ^{13}C -NMR APT experiments were carried out with 1024 scans, using 50 mg of material. The obtained NMR data were used to determine the conversion of the end groups and the degree of polymerization. This data was also used to determine the ratio of the constituents of the chains by comparing the normalized integrals of the monomeric units in the polymer chain.

Gel permeation chromatography (GPC) was conducted on a Shimadzu Prominence-i LC-2030 HPLC system fitted with a Shimadzu RID-20A detector. The measurements were run with isocratic elution of chloroform at 1 mL/min on a Shodex KF-805L column (10 mm by 300 mm, 10 μm pore size) operating at 40 °C. Samples were prepared by making 1 mg/mL solutions in chloroform and filtered over a 0.2 μm PTFE filter. GPC was used to determine the molecular weight distribution of the obtained polymers as compared to polystyrene standards.

Differential scanning calorimetry (DSC) thermograms were recorded on 2 to 7 mg samples in pierced lid pans on a Netzsch Polyma 14 machine at heating and cooling rates of 10 °C/min from -40 °C to 200 °C with 3 min isothermals at those temperatures. Two temperature cycles were measured with the melting (T_m) and crystallization temperatures (T_c) of the second cycle being reported. Glass transition temperatures (T_g) are reported as the inflection point of the first observed change in enthalpy in the second cycle.

Rheological Measurements, the viscoelastic properties of the synthesized polymers were investigated on an Anton Paar MCR 702 MultiDrive rheometer. The measurements were conducted in oscillatory shear mode with a plate-plate geometry. The plates were 15 mm and 50 mm in diameter, with a 1.000 mm gap for all the measured samples.

Compression Test

The cylinders used for the test were prepared as described above and subjected to uniaxial compression on a Zwick/Roell Zo20 table-top universal testing machine with a maximum test load of 20 kN. Before the measurements, frame compliance was recorded. The compliance was 3.618 $\mu\text{m}/\text{N}$ and the applied true strain speed 0.001/s. Samples were covered with polyethylene tape on both testing surfaces and a drop of dishwashing detergent in water was added to ensure the load was divided equally over the entire sample surface.

Tensile Test

Tensile tests were performed using a Linkam TST350 tensile stage, equipped with a temperature controller (operating range $-190\text{ }^{\circ}\text{C}$ to $350\text{ }^{\circ}\text{C}$) and a 200 N load cell. Per sample 5 tests were conducted at both room temperature ($\sim 25\text{ }^{\circ}\text{C}$) and at $-20\text{ }^{\circ}\text{C}$ with a strain rate of 100 $\mu\text{m}/\text{s}$. The samples were cooled for 5 minutes before the beginning of the measurement to be completely frozen.

In both the compression and tensile tests, the Young's modulus was determined by taking the slope of the stress-strain curve immediately after the start of the measurement. The yield stress, σ_y , was calculated by determining the 1% offset yield strain, forming a line with a slope equal to the Young's modulus with that yield strain as the x-intercept, and locating the point where this line intersected the stress-strain curve. The maximum stress was determined by finding the local maximum of the stress-strain curve before fracture of the samples occurred. For the compression tests, elongation was taken as the maximum strain and represents compressibility. For the tensile tests, elongation at break was taken as the strain at the abrupt loss of stress.

Impact Test

Impact tests were carried out on a Zwick/Roell HIT5.5P Pendulum Impact Tester at room temperature, according to ISO 180 standard (Notched Izod Impact Test). Three measurements were collected, on impact bars that had been prepared by injection molding. Before the test, the specimens were notched, with a V-shaped notch, in the direction of the blow. Each sample was fixed vertically, and it was broken by striking it from the notched side. All the samples broke completely. The Izod impact value (kJ/m^2) was calculated by dividing the fracture energy by the width of the specimen.

Results and discussion

Synthesis of DMDPP-C6

The aim of this work was to determine the mechanical properties of DMDPP-C6. Mechanical properties are highly dependent on several factors such as, thermal properties, processing conditions, crystallinity and molecular weight. As stated in the Introduction, the importance of the molecular weight on the mechanical properties is due to entanglements. The small-scale reactions of DMDPP-C6 described in Chapter 2 already resulted in relatively high molecular weight. A batch with a M_n of 33000 g/mol could be cold-drawn, a good indicator of sufficient entanglements for good mechanical properties. This molecular weight was thus considered the minimum required for representative mechanical properties.

To determine at which molecular weight sufficient entanglements are present, several polymerization reactions of Me₂DMDPP with 1,6-hexanediol were performed (see **Table 1**). In all cases, the progress of the reactions was followed by ¹H-NMR spectroscopy studies and any monomer depletion was compensated immediately to maintain a stoichiometry. Upon reaching 95% conversion, vacuum was applied and the reactions tracked by GPC analysis of periodic samples. A series of several increasing molecular weights was targeted and when a desired weight was reached, the polymerization was considered complete and stopped.

In our experiments, two different types of catalysts were used. Initially, tin(II) 2-ethylhexanoate (SnOct₂) was selected, since this performed well in the small scale batch-reactions described in Chapter 2. On larger scales however, SnOct₂ did not increase the molecular weight as fast as expected, with the reaction taking multiple days. Therefore we decided to use dibutyltin(IV) oxide (DBTO) instead, which showed a definite increase in reaction rates for a similar polymerization.^[9] This increase in rate was also found in our reactions. The final molecular weights values for the synthesized polymers were determined via chloroform GPC. GPC analysis was also performed after several processing stages and these values will be used throughout the rest of this chapter.^[10]

Table 1: Overview of the performed polycondensations at 160 – 180 °C.

Batch	Scale (g)	Polymer Isolated (g)	M_n (g/mol) GPC	M_w (g/mol) GPC	\bar{D}	Catalyst	Diol conversion (%)	Reaction time (h)	M_n (g/mol) $^1\text{H-NMR}^{[11]}$
1	5	4.9	25000	53000	2.1	SnOct ₂	92	20	6600
2	10	6.8	22000	42500	2.0	SnOct ₂	95	54	8900
3	10	7.0	40000	72000	1.8	SnOct ₂ /DBTO	98	41	21100
4	10	7.0	64000	121000	1.9	DBTO	99	36	40800
5	30	17.0	42000	89500	2.1	DBTO	99	43	29400

Thermal properties - Crystallization study

Since DMDPP-C6 is a semi-crystalline polymer and crystal polymorphism can have a major effect on the mechanical properties of a material, it was important to investigate the crystallization behavior.^[12] Several batches of DMDPP-C6 had already been made while developing the synthesis procedure and subjected to DSC analysis. These were all found to have two melting points with no negative enthalpy in between. These two melting points could either be due to different polymorphs or arise due to differences in lamellar thickness. An average batch of DMDPP-C6 ($M_n = 35,000$ g/mol, $\bar{D} = 2.0$) showed a glass transition temperature (T_g) of 4 - 6 °C, a melting temperature (T_m) of 145 °C ($\Delta H_m = 65$ J/g) and a crystallization temperature (T_c) of 106 - 110 °C ($\Delta H_{cryst} = -80$ J/g) when measured at 10 °C/min.

In order to determine whether crystallization should be considered for the mechanical testing, a sample of DMDPP-C6 (batch 1, $M_n = 25,000$ g/mol, $\bar{D} = 2.1$) was subjected to different cooling rates. These rates were 1 °C/min, 5 °C/min, 10 °C/min and 20 °C/min while the heating rate was kept constant at 10 °C/min. The results from the second cooling and second heating cycles are depicted in **Figure 1**. These data show that the 10 °C/min heating and cooling graph is very similar to the previously measured batches of DMDPP-C6 at these rates; the material is thus a representative sample.

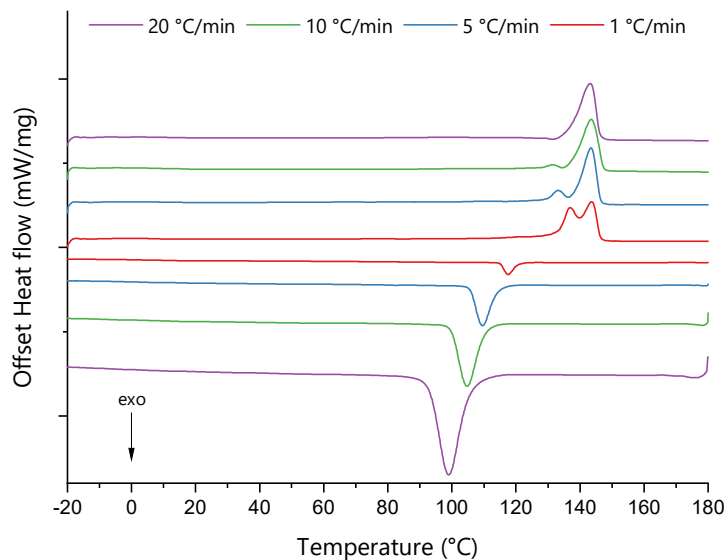


Figure 1: DSC measurements at different cooling rates on the polyester, heating rate constant at 10 °C/min.

When we examined the crystallization temperature, a drop to lower temperatures combined with an increase in enthalpy was observed at increasing cooling rates. This behavior can be attributed to the effect of undercooling on the crystallization kinetics.^[13] In short, if crystallization can take place at a high temperature and the sample is rapidly cooled below this point, the apparent crystallization temperature will be lower and the corresponding enthalpy higher.

Turning towards the melting temperatures, regardless of the cooling rate, the highest melting peak remains around 143 °C. This suggests that this peak is associated with the most stable crystalline phase. An interesting observation is that at the lowest cooling rate, a lower melting peak increased significantly. This behavior is opposite of the usual effect seen for polymers, described by the Hoffman-Lauritzen chain folding theory.^[14] Low cooling rates usually result in slower crystallization, thus better crystals, which in turn melt at higher temperatures. This unexpected behavior is however also observed in the structurally relatively similar poly(hexamethylene terephthalate)(PHT).^[7] In PHT up to 5 different melting enthalpies are observed depending on cooling and heating rates, the highest melting of these is only observed at crystallization temperatures close to the melt. The observed melting at 143 °C might thus not be the most stable crystal. At lower crystallization temperatures, the 5 enthalpies change in intensity and the corresponding crystals may undergo reorganizations.

Such reorganizations, although not resulting in an observed negative enthalpy, are most likely the cause of the apparent deviation from theory in DMDPP-C6. This is corroborated by the lower melting enthalpies for the crystals formed at higher rates, compared to those at lower rates. Besides this, lower rates also result in a smaller difference between the melting and crystallization enthalpy, suggesting less reorganization has to take place.

Since all the observations above indicate complex crystallization behavior and thus polymorphism, the question arises whether these fine details matter for the mechanical properties. In this regard and considering that, the real-world cooling rates for the samples will be in the range of 10 to 20 °C/min and up, the differences between these two rates are minimal. This, combined with the fact that the highest melting crystal dominates, we conclude that for initial determination of properties, crystallization does not need to be taken into account.

Rheological measurements

As stated in the Introduction entanglements play a major role in the mechanical properties of polymers. With too little entanglements, mechanical properties are not yet stable and interpretation of mechanical tests is difficult. It is therefore imperative that the entanglement molecular weight (M_e) of DMDPP-C6 is determined or that it is at least known whether an entanglement network was present. To address this frequency sweep measurements at different temperatures of three batches of DMDPP-C6 (batches 1, 3 and 4 in **Table 2**) were performed. We anticipated that with the obtained data, the rubber plateau and thus the M_e could be determined.

Prior to the determination of the M_e , the *linear viscoelastic region* (LVE) was determined by performing an amplitude sweep at constant angular frequency ($\omega = 10$ rad/s) and temperature (180 °C). This region indicates the range in which the test can be carried out without perturbing the equilibrium structure of the sample.^[15] From this we concluded that measurements between 0.1 to 100 rad/s at 1% strain would be within the limits of linear viscoelasticity, working in the optimum torque range of the transducer and still within reasonable experiment times. As such, frequency sweeps were performed under those conditions at different temperatures. Initially the test temperatures were between 180 and 130 °C. For both batches 1 and 3 it was found that some degradation took place at 180 °C, as determined by significant discoloration of the sample. To prevent this, batch 4 was only measured up to 160 °C.

Table 2: Polyester properties and experimental temperatures for the M_e determination measurements.

Batch	M_n (g/mol)	M_w (g/mol)	\bar{D}	Temperature range (°C)	M_n (g/mol) after	M_w (g/mol) after
1	25000	53000	2.1	180-130	26500	51000
3	40000	72000	1.8	180-130	50000	94500
4	64000	121000	1.9	160-130	67000	132500

For the lowest molecular weight material, polyester 1, an oscillatory response was obtained in the storage modulus G' at low frequencies regardless of temperature (see **Figure A1**). This is most likely due to low viscosity resulting from the low molecular weight. It can be stated that the material shows little to no entanglements and can therefore be excluded from further discussion.

The two other molecular weights reveal an important aspect. The loss modulus (G'') lies above the storage modulus (G') suggesting that the dynamics of the polymer are most likely in the terminal regime.^[16] Here the measured dynamics are mostly due to diffusion of the bulk material and no chain dynamics are observed, the material behaves mostly as a Newtonian fluid. The anticipated power laws for this regime i.e. $G'(\omega) \propto \omega^2$ and $G''(\omega) \propto \omega$ however, are not obeyed as is evident in the storage modulus data. Both moduli do scale differently with frequency confirming the terminal regime is observed. The deviation from the expected power laws might be due to two reasons. Either, the dispersity of the samples, which is about two, contributes to deviations from the expected response. Or, the observed behavior at low frequencies is due to the presence of transient interactions such as hydrogen bonding. Such interactions would prevent large-scale motion (terminal relaxation) of the chains (or fraction of the chains), giving rise to the non-ideal behavior together with dispersity effects. In other words, the friction that chains experience is not uniform.

To determine M_e it is necessary to find the plateau modulus, a regime where G' is stable regardless of measurement frequency. Since none of the measurements manifest a cross-over between G' and G'' this means that a plateau modulus is not reached and M_e cannot be determined. Further cooling of the samples to obtain a measurement window where the plateau modulus would be visible was not a viable option, due to crystallization of the polyesters. This was already clearly observed at low frequency in batch 4, where the modulus increases rapidly. The degree of convergence between the moduli suggest that the crossover point could be reached, under the applied measurement conditions if the M_w of the polyester was approximately twice as high as batch 4 (121kDa).

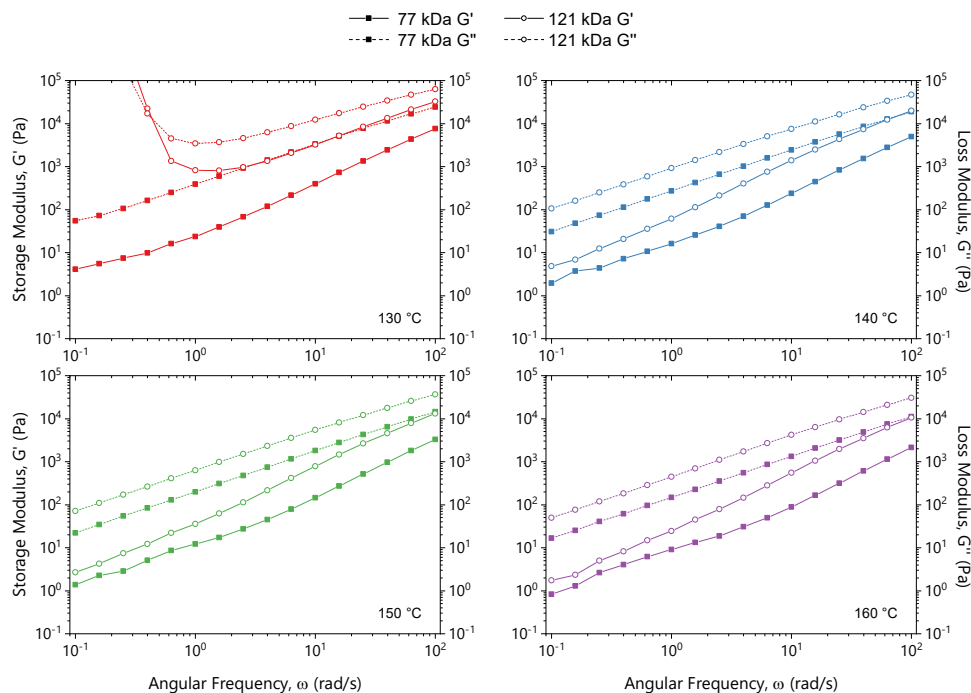


Figure 2: Storage (G') and the loss (G'') moduli for batch 3 (squares) and batch 4 (circles) at four different temperatures.

After both experiments were finalized, samples of both polymers were analyzed by GPC to track if any changes occurred in the molecular weights. It was found that an increase of the initial values of the polyesters could be observed together with significant color changes. The length of the measurements at elevated temperature in air might be the cause of these differences. Taking into account the thermal instability of the polymer, as shown in Chapter 2, processing should either be fast or take place under inert atmosphere.

Compression Test

As stated in the Introduction, testing the uniaxial compression is the best first approach to determine the mechanical properties of DMDPP-C6. However, with unknown M_e more cautious interpretation of any mechanical data is necessary. Nevertheless, we proceeded with compression testing. To prepare the samples two batches of polyester with different molecular weights were molded into cylinders as described in the experimental section. A total of ten cylinders was prepared; five from each batch (batches 3 and 4 in **Table 1**). After this, GPC measurements show that under used processing conditions there was a significant reduction in molecular weights (see **Table 3**). This reduction can be attributed to the polymer degradation at

processing temperature (175 °C) or to the material not being dried prior to processing resulting in some hydrolysis. These noticeable losses signify that processing conditions should be reconsidered in future studies.

Table 3: Differences in molecular weight before and after formation of cylinders as determined by GPC.

Batch	M_n (g/mol) before	\bar{D} before	M_n (g/mol) after	\bar{D} after	Difference (%)
3	40000	1.8	33000	1.9	-17
4	64000	1.9	42000	2.0	-35

The samples were still considered acceptable for testing. Prior to the compression test, the cylinders were dried *in vacuo* at 40 °C to prevent any plasticizing effect of water. The initial dimensions of the specimens can be found in the appendix (**Table A1**). The dried cylinders were measured and the obtained average true stress-strain curves can be found in **Figure 3** (the individual data can be found in **Figure A2** and **A3**).

The materials behaved fully ductile as can be concluded from the shape of both averaged curves. No fracture was found after the initial elastic regime up to the machine limit of 20kN except for one sample. The Young's modulus of both materials was found to be between 0.6 to 0.8 GPa, which is relatively low compared to other semi-aromatic polyesters, but higher than poly(caprolactone) (PCL) and similar to both poly(caprolactam) (PA6), isotactic poly(propylene) (iPP), poly(hexamethylene terephthalate) and poly(hexamethylene furanoate).^[17-19]

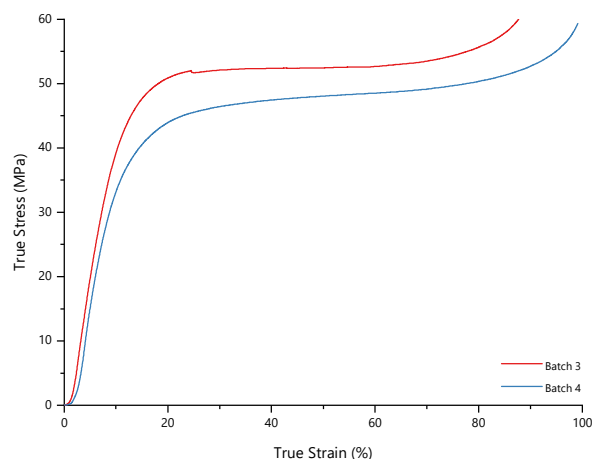


Figure 3: Average true stress – true strain curves for batch 3 and 4 under uniaxial compression.

A low Young's modulus is not unexpected for DMDPP-C6 considering the low T_g of the polymer. Having measured well above T_g the amorphous phase between the crystallites is highly mobile and thus little stress needs to be applied to achieve

significant strain. The yield stress of the materials was between 35 and 45 MPa after which minimal to no plastic flow was observed. This latter effect might be due to high crystallinity leaving little amorphous phase to deform, with the crystallites themselves being tough not brittle. The fact that the higher molecular weight batch 4 showed a lower yield stress but longer elongation is likely also due to crystallinity. Higher molecular weight materials usually show lower degrees of crystallinity due to crystal imperfections and impeded chain folding. Consequently, the larger amorphous fraction results in a lower Young's modulus, lower yield stress and a higher elongation. The calculated average values of the mechanical properties for batches 3 and 4 are summarized in **Table 4**. The materials also showed strain hardening as indicated by the rising stress at high strains. Having reached the machine limit without failure however, it cannot be determined whether this hardening is due to material properties or the measurement method.

Regardless of molecular weight, the polyester behaves mostly ductile and is of relatively low strength. The fact that rheology indicated that the entanglement network seems low was not confirmed by early brittle failure. Due to its geometry, a compression test does not always show such failure. Examining the samples after testing showed that the edges of the cylinders had small tears. These could be caused by different failure mechanisms, among which brittle failure due lack of entanglements.

Table 4: Average compressive mechanical properties for batches 3 and 4 with standard deviations.

Batch	Young's Modulus (MPa) [std]	Yield Stress (MPa) [std]	Ultimate Yield Strength (MPa) [std]	Maximum strain (%) [std]
3	787 [166]	28.8 [5.8]	66.8 [6.4]	60.4 [1.2]
4	675 [60]	25.4 [3.0]	64.0 [2.7]	64.2 [1.4]

Tensile Test

The prevalent failure mechanism of a material is often probed by tensile testing. This testing method was not initially used because traditional injection molded tensile bars require significantly more material than the cylinders used for compression testing. Having obtained mechanical data via compression, we felt it appropriate to use a less accurate mini tensile stage to investigate the failure mechanism. An added advantage of the use of this mini tensile stage is that it allows for cooling of the sample below the T_g . Temperature has a significant effect on the material's mechanical performance by limiting chain mobility below T_g . To prepare samples the cylinders used in the compression test were dissolved in chloroform, cast and finally compressed into a film (see experimental). Each of the molecular weights tested in compression was formed into their own film to compare the effect of molecular weight. Prior to the

measurements, the effect of the dissolution and reprocessing was examined by GPC. The molecular weights of both films had dropped significantly when compared to the cylinders used for compression testing as can be seen in **Table 5**, this is most likely due to the effects of residual moisture. Besides this, both films contained significant impurities (e.g. dust) resulting from processing (see **Figure 4**). The tensile bars were punched attempting to limit the influence of these impurities. As such, the two polyesters were nevertheless subjected to tensile measurements at two different temperatures as described in the experimental.

Table 5: Differences in molecular weight before and after the dissolution of the cylinders and the subsequent compression into thin films as determined by GPC.

Batch	M_n (g/mol) before	\bar{D} before	M_n (g/mol) after	\bar{D} after	Difference (%)
3	33000	1.9	24000	2.2	-27
4	42000	2.0	27500	2.2	-35

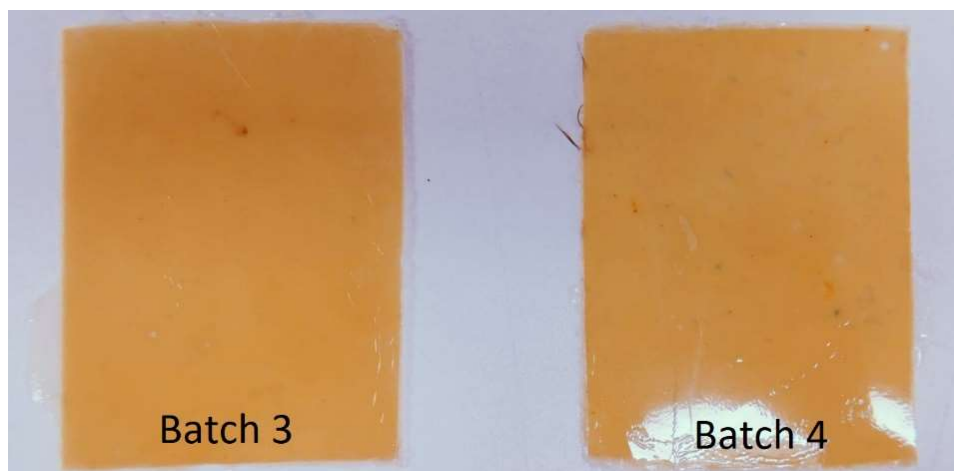


Figure 4: Compressed films of batch 3 (left) and batch 4 (right).

The stress-strain curves at room temperature (see **Figure 5 A and B**) and the resulting data (see **Table 6**) reveal a significant effect of impurities on the mechanical properties. For the film with the least impurities, a Young's modulus close to that of the compression test is observed. This, can therefore be considered a representative modulus for DMDPP-C6 at low molecular weights. The effect of impurities on the Young's modulus is quite large, dropping by about 25%. The yield stress is slightly lower than obtained by compression testing, this however, is most likely a molecular weight effect. The ultimate yield strength is significantly lower in tensile than compression, this is most likely due to the measurement geometry.

The tensile test reveals the actual failure of the material where the compression test did not. The ultimate yield strength of DMDPP-C6 is between 30 and 40 MPa, with a strain at break between 13 and 70%. Two major factors determine the measured yield strength and strain at break. First, the impurities in the film clearly cause early failure. Second, the lack of entanglement network at the measured molecular weight resulting in non-representative values for the material properties. Although the Young's modulus and ultimate yield strength are reasonably reproducible, the measurement also show that the elongation at break is not. This is most likely due to both the impurities as well as the low molecular weight.

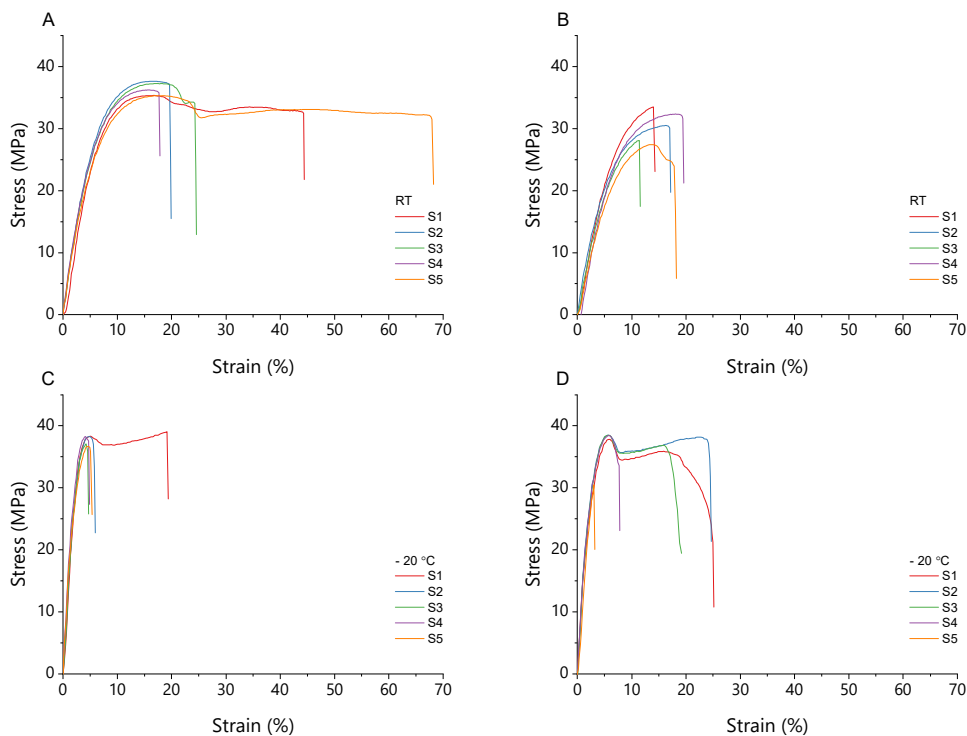


Figure 5: Stress – strain curves under tension for batch 3 (panel A) and batch 4 (panel B) at room temperature and the stress – strain curves under tension for batch 3 (panel C) and batch 4 (panel D) at – 20 °C.

Table 6: Average tensile mechanical properties for batches 3 and 4 at room temperature and -20 °C.

Batch	Temperature (°C)	Young's Modulus (MPa) [std]	Yield Stress (MPa) [std]	Ultimate Yield Strength (MPa) [std]	Elongation at break (%) [std]
3	25	613 [23]	23.5 [1.7]	30.4 [2.4]	35 [19]
4	25	469 [39]	19.9 [2.1]	36.4 [1.0]	16 [3]
3	-20	1457 [59]	36.0 [0.9]	38.1 [2.2]	8 [6]
4	-20	1344 [60]	33.6 [0.3]	36.7 [3.1]	16 [9]

Turning towards the changes in mechanical properties below T_g , the Young's modulus shows a significant increase (see **Figure 5C and D**). This was expected based on lack of mobility in the amorphous phase below T_g , stiffening the material. The effect of impurities is also significantly less as both samples show a modulus within the standard deviation. Because of rigidity in the amorphous phase, the yield stress shows a small increase. The ultimate yield strength and elongation at break of the sample with impurities remain virtually the same above and below T_g . This indicates that the impurities dominate the mechanical behavior of this sample. The other sample on the other hand, shows the expected effect of increased rigidity below T_g , a decrease in elongation at break and an increase in ultimate yield strength. Also, below T_g the reproducibility of the elongation at break is lacking.

Summarizing, DMDPP-C6 shows similar behavior in tensile as in compression, when it concerns the Young's modulus. Besides this, the expected effects of measuring below T_g are observed. Failure of the samples is predominantly brittle at this molecular weight due to lack of entanglements. Higher molecular weight will most likely show more ductile behavior as observed for some of the samples.

Impact Test

Generally, an impact test is used to determine material behavior under high strain-rates. Such a test is also employed to assess resistance of a material against rapid and sudden applied loads. The impact value obtained provides a measure for the toughness of a material, the capacity to absorb energy and deform without fracturing. The higher the impact value of a material is, the higher the toughness of the material. An impact test can also give an indication on which fracture mode, brittle or ductile, is prevalent. As such, impact tests are often performed to determine whether materials are suitable for high strain applications and when precautions should be taken against catastrophic failure.

We performed impact tests on DMDPP-C6 to have some indication of the expected toughness. To prepare impact bars a large batch of polymer (batch 5 in **Table 1**) was

synthesized, which was found to have a $M_n = 42000$ g/mol and $\bar{D} = 2.1$. Unfortunately, this molecular weight was rather low taking entanglements in to consideration. Nevertheless, seventeen grams of the polyester were processed into impact bars with the dimensions listed in **Table 7** below:

Table 7: Specifications of the impact bars.

Specimen	Length (mm)	Width (mm)	Height (mm)	Weight (g)	Impact value (kJ/m ²)
1	70	9	4	3.18	3.36
2	65	9	4	2.63	4.02
3	65	9	4	2.94	3.62

Weighing each plate showed more than half of the initial amount of the material was lost during the extrusion. This did result in deviation from the dimensions required for an ISO 180 standard test (80 x 10 x 4 mm). In addition, the lack of initial material and the loss during processing meant the sample pool was rather small, as a typical sample pool for this test requires at least 10 samples.

An Izod style test was performed nonetheless (see characterization) and the Izod impact value (kJ/m²) was calculated by dividing the fracture energy by the width of the specimen. An average value of 3.67 kJ/m² was obtained, this is about half the value of commercial poly(butylene terephthalate) grades (~5.3 kJ/m²), about one third of poly(ethylene terephthalate) grades (~9.0 kJ/m²) and similar to isotactic poly(propylene) (~2.7 kJ/m²).^[18] To take into consideration the effect of processing at relatively high temperatures, GPC data were recorded after processing. After processing, the molecular weight was $M_n = 36.000$ g/mol with $\bar{D} = 2.0$, indicating degradation had taken place. The fracture interface of the samples was also mostly straight, indicating brittle failure due to low entanglements. The obtained impact value can thus most likely be considered a lower limit for DMDPP-C6 and higher molecular weights might result in a decent engineering plastic. Besides this, the degradation again confirms that care must be taken when processing this polyester and that the processing window is small.

Mechanical properties overview

The obtained mechanical property data for DMDPP-C6 is summarized below in **Table 8**, together with relevant literature data for comparable polymers. Although comparison with literature data is usually hindered by differences in processing and experimental conditions, the observed trends in properties are representative. From the comparison between different materials, it can be concluded that DMDPP-C6 has a Young's modulus is similar, to slightly higher than other 1,6-hexanediol aromatic polymers. Compared to linear aliphatic polyesters such as PCL, the Young's modulus

of DMDPP-C6 is significantly higher, while when comparing to PBT and iPP the Young's modulus is lower for DMDPP-C6.

Comparison of the yield stress is unfortunately not possible due to lack of data and different definitions. However, the ultimate yield strength can be compared. For DMDPP-C6 this similar to PHF and iPP while being slightly lower than the yield strength of PBT. The accompanying elongation at break is very low for DMDPP-C6 but this can attributed to the low molecular weight of the analysed samples as state above.

The overall properties of DMDPP-C6 at the measured molecular weight are comparable to other 1,6-hexandiol aromatic polyesters and slightly lower than PBT and iPP. Considering the lack of entanglements and processing condition optimization DMDPP-C6 can be considered a low to medium strength engineering plastic.

Table 8: Overview and comparison of DMDPP-C6 properties with other hexanediol polymers and comparable polymers.

	Young's modulus (GPa)	Yield stress (MPa)	Ultimate yield strength (MPa)	Elongation at brake (%)	Impact value (kJ/m ²)
DMDPP-C6	0.6 – 0.8	20 – 30	30 – 40	16 – 35	3.7
poly(hexamethylene furanoate) ^[8, 17, 19-20]	0.4 – 0.8	-	28 – 37	160 – 220	-
poly(hexamethylene terephthalate) ^[17]	0.4 – 0.5	-	25 – 30	400 – 500	-
poly(caprolactone) ^[21]	0.3 – 0.4	10	15 – 17	400 – 700	-
poly(butylene terephthalate) ^[18]	2.6	-	52	200 – 300	5.3
isotactic poly(propylene) ^[18, 22]	1.2 – 1.4	-	35	500 – 700	2.7

Solid state post-condensation (SSP)

Rheology had revealed that the molecular weights initially used to determine the mechanical properties were below the entanglement molecular weight, making the obtained data less representative. During the synthesis of the different batches of DMDPP-C6 it was found that increasing the molecular weight was difficult. This is most likely due to the reaction becoming diffusion limited, the last methanol and especially 1,6-hexandiol condensate cannot be removed effectively at 180 °C to obtain higher conversions. In most other cases, a polycondensation would be heated to higher temperature to overcome this limitation. In the case of DMDPP-C6 however, this is not possible due to the degradation temperature of the polymer.

It was therefore decided to attempt solid-state post-condensation (*SSP*) on DMDPP-C6 to increase the molecular weight.^[23] *SSP* is a technique initially developed for the synthesis of polyamide 4.6. This polyamide has a high melting point and very interesting mechanical properties but also suffers from a relatively low degradation temperature. To obtain polyamide 4.6 of sufficient molecular weight for applications, a low molecular weight pre-polymer is treated in a stream of hot nitrogen below the melting point. This results in further condensation of the end-groups without degradation taking place, increasing the molecular weight. *SSP* has successfully been used in the finishing of other polymers as well and is especially useful for semi-crystalline polymers. This latter fact is due to the end-groups of semi-crystalline polymers mostly residing the amorphous phase between crystallites effectively increasing the end-group concentration and making further condensation easier.

To test whether *SSP* would be suitable for DMDPP-C6 a new batch of the polymer was synthesized at 10 g scale (batch 6). Initially, a sample for *SSP* was placed on a TGA pan and then heated isothermally under a stream of nitrogen for 24 hours at 130 °C. This results in a weight loss of 2% and an increase in M_n (GPC) from 18200 g/mol (D 2.6) to 66600 g/mol (D 2.0). This significant increase indicated *SSP* was indeed a viable means to obtain high molecular weight DMDPP-C6. Scale-up of the procedure was subsequently attempted by various means, for which the polymer was first ground into a fine powder.

A thin layer of powder was heated in an oven at 130 °C for 18 hours, either under nitrogen or under vacuum (10 mbar) resulted in no appreciable increase of molecular weight. Indicating a stream of nitrogen is necessary for any formed condensate to be removed and drive the post-condensation or the vacuum is not deep enough to achieve the same. To this end, a specially designed reactor was employed consisting of a 2.5 cm diameter glass frit at the bottom of a glass tube with a gas inlet at the bottom. The gas inlet is fed by a glass coil encircling the tube eight times. A small amount of polymer powder was placed on the frit and the entire reactor submerged in a 130 °C oil bath while a low flow of nitrogen (<0.5 L/min) was fed through the coil for 18 hours. No physical changes were observed in the powder, but GPC analysis revealed that the M_n had increased to 55000 and 70000 g/mol when two different samples were taken. The inhomogeneity of the reaction and the small scale of the reactor (maximum of 500 mg) are the major issues and a different system was sought.

Since a proper large-scale fluidized bed reactor was not available, a flask with magnetic stirring in an oil bath at 130 °C under nitrogen flow was used to improve mixing. The setup displays a large difference in temperature. At the top 80 °C was observed, while at the walls of the flask temperatures of 130 °C were recorded. Next to this, significant

sintering of the polymer powder on the walls took place and sampling of different spots in the reactor gave different molecular weights. The reaction worked to some extent with the M_n increasing from 18200 g/mol to 35000 g/mol, however this is still below the entanglement molecular weight and inhomogeneous.

To improve mixing, rotation seemed the best available approach to obtain a homogenous *SSP* system. A rotavap was therefore adapted by fitting it with a nitrogen inlet via a long hollow rod. This setup was fitted with a 250 mL flask filled with about 10 grams of freshly synthesized polymer powder which was heated to 130 °C under low nitrogen flow (<0.5 L/min). This setup was left for a total of 18 hours with periodic sampling. The M_n increased from 19400 g/mol to 24000 g/mol and in this case, the material proved homogenous. An attempt to push the reaction further using deep vacuum in this system ($1.0 \cdot 10^{-2}$ mbar) did not increase the molecular weight either. The small increase in M_n was attributed to the limited heat transfer from the wall of the rotating flask to the middle of the polymer powder.

To improve the heat transfer the reaction was repeated in a Kugelrohr apparatus, which provides even heating due to its glass oven. The Kugelrohr unfortunately only accommodated 5 grams of polymer powder but running this at 130 °C under nitrogen flow for 24 hours increased the M_n from 19400 g/mol to 33000 g/mol. A further 12 hours under vacuum ($1.0 \cdot 10^{-2}$ mbar) pushed the M_n to 51000 g/mol.

Overall, *SSP* seemed to work reasonably well for DMDPP-C6. However, limitations in equipment prevent the formation of high enough molecular weight material to reach a significant entanglement network. The lack of a heated nitrogen gas source is a severely limiting factor for the tested reactions, especially considering the success of the TGA test experiment. Therefore, a properly heated nitrogen gas source together with a higher molecular weight starting polymer should result in a good *SSP* reaction in DMDPP-C6 circumventing the degradation temperature/diffusion limitation issues of the melt polycondensation.

A final attempt towards an increased molecular weight starting polymer to serve as input for an *SSP* reaction was performed by use of the very active polymerization catalyst titanium butoxide.^[24] Unfortunately, this catalyst did not result in a significantly higher molecular weight (M_n 34500 *D* 2.2) compared to that obtained with tin-based catalysts. More thorough screening and optimization of both the reaction conditions as well as the catalysts type, loading and diol feed will be necessary to eventually obtain high molecular weight DMDPP-C6, with or without the use of *SSP*.

Conclusions

This Chapter describes our pursuit to determine the mechanical properties of the co-polyester of 1,6-hexanediol with the pyrazine-containing monomer DMDPP. The goal was to establish a potential application niche for this material. The synthesis of the polymer works well, especially after switching to a more active catalyst (dibutyl tin(VI)oxide). A few batches of different molecular weights were obtained for mechanical testing. With DSC we found that, although DMDPP-C6 is semi-crystalline, the crystallinity and cooling rates do not necessarily need to be considered in the initial determination of the mechanical properties. Rheological measurements of the synthesized batches show all of them to be below the entanglement molecular weight. The obtained mechanical properties are thus only an indication of the final properties. Mechanical testing was nevertheless performed and the properties of DMDPP-C6 were similar to both iPP as well as aromatic 1,6-hexanediol-based materials. Higher molecular weight material still needs to be tested to determine the dominant failure behavior (brittle vs ductile). Attempts at achieving higher molecular weight using the very active titanium butoxide catalyst or by use of solid-state post-condensation were unfortunately unsuccessful. The latter mostly due to lack of a heated nitrogen gas source, which is necessary for the reaction to take place efficiently. Overall, the DMDPP-C6 polymer can be considered a low to medium strength engineering plastic with a low T_g and high crystallinity. Potential applications of the material will be in similar niches to poly(butylene terephthalate) and highly depended on the chemical properties of the pyrazine, which are still being explored.

References

- [1] H. E. H. Meijer, L. E. Govaert, *Prog. Polym. Sci.* **2005**, *30*, 915-938
- [2] A. Pawlak, *Macromol. Chem. Phys.* **2019**, *220*, 1900043
- [3] Z. Dobkowski, *Rheol. Acta* **1995**, *34*, 578-585
- [4] C. Liu, J. He, E. v. Ruymbeke, R. Keunings, C. Bailly, *Polymer* **2006**, *47*, 4461-4479
- [5] M. A. Würdemann, K. V. Bernaerts, *ACS. Sustain. Chem. Eng.* **2020**, *8*, 12045-12052
- [6] M. Gilbert, F. J. Hybart, *Polymer* **1972**, *13*, 327-332
- [7] A. K. Ghosh, E. M. Woo, Y.-S. Sun, L.-T. Lee, M.-C. Wu, *Macromolecules* **2005**, *38*, 4780-4790
- [8] M. Jiang, Q. Liu, Q. Zhang, C. Ye, G. Zhou, *J. Polym. Sci., Part A: Polym. Chem.* **2012**, *50*, 1026-1036
- [9] I. Gavrilă, P. Raffa, F. Picchioni, *Polymers* **2018**, *10*, 248
- [10] After the mechanical studies were complete, the molecular weight of the initial batches of polymer was also determined using NMR end-group analysis. Unfortunately, we observed quite a significant disparity between the molecular weights measured by these two techniques. The molecular weight measured by NMR was significantly lower than that measured by GPC. This difference should also be taken into account when assessing the mechanical data, although this insight does not influence the conclusions.
- [11] NMR molecular weight was calculated in the same way as described in Chapter 2.
- [12] B. A. G. Schrauwen, R. P. M. Janssen, L. E. Govaert, H. E. H. Meijer, *Macromolecules* **2004**, *37*, 6069-6078
- [13] M. L. Di Lorenzo, C. Silvestre, *Prog. Polym. Sci.* **1999**, *24*, 917-950
- [14] J. D. Hoffman, J. I. Lauritzen, Jr., *J Res Natl Bur Stand A Phys Chem* **1961**, *65A*, 297-336
- [15] O. Starkova, A. Aniskevich, *Mechanics of Time-Dependent Materials* **2007**, *11*, 111-126
- [16] M. Rubinstein, R. H. Colby, *Polymer Physics*, OUP Oxford, **2003**.
- [17] J. Min, L. Tingting, Z. Qiang, C. Ying, Z. Guangyuan, *Journal of Renewable Materials* **2015**, *3*, 120-141
- [18] J. E. Mark, *Polymer Data Handbook*, Oxford University Press, **2009**.
- [19] J. Zhang, Q. Liang, W. Xie, L. Peng, L. He, Z. He, S. P. Chowdhury, R. Christensen, Y. Ni, *Polymers* **2019**, *11*, 197
- [20] X. Qu, G. Zhou, R. Wang, H. Zhang, Z. Wang, M. Jiang, J. Tang, *Journal of Industrial and Engineering Chemistry* **2021**, *99*, 422-430
- [21] S. Eshraghi, S. Das, *Acta Biomaterialia* **2010**, *6*, 2467-2476
- [22] J. Li, Z. Zhu, T. Li, X. Peng, S. Jiang, L.-S. Turng, *J. Appl. Polym. Sci.* **2020**, *137*, 48581
- [23] C. D. Papaspyrides, S. N. Vouyiouka, *Solid State Polymerization*, Wiley, **2009**.
- [24] K. Tomita, *Polymer* **1976**, *17*, 221-224

Appendix

Figure A1: Rheology data for frequency sweep measurements of batch 1.

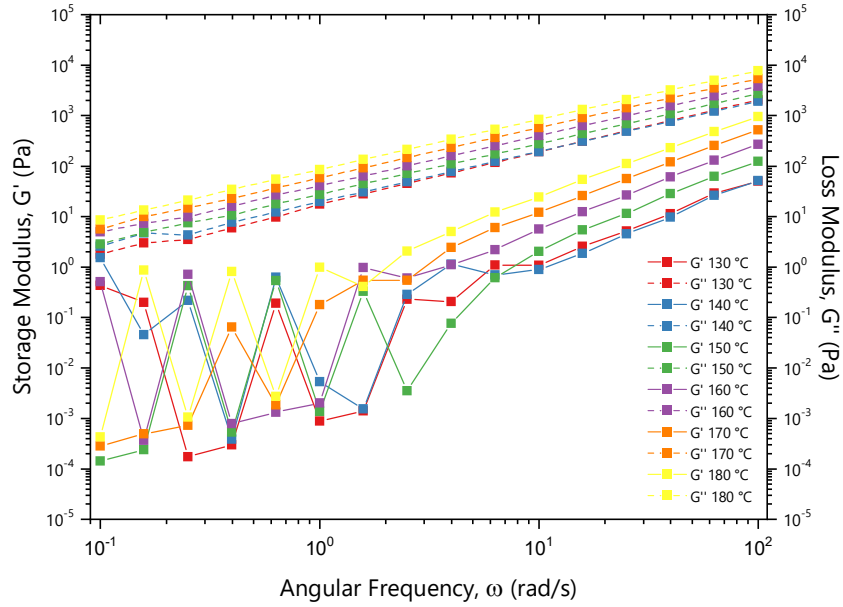


Table A1: Initial dimensions of the cylinders for compression tests.

Specimen	Diameter (mm)	Height (mm)
B3 – S1	11.85	8.07
B3 – S2	11.81	8.18
B3 – S3	11.87	7.20
B3 – S4	11.85	8.52
B3 – S5	11.85	7.34
B4 – S1	11.80	9.20
B4 – S2	11.80	9.07
B4 – S3	11.82	10.29
B4 – S4	11.85	9.15
B4 – S5	11.82	10.18

Figure A2: Stress-strain curves for the compression test of batch 3.

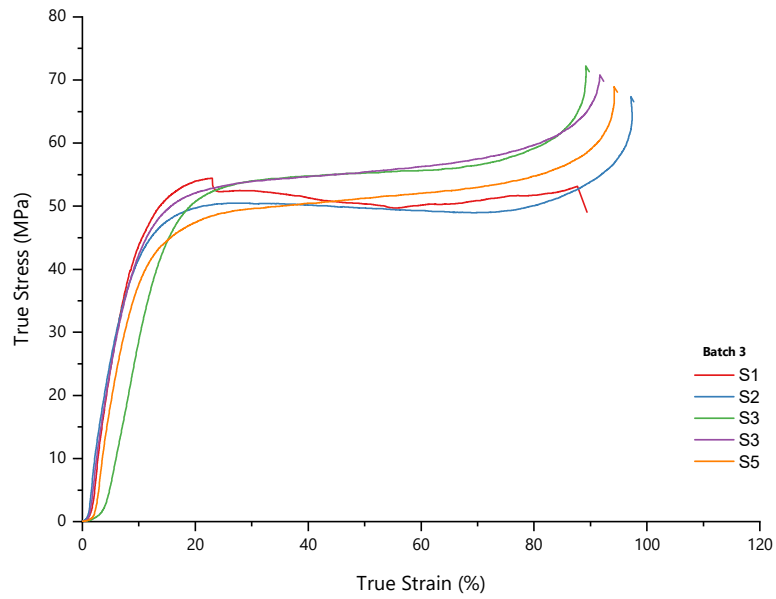
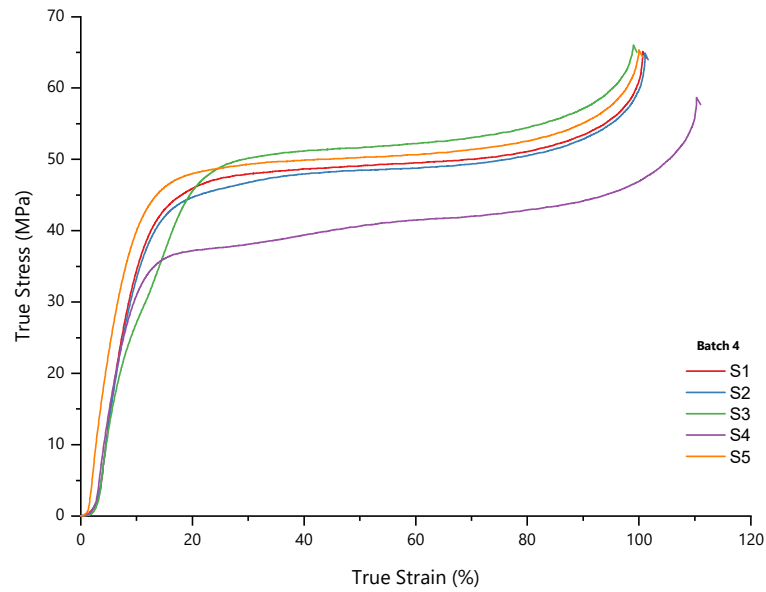


Figure A3 Stress-strain curves for the compression test of batch 4.



Chapter 4

Post-modification of biobased pyrazines and their polyesters

Published as:

M.A. Würdemann, T. Faber, J.A.W. Harings, K.V. Bernaerts, R.V.A. Orru, A. Pich, *Macromolecules* **2021**, 54 (23), 10850-10859

Abstract

Monomers and polymers from biobased pyrazine underwent post-modification reactions to synthesize series of novel tailored polyesters with tunable structure and adjustable physico-chemical properties. Modification using $\text{Me}_3\text{O}\cdot\text{BF}_4$ gave poorly soluble and unstable polymers that could not be isolated nor characterized. However, controlled oxidative post-modification is possible, without loss of molecular weight. The degree of oxidation has a large effect on the thermal properties of the polyesters. One of the polyesters shows loss of crystallinity combined with an increase in glass transition temperature at increasing degrees of oxidation. For the other polyester oxidation results in an elevated melting point. Weak hydrogen bonds are responsible for the latter observation as demonstrated by infrared spectroscopy. Surface modification of a polymer film results in different wetting behaviour. Our biobased pyrazine building blocks and their ability to be post-modified offer interesting opportunities in added functionality materials of the future.

Introduction

Synthetic polymers has increased living standards significantly over the past century^[1-2] however, serious environmental concerns exist using materials based on these polymers. The monomers frequently used in synthetic polymers are mainly sourced from fossil-oil feedstocks and consequently inherently less sustainable. Further, most of these polymeric materials are not (bio)-degradable and hence pose a waste problem.^[3] In pursuit of more sustainable environmentally compatible synthetic polymers, current research mostly focuses on oxygen containing lingo-cellulosic biomass as feedstock to source the required monomeric building blocks.^[4] On the other hand, nitrogen-rich biomass receives, as of yet, relatively little attention as a source of biogenic carbon for the synthesis of advance polymers.^[5] Our group recently developed a number of pyrazine-containing polyesters from nitrogen-rich biomass.^[6] More specific, biobased pyrazine diacids namely, dimethyldipropionic and dipropionic acid pyrazine (DMDPP and DPP, respectively) (see **Figure 1**) prepared via a straight-forward process from simple amino acids (glutamic- and δ -amino-levulinic acid), were employed to access our polyesters.^[7]

Both nitrogen atoms in the pyrazine core still have an electron lone pair available for post-modification reactions. This feature in combination with their specific aromatic character make pyrazines interesting building block candidates for added functionality materials. Thus far, only scattered examples of pyrazines as constituents of polycondensates like polyesters exist. On the other hand, the modification of the pyrazine core via a variety of different reactions, including oxidation and alkylation, is well established.^[8-9] These reactions can also be used to post-modify pyrazine-containing polymers. Post-modification of polymers is a frequently employed strategy to enable specific changes in material properties, such as crystallinity, thermal properties, different surface behavior or better (bio)-degradability. We believe that post-modification could be an effective approach to establish pyrazine-containing polymers as biobased added-functionality materials with tunable properties. The current work describes the use of alkylation and oxidation reactions to enable the post-modification of pyrazine-containing polyesters and provides a proof of principle to further elaborate these strategies towards tunable biobased functional materials.

This study focuses on several modification procedures starting with two specific monomers (Me_2DMDPP and Me_2DPP) available from our earlier work in this area. Subsequent reactions of these pyrazine building blocks and 1,6-hexanediol produces biobased polyesters that were subjected to the same modifications (see **Figure 1**). These polyesters are semi-crystalline and post-modification would induce major changes in observed thermal properties making these ideal for our proof of principle study.

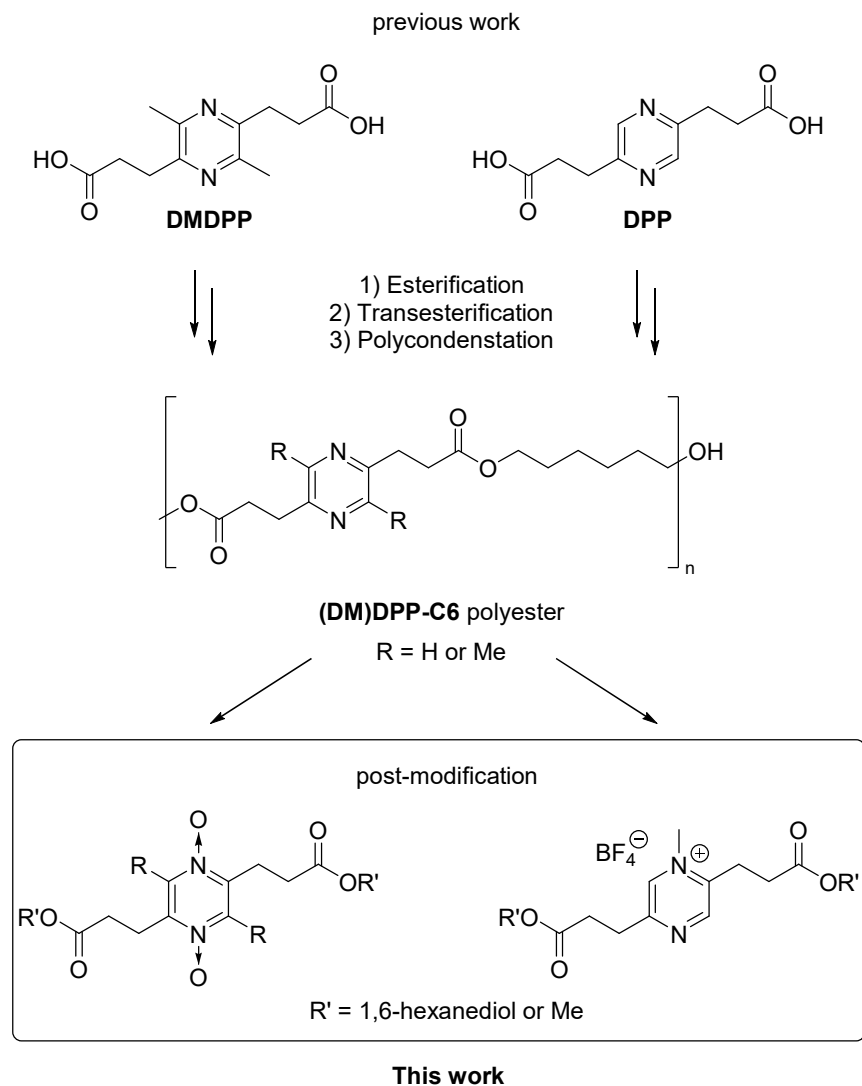


Figure 1: Structures of the pyrazine monomers DMDPP and DPP, the 1,6-hexanediol polyesters used in this study and the post-modification.

Experimental

Materials

Monomers Me₂DMDPP & Me₂DPP and polymers DMDPP-C6 & DPP-C6 were synthesized according to literature.^[6] Trimethyloxonium tetrafluoroborate and trifluoroacetic acid were supplied by TCI in >95% purity, 3-chloroperbenzoic acid (mCPBA) 77 wt% purity, sodium thiosulphate and sodium bicarbonate were supplied by Sigma-Aldrich and all were used as received. Silica gel (Davisil 60A) was supplied by Grace. All solvents were supplied by Biosolve in at least analytical reagent grade purity and used as received. Deuterated chloroform (CDCl₃) and deuterium oxide (D₂O) were supplied by Cambridge isotopes and kept over 4Å molecular sieves obtained from Sigma-Aldrich.

Alkylation of Me₂DPP

A 25 mL Schlenk vial was loaded with Me₂DPP (126 mg, 0.50 mmol), Me₂O·BF₄ (74 mg, 0.50 mmol) and a magnetic stirrer. After addition of 2 mL of chloroform (CHCl₃) the vial was sealed and left to stir for 19h. After this time, the solvent was removed by a flow of nitrogen, followed by concentration *in vacuo*. The resulting greenish oil was washed with 3x 5 mL ethylacetate (EtOAc) in the Schlenk and again concentrated, resulting in the desired product as a brown viscous oil (130 mg, 0.37 mmol, 73% yield).

(2,5-bis(3-methoxy-3-oxopropyl)-1-methylpyrazin-1-ium tetrafluoroborate)

HRMS [M - BF₄]⁻ C₁₃H₁₉N₂O₄ calcd 267.1339, found 267.1339; ¹H-NMR (300 MHz, D₂O) δ 9.22 (s, 1H), 8.88 (s, 1H), 4.43 (s, 3H), 3.73 (s, 3H), 3.70 (s, 3H), 3.51 (t, J = 7.1 Hz, 2H), 3.37 (t, J = 6.9 Hz, 2H), 3.08 (t, J = 7.2 Hz, 2H), 2.99 (t, J = 6.9 Hz, 2H); ¹³C-NMR (75 MHz, D₂O) δ 175.1, 173.8, 159.9, 150.2, 147.9 (t, ¹⁴N-J = 9.3 Hz), 147.8, 137.8 (t, ¹⁴N-J = 9.6 Hz), 52.6, 52.4, 46.2 (t, ¹⁴N-J = 4.8 Hz) 31.3, 30.3, 29.2, 24.8; ¹⁹F-NMR (282 MHz, D₂O) δ -150.5 (BF₄⁻); (FT-IR $\tilde{\nu}$ 2958, 1727, 1499, 1439, 1203, 1175, 1032, 892, 838, 521 cm⁻¹; LC-MS (ESI⁺) m/z 267 ([M]).

General procedure for the oxidation of Me₂DMDPP and Me₂DPP

A flask was loaded with 1 equiv. of diester and dissolved in CHCl₃ to form a 0.1 M solution. To this solution was added either 1 or 3 equiv. of mCPBA (77wt%) and then left to stir overnight. The resulting suspension was quenched by addition of sodium thiosulfate (0.5 equiv. of a 0.1 M solution). The organic layer was extracted with satd. NaHCO₃, dried over Na₂SO₄ and concentrated *in vacuo*. The mono-oxides were subjected to column chromatography over silica using 50/50 EtOAc/hexane. The dioxides could be isolated by washing with a minimal amount of hot methanol (MeOH).

Me₂DMDPP-O (2,5-bis(3-methoxy-3-oxopropyl)-3,6-dimethylpyrazine 1-oxide)

Isolated as a colorless solid in 46% yield (485 mg, 1.63 mmol); Mp: 96 – 98 °C; Elemental analysis calcd (%) for C₁₄H₂₀N₂O₅: C 56.75, H 6.80, N 9.45; found (%): C 56.91, H 6.63, N 9.46; ¹H-NMR (300 MHz, CDCl₃) δ 3.67 (s, 3H), 3.65 (s, 3H), 3.17 (t, J = 7.4 Hz, 2H), 3.06 (t, J = 7.1 Hz, 2H), 2.85 – 2.69 (m, 4H), 2.53 (s, 3H), 2.45 (s, 3H); ¹³C-NMR (75 MHz, CDCl₃) δ 173.5, 173.3, 152.7, 151.4, 141.1, 139.9, 51.9, 51.8, 31.5, 29.4, 29.2, 23.1, 22.1, 12.7; FT-IR $\tilde{\nu}$ 2951, 1722, 1582, 1430, 1281, 1175, 1154, 859, 597, 411 cm⁻¹; LC-MS (ESI⁺) m/z 297 ([M+1]).

Me₃DMDPP-O₂ (2,5-bis(3-methoxy-3-oxopropyl)-3,6-dimethylpyrazine 1,4-dioxide)

Isolated as a colorless solid in 73% yield (854 mg, 2.73 mmol); Mp: 191 – 193 °C; Elemental analysis calcd (%) for C₁₄H₂₀N₂O₆: C 53.84, H 6.13, N 8.97; found (%): C 53.57, H 6.45, N 9.04; ¹H-NMR (300 MHz, CDCl₃) δ 3.67 (s, 6H), 3.25 (t, J = 7.2 Hz, 4H), 2.80 (t, J = 7.2 Hz, 4H), 2.57 (s, 6H); ¹³C-NMR (75 MHz, CDCl₃) δ 172.9, 144.5, 143.4, 52.1, 29.4, 24.1, 14.3; FT-IR $\tilde{\nu}$ 2956, 1721, 1517, 1423, 1280, 1191, 1081, 861, 634, 448 cm⁻¹; LC-MS (ESI+) m/z 313 ([M+1]).

Me₂DPP-O (2,5-bis(3-methoxy-3-oxopropyl)pyrazine 1-oxide)

Isolated as a yellow solid in 55% yield (148 mg, 0.55 mmol); Mp: 73 – 75 °C; Elemental analysis calcd (%) for C₁₂H₁₆N₂O₅: C 53.73, H 6.01, N 10.44; found (%): C 53.59, H 6.04, N 10.28; ¹H-NMR (300 MHz, CDCl₃) δ 8.40 (s, 1H), 8.05 (s, 1H), 3.68 (s, 3H), 3.67 (s, 3H), 3.12 (t, J = 7.0 Hz, 2H), 3.02 (t, J = 7.1 Hz, 2H), 2.81 (t, J = 7.0 Hz, 4H); ¹³C-NMR (75 MHz, CDCl₃) δ 172.8, 157.3, 147.3, 143.2, 132.8, 52.0, 52.0, 31.9, 29.8, 29.5, 23.6; FT-IR $\tilde{\nu}$ 2955, 1727, 1598, 1432, 1278, 1171, 1052, 861, 803, 490 cm⁻¹; LC-MS (ESI+) m/z 269 ([M+1])

Me₂DPP-O₂ (2,5-bis(3-methoxy-3-oxopropyl)pyrazine 1,4-dioxide)

Isolated as a colorless solid in 63% yield (180 mg, 0.63 mmol); Mp: 185 – 188 °C; Elemental analysis calcd (%) for C₁₂H₁₆N₂O₆: C 50.70, H 5.67, N 9.85; found (%): C 50.49, H 5.44, N 9.78; ¹H-NMR (300 MHz, CDCl₃) δ 8.10 (s, 2H), 3.66 (s, 6H), 3.04 (t, J = 6.8 Hz, 4H), 2.79 (t, J = 6.8 Hz, 4H); ¹³C-NMR (75 MHz, CDCl₃) δ 172.3, 146.5, 135.9, 52.1, 29.2, 23.9; FT-IR $\tilde{\nu}$ 3030, 1733, 1533, 1426, 1383, 1329, 1206, 881, 687, 441 cm⁻¹; LC-MS (ESI+) m/z 285 ([M+1])

General procedure for the oxidation of DMDPP-C6 and DPP-C6

Eight vials were loaded with 1 ml of a stock solution of the polymer under test dissolved in CHCl₃ (400 mg in 8 mL, 0.15M or 0.16M) and a magnetic stirrer. To the vials was added 0.0, 0.05, 0.25, 0.5, 1.0, 1.5, 2, and 3 equiv. of mCPBA, a magnetic stirrer and 0.5 mL of CHCl₃. The resulting solutions were left to stir in closed vials overnight (~19h). After which the reaction mixtures were precipitated in 30 mL of cold MeOH and the precipitate isolated by filtration. The obtained colorless solids were dried *in vacuo* at 40 °C and subsequently analysed by NMR, GPC and DSC.

Surface modification

A DMDPP-C6 polymer film was made by compression moulding (COLLIN Laboratory Platen Press P200E at 175 °C, 5 bar for 2 minutes, the pressure was increased at 40 bar for 1 minute, left to cool at 40 bar and removed from the mould). A 1x4 cm section of film was submerged overnight in a solution of 2 g of mCPBA in 10 mL of EtOAc, after which it was removed and dried *in vacuo*. The modified film and a similar size of virgin film were analysed by IR.

Samples for water contact angle measurements were prepared by spin coating a 0.01 w% solution of DMDPP-C6 in CHCl₃ on glass microscope slides using a Laurell WS-650MZ-23NPPB spincoater. Per sample 400 µL of solution were pipetted on the slide, which was accelerated at 200 x and spun at 2000 rpm for 30 seconds. This procedure resulted in six reasonable films (see **Figure S33**). Half of the films was subjected to a solution of mCPBA in EtOAc overnight, the control films were subjected to just EtOAc. The following day the films were removed from their respective solutions, washed with EtOAc and EtOH and dried *in vacuo* overnight at 40 °C.

Characterization

The polymers were dried *in vacuo* overnight at 40 °C before analysis.

Gel permeation chromatography (GPC) was conducted on a Shimadzu Prominence-i LC-2030 HPLC system fitted with a Shimadzu RID-20A detector. The measurements were run with isocratic elution of chloroform at 1 mL/min on a Shodex KF-805L column (10 mm by 300 mm, 10 µm pore size) operating at 40 °C. Samples were prepared by making 1 mg/mL solutions in chloroform and filtered over a 0.2µm PTFE filter. GPC was used to determine the molecular weight distribution of the obtained polymers as compared to polystyrene standards.

Nuclear magnetic resonance (NMR) spectroscopy was conducted on a Bruker AVANCE 300 MHz apparatus. Measurements were run in d-chloroform using 5-10 mg of polymer. The ¹H-NMR (300 MHz) spectra were recorded with 16 scans and the ¹³C-NMR (75 MHz) APT spectra were recorded at 1024 scans. The obtained NMR data was used to determine the conversion of the end groups and the degree of polymerization. This data was also used to determine the ratio of the constituents of the chains by comparing the normalized integrals of the monomeric units in the polymer chain.

Infrared spectra were recorded on a Perkin Elmer Frontier apparatus equipped with a PIKE-GladiATR using 32 scans. The spectral range was from 4000-400 cm⁻¹ with a resolution of 2 cm⁻¹. Spectra in the melt were recorded 10 °C above the melting temperature.

Thermal stability of the polymers was determined by use of thermal gravimetric analysis (TGA) by heating 3 to 10 mg samples at 10 °C/min up to 700 °C under a nitrogen atmosphere on a TA instruments TGA 500 machine. The degradation temperature (*T_d*) was set as 5% weight loss.

Differential scanning calorimetry (DSC) thermograms were recorded on 2 to 7 mg samples in pierced lid pans on a Netzsch Polyma 14 machine at heating and cooling rates of 10 °C/min from -40 °C to 200 °C with 3 min isothermals at those temperatures. Two temperature cycles were measured with the melting (*T_m*) and crystallization temperatures (*T_c*) of the second cycle being reported. Glass transition temperatures (*T_g*) are reported as the inflection point of the first observed change in in heat flow in the second cycle.

Melting points of the monomer di-esters and oxides were recorded in triplicate on a Mettler Toledo MP90 melting point system using open capillaries and are uncorrected.

Liquid Chromatography – Mass Spectrometry (LC-MS) analysis was performed on a Shimadzu Nexera 2 UHPLC system equipped with a Shimadzu LC-30AD pump, a SPD-M30A photodiode array detector and LCMS-2020 single quadrupole detector. The system runs on MilliQ water and LC-MS grade acetonitrile both modified with 0.1% formic acid. A Waters XSelect CSH-C18 column (3.0 mm x 75 mm with a particle size of 3.5 µm) was used operating at 30 °C. The method was set up with a gradient of 5% acetonitrile in water for 2 min, an increase to 95% acetonitrile over 6 min, 1 min at 95% followed by flushing back to 5% acetonitrile. Samples were prepared by dissolving the reaction mixture in methanol at ± 1 mg/mL in case of the dioxides a few drops of DMSO where added.

The water contact angle was determined on a OneAttention Theta Light machine using a 5.0 µL sensile drop tests at 60 fps for a measurement of 10 seconds. Between 8 and 9 drops per film were measured. A total of 27 measurements were done for the unmodified film and 26 for the modified film.

Results and discussion

Both alkylation and oxidation post-modification reactions were explored at the monomer, as well as the polymer stage for both Me₂DMDPP and Me₂DPP. The results are discussed below.

Alkylation

Mono- or dipyrazinium salts may form (stable) radicals^[10-14] and complexes with a range of metals.^[15-18] They also catalyse oxidation reactions.^[19-21] These interesting features may be transferred to specialized materials with added functionality via post-alkylation of pyrazine-containing polymers. Alkylation of pyrazines takes place under various conditions.^[8-9] To identify, which of these are suitable to access added-value polymers several factors must be considered. First, the post-modification alkylation should take place under mild conditions to prevent loss of molecular weight. Further, our polyesters only dissolve in well in chloroform or dichloromethane (DCM), which makes them the solvent of choice of post-alkylation. Finally, the safety profile of the applied alkylating agent should be acceptable, especially the toxicity and exposure routes. With these factors in mind, we decided to first test potentially suitable reagents and reaction conditions for the post-alkylation of the monomeric pyrazine building blocks, after that we turned our attention to post-alkylation of the 1,6-hexanediol polymers.

Since mono-alkylation of pyrazines proceeds smoothly with methyl iodide, we started with this rather straightforward methylation.^[22-27] Using an excess of methyl iodide with either Me₂DMDPP or Me₂DPP in chloroform at room temperature, did not result in any observable alkylation by NMR even after several days. Running the reaction at elevated temperature and pressure in a microwave (150 °C, ± 3 bar, 90 min) did not result methylation either. These conditions were also applied to post-methylate the corresponding polyesters, unfortunately without success. Methyl iodide apparently is not reactive enough to alkylate either of the pyrazine monomers nor the pyrazine containing polyesters.

Besides methyl iodide, other more active alkylating agents have been used to form pyrazinium salts. Dimethylsulfate (DMS) for example is known to alkylate tetra-substituted pyrazines similar to DMDPP. However, the poor safety profile prevented us to explore DMS as an alkylating agent.^[28-29] Meerwein's salts (trialkylxonium tetrafluoroborates) also very effectively alkylate pyrazines.^[10-11, 30-31] Unfortunately, in our hands, triethyloxonium tetrafluoroborate (Et₃O·BF₄) and the less sterically demanding trimethyloxonium tetrafluoroborate (Me₃O·BF₄) in DCM or chloroform proved unsuccessful to alkylate Me₂DMDPP. It is has been reported that

substituted pyrazines are increasingly difficult to alkylate, with tetramethylpyrazine only forming 5% dipyrazinium salt under forcing conditions with $\text{Et}_3\text{O}\cdot\text{BF}_4$ in dichloroethane.^[1] Apparently the methyl substituted DMDPP monomer is too sterically hindered for post-modification by alkylation under these conditions.

However, we were happy to find by LC-MS analysis and NMR (see appendix **Figure A1-2**) that post-alkylation of Me_2DPP was successful using $\text{Me}_3\text{O}\cdot\text{BF}_4$ after an overnight reaction in chloroform. We were able to control the degree of alkylation to a certain extent by adjusting the amount of alkylating agent. With one equivalent of $\text{Me}_3\text{O}\cdot\text{BF}_4$ only mono alkylation was observed but at incomplete conversion (see **Figure 2**). The alkylated material could be isolated as a green to brown, hygroscopic oil. Using two or three equivalents, however, the mass of the dialkylated species was not found using LC-MS (see appendix **Figure A2**). Instead, we observed the oxidized dialkylated species (not isolated) matching earlier reports on the stability of diquarternary pyrazinium salts (see **Figure 2**).^[32] Overall stability of the salts is low, showing both spontaneous decomposition as well as reactions with oxygen, water and alcohols via radical mechanisms.^[1]

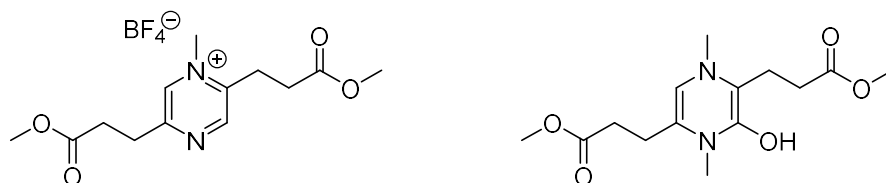


Figure 2: Alkylation products of Me_2DPP with $\text{Me}_3\text{O}\cdot\text{BF}_4$, mono and dialkylation/oxidation respectively.

After successful alkylation of the Me_2DPP monomer the DPP-C6 polyester was also treated with varying equivalents of $\text{Me}_3\text{O}\cdot\text{BF}_4$ in chloroform. Depending on the amount of $\text{Me}_3\text{O}\cdot\text{BF}_4$ used more or less of a colorless to grey non-soluble gel formed. Analysis of the reaction solvent revealed only unreacted polymer. This indicates the gel consists of either the desired alkylated material or unreacted $\text{Me}_3\text{O}\cdot\text{BF}_4$. Further, the gel turns yellowish/brown after prolonged exposure to air and/or exposure to water after which, this material did not dissolve in any solvent. We believe that either crosslinks are formed or post-alkylation results in very strong interchain interactions making the resulting polymeric material no longer soluble in any convenient solvent. Thus, although alkylation of DPP in a polymer seems possible, such a process is highly impractical. The 1,6-hexanediol spacer is not ideal for this kind of post-modification, since it limits the solubility of the polymer to chloroform and DCM. Further work on the alkylation of other polymers containing pyrazines may still be of interest. At this stage, we stopped however, our studies in this direction and turned our attention to oxidation post-modification reactions.

Oxidation

Pyrazines can be oxidized to the corresponding N-oxides. Similar to N-alkyl pyrazinium salts, these N-oxides have interesting chemical and functional properties. Most important to note is that mono-oxidation lowers the pK_a of the pyrazine ring.^[33] Besides this, pyrazine N-oxides can undergo several types of electrochemical^[34-37] and photo-chemical reactions.^[38-39] They also easily form complexes with metal ions^[40-46] additionally oxidation opens new reaction pathways on the pyrazine ring.^[47-52]

N-oxide formation can be achieved by reaction with several types of oxidizing agents, such as hydrogen peroxide, peroxyacetic acid and meta-chloroperbenzoic acid (mCPBA).^[8-9] The latter has been identified as a general and versatile oxidant for pyrazines and was our initial reagent of choice to test the post-oxidation of pyrazine-containing polyesters. Moreover, mCPBA can be used under anhydrous conditions limiting potential ester hydrolysis.

Monomers

The oxidative post-modification of both Me₂DMDPP and Me₂DPP with mCPBA in chloroform was explored in detail. Reactions with one or three equivalents of oxidant were stirred overnight at room temperature in chloroform or DCM to access the desired mono- and dioxides. Extraction of the resulting suspensions with aqueous base, concentration of the organic layers and further work-up (see experimental) allows isolation of both mono and di oxo pyrazines (see **Figure 3**) as crystalline solids. The NMR spectra of these products showed the expected breaking of symmetry for the mono-oxides and return of symmetry for the di-oxides. The mono-oxides melt at temperatures very similar to the starting materials, but surprisingly, the di-oxides show much higher melting points, (90 to 110 °C) compared to their starting materials. Hydrogen bonding of the acceptor N-oxide functionality and a C-H group as a weak donor may account for this melting point behaviour, as discussed later in this paper. The relative kinetics of the oxidation reaction was determined by LC-MS and shows that mono-oxidation is completed after 3 hours, while di-oxidation is only completed after 18 hours (see appendix **Figure A7**).

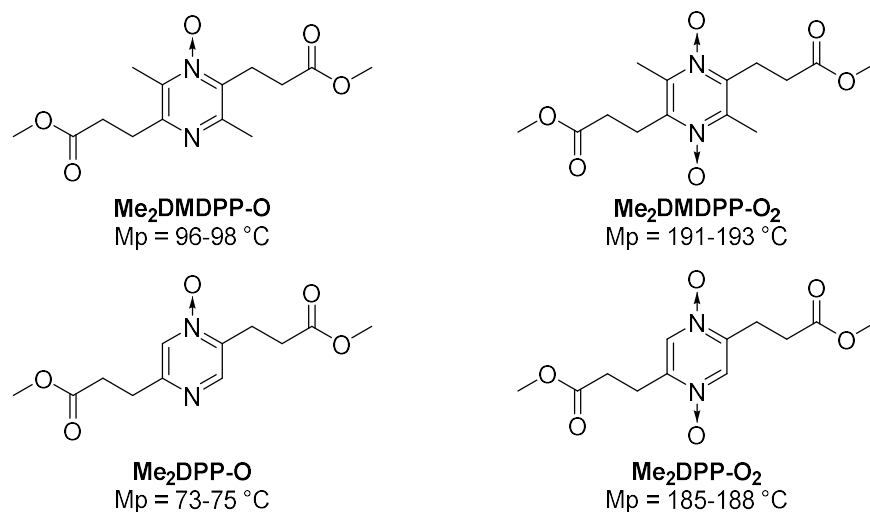


Figure 3: Structures of the mono- and di-oxides of Me₂DMDPP and Me₂DPP, with their melting points.

Polymers

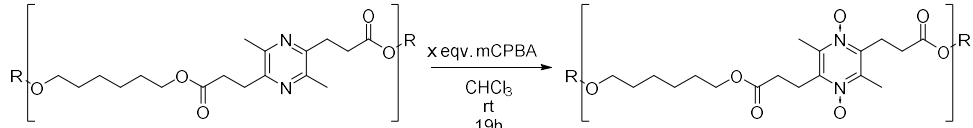
The successful isolation of the monomeric oxides, prompted us to study the oxidation of the corresponding pyrazine polyesters. After stirring our polyesters dissolved in chloroform at room temperature overnight with an excess of mCPBA a colourless precipitate was formed. This was treated with cold methanol, isolated by filtration and washed on the filter. NMR spectra showed the material was fully oxidized on both pyrazine nitrogens and the precipitation procedure had removed all oxidant residues. The oxidation post-modification is thus not hampered when the pyrazine building block is already incorporated in a polymer. Since control over the extent of oxidation proved possible with the monomers by adjusting the oxidant loading, we varied the mCPBA equivalents for the polymer post-oxidation as well. The NMR analysis demonstrates controlled access to the desired oxidized polymers. The results are listed in **Tables 1 and 2**.

Preferably, a post-modification procedure should not affect the overall molecular weight of a polymer while at the same time no or very limited side-reactions take place. In case of DMDPP-C6 our post-oxidation protocol seems to influence the molecular weight to a limited extent as shown by both NMR and GPC (see **Table 1**). However, taking the limitations of both techniques in consideration it is difficult to assess whether hydrolysis takes place or the observed differences are due to experimental error. Especially, since GPC is a relative measurement depending on hydrodynamic volume, which will change upon oxidation. But also, NMR as an analysis technique to determine molecular weight has its limitations since resolution and integration largely influence the calculated molecular weight. The dispersity of

the material was also not significantly influenced by oxidation, which together with complete solubility of any polymer samples indicated no cross-linking took place. These observations also indicate that little to no degradation via chain scission takes place during oxidation. It is thus safe to conclude that oxidation of DMDPP-C6 in chloroform with mCPBA has no major effect on the overall molecular weight and the polymer is stable under the applied conditions.

All prepared polymers, regardless of their oxidation state, were crystalline in the first heating cycle on DSC. The melting point in the second DSC heating cycle for the DMDPP-C6 polymer decreased. However, with increasing levels of oxidation and with more than 1 equivalent (or >50% mono-oxide) of oxidant, crystallinity was lost altogether (see **Figure 4**). Repeating the DSC-analysis after a week did not show any crystal formation, and crystallinity observed during the initial DSC heating may therefore be solvent induced. At higher levels of oxidation, the T_g of the DMDPP-C6 polymer also increased from 4 °C⁶ for the nascent material to 31 °C upon complete di-oxidation.

Table 1: Results for the oxidation of DMDPP-C6 polymer using different amounts of oxidant.



Entry	Eqv. mCPBA	O ⁰ / O ¹ / O ² (%) ^[c]	M _n (g/mol) NMR ^[d]	M _n (g/mol) GPC	\bar{D}	T _m (°C) 1 st cycle	T _m (°C) 2 nd cycle	T _g (°C)	T _d (°C) 5 wt%
1 ^[a]	0	100 / 0 / 0	9700	27300*	1.9	144	144	-	324
2 ^[b]	0	100 / 0 / 0	11000	29100	1.8	145	144	-	-
3	0.05	94 / 6 / 0	8700	25400*	2.0	142	142	-	-
4	0.25	75 / 25 / 0	10700	23000*	2.1	128	128	-	-
5	0.5	50 / 48 / 2	9700	24600*	1.8	106	106	0	-
6	1	16 / 78 / 6	9400	29700*	1.7	79	-	7	303
7	1.5	0 / 61 / 39	8400	23900	1.9	101	-	20	-
8	2	0 / 32 / 68	10700	26800	1.8	122	-	27	-
9	3	0 / 7 / 93	8600	24300	1.8	131	-	31	255

*Low M_n material still present

[a] starting polymer used for other entries, [b] precipitated starting polymer, [c] integral ratio for unoxidized, mono-oxide and di-oxide see appendix for assignment and calculation, [d] calculation in appendix

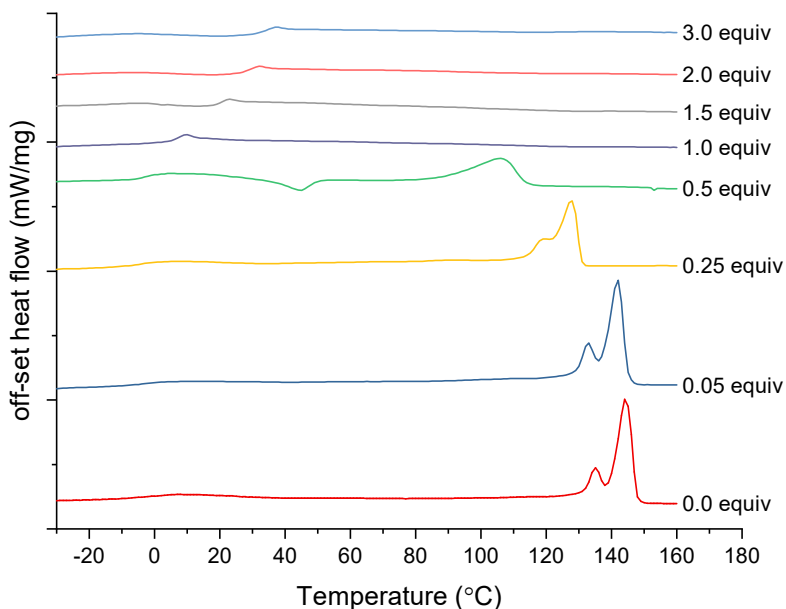


Figure 4: The second cycle DSC thermograms of the entries in Table 1.

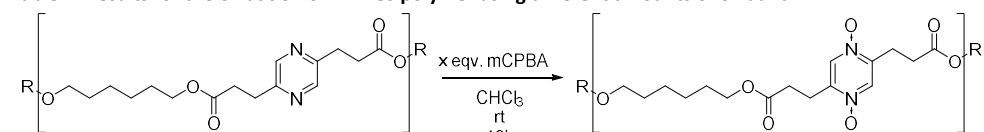
At first glance, the DPP-C6 polymer seems to behave similar to the DMDPP-C6 polymer certainly until 1 equivalent of oxidant is added (see Table 2). However, at higher oxidation levels, the solubility of the polymer product decreases rapidly in chloroform. Fortunately, NMR measurements using end-group determination were still possible after adding TFA. This shows little change in molecular weight in all but the fully oxidized polymer (Table 2, entry 9). For more oxidized polymeric materials, the GPC analysis was inconclusive due to the lack of solubility. In terms of polymer stability we conclude, as for DMDPP-C6, that no major degradation or chain scission takes place during oxidation.

The observed changes in the thermal properties upon post-oxidation of the DPP-C6 polymer follow a similar trend as was found for the DMDPP-C6 polymer. At increased oxidation levels, the crystallinity of the material decreases and the T_g increases (see Figure 5). Similar steric arguments as discussed for the DMDPP-C6 case, seem to account of the observed thermal behaviour in the DPP-C6 polymer. However, in case of DPP-C6 this is less pronounced and at >50% oxidation a new crystalline phase is obtained, that melts at significantly higher temperatures than the initial polymer. Moreover, this is accompanied by a decrease in solubility of the material. The melting point increases to such an extent that it supersedes the melting point of non-oxidized DMDPP-C6, which already melts 80 °C higher than DPP-C6.

Similar to the di-oxidized monomers, we believe that this increase in melting point is most likely due to hydrogen bonding as we will discuss in more detail below.

Next, we found that the degradation temperature of the oxidized polymers decreases with increasing oxidation level compared to the degradation temperature of the starting polymers. This is however, taking 5% weight loss as the cut-off for degradation. The DMDPP-C6 polymer already degrades below this cut-off via intramolecular nucleophilic attack of the pyrazine nitrogen to the ester bond.^[6] Oxidation may block this reaction pathway but also changes the electronic character. Besides, oxidation has been reported to change the reactivity of pyrazines to a large extent. As such, the 5% weight loss limit might not reflect the actual useable temperature window for the oxidized polymers. Of note is the char formation of the materials, under inert conditions significant (40%-20%) char is formed, under an oxygen atmosphere however, no char remains (see appendix).

Table 2: Results for the oxidation of DPP-C6 polymer using different amounts of oxidant.



Entry	Eqv. mCPBA	O ⁰ / O ¹ / O ² (%) ^[c]	M _n (g/mol) NMR ^[d]	M _n (g/mol) GPC	Đ	T _m (°C) 1 st cycle	T _m (°C) 2 nd cycle	T _g (°C)	T _d (°C) 5 wt%
1 ^[a]	0	100 / 0 / 0	10400	31700	2.1	65	64	-31	318
2 ^[b]	0	100 / 0 / 0	10100	26900	2.1	68	64	-35	-
3	0.05	93 / 7 / 0	9200	27900	2.1	65	62	-30	-
4	0.25	72 / 28 / 0	10400	31200	2.1	72	-	-21	-
5	0.5	49 / 50 / 1	11000	28800	2.0	76	-	-16	-
6	1	7 / 83 / 10	11000*	22800**	2.3	92	-	-2	303
7	1,5	0 / 66 / 34	9500*	15100**	2.6	129	131	8	-
8	2	0 / 37 / 63	9200*	n.d.**	n.d.	170	158	17	-
9	3	0 / 13 / 87	n.d.*	n.d.**	n.d.	200	195	32	264

* TFA added **solubility low

[a] starting polymer used for other entries, [b] precipitated starting polymer, [c] integral ratio for unoxidized, mono-oxide and di-oxide see appendix for assignment and calculation, [d] calculation in appendix

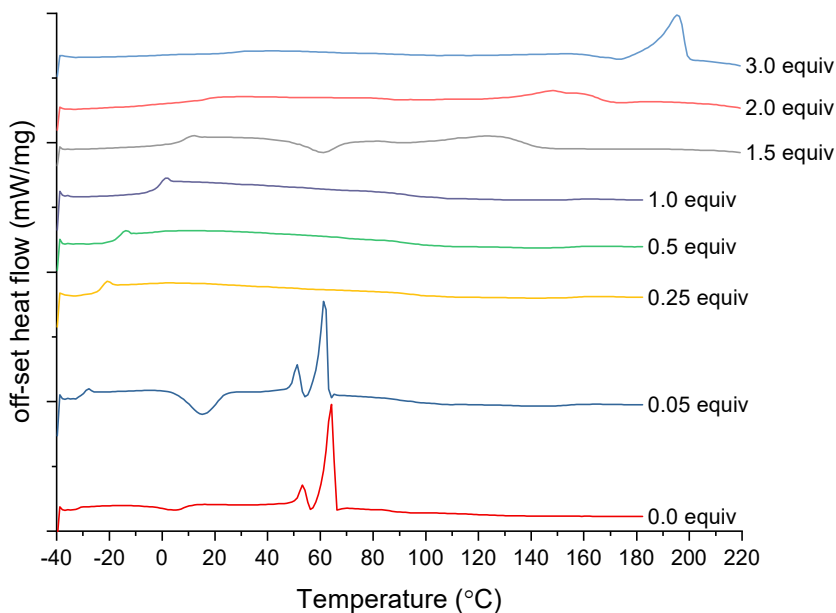


Figure 5: The second cycle DSC thermograms of the entries in Table 2.

Melting point & hydrogen bonding

We hypothesise that (weak)-hydrogen bonding is responsible for the increased melting point of the pyrazine di-N-oxides and fully oxidized DPP-C6 polymer (Table 2, entry 9). Although not explicitly reported, there is some precedent. The anticipated type of weak C-H...O bonds were demonstrated in crystal structures of poly(lactic acid), poly(hydroxyalkanoates) and several small molecules.^[53-58] For the dioxides of both 2,5-dimethylpyrazine and tetramethylpyrazine the crystal structures have been reported.^[59-60] Close examination of these structures for the possible presence of weak hydrogen bonds using the CCDC Mercury program^[61] revealed a number of short contacts. More specific, the distance between the N-oxides and hydrogens on the ring and the methyl groups is shorter than their van der Waals sum and the geometry fulfils the required definition (bond length $<2.8 \text{ \AA}$ and donor acceptor angle $\geq 120^\circ$).^[62-63] This indicates that hydrogen bonding is present in these model compounds and it accounts for the increase in melting point compared to their starting materials.^[64-66]

To confirm or discard hydrogen bonding in our oxidized DPP-polymer, we decided to use well-established Fourier transform infra-red (FTIR) spectroscopy as an independent analysis. Discrimination between the amorphous and crystalline phase of semi-crystalline samples needs to be considered in assigning vibrational modes. To identify vibrational modes sensitive to variations in hydrogen bonding efficiencies FTIR spectra are recorded in different physical states; one where bonding is highly

efficient and expressive like the in crystalline phase, and one where efficiency low due to high conformational and translational molecular motion like in the melt (liquid) state. A shift in wavenumber and transmittance/absorbance for the same vibration between the two states would then indicate variations in hydrogen bonding efficiency. Using reported band assignments for pyrazine dioxides^[67-69], the bond vibrations involved in hydrogen bonding can be examined.

Starting in the C-H stretch region (between 3200 and 2700 cm^{-1}) it is clear that $\text{Me}_2\text{DPP-O}_2$ has a very distinctive peak at 3030 cm^{-1} when compared with Me_2DPP (see **Figure 6**). It is observed that upon di-oxidation, the C-H stretch vibration red shifts (ν_{CH}) to an intense peak at 3030 cm^{-1} . This peak also moves on melting to a peak at 3080 cm^{-1} , close to the assigned aromatic C-H stretch in both pyrazine dioxide as well as 2,5-dimethylpyrazine^[68-71]. This same shift is found in DPP-C6 dioxide (**Table 2**, entry 9) (DPP-C6-O_2) although less pronounced due to the relative intensity of the hexanediol methylene stretch vibrations. Hydrogen bonding is reflected in the increased IR intensity and a red-shift of vibrations upon bond lengthening.^[72-73] The observed change in the aromatic C-H stretch for both $\text{Me}_2\text{DPP-O}_2$ and DPP-C6-O_2 thus clearly suggests these atoms are involved in hydrogen bonding, especially since the proton involved is the most acidic one in the molecule and thus the strongest hydrogen bond donor.

Turning towards spectral range between 1600-1000 cm^{-1} the comparison of both Me_2DPP and $\text{Me}_2\text{DPP-O}_2$ above and below the melt (see **Figure 7**) provides further insight regarding any hydrogen bonding. Especially since the proposed weak hydrogen bonding is expected to affect the electron distribution in the aromatic ring. There to any relevant peaks first need to be assigned to a vibrational mode. For aromatic systems this is traditionally done by use of Wilson modes.^[74] Unfortunately, these modes are not assigned unambiguously and change considerably with changes in symmetry and the mass of substituents. Although a new system has recently been proposed to remove ambiguity^[75], this has not yet been implemented for pyrazines nor for double para substituted systems such as 2,5-dimethylpyrazine and DPP. We will therefore mostly refer to the earlier notation.

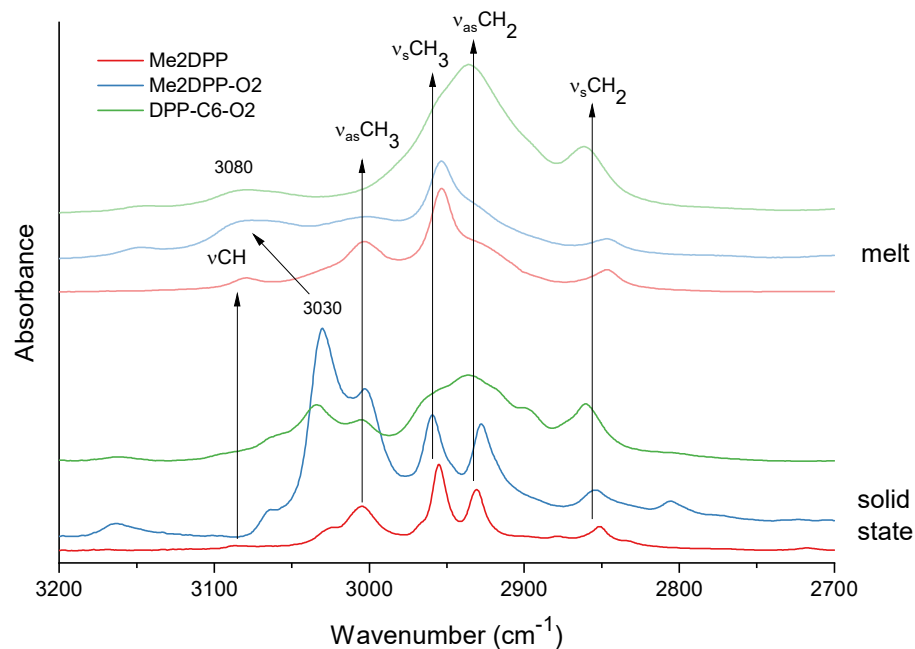


Figure 6: Infrared spectra Me₂DPP (red) & Me₂DPP dioxide (blue) and DPP-C₆-O₂ (green) in the 3200-2700 cm⁻¹ range above and below the melt.

Starting by comparing the molten state, where solid-state effects are minimized, three major differences between both molecules are found. Firstly, the highest wavenumber peak is found at 1518 cm⁻¹ in Me₂DPP-O₂ instead of 1486 cm⁻¹ in Me₂DPP. Secondly, Me₂DPP-O₂ shows a prominent peak at 1382 cm⁻¹ which is not present in the molten Me₂DPP. Finally, Me₂DPP shows a prominent peak at 1033 cm⁻¹ which is lacking in Me₂DPP-O₂. Any other major differences between the two molecules are obscured by the methylene wagging (ω CH₂), symmetric carbon-carbon stretches (ν_s CC) and oxygen-methyl(ene) rocking vibrations (ρ OCH_x) between 1300 and 1100 cm⁻¹ (these bands are present in the molten state for Me₂DMDPP and its oxides as well).

The differences observed between the molecules in the melt can be assigned to the following vibrations. The peaks at 1518 cm⁻¹ in Me₂DPP-O₂ and 1486 cm⁻¹ in Me₂DPP are certainly semi-circle stretches modes 19a and 19b. For Me₂DPP, mode 19a can be assigned to this wavenumber by analogy with 2,5-dimethylpyrazine.^[70] For Me₂DPP-O₂ this assignment of either 19a or 19b is unclear, in tetra substituted benzenes higher frequency vibration is 19b while in para substituted ones this is 19a.^[76] The other prominent peak in Me₂DPP-O₂ at 1382 cm⁻¹ is most likely the other semi-circle stretch, especially considering that the peak at 1436 cm⁻¹ originates in methyl and methylene deformations (δ (CH₃) & δ (CH₂)).^[77] This latter assignment is confirmed by the splitting of this peak in the solid state.

In the solid state several other new bands arise due to crystallinity, other changes also occur, and the peak at 1518 cm^{-1} in $\text{Me}_2\text{DPP-O}_2$ moves to 1532 cm^{-1} while increasing in intensity. This shift is most likely due to hydrogen bonding induced changes in electron density influencing the N-O and C-H stretching contributions to this mode. Next to this, the peak at 1382 cm^{-1} shows no changes suggesting this semi-circle stretch has no N-O stretching contribution and is vibration 19b.^[68] $\text{Me}_2\text{DPP-O}_2$ in the solid state shows a new band at 1330 cm^{-1} which would be the lower limit for mode 13, which has the highest N-O stretching contribution.^[64, 78] This band is absent in the melt, suggesting that it is indeed the N-O stretching vibration. This band is sensitive for hydrogen bonding with red-shifts upon hydrogen bonding of 20 cm^{-1} being reported.^[79-80] In the molten state this band actually appears as a shoulder at 1358 cm^{-1} where the observed shifts in wavenumber marks hydrogen bonding a lower temperatures.

As can be seen in **Figure 7**, DPP-C6-O_2 shows the same changes between the solid state and the melt as $\text{Me}_2\text{DPP-O}_2$ proving that hydrogen bonding is responsible for the increased melting point of this polymer. The semi-crystalline nature of the polymer is also reflected in the broadening of the 19a vibration at 1532 cm^{-1} .

The aforementioned peak in Me_2DPP at 1033 cm^{-1} has previously been assigned to ring vibration 12 in 2,5-dimethylpyrazine.^[70] The corresponding vibration in pyrazine-N,N'-dioxide however, has been reported at 874 cm^{-1} .^[69] Turning towards the $1000\text{-}400\text{ cm}^{-1}$ spectral range (**Figure 8**) this peak can indeed be identified in molten $\text{Me}_2\text{DPP-O}_2$ at 862 cm^{-1} which blue-shifts to 881 cm^{-1} in the solid state. In the Wilson representation mode 12 has mostly stretching contributions in the newer representation however, the equivalent vibration D_{10} ^[75] has C-H bending contributions next to the N-O stretching vibration. Bending vibrations are known to blue-shift upon hydrogen bonding explaining the blue-shift of this peak between the melt and the solid state.^[73]

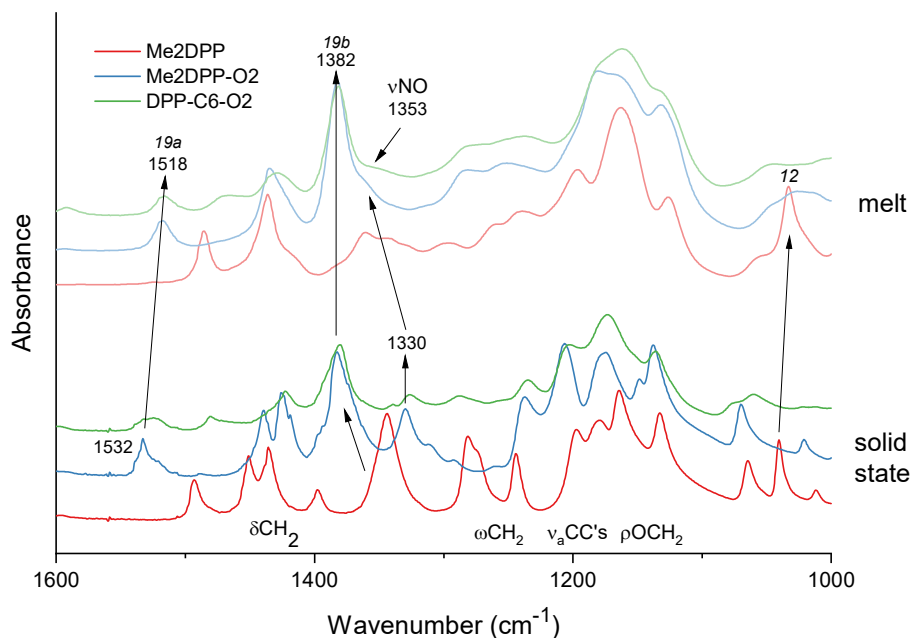


Figure 7: Infrared spectra of Me₂DPP (red) & Me₂DPP-O₂ (blue) and DPP-C6-O₂ (green) in the 1600-1000 cm⁻¹ range above and below the melt.

Concerning other bending vibrations, the C-H in-plane bending vibrations (γ_{CH}) can be found in Me₂DPP at 892 cm⁻¹ in the melt, which increase in intensity in the solid state. In Me₂DPP-O₂, this vibration seems obscured in the melt, but in the solid-state two peaks at 927 cm⁻¹ are observed. This suggests that the C-H in-plane bending vibrations are involved in hydrogen bonding and are blue shifted in the solid state. The blue shifting of bending vibrations upon hydrogen bonding is also seen below 500 cm⁻¹ where the out-of-plane bending vibrations reside. Due to the spectral range limit of 400 cm⁻¹ the shift to lower wavenumbers cannot be monitored, preventing peak assignment. The only peak that can be assigned is the prominent peak in Me₂DPP which is vibration 16b by analogy with 2,5-dimethylpyrazine.

Also in the 1000-400 cm⁻¹ spectral range the oxidized polymer DPP-C6-O₂ shows similar changes to Me₂DPP-O₂ when taking into account semi-crystallinity. This latter effect explains the lack of intense peaks in the C-H stretch region and the broader N-O peak at 881 cm⁻¹.

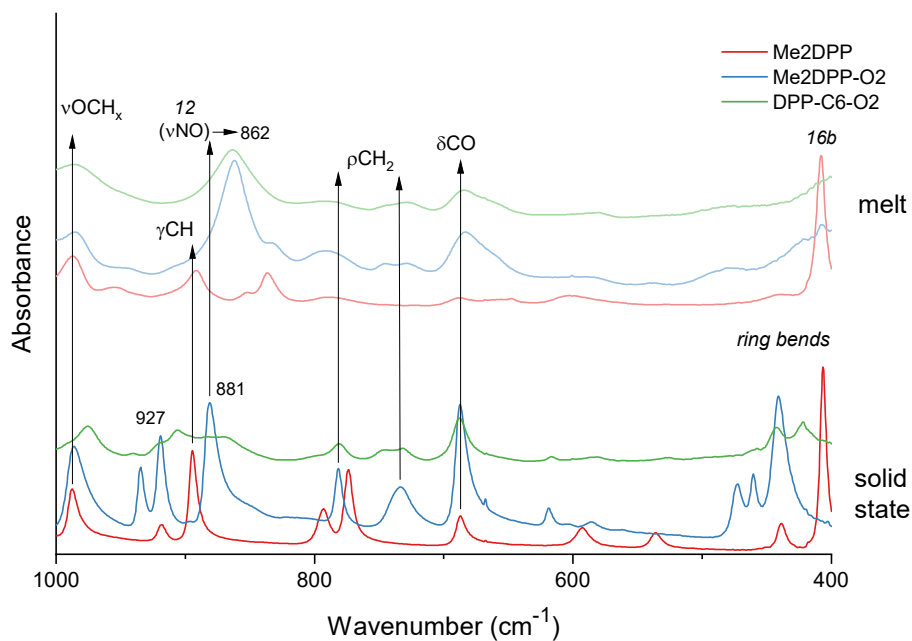


Figure 8: Infrared spectra of Me₂DPP (red) & Me₂DPP-O₂ (blue) and DPP-C₆-O₂ (green) in the 1600-1000 cm⁻¹ range above and below the melt.

Although Me₂DMDPP-O₂ also shows a significant increase in melting point, hydrogen bonding could not be confirmed in a similar manner as above due to the lack of fully resolved aromatic C-H stretches, a more dense vNO region and smaller changes between the solid state and the melt (see **Figure A4**). The latter is most likely due to methyl groups being weaker hydrogen bond donors than aromatic C-H bonds.

The changes observed in the infrared spectra between the solid state and the melt for both Me₂DPP-O₂ and DPP-C₆-O₂, can be adequately explained by the presence of weak hydrogen bonds. This hydrogen bonding in turn results in the observed increase in melting point between the oxidized and non-oxidized species.

Surface modification of DMDPP-C₆ polymer

Since oxidative post-modification is feasible in solution, we turned our attention to surface modification. Selective introduction of different properties on a surface could be of interest, as the presence of N-oxide groups may determine wettability or improve biocompatibility. Thus, we treated a film of DMDPP-C₆ polymer with mCPBA in ethylacetate. The modified and unmodified films were subsequently analysed by IR using ATR sampling. Since ATR only penetrates a sample to about 5 μm^[81] it gives a reasonable measure of surface modification. From the spectra it becomes clear that modification indeed results in additional peaks while the peaks of the unmodified

material remain (see **Figure 9**, blue) visible as well. A number of peaks can be specifically attributed to the N-O vibrations. These include a change in the semi-circle stretch at 1515 cm^{-1} , the νNO vibration at 1256 cm^{-1} , a NO combination band at 830 cm^{-1} and the αNO band at 445 cm^{-1} . The difference spectrum obtained by subtracting the unmodified film spectrum from the modified film spectrum is extremely similar to the spectrum of the fully oxidized DMDPP-C6 polymer (**Table 1**, entry 9), (see **Figure 9**, green). Considering these changes in IR combined with the sampling technique selective surface modification seems possible. For further proof of surface modification, the films were analysed by X-ray Photon Spectroscopy (XPS), a surface selective technique. The spectra showed clear formation of new nitrogen associated photons (see **Figure A32**), further confirming the surface modification.

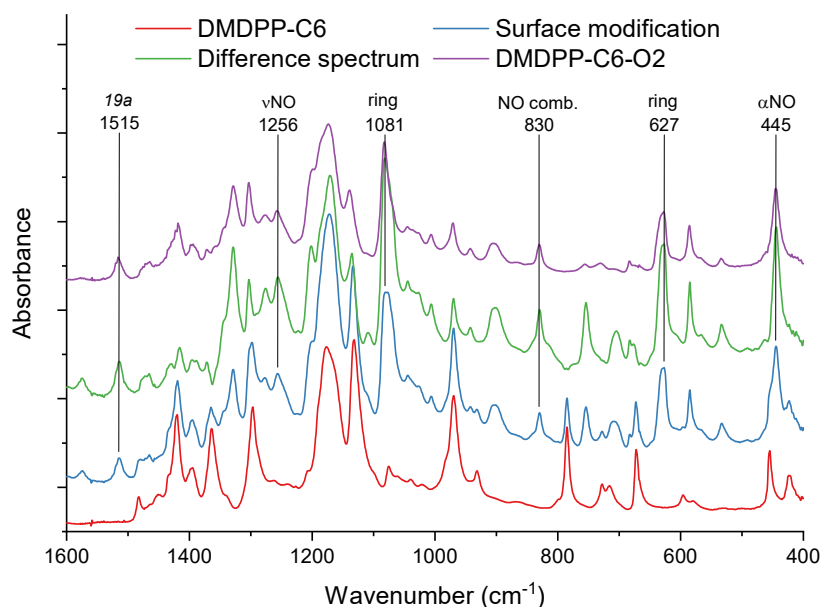


Figure 9: Infrared spectra of DMDPP-C6 polyester (red), after surface modification (blue), difference spectrum (green) and the DMDPP-C6-O2 polyester (purple).

Further proof of the surface modification and the effect on wettability was obtained by water contact angle measurements on both modified and unmodified spincoated plates. For the unmodified plates the average contact angle was $71^\circ \pm 3^\circ$ and the modified plates had an angle of $56^\circ \pm 4^\circ$. This indicates that the introduction of oxygen on the surface is successful and results in different wetting behaviour, with the surface becoming more hydrophilic. The surface properties thus can be tuned in this fashion.

Conclusions

The recently reported biobased pyrazine containing building blocks Me₂DMDPP and Me₂DPP and their 1,6-hexanediol derived polymers (DMDPP-C6 and DPP-C6) were used for a proof of principle post-modification study. Post-modification by alkylation is not possible for the DMDPP monomer and its polymer. Most likely steric effects hamper reaction of the relatively weak nucleophilic pyrazine nitrogen lone-pairs to the electrophilic alkylation agents used. Alkylation with trimethyloxonium tetrafluoroborate proves, however feasible at least in case of Me₂DPP and most likely for its 1,6-hexanediol-based polymer. However, solubility and stability issues made isolation and characterization of the modified polymer not practical. Polymers of DPP with other co-monomers may prove better targets for future post-alkylation studies.

On the other hand, oxidative post-modification of both monomers and polymers is facile in the presence of *m*-chloroperbenzoic acid. This oxidation has a large effect on the thermal properties of the materials. With increasing degree of oxidation, the DMDPP-based polymer showed complete loss of semi-crystallinity, which coincided with an increase in glass transition temperature. The Me₂DPP monomer and the DPP-C6 polymer, on the other hand, show a surprising increase in melting point at high degrees of oxidation. Using infrared spectroscopy, we were able to demonstrate that (weak) hydrogen bonds between the aromatic C-H and N-O groups may account for this increase in melting point. Next to this, selective surface modification of a polymer film by exposing it to oxidant in a non-solvent is also possible as was demonstrated after infra-red and XPS analyses of the oxidized film materials. Surface modification results in higher wettability of the polymer compared to the unmodified material.

The thermal properties of any polymer containing either of these pyrazines can thus be adjusted by oxidative post-modification. Next to this, the presence of N-oxides in the polymer enables access to other chemistries and reactivity, which we will explore in the future. Overall, the biobased nature of the reported pyrazines and their ability to undergo post-modification make them interesting building blocks for further study as added functionality materials with tunable properties.

References

- [1] A. L. Andradý, M. A. Neal, *Philosophical Transactions of the Royal Society B: Biological Sciences* **2009**, 364, 1977-1984
- [2] H. Millet, P. Vangheluwe, C. Block, A. Sevenster, L. Garcia, R. Antonopoulos, in *Plastics and the Environment*, The Royal Society of Chemistry, **2019**, pp. 1-20.
- [3] R. Geyer, J. R. Jambeck, K. L. Law, *Science Advances* **2017**, 3, e1700782
- [4] F. H. Isikgor, C. R. Becer, *Polym. Chem.* **2015**, 6, 4497-4559
- [5] F. De Schouwer, L. Claes, A. Vandekerckhove, J. Verduyck, D. E. De Vos, *ChemSusChem* **2019**, 12, 1272-1303
- [6] M. A. Würdemann, K. V. Bernaerts, *ACS Sustain. Chem. Eng.* **2020**, 8, 12045-12052
- [7] M. A. Würdemann, C. Nitu, S. M. A. De Wildeman, K. V. Bernaerts, R. V. A. Orru, *Chem. Eur. J.* **2020**, 26, 8090-8100
- [8] G. B. Barlin, *The Pyrazines*, Wiley, New York, **1982**.
- [9] D. J. Brown, *The Pyrazines: Supplement I*, Wiley, New York, **2003**.
- [10] T. J. Curphey, *J. Am. Chem. Soc.* **1965**, 87, 2063-2064
- [11] T. J. Curphey, K. S. Prasad, *J. Org. Chem.* **1972**, 37, 2259-2266
- [12] H.-D. Hausen, A. Schulz, W. Kaim, *Chem. Ber.* **1988**, 121, 2059-2061
- [13] A. Schulz, W. Kaim, H.-D. Hausen, *J. Chem. Soc. Farad. T.* **1988**, 84, 3207-3214
- [14] W. Kaim, A. Schulz, F. Hilgers, H. D. Hausen, M. Moscherosch, A. Lichtblau, J. Jordanov, E. Roth, S. Zalis, *Res. Chem. Intermed.* **1993**, 19, 603-615
- [15] W. L. Darby, L. M. Vallarino, *Inorg. Chim. Acta* **1983**, 75, 65-71
- [16] E. Waldhor, W. Kaim, J. A. Olabe, L. D. Slep, J. Fiedler, *Inorg. Chem.* **1997**, 36, 2969-2974
- [17] C. Yang, M.-S. Wang, Z.-N. Xu, F. Chen, G.-N. Liu, G. Xu, G.-C. Guo, J.-S. Huang, *Inorg. Chem. Commun.* **2010**, 13, 326-329
- [18] D. R. Eaton, J. M. Watkins, R. J. Buist, *J. Am. Chem. Soc.* **1985**, 107, 5604-5609
- [19] P. Ménová, F. Kafka, H. Dvořáková, S. Gunnoo, M. Šanda, R. Cibulka, *Adv. Synth. Catal.* **2011**, 353, 865-870
- [20] J. Sturala, S. Bohacova, J. Chudoba, R. Metelkova, R. Cibulka, *J. Org. Chem.* **2015**, 80, 2676-2699
- [21] R. Brisar, D. Hollmann, E. Mejia, *Eur. J. Org. Chem.* **2017**, 2017, 5391-5398
- [22] J. Lu, J. K. Kochi, *Cryst. Growth Des.* **2009**, 9, 291-296
- [23] L. W. Deady, J. A. Zoltewicz, *J. Am. Chem. Soc.* **1971**, 93, 5475-5477
- [24] C. Stoehr, *J. Prakt. Chem.* **1893**, 47, 439-522
- [25] C. Stoehr, *J. Prakt. Chem.* **1894**, 49, 392-403
- [26] C. Stoehr, *J. Prakt. Chem.* **1894**, 51, 449-476
- [27] C. Stoehr, P. Brandes, *J. Prakt. Chem.* **1896**, 53, 501-512
- [28] H. J. Scholl, (Bayer AG), DE3427400A1, **1986**
- [29] M. Lucarini, G. F. Pedulli, L. Valgimigli, *Gazz. Chim. Ital.* **1994**, 124, 455-457
- [30] Y. Gao, J. n. M. Shreeve, *Synthesis* **2004**, 2004, 1072-1082
- [31] B. Geurtsen, D. A. de Bie, H. C. van der Plas, *Tetrahedron* **1989**, 45, 6519-6530
- [32] T. Hofmann, W. Bors, K. Stettmaier, *J. Agric. Food. Chem.* **1999**, 47, 379-390
- [33] W. W. Paudler, S. A. Humphrey, *J. Org. Chem.* **1970**, 35, 3467-3470
- [34] H. Miyazaki, Y. Matsuhisa, T. Kubota, *Bull. Chem. Soc. Jpn.* **1981**, 54, 3850-3853
- [35] S. I. Kulakovskaya, A. V. Kulikov, A. F. Shestakov, *Russ. J. Electrochem.* **2007**, 43, 1156-1163
- [36] S. I. Kulakovskaya, A. V. Kulikov, A. F. Shestakov, *Russ. J. Electrochem.* **2009**, 45, 1368-1375
- [37] S. I. Kulakovskaya, A. V. Kulikov, A. F. Shestakov, *Russ. J. Electrochem.* **2010**, 46, 1047-1055
- [38] N. Ikekawa, Y. Honma, R. Kenkyusho, *Tetrahedron Lett.* **1967**, 8, 1197-1200
- [39] P. Deledalle, A. Lablache-Combier, C. Loucheux, *J. Appl. Polym. Sci.* **1984**, 29, 125-140
- [40] C. J. Popp, G. D. Garlough, *J. Inorg. Nucl. Chem.* **1981**, 43, 501-507
- [41] R. Puttreddy, J. R. A. Cottam, P. J. Steel, *RSC Advances* **2014**, 4, 22449-22454
- [42] J. A. Schlueter, H. Park, G. J. Halder, W. R. Armand, C. Dunmars, K. W. Chapman, J. L. Manson, J. Singleton, R. McDonald, A. Plonczak, J. Kang, C. Lee, M.-H. Whangbo, T. Lancaster, A. J. Steele, I. Franke, J. D. Wright, S. J. Blundell, F. L. Pratt, J. deGeorge, M. M. Turnbull, C. P. Landee, *Inorg. Chem.* **2012**, 51, 2121-2129
- [43] B.-Q. Ma, H.-L. Sun, S. Gao, G. Su, *Chem. Mater.* **2001**, 13, 1946-1948
- [44] H. L. Sun, S. Gao, B. Q. Ma, G. Su, *Inorg. Chem.* **2003**, 42, 5399-5404

- [45] H.-L. Sun, S. Gao, B.-Q. Ma, F. Chang, W.-F. Fu, *Microporous Mesoporous Mater.* **2004**, *73*, 89-95
- [46] R. Podgajny, D. Pinkowicz, B. Czarnecki, M. Koziel, S. Chorąży, M. Wis, W. Nitek, M. Rams, B. Sieklucka, *Cryst. Growth Des.* **2014**, *14*, 4030-4040
- [47] B. Klein, J. Berkowitz, N. E. Hetman, *J. Org. Chem.* **1961**, *26*, 126-131
- [48] N. Sato, M. Fujii, *J. Heterocycl. Chem.* **1994**, *31*, 1177-1180
- [49] N. Sato, N. Miwa, H. Suzuki, T. Sakakibara, *J. Heterocycl. Chem.* **1994**, *31*, 1229-1233
- [50] S. K. Das, J. Frey, *Tetrahedron Lett.* **2012**, *53*, 3869-3872
- [51] D. J. Schipper, M. El-Salfiti, C. J. Whipp, K. Fagnou, *Tetrahedron* **2009**, *65*, 4977-4983
- [52] H. Andersson, T. S. Banchelin, S. Das, M. Gustafsson, R. Olsson, F. Almqvist, *Org. Lett.* **2010**, *12*, 284-286
- [53] T. Steiner, *Crystallography Reviews* **2006**, *6*, 1-51
- [54] H. Sato, R. Murakami, A. Padermshoke, F. Hirose, K. Senda, I. Noda, Y. Ozaki, *Macromolecules* **2004**, *37*, 7203-7213
- [55] H. Sato, J. Dybal, R. Murakami, I. Noda, Y. Ozaki, *J. Mol. Struct.* **2005**, *744-747*, 35-46
- [56] J. Zhang, H. Sato, H. Tsuji, I. Noda, Y. Ozaki, *J. Mol. Struct.* **2005**, *735-736*, 249-257
- [57] H. Sato, Y. Ando, J. Dybal, T. Iwata, I. Noda, Y. Ozaki, *Macromolecules* **2008**, *41*, 4305-4312
- [58] H. Sato, M. Miyada, S. Yamamoto, K. Raghunatha Reddy, Y. Ozaki, *RSC Advances* **2016**, *6*, 16817-16823
- [59] C. B. Aakeroy, T. K. Wijethunga, J. Benton, J. Desper, *Chem. Commun.* **2015**, *51*, 2425-2428
- [60] C. J. Brown, J. M. Knaust, *Acta Crystallographica Section E - Structure Reports Online* **2009**, *65*, 03052
- [61] C. F. Macrae, I. Sovago, S. J. Cottrell, P. T. A. Galek, P. McCabe, E. Pidcock, M. Platings, G. P. Shields, J. S. Stevens, M. Towler, P. A. Wood, *J. Appl. Crystallogr.* **2020**, *53*, 226-235
- [62] G. R. Desiraju, *Acc. Chem. Res.* **1991**, *24*, 290-296
- [63] T. Steiner, *Chem. Commun.* **1999**, 313-314
- [64] B. Klein, J. Berkowitz, *J. Am. Chem. Soc.* **1959**, *81*, 5160-5166
- [65] C. F. Koelsch, W. H. Gumprecht, *J. Org. Chem.* **1958**, *23*, 1603-1606
- [66] A. Ohta, M. Ohta, *Synthesis* **1985**, *1985*, 216-217
- [67] R. A. Aitken, B. Fodi, M. H. Palmer, A. M. Z. Slawin, J. Yang, *Tetrahedron* **2012**, *68*, 5845-5851
- [68] R. A. Yadav, V. Mukherjee, M. Kumar, R. Singh, *Spectrochim. Acta, Part A* **2007**, *66*, 964-971
- [69] D. A. Thornton, P. F. M. Verhoeven, G. M. Watkins, H. O. Desseyn, B. J. Van der Veken, *Spectrochim. Acta A-M* **1990**, *46*, 1439-1451
- [70] J. F. Arenas, S. P. Centeno, I. López-Tocón, J. C. Otero, *J. Mol. Struct.* **2005**, *744-747*, 289-293
- [71] J. F. Arenas, J. T. López-Navarrete, J. I. Marcos, J. C. Otero, *J. Mol. Struct.* **1987**, *162*, 263-272
- [72] G. Desiraju, T. Steiner, *The Weak Hydrogen Bond: In Structural Chemistry and Biology* (Eds.: G. Desiraju, T. Steiner), Oxford Univ. Press, Oxford, **2001**, pp 29-121.
- [73] N. B. Colthup, L. H. Daly, S. E. Wiberley, in *Introduction to Infrared and Raman Spectroscopy* (Third Edition) (Eds.: N. B. Colthup, L. H. Daly, S. E. Wiberley), Academic Press, San Diego, **1990**, pp. 171-213.
- [74] R. C. Lord, A. L. Marston, F. A. Miller, *Spectrochim. Acta* **1957**, *9*, 113-125
- [75] A. Andrejeva, A. M. Gardner, W. D. Tuttle, T. G. Wright, *J. Mol. Spectrosc.* **2016**, *321*, 28-49
- [76] G. Varsányi, in *Vibrational Spectra of Benzene Derivatives* (Ed.: G. Varsányi), Academic Press, **1969**, pp. 141-393.
- [77] R. M. Moravie, J. Corset, *J. Mol. Struct.* **1975**, *24*, 91-108
- [78] D. A. Thornton, G. M. Watkins, *Spectrosc. Lett.* **1992**, *25*, 1023-1036
- [79] H. Shindo, *Chemical & Pharmaceutical Bulletin* **1959**, *7*, 791-800
- [80] H. Shindo, *Chemical & Pharmaceutical Bulletin* **1960**, *8*, 33-45
- [81] F. M. Mirabella, *Applied Spectroscopy Reviews* **1985**, *21*, 45-178

Appendix

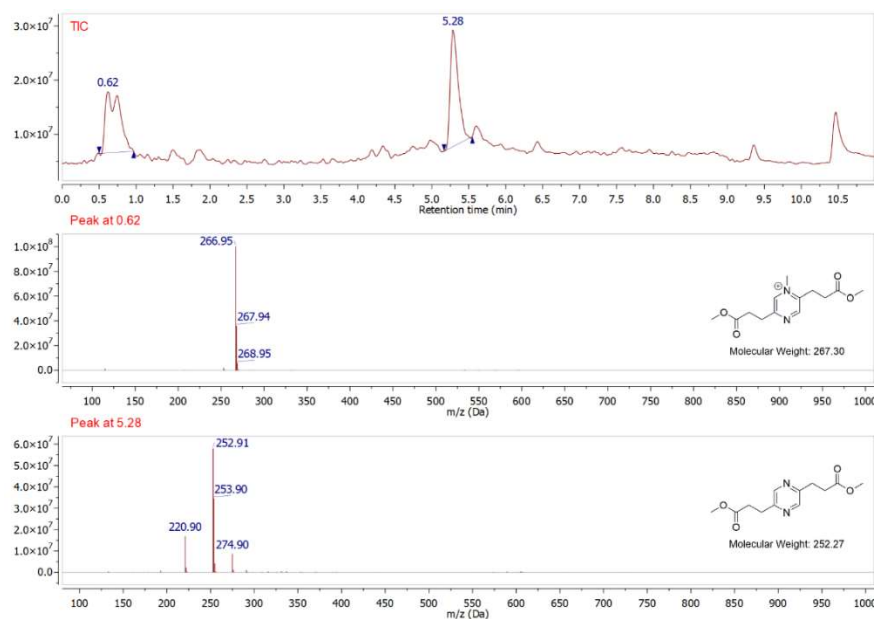


Figure A1: LC-MS Total Ion Count of mono-alkylation attempt.

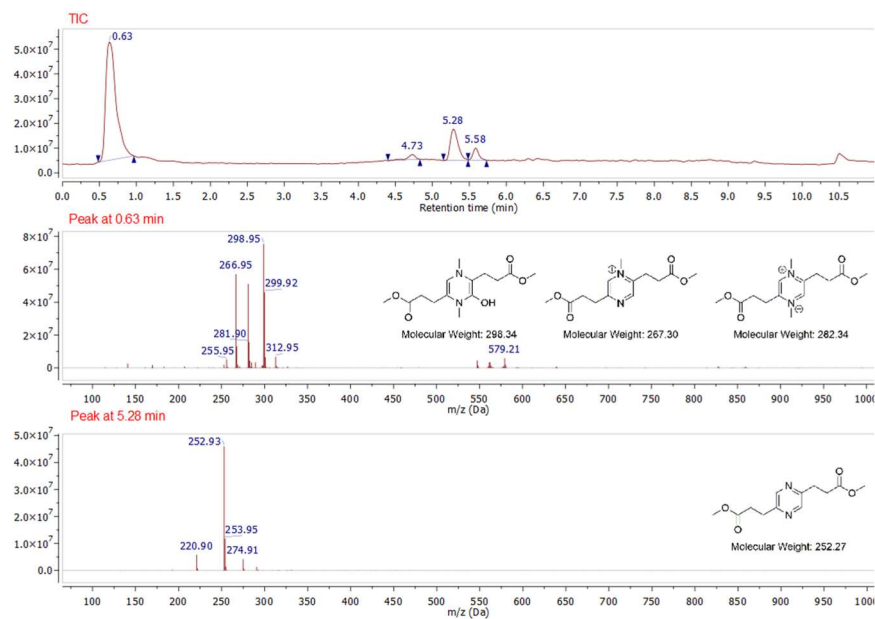
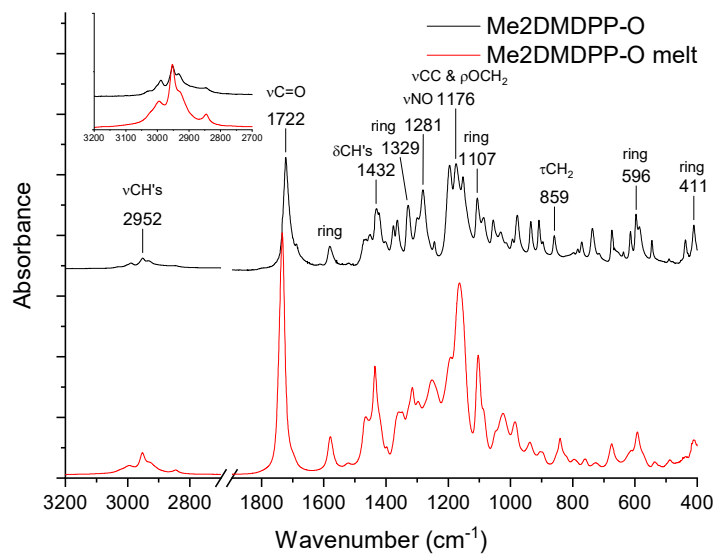
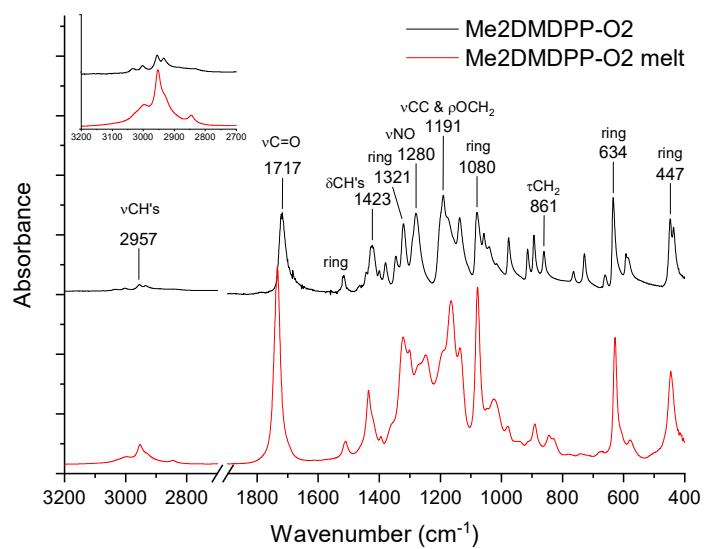


Figure A2: LC-MS TIC for dialkylation attempt, peak at 0.63 min clearly shows the lack of the expected dialkylated mass of 282 g/mol.

IR data monomers

Figure A3: IR spectrum below and above the melt for Me₂DMDPP-O.Figure A4: IR spectrum below and above the melt for Me₂DMDPP-O₂.

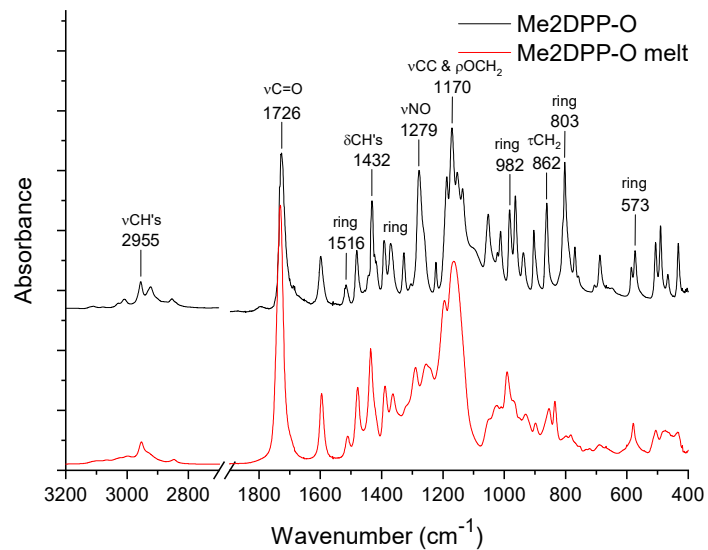


Figure A5: IR spectrum below and above the melt for Me₂DPP-O.

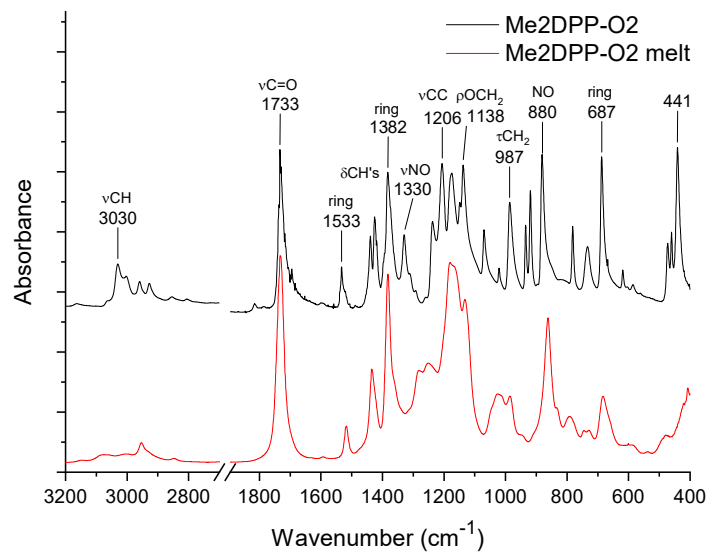


Figure A6: IR spectrum below and above the melt for Me₂DPP-O₂.

Conversion kinetics of oxidation

Two simple kinetics experiments were set up to monitor the minimal reaction time necessary for the oxidation to take place. One experiment was run with 1 eqv. of mCPBA and one with 3 eqv.

A vial fitted with a magnetic stirrer was loaded with Me₂DMDPP (50 mg, 0.178 mmol, 1.00 eqv.) and biphenyl (27.4 mg, 0.178 mmol, 1.00 eqv.) both of which were dissolved in 1 mL of CHCl₃. To this was added a solution of mCPBA (40.6 mg, 0.178 mmol, 1.00 eq or 120 mg, 0.534 mmol, 3.00 eqv.) in 1 mL of CHCl₃. Aliquots of 40 μL were taken from the reaction mixture at several time intervals and added to 40 μL (if 1.0eq. of mCPBA was used) or 120 μL (if 3.0 eqv. of mCPBA was used) of a 0.1M solution of sodium thiosulphate. This quenched mixture was then diluted in 1mL of acetonitrile, filtered and analyzed by LC-MS (1 μL injection).

The data was analyzed at 277 ± 10 nm wavelength (absorption maximum of Me₂DMDPP). The obtained peak areas were corrected for the sampling error by use of the biphenyl standard and for the response factors of both Me₂DMDPP and Me₂DMDPP-O. The final areas were converted to an area percentage and plotted below. Mono oxidation conversion stops in about 3 hours, while dioxidation requires at least 18h for conversion to seize.

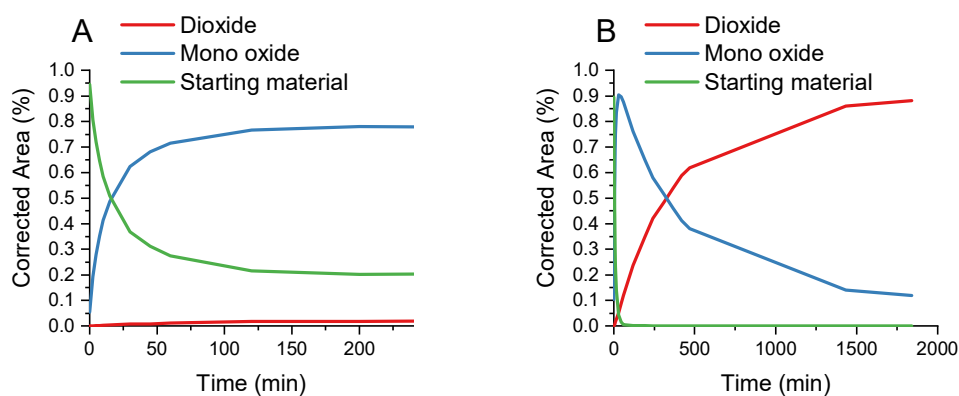
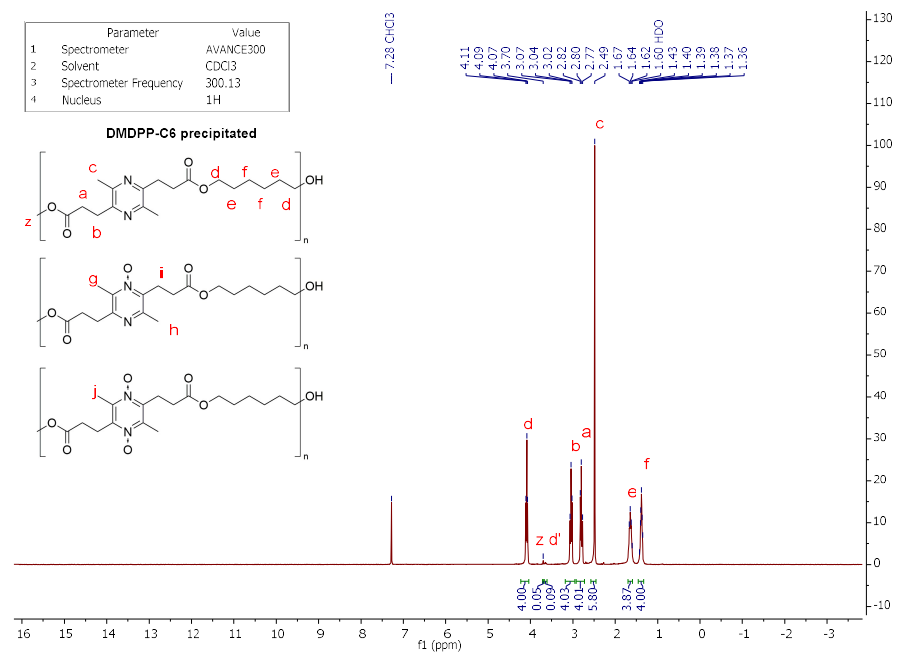
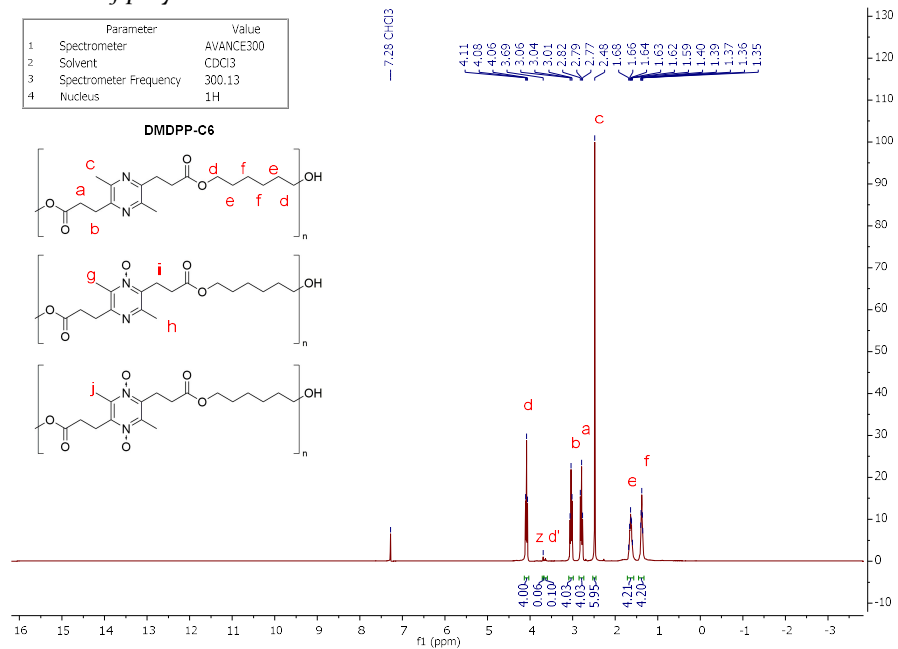
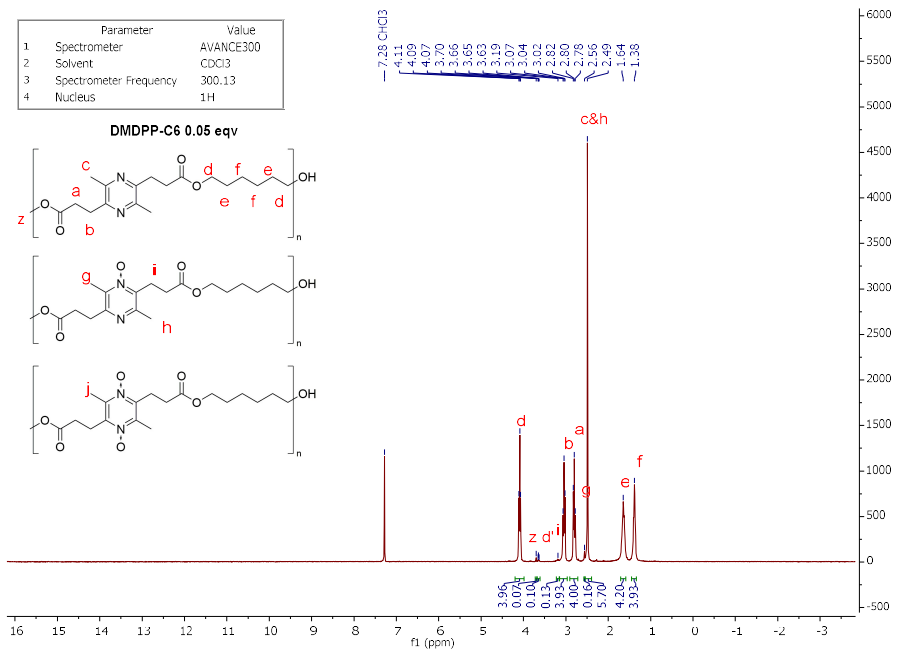
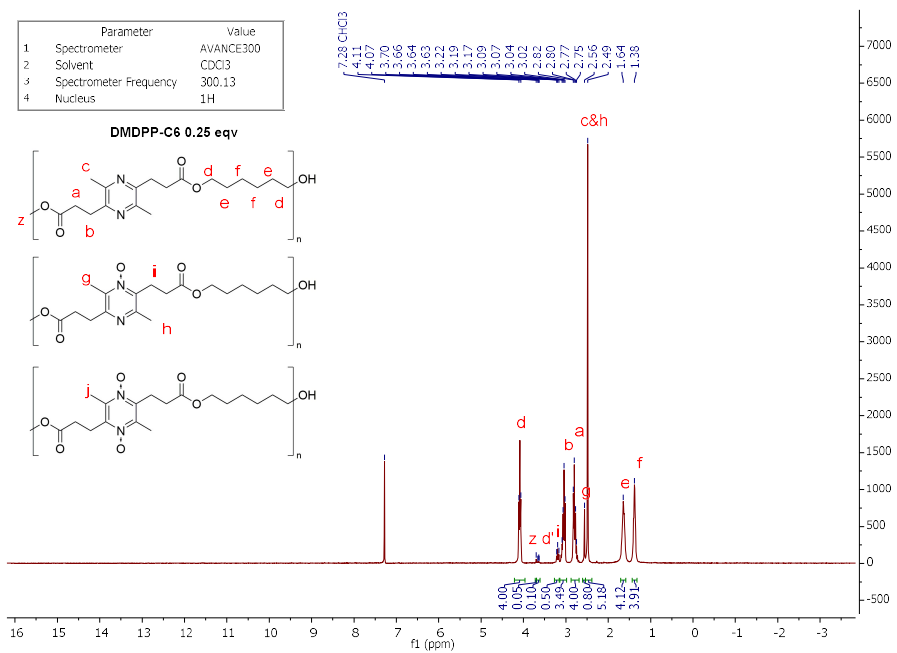


Figure A7: Conversion kinetics plots for the oxidation of Me₂DMDPP, both mono- (panel A) and dioxidation (panel B).

NMR data of polymers in Table 1



Figure A10: ¹H-NMR for entry 3.Figure A11: ¹H-NMR for entry 4.

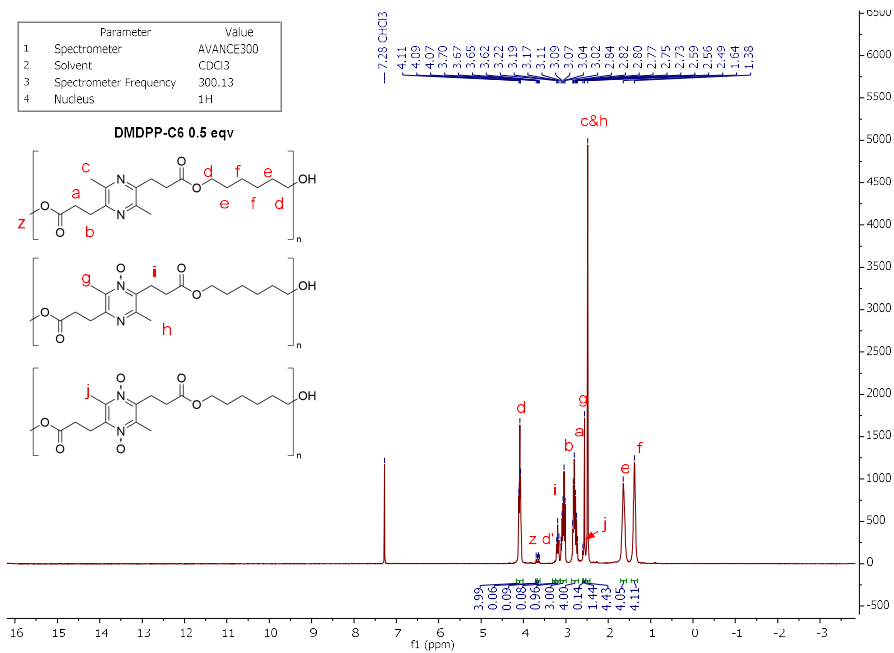


Figure A12: ¹H-NMR for entry 5.

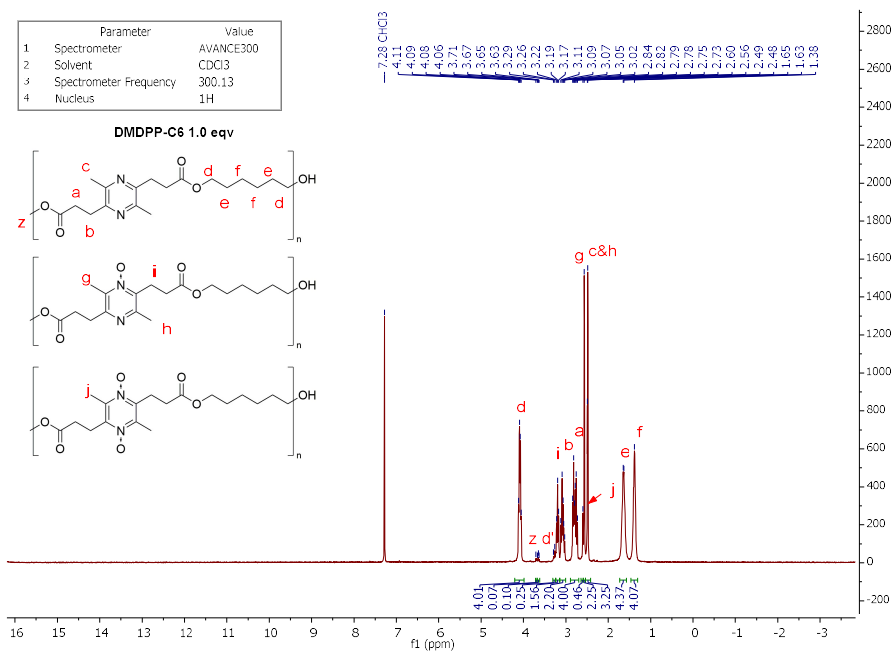
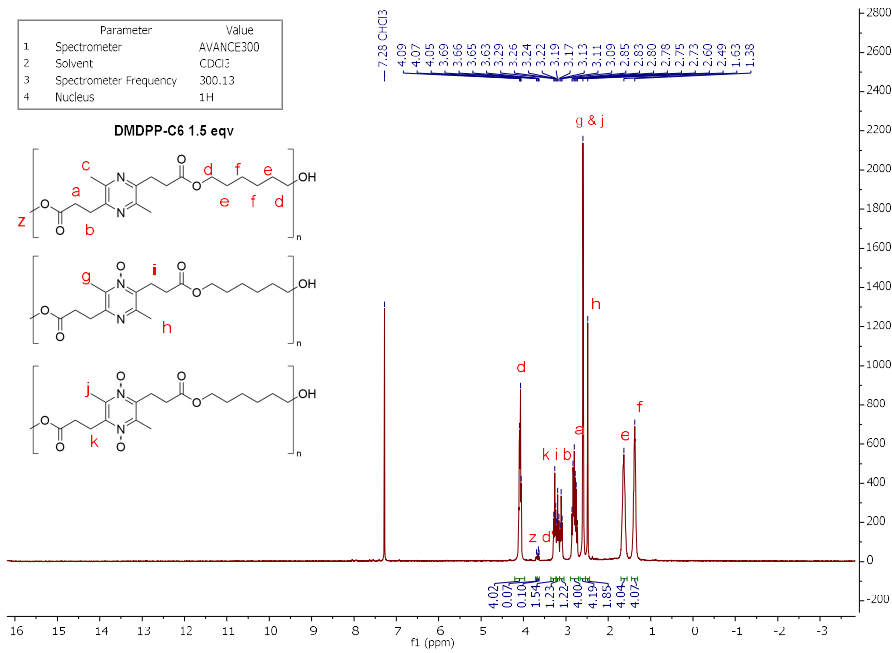
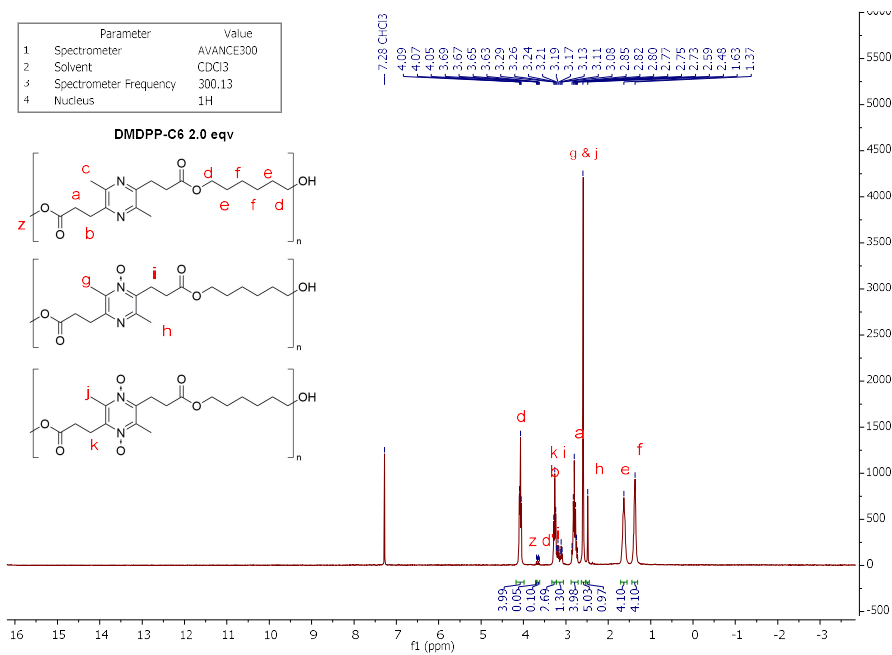
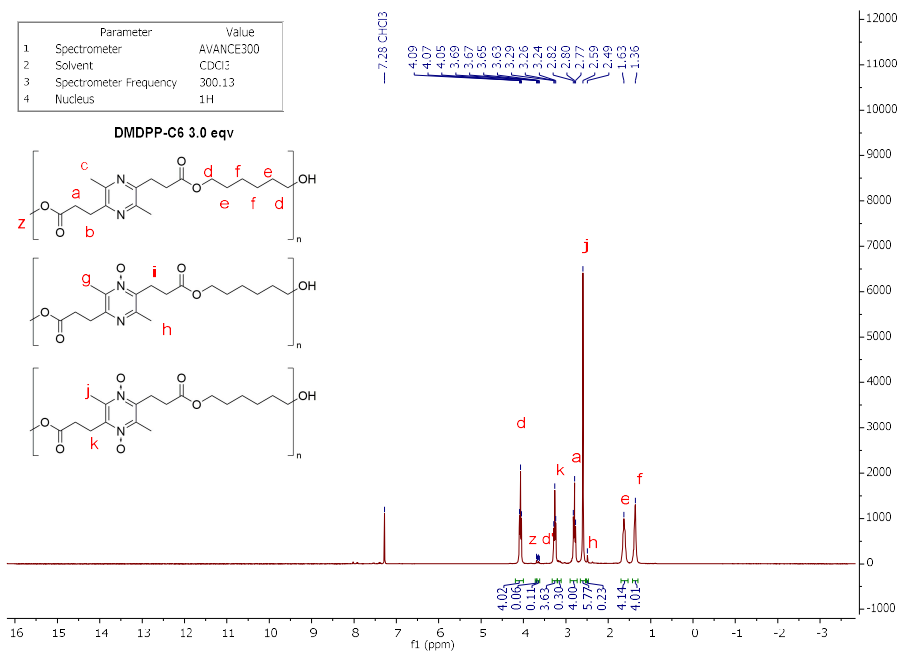
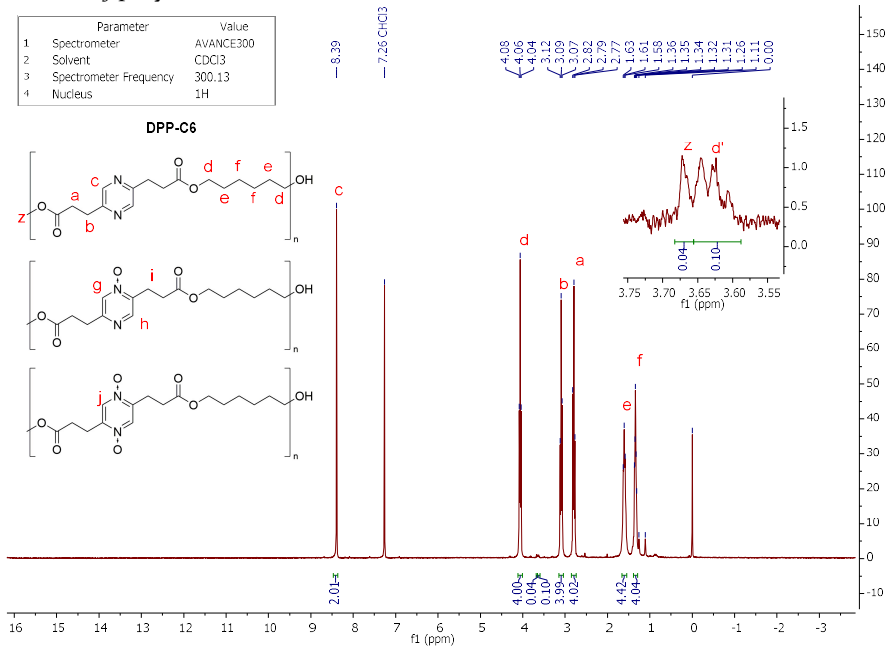


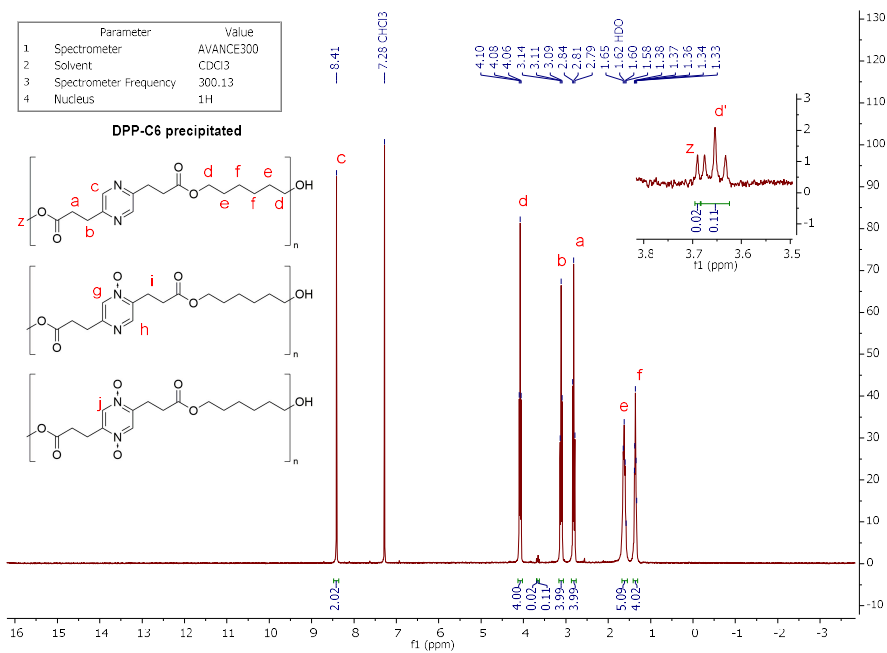
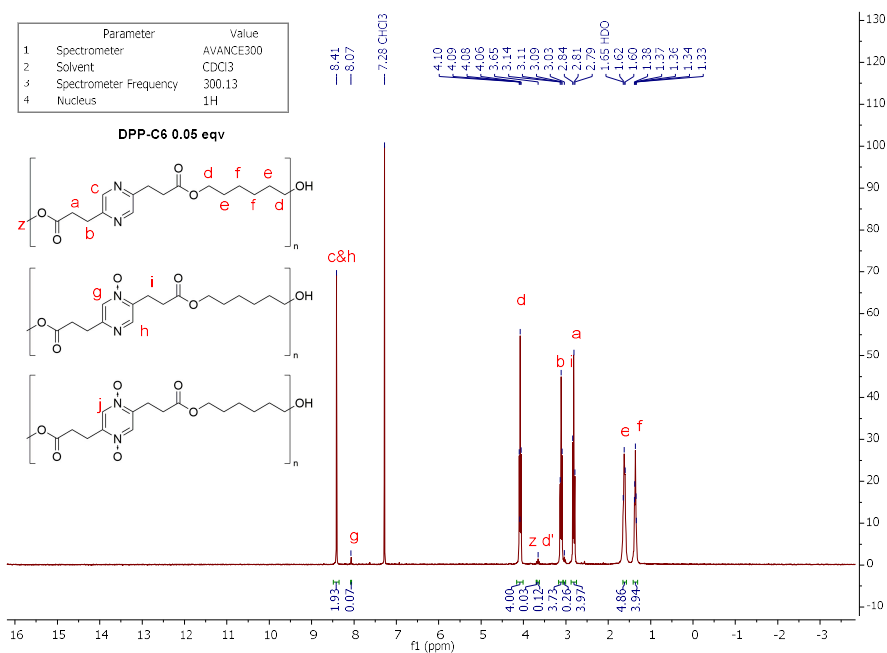
Figure A13: ¹H-NMR for entry 6.

Figure A14: ¹H-NMR for entry 7.Figure A15: ¹H-NMR for entry 8.



NMR data of polymers in Table 2



Figure A18: ¹H-NMR of entry 2.Figure A19: ¹H-NMR of entry 3.

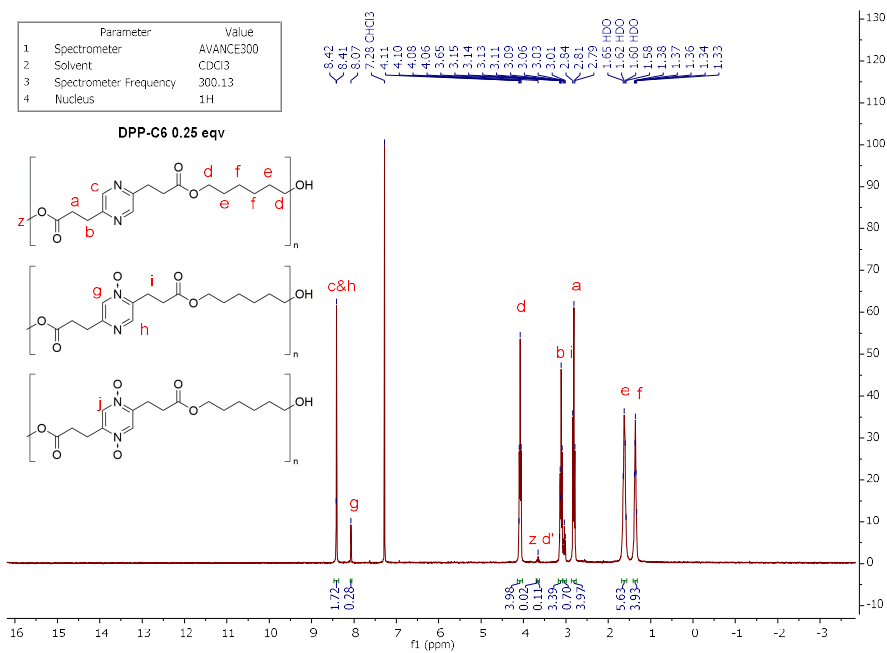


Figure A20: ¹H-NMR of entry 4.

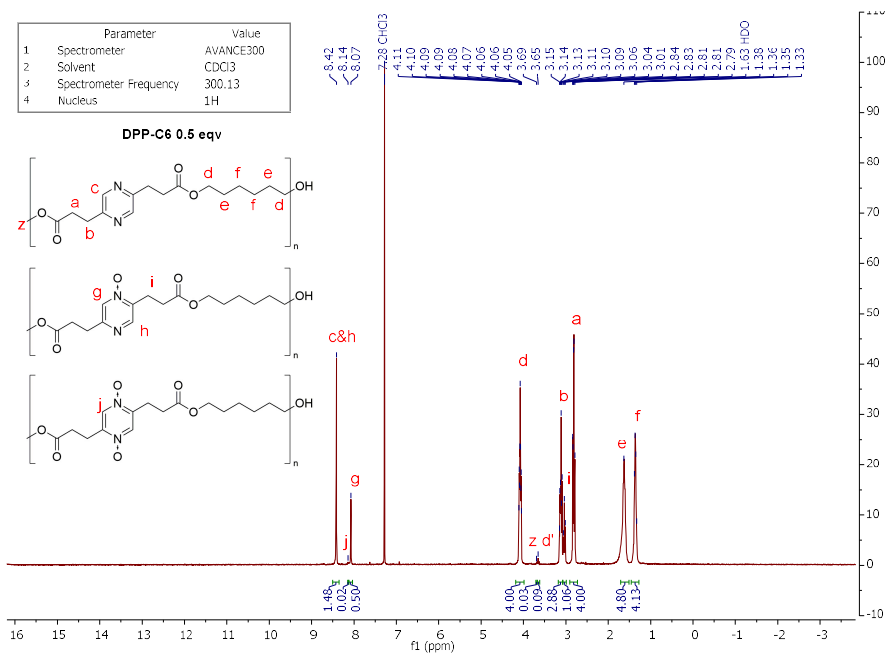
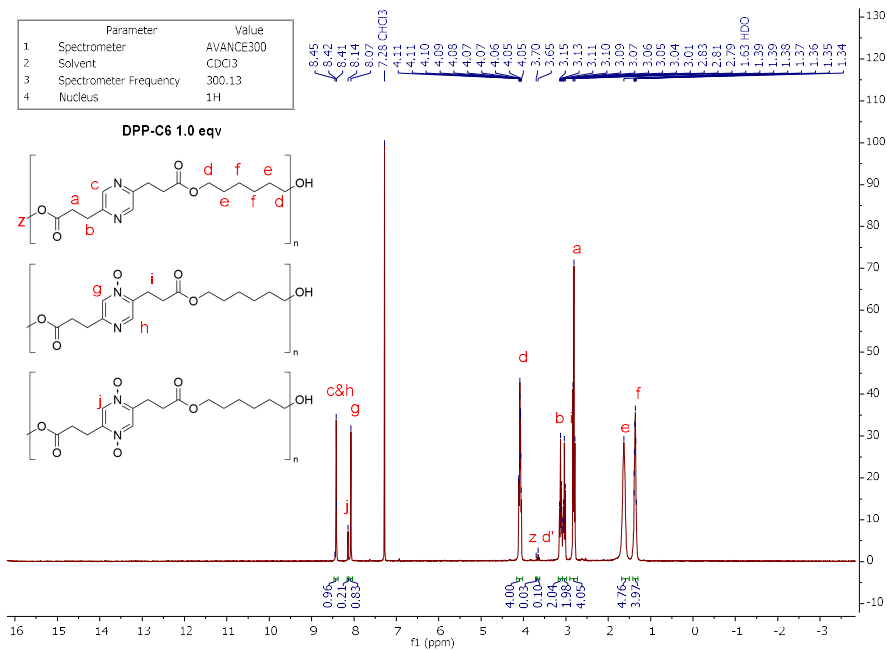
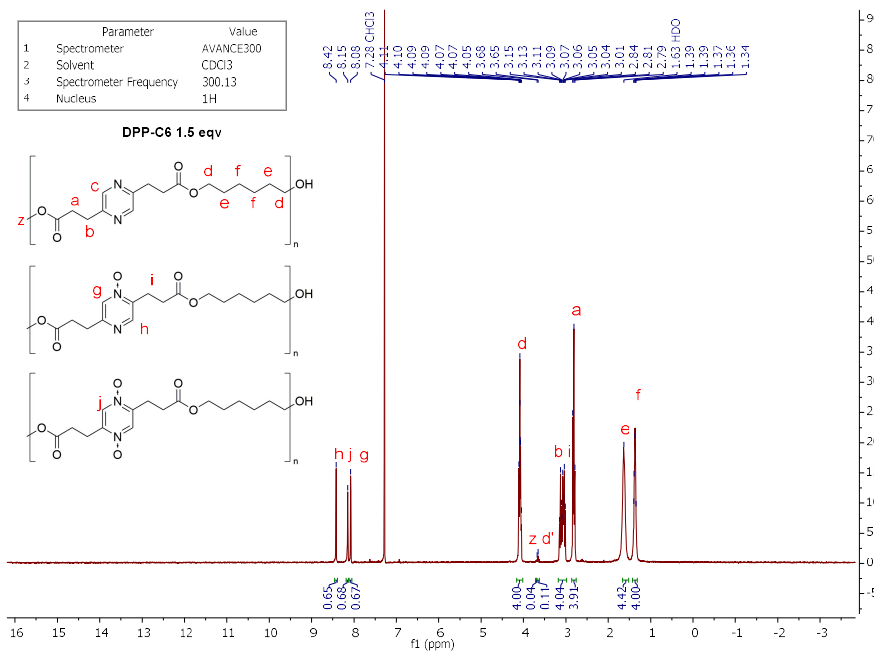


Figure A21: ¹H-NMR of entry 5.

Figure A22: ¹H-NMR of entry 6.Figure A24: ¹H-NMR of entry 7.

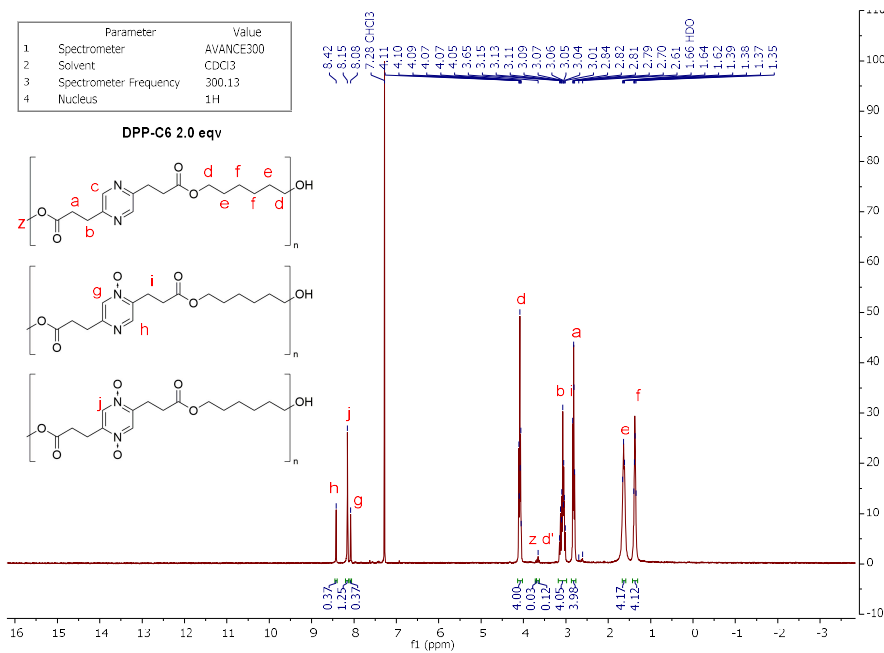


Figure S25: ¹H-NMR of entry 8.

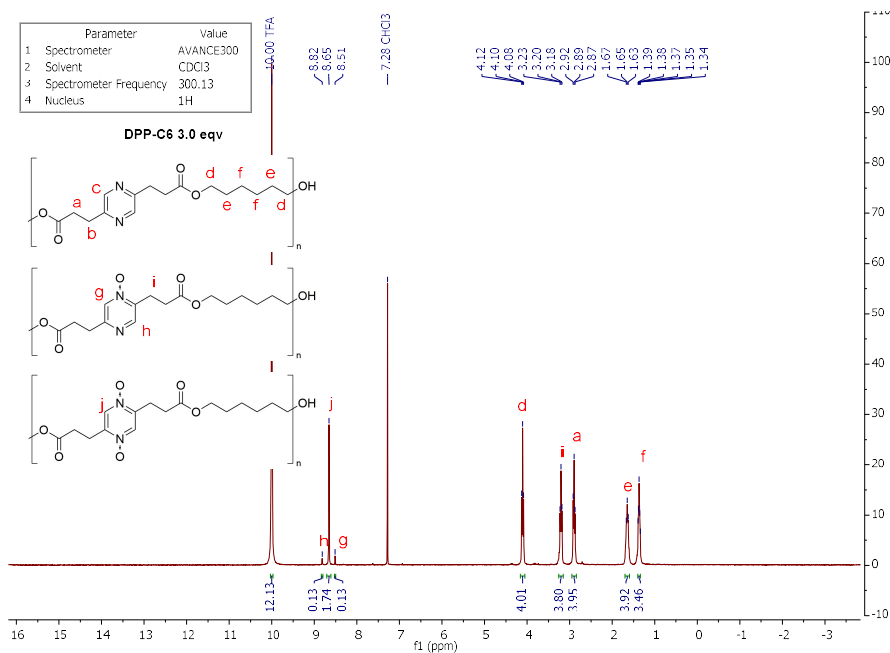


Figure A26: ¹H-NMR of entry 9.

NMR calculations

The end-group distribution of the synthesized polymers can be calculated from the ratio between both end-groups corrected for the number of protons of each end-group. This ratio is then translated to a percentage based on 200% (since there are 2 end-groups per chain). **Equation 1** provides an example using the peak labeling above. Using this formula for all polymers provides the distributions in **Tables A1&A2**.

$$\text{Eq 1: } \text{End - group distribution} = \frac{d'}{2} / \left(\frac{d'}{2} + \frac{z}{3} \right) \times 200\%$$

The degree of polymerization (*DP*) can be calculated from NMR end-groups as long as these can be integrated properly and used in **equation 2**.

$$\text{Eq 2: } \overline{DP} = \frac{(I_{ru} \times m_{end} \times n_{end})}{(I_{end} \times m_{ru})}$$

In this equation I_{ru} is the integral of the repeating unit, m_{end} is the number of protons for the end-groups, n_{end} is the number of end-groups, I_{end} is the integral for the end groups and m_{ru} is the number of protons for the repeating unit.

Since most of the polymers synthesized still show both end-groups on NMR, the number of end-groups has to be corrected for the end-group distribution. Using this correction either end-group can be used to calculate the *DP*. For these *DP* calculations, the repeating unit was defined as the glycol ester protons labeled **d** and being 4 protons. The end-group was defined as the alcohol end group peak **d'** being 2 protons and the number of end-groups corrected for the distribution. As an example of the calculations, the data for DMDPP-C6 was used.

Here I_{ru} is 4.00, m_{end} is 2, n_{end} is the fraction of alcohol end-groups and m_{ru} is 4. The end-group integral I_{end} is 0.102 in this case (peak **d'**). Filling these numbers in **equation 1** give the approximate *DP* of DMDPP-C2 (see **equation 3**). By using the fraction of the alcohol end-groups the degree of polymerization is not over-estimated as it would be when this number were set to the theoretical maximum of two.

$$\text{Eq 3: } \overline{DP} = \frac{(4.00 \times 2 \times 1.41)}{(0.102 \times 4)} = 28$$

These calculations were done for all polymers and the resulting *DP* values are found in **Tables 1&2** of the main manuscript and **Tables A1&A2** below.

Using the approximate *DP* values calculated, the M_n can be calculated by multiplying this number by the repeating unit weight and adding the end-group weights corrected for their distribution. No correction for the degree of oxidation was applied. These M_n values were rounded to the nearest 100 and are listed in **Tables A1&A2** below.

Table A1: NMR calculations overview for Table 1.

Polymer	End-group conv. ratio (%)	Repeating unit molecular weight (g/mol)	Ester end-group weight (g/mol)	Alcohol end-group weight (g/mol)	End-group distribution (alcohol/ ester) (%)	DP	M_n - NMR (g/mol)
Entry 1	97,9/95,2	334,42	265,29	117,17	141 / 59	28	9700
Entry 2	98,2/95,2	334,42	265,29	117,17	147 / 53	32	11000
Entry 3	98,2/95,6	334,42	265,29	117,17	144 / 56	25	8700
Entry 4	97,9/94,8	334,42	265,29	117,17	143 / 57	31	10700
Entry 5	98,5/94,7	334,42	265,29	117,17	158 / 42	28	9700
Entry 6	97,6/95,3	334,42	265,29	117,17	135 / 65	27	9400
Entry 7	97,5/94,8	334,42	265,29	117,17	137 / 63	24	8400
Entry 8	98,1/95,7	334,42	265,29	117,17	141 / 59	31	10700
Entry 9	98,2/94,0	334,42	265,29	117,17	163 / 37	25	8600

Table A2: NMR calculations overview for Table 2.

Polymer	End-group conv. ratio (%)	Repeating unit molecular weight (g/mol)	Ester end-group weight (g/mol)	Alcohol end-group weight (g/mol)	End-group distribution (alcohol/ ester) (%)	DP	M_n - NMR (g/mol)
Entry 1	98,7/95,8	306,36	237,24	117,17	158 / 42	33	10400
Entry 2	99,3/95,2	306,36	237,24	117,17	178 / 22	32	10100
Entry 3	99,1/94,7	306,36	237,24	117,17	173 / 27	29	9200
Entry 4	99,2/95,5	306,36	237,24	117,17	174 / 26	33	10400
Entry 5	99,0/95,8	306,36	237,24	117,17	164 / 36	35	11000
Entry 6	99,1/95,7	306,36	237,24	117,17	167 / 33	35	11000
Entry 7	98,6/95,2	306,36	237,24	117,17	157 / 43	30	9500
Entry 8	98,9/94,6	306,36	237,24	117,17	168 / 32	29	9200
Entry 9	-	306,36	237,24	117,17	-	-	-

NMR calculations oxidation ratios

The ratio of N-oxide versus non-oxidized pyrazines in the polymers as, given in **Tables 1 and 2** of the main manuscript, was calculated by integrating the peak belonging to the signals most influenced by the oxidation. These integrals were divided by the theoretical number of protons for each shift, the resulting number was rounded and normalized to 100%.

For DMDPP-C6 the peaks use were associated with the methylenes **b**, **i** and **k** in the assignments above, with **b** at no oxidation, **i** at mono-oxidation and **k** at di-oxidation. The integral for **k** represents 4 protons, the integral for **i** represents 2 protons and the integral for **b** represents 4 protons after subtraction of the integral of **i**. This correction is because at mono-oxidation one methylene shifts significantly while the other overlaps with **b**. At 2 and 3 equivalents of oxidant peak **b** is no longer present and peak **i** represents 4 protons and its integral is divided by 4. As an example, the case of the 1.0 equivalent reaction is given.

The number of double oxidized pyrazines is given by $(I_k \div 4) \times 100\% = O_2$

filling in with $I_k = 0.25$ gives $O_2 \approx 6\%$

The number of single oxidized pyrazines in given by $(I_i \div 2) \times 100\% = O_1$

filling in with $I_i = 1.56$ gives $O_1 \approx 78\%$

The number of non-oxidized pyrazines in given by $((I_b - I_i) \div 4) \times 100\% = O_0$

filling in with $I_b = 2.20$ and $I_i = 1.56$ gives $O_0 \approx 16\%$

For DPP-C6 oxidations the peaks of the aromatic pyrazine protons used were **c**, **g**, **h**, **j** in the assignments above, with **c** at no oxidation, **g** and **h** at mono-oxidation and **j** at di-oxidation. The integral for **j** represents 2 protons, the integral for **g** and **h** represent 1 protons and the integral for **c** represents 2 protons after subtraction of the integral of **g**. The correction is because at mono-oxidation the one proton shifts significantly while the other overlaps with **c**. As an example, the case of the 1.0 equivalent reaction is given.

The number of double oxidized pyrazines is given by $(I_j \div 2) \times 100\% = O_2$

filling in with $I_j = 0.21$ gives $O_2 \approx 10\%$

The number of single oxidized pyrazines in given by $(I_g \div 1) \times 100\% = O_1$

filling in with $I_g = 0.88$ gives $O_1 \approx 87\%$

The number of non-oxidized pyrazines in given by $((I_c - I_g) \div 2) \times 100\% = O_0$

filling in with $I_c = 0.96$ and $I_g = 0.88$ gives $O_0 \approx 2\%$

DSC data first heating cycles

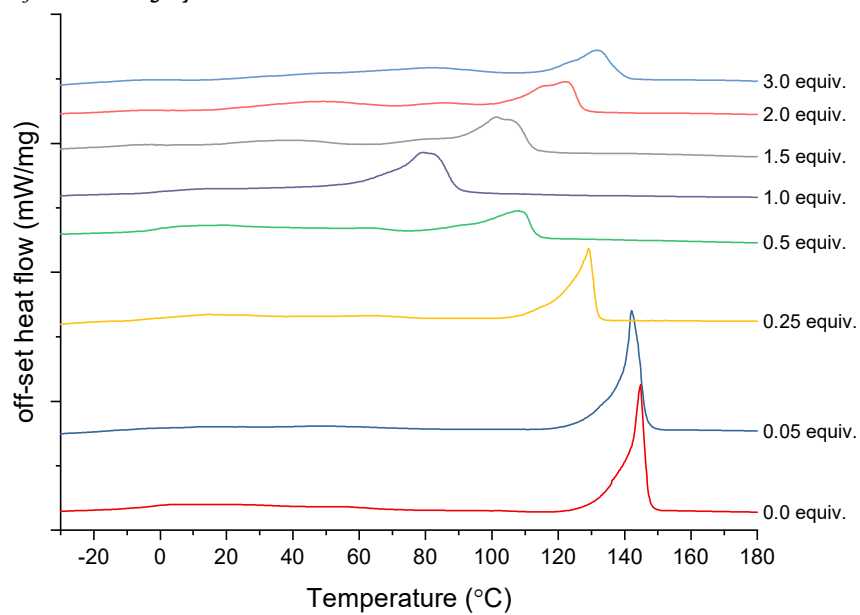


Figure A27: First heating cycles of DMDPP-C6 oxidations

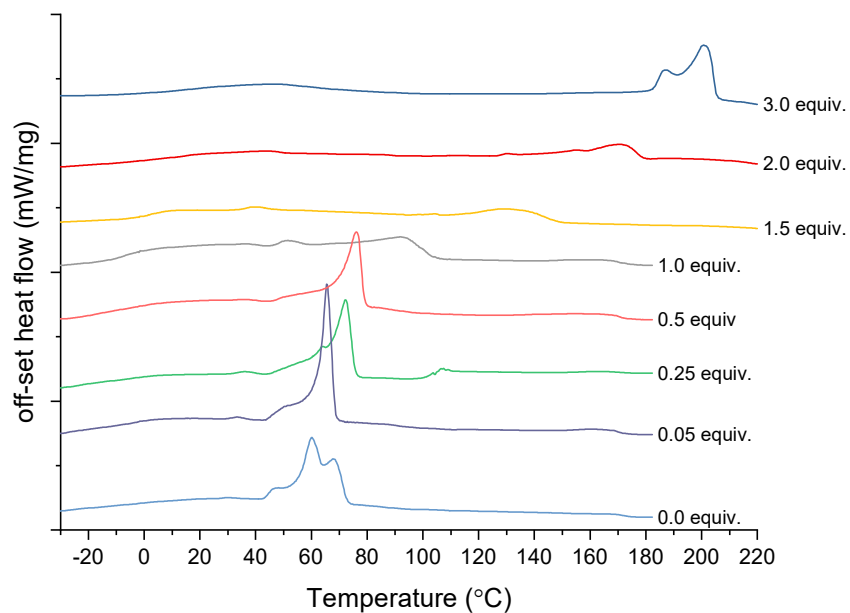


Figure A28: First heating cycles of DPP-C6 oxidations.

TGA data

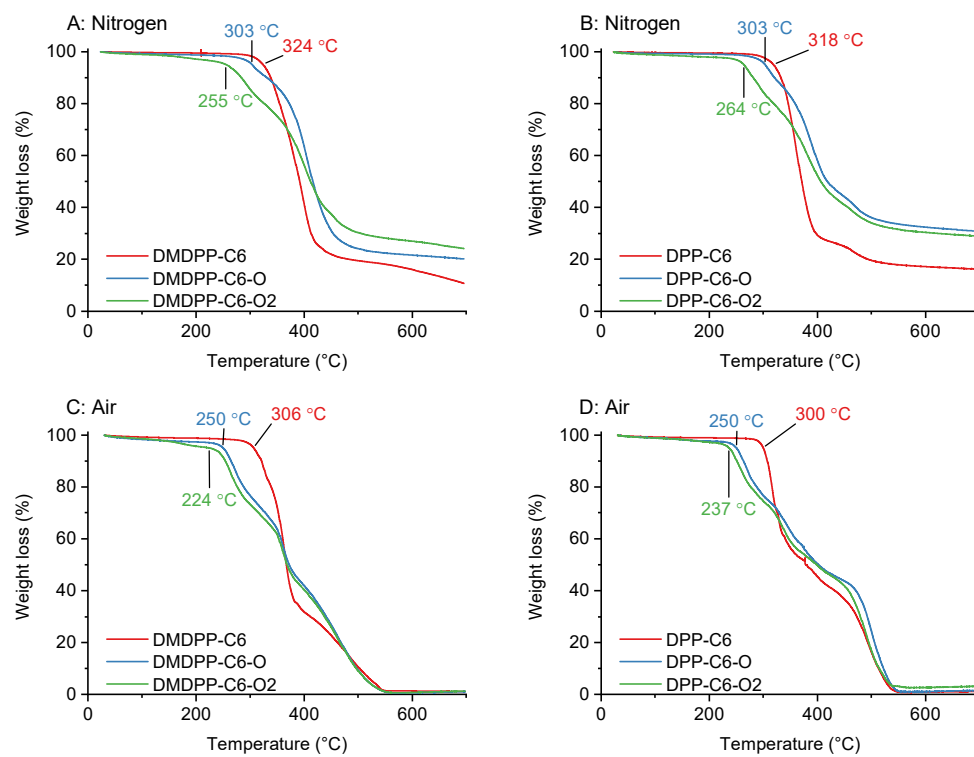


Figure A29: TGA data for the reported polymers.

IR data of polymers

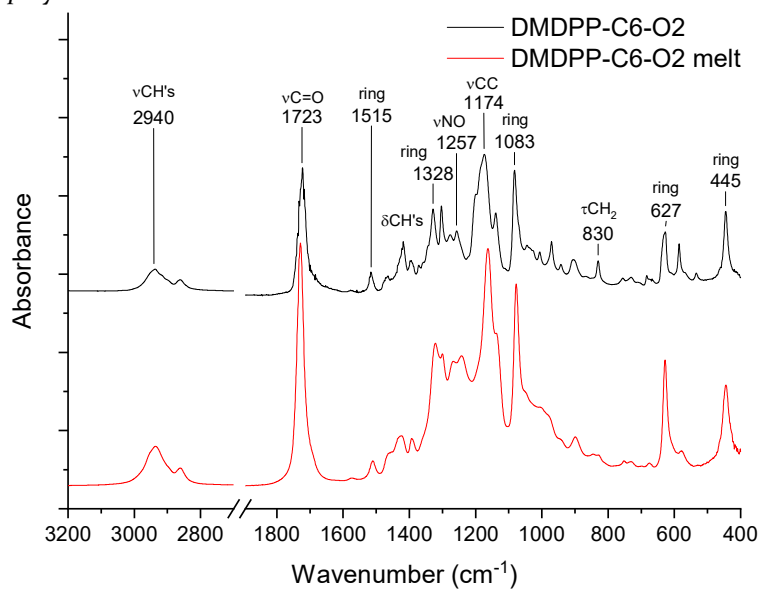


Figure A30: IR spectrum below and above the melt for DMDPP-C6-O2 (table 1, entry 9).

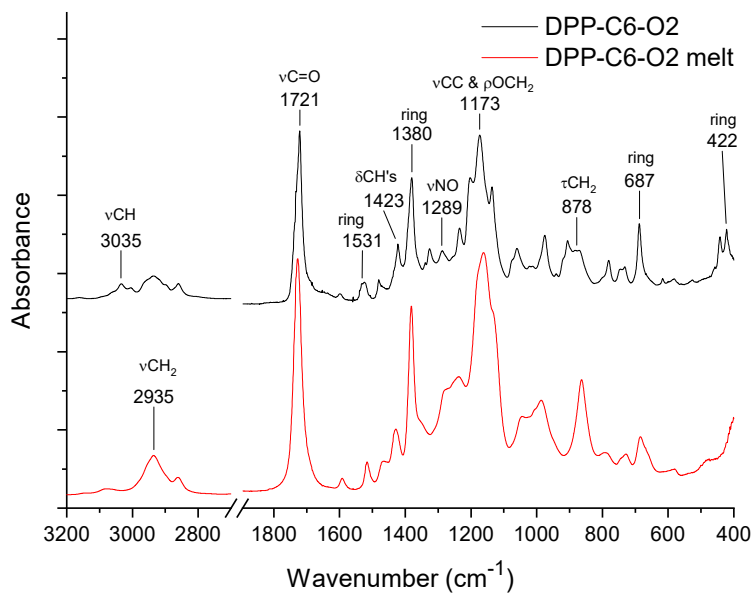


Figure A31: IR spectrum below and above the melt for DPP-C6-O2 (table 2, entry 9).

XPS results

The surface modified films were subjected to X-ray photoelectron spectroscopy (XPS) on an Axis Ultra spectrometer (Kratos Analytical). The samples were irradiated with monoenergetic Al $K_{\alpha,2}$ radiation (1486.6 eV) and the spectra were taken at a power of 144 W (12 kV x 12 mA).

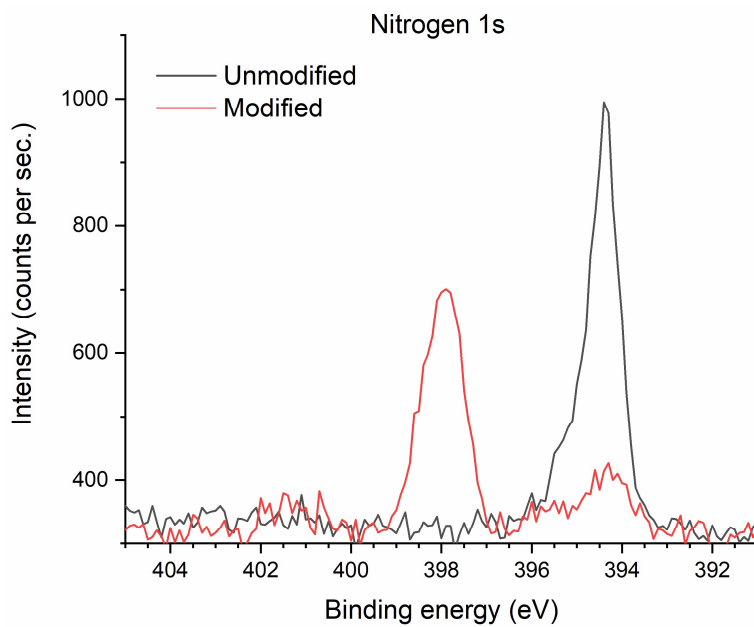


Figure A32: XPS nitrogen 1s data for the unmodified film (black) and modified film (red)

Contact angle measurements



Figure A33: Spincoated microscope slides for contact angle measurement

Chapter 5

Crystal structure and polymorphism of biobased aromatic polyesters: Elucidation of melting temperature differences

Published as:

Martien A. Würdemann, Enno A. Klop, Junyu Li, Katrien V. Bernaerts, Romano V.A. Orru, Jules A.W. Harings, *Manuscript submitted*.

Abstract

The physical origin of the difference in melting temperature between two structurally similar biobased pyrazine containing polyesters was elucidated by synthesis and study of a series of analogs. The effects of both methyl-group introduction on the hetero-aromatic pyrazine ring and the difference between phenyl- and pyrazine-rings was studied in detail. Fiber and powder X-ray diffraction allowed structure determination of two polymorphs. Based on these structures (weak) hydrogen-bonding interactions prove the basis of the observed melting temperature differences.

Introduction

The development of new, more renewable hetero-aromatic building blocks to replace fossil-based ones in polymeric materials parallels the transition to a biobased, circular society. To date, these efforts have been mostly focused on ligno-cellulosic biomass as a sustainable feedstock, with depolymerized lignin and especially furandicarboxylic acid being the most promising.^[1] Other sources of biomass, such as nitrogen-rich fractions, have received less attention.^[2] We have developed a method to utilize such nitrogen-rich fractions, in this case amino acids, to obtain pyrazine containing building blocks.^[3] This class of aromatic compounds is underreported as a building block for polymer synthesis, which prompted us to develop a new class of polyesters.

In that light, we recently reported the synthesis and thermal characterization of pyrazine containing polyesters containing dimethyl dipropionic acid pyrazine (DMDPP) and dipropionic acid pyrazine (DPP) (see **Figure 1**).^[4] Besides being the first pyrazine containing polyesters, these materials also present an interesting opportunity to study the effect of methyl-group substitution on the physical properties of aromatic polyesters. The polyesters based on DMDPP show markedly different thermal behavior compared to those based on DPP. The melting temperatures of DMDPP-based polyesters were found to be up to 80 °C higher than their corresponding DPP analogs. Further comparison with literature values for both aliphatic and aromatic semi-crystalline polyesters, such as those based on terephthalic acid or sebacic acid, indicate that DPP behaves as expected based on its structure. This means, as soon as conjugation between the aromatic ring and the monomeric acid group is broken, the character of the material changes to that of a completely aliphatic polyester. This line of reasoning, originally proposed for polyester of phenylene diacetate^[5], explains the melting temperature of DPP well.

The melting temperature of DMDPP-based polyesters with longer aliphatic diols however, are similar to those of conjugated aromatic polyesters of terephthalic acid and furandicarboxylic acid.^[4] We hypothesized that the difference in thermal properties of DMDPP originates from the steric effects of methyl-groups on the pyrazine ring or from secondary interactions, such as hydrogen bonding. The large increase in the thermal properties of the pyrazine polyesters with methyl groups that positions these renewable polyesters competitively as engineering material, prompted further investigation. Especially, since the only existing report for methyl-substituted polyethylene terephthalate shows that the melting temperature of the substituted polymer is lower than that of the unsubstituted one.^[6]

To study how methyl group introduction affects melting, a series of polyesters with different diacids was synthesized and a structure–function relationship examined. The chosen diacids were designed to isolate the different structural features accountable for the observed behavior systematically. The diacids DMDPP, DPP, their phenylene analogs, terephthalic acid and 2,5-dimethylterephthalic acid (see **Figure 1**) were subsequently polymerized with 1,6-hexanediol as the diol of choice. In this series, we anticipated that the effect of methyl group introduction in aromatic polyesters as well as the effect of pyrazines as phenylene replacements on their melting temperatures could be studied independently. For the synthesis we employed our earlier transesterification procedure for pyrazine polyesters.^[4] Now, we report our findings on the structural basis of the melting temperature differences between DMDPP and DPP.

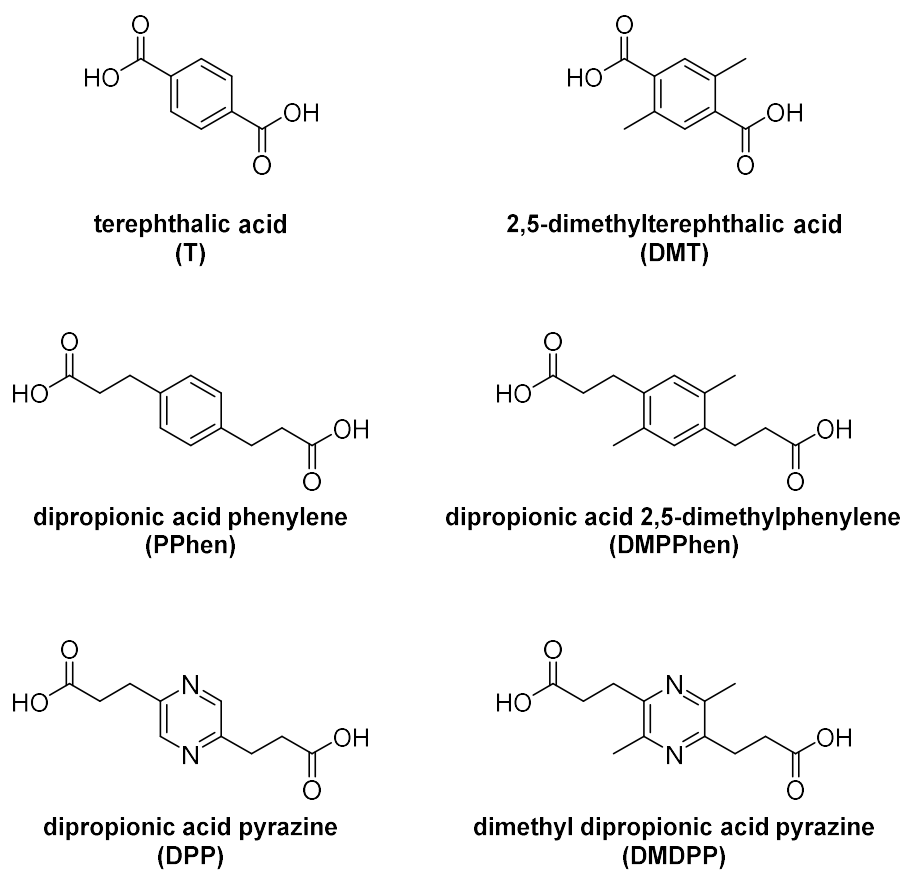


Figure 1: Monomers used to study the difference in melting temperature of DPP-C6 and DMDPP-C6.

Experimental

Materials

DMDPP, DPP and their dimethyl esters were synthesized according to our previously reported procedures.^[3-4] 1,4-Dipropionic acid benzene was supplied by Sigma-Aldrich in 98% purity and its methyl ester synthesized by esterification in methanol with thionyl chloride. Dipropionic acid xylene was synthesized via a Heck reaction according to an adapted procedure from Lebel *et al.*^[7] followed by reduction according to Paryzek *et al.*^[8] (see appendix). Dimethylterephthalate was supplied by Sigma-Aldrich in 98% purity. 2,5-Dimethylterephthalic acid was supplied by Combi-Blocks in 96% purity and its methyl ester synthesized by Fisher esterification in methanol (see appendix). 1,6-hexanediol and m-xylene were supplied by Sigma-Aldrich in >97% purity and used as received. Tin(II)-2-ethylhexanoate was supplied by Sigma-Aldrich in 97% purity and used to make a 1 M stock solution in m-xylene. Methanol and chloroform were supplied by Biosolve in at least analytical reagent grade purity and used as received. Deuterated chloroform (CDCl₃) was supplied by Cambridge isotopes and kept over 4Å molecular sieves (obtained from Sigma-Aldrich).

Polymer synthesis

Small-scale polymerization reactions were carried out for the synthesis of reported materials. The chosen scale was 1 gram of diester per reaction with a 10 mol% excess of diol. The syntheses were performed in a 20 mL cylindrical three necked flask fitted with a nitrogen inlet, an overhead stirrer, and a vigreux connected to a distillation bridge. The flask was loaded with the required diester and diol followed by 2 mL of m-xylene, this mixture was then heated to 130 °C to azeotropically remove any water. Each synthesis was subsequently performed in a two-step procedure in the presence of 0.5 mol% tin(II) 2-ethylhexanoate (Sn(II)Oct₂) as catalyst. The first step consisted of a transesterification reaction at 160-180 °C until the methyl ester peak on ¹H-NMR was less than 5%. m-Xylene (2 mL) was added to this reaction step to facilitate removal of condensate. The second reaction step consisted of polycondensation *in vacuo* at 180-200 °C until the ratio between both monomers was within 1% of 1:1 on ¹H-NMR. Polymerizations with dimethyl terephthalate and dimethyl 2,5-dimethylterephthalate had to be heated to 220-240 °C to maintain molten. If the ratio between the unreacted diacid and the diol dropped to lower than 1:1, more of the starting diol was added to the reaction mixture. A series of polyesters was synthesized under these conditions using the dimethyl esters of the acids listed in **Figure 1**. A representative example of the procedure is presented below.

Example polymerization: DMDPP-C6

A 20 mL cylindrical three-necked flask was loaded with Me₂DMDPP (991 mg, 3.54 mmol), hexane-1,6-diol (463 mg, 3.92 mmol) and 2 mL m-xylene. The resulting suspension was heated to 160 °C under open nitrogen flow. A clear melt soon formed and after 15 min an aliquot of a 1M Sn(II)Oct₂ solution in m-xylene (18 µL, 0.5 mol%, 18 µmol) was added to the reaction and the nitrogen flow was closed. After 1.5h, nitrogen flow over the reaction was opened in order to help the removal of condensate. After 1h the reaction was heated to 180 °C, another hour later the reaction was sampled and analyzed by NMR. The methyl ester peak was still more than 5% and the reaction was heated for another 2 hours. Another sample indicated the methyl ester peak had dropped below 5%, the vigreux was removed from the setup and vacuum was applied (3*10⁻¹ mBar). The reaction was kept under vacuum and analyzed by NMR until the last sample showed the monomer ratio to be close to 1:1 (5h). The resulting melt was removed while hot and crystallized into a cream colored solid.

DMDPP-C6

$^1\text{H-NMR}$ (300 MHz, CDCl_3) δ (ppm) 4.00 (t, $J = 6.7$ Hz, 4H), 2.96 (t, $J = 7.3$ Hz, 4H), 2.71 (t, $J = 7.3$ Hz, 4H), 2.41 (s, 6H), 1.63 – 1.48 (m, 4H), 1.36 – 1.24 (m, 4H); $^{13}\text{C-NMR}$ (75 MHz, CDCl_3) δ (ppm) = 173.4, 149.4, 148.0, 64.4, 31.7, 28.5, 25.6, 20.9.

Characterization

Gel Permeation Chromatography (GPC) was conducted on a Shimadzu Prominence-i LC-2030 HPLC system fitted with a Shimadzu RID-20A detector. The measurements were run with isocratic elution of chloroform at 1 mL/min on a Shodex KF-805L column (10 mm by 300 mm, 10 μm) operating at 40 $^\circ\text{C}$. Samples were prepared by making 1 mg/mL solutions in chloroform and filtered over a 0.2 μm PTFE filter. GPC was used to determine the molecular weight distribution of the obtained polymers as compared to polystyrene standards.

Nuclear Magnetic Resonance (NMR) was conducted on a Bruker AVANCE III HD Nanobay 300 MHz apparatus. Measurements were run in *d*-chloroform using 5-10 mg of polymer. The $^1\text{H-NMR}$ (300 MHz) spectra were recorded with 16 scans and the $^{13}\text{C-NMR}$ (75 MHz) spectra were recorded at 1024 scans. The obtained NMR data was used to determine the degree of polymerization by end-group analysis. This data was subsequently used to calculate the NMR molecular weight after correcting for the ratio of the end-groups.

Thermal stability of the polymers was determined by use of Thermal Gravimetric Analysis (TGA) by heating 3 to 10 mg samples at 10 $^\circ\text{C}/\text{min}$ up to 700 $^\circ\text{C}$ under a nitrogen atmosphere on a TA instruments TGA 500 machine. The degradation temperature (T_d) was set at 5% weight loss.

Differential Scanning Calorimetry (DSC) thermograms were recorded on 2 to 7 mg samples on a TA instruments Q2000 DSC using Tzero Hermetic pans. Heating and cooling rates of 10 $^\circ\text{C}/\text{min}$ were used from -40 $^\circ\text{C}$ to 180 $^\circ\text{C}$ with 3 min isothermals at those temperatures unless stated otherwise. Two temperature cycles were measured with the melting (T_m) and crystallization temperatures (T_c) of the second cycle being reported.

Dynamic Mechanical Analysis in torsional mode (DMA) was conducted on an Anton Paar MCR 702 twin drive rheometer. A 5 mm and 50 mm spindle with a 1 mm gap were used at a frequency of 10 rad/s while cooling from 30 $^\circ\text{C}$ above the melt to -50 $^\circ\text{C}$. The glass transition temperature T_g was determined as the temperature at the maximum of the loss factor ($\tan \delta$).

Fourier Transform InfraRed (FTIR) spectra were recorded on a Perkin-Elmer Frontier apparatus fitted with a Perkin-Elmer Spotlight IR microscope in transmission mode accumulating 32 scans. A sample of each polymer was molten on a ZnSe plate, spread into a thin film and subsequently cooled to crystallize. The spectral range was from 4000-600 cm^{-1} with a resolution of 2 cm^{-1} .

All X-ray diffraction measurements were conducted on a SAXSlab Ganesha diffractometer with a Genix microfocus Cu source at a wavelength of 1.5418 Å ($\text{CuK}\alpha$), Multilayer optic "3D version" optics with 0.9 x 0.9 mm^2 primary slits and 0.7 x 0.7 mm^2 guard slits. The detector used was a flat plate Pilatus 300K with 487 x 619 pixels of 0.172 mm size. The sample-to-detector distance was 120.4 mm calibrated using silver behenate and poly(ethylene). The samples were measured in vacuum using 600 s exposure times for powders and 1800 s for fibers.

The relative degree of crystallinity was determined from diffraction data. Samples were prepared in the DSC by heating to 30 $^\circ\text{C}$ above the melt for 3 min for each polymer and subsequently cooled to room temperature at 10 $^\circ\text{C}/\text{min}$. The samples were removed from the DSC pan and kept in place in the X-ray beam using Kapton tape. The diffractogram was corrected for the presence of kapton using SAXSGUI^[9] and the corrected data was fitted using Fityk.^[10] The amorphous halo was fitted as a Gaussian peak and the crystalline peaks were fitted as PearsonVII peaks. The total area under the curve was obtained by summation of both the crystalline peak areas as well as the amorphous halo area. The sum of the crystalline peak areas was divided by the total area to calculate the relative degree of crystallinity.

The fiber diffraction pattern of DMDPP-C6 was recorded on a fiber pulled from molten material, hand drawn to a ratio of 300-500% and subsequently annealed at 130 °C overnight under tension. All pictured fiber diffraction patterns are composite images generated by inversion and mirroring of two different fiber exposures. Peak positions were measured using SAXSGUI. The resulting diffraction data were used for molecular modeling, molecular mechanics and diffraction pattern simulation using Biovia 4.2 with the COMPASS force field.^[11] The crystallite size, temperature factor and degree of arcing due to crystallite disorientation were chosen to match the observed X-ray diffraction patterns. The indexing problem was solved using the method of *Klop and Lammers*.^[12] Lorentz, polarization factors and reflection multiplicities are included in the intensity calculation in **Table 3**. The resulting crystal structures were exported as .CIF files and further analyzed using the CCDC Mercury program.^[13]

Results and discussion

Polymer synthesis

Polymer synthesis for the studied materials (**Table 1**; entries 1-6) was conducted in the same way as in our earlier report on the pyrazine polyesters.^[4] This transesterification method proved adequate for the other dimethyl esters used in this study, albeit that, for dimethylterephthalate and the dimethyl ester of 2,5-dimethylterephthalic acid the reaction temperature had to be raised to 200 °C to keep the reaction mixture fully molten. The reactions were monitored by NMR analysis and stopped at sufficiently high end-group conversions. Chloroform GPC analysis of the final materials showed high molecular weights and the expected dispersities \bar{D} of about 2. However, NMR end-group analysis revealed significantly lower molecular weights. Regardless of the analysis technique, the molecular weights were in a sufficiently small range for the different monomers to justify comparison of the thermal and thermomechanical analyses (see **Table 1**).

Table 1: Analysis results of the synthesized polymers.

#		M_n ,GPC (g/mol)	\bar{D}	M_n ,NMR (g/mol) ^[a]	T_g (°C)	T_m (°C)	ΔH (J/g)	ΔH (J/mol)	Crystallinity (%)
1	T-C6	23500	1.8	9200	20	147	40.2	9970	48
2	DMT-C6	31000	2.0	11600	26	163	54.1	14932	71
3	PPhen-C6	38000	1.9	13800	-23	65	39.6	12038	42
4	DMPPhen-C6	26500	1.9	8600	-12	92	33.4	10990	42
5	DPP-C6	32000	2.1	15400	-24	64	38.6	11812	43
6	DMDPP-C6	28500	1.9	13100	4	144	48.3	16132	60

[a] For calculation see appendix

Structure property relationship – glass transition

The DSC thermograms of DMDPP-based polyesters (see the appendix of Chapter 2) showed no clear glass transitions, suggesting relatively high crystallinities. Therefore the loss factor peak ($\tan \delta$) obtained in DMA was used to determine the T_g of all materials (see appendix). The differences in T_g observed for the series of polyesters clearly show a trend, polymers of the methyl-substituted monomers (DMT-C6, DMPPhen-C6, DMDPP-C6) having higher glass transition temperatures than the non-substituted aromatic analogues. We expected this behavior taking the differences in steric hindrance and diminished conformational mobility upon substitution into account. The higher T_g of the terephthalates (**Table 1**; entries 1 and 2) compared to the other polymers can be explained by the lack of ester-group conjugation with the aromatic ring in the latter case. This lack of conjugation results in higher chain flexibility that is further promoted by the facile conformational motion of the

methylene segments upon heating and thus lowering the T_g . The magnitude of the effect of methyl group introduction varies for the studied materials. This is most likely caused by other factors influencing the T_g , such as degree of crystallinity, the rigid amorphous phase and dispersive forces.^[14]

Structure property relationship – melting temperature

Comparing the melting temperatures of the different polymers, several trends can be observed. One obvious observation is that the introduction of methyl-groups on the aromatic core clearly increases the melting point, but to differing degrees. In case of the terephthalates, the melting point of DMT is around 16 °C higher than T (**Table 1**, entries 1 and 2). For the phenylenes the melting point of DMPPhen is around 27 °C higher than for PPhen (**Table 1**, entries 3 and 4). As reported previously, for the pyrazines a much larger difference was observed with DMDPP that shows a melting point of 80 °C higher than DPP (**Table 1**, entries 5 and 6). The comparison between the phenylenes and the pyrazines in this case is especially valuable, since it isolates the effect of the nitrogens in the pyrazine aromatic core. Furthermore, pyrazine itself is electronically quite similar to benzene with 89% aromaticity.^[15] This similarity is reflected when the melting points of PPhen and DPP (**Table 1**, entries 3 and 5) are compared showing almost identical values (65 °C and 64 °C, respectively). Since the enthalpies of melting are also identical, the inclusion of the nitrogens in the aromatic core does not entail any differences in conformational degrees of freedom.

Thus, the introduction of two extra methyl-groups on the aromatic ring raises the melting temperature in DMPPhen by about 27 °C compared to PPhen. Furthermore, we see that the melting temperatures of phenylene and pyrazine are similar. By extrapolation, the addition of two methyl-groups on DPP should then result in an increase in melting temperature of a similar magnitude i.e. ~27 °C as well. As already noted, the melting temperature difference between DPP and DMDPP is however 80 °C, which indicates that the introduction of two methyl groups and conformational degrees of freedom above T_g in this case does not fully account for this and other factors must additionally be considered to explain for this rise in the melting temperature.

Several factors influence the melting of crystalline domains in polymers, such as lamellar thickness, degree of crystal perfection or disorder, polymorphism, and secondary interactions between molecules. In fact, DSC measurements reveal that the enthalpy of melting observed in the DMDPP sample is significantly higher than DPP and DMPPhen. The increased melting enthalpy may originate from differences in crystallinity or increased secondary interactions. To examine the differences in the materials in this regard, Wide-Angle X-ray Diffraction (WAXD) was recorded for all

samples. To provide a good comparison between the samples they were given the same thermal history in the DSC. That is, the samples were heated to 30 °C above their melting point, kept isothermal for 3 min and cooled to room temperature at 10 °C/min. When comparing the resulting diffraction patterns it becomes clear that the crystal structure is not the same for the pyrazines and their phenylene analogs (see **Figure 2**). The polymer chains thus pack differently even though they are structurally similar.

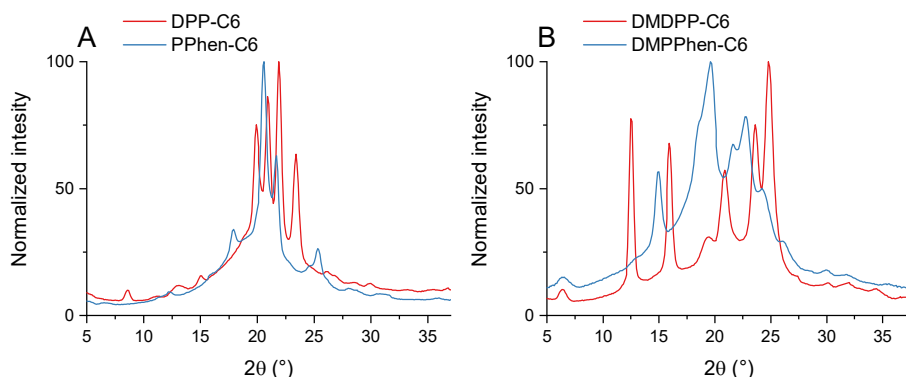


Figure 2: WAXD patterns of DPP-C6 and PPhen-C6 (A) and DMDPP-C6 and DMPPhen-C6 (B).

The exact differences in chain packing are difficult to determine based on WAXD alone, especially since there are already numerous suggested polymorphs of T-C6 of which the existence in quiescent conditions depends on the cooling rate.^[16-18] The data however, can be used to judge whether the degree of crystallinity differs and whether it can solely or in combination with increased secondary interactions account for the increased melting temperature of DMDPP-C6. Hereto, the melting enthalpy per mole of polymer was first determined by DSC. At first glance, these data show relatively large differences (see **Table 1**), however, when corrected for the degree of crystallinity obtained from the WAXD data the melting enthalpies of both the phenylenes and pyrazines are in the same order of magnitude. This approach shows that the degree of crystallinity, although higher for DMDPP-C6, is not the major additional factor to account for the increase of the melting temperature observed. To elucidate whether unique secondary interactions exist the molecular conformations and chain packing in the crystal lattice are examined.

Fiber diffraction and chain packing

To reveal molecular conformations and spatial position of moieties engaged in secondary interactions accounting for the observed high melting point of DMDPP-C6, structure determination was performed starting from fiber diffraction data. It is an alternative method to the analysis of electron diffraction data of polymer single

crystals^[19]. A fiber of DMDPP-C6 was pulled from molten polymer, stretched by hand 300-500% and annealed under tension overnight at 130 °C. The resulting fiber was analyzed by X-ray diffraction providing a higher resolved anisotropic diffraction pattern (**Figure 3**, left). Solving the indexing problem for fiber patterns is non-trivial, especially considering the limited number of reflections usually obtained. The indexing problem can be solved for fiber patterns with a limited number of reflections via the approach of *Klop and Lammers*.^[12] This approach was used for the DMDPP-C6 pattern and a well matching simulated pattern was obtained (**Figure 3**, right). The DMDPP-C6 fiber was successfully indexed in a triclinic unit cell with the following parameters: $a = 4.41 \text{ \AA}$, $b = 7.62 \text{ \AA}$, $c = 21.22 \text{ \AA}$, $\alpha = 129.6^\circ$, $\beta = 119.6^\circ$, $\gamma = 84.5^\circ$.

During indexing and further modelling of the polymer structure the two possible conformations of the pyrazine ring were taken into account. These conformations arise from the rotational asymmetry of the ring with respect to the fiber axis and consist of two forms similar to those found in poly(ethylene naphthalate)(PEN)^[20], which we assigned the α and β forms (**Figure 4**).

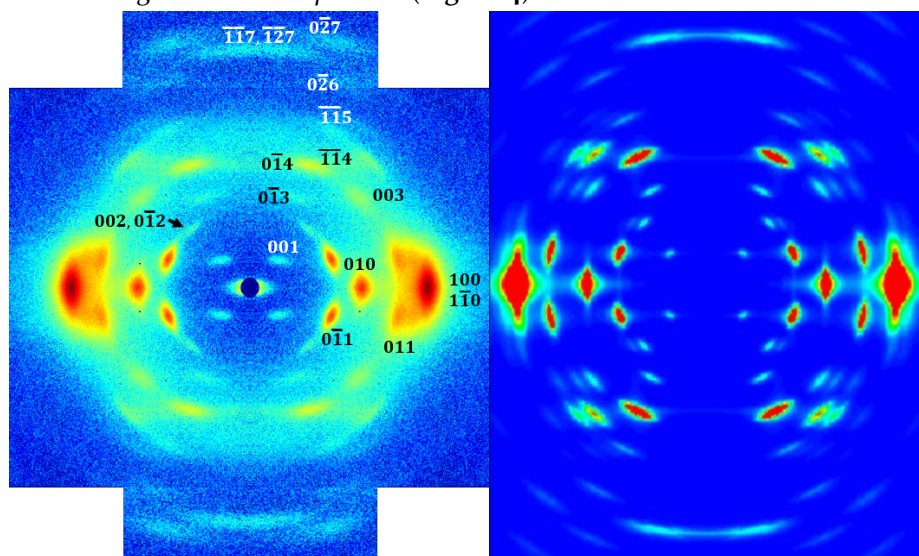


Figure 3: The observed fiber diffraction pattern of DMDPP-C6 including indexing (logarithmic intensity) (left) and the simulated pattern (right).

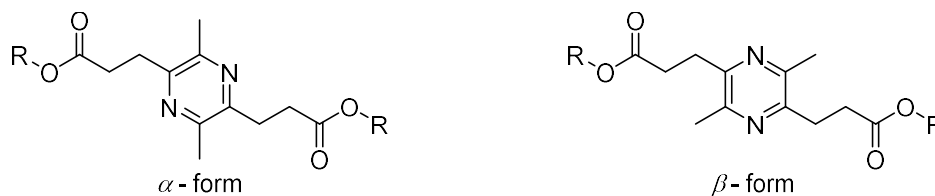


Figure 4: The α - conformation (left) and the β - conformation (right) of DMDPP.

From the unit cell dimensions, especially the *c*-axis, it was clear that the polymer adopts an extended chain conformation. Next to this, the size of the *ab*-plane dictates that only a single chain can occupy the cell. Both ring conformations were used to model the measured diffraction pattern, which revealed that the α conformation of the pyrazine ring results in a very good match between the simulated and the measured pattern (**Figure 3** and **Table 2**). Also, the higher order reflections match well, validating the model. The fiber can thus be considered to consist of the α form, for which the packing of chains of DMDPP-C6 was designated the α -polymorph.

The calculated powder diffraction pattern of the α -polymorph was compared to earlier powder data obtained for DMDPP-C6 which did not match, suggesting the bulk crystallized materials consists of a different polymorph or disordered phase. Upon modeling DMDPP-C6 in the β form, the earlier powder data indeed did match (**Figure 5**) especially the splitting of the main reflection at $2\theta = 24.6^\circ$. The chain packing of DMDPP-C6 in this form was designated the β -polymorph, and the match with the diffraction data justifies the conclusion that the bulk crystallized DMDPP-C6 consists mostly of the β -polymorph (see **Table 3**). Since the fiber is the α -polymorph, it is likely that the β -polymorph transformed into the α -polymorph upon fiber drawing and/or annealing. Refining the model of the β -polymorph with the measured powder reflections resulted in the following unit cell parameters $a = 4.73 \text{ \AA}$, $b = 9.46 \text{ \AA}$, $c = 21.70 \text{ \AA}$, $\alpha = 140.1^\circ$, $\beta = 124.5^\circ$, $\gamma = 50.4^\circ$ (unit cell I). The β -polymorph shows a much larger *c*-axis shift of neighboring polymer chains (stagger) compared to the α -polymorph. The calculated crystalline density was 1.172 g/cm^3 , very close to the measured value of 1.15 g/cm^3 .

Table 2: Indexing of reflections and comparison between observed and calculated intensities.
 (vs = very strong, s = strong, m = medium, w = weak, diff = diffuse)

$2\theta^{\text{obs}}$ ($^{\circ}$) ^[a]	$2\theta^{\text{calc}}$ ($^{\circ}$)	d^{calc} (\AA)	h	k	l	I^{obs}	I^{calc} [12]
15.95	15.97	5.549	0	1	0	s	215.5
24.57	24.58	3.622	1	-1	0	vs	129.3
	24.59	3.620	1	0	0		1000
6.33	6.55	13.494	0	0	1	w	0.8
12.54	12.44	7.115	0	-1	1	s	111.9
21.18	21.06	4.218	0	1	1	s	99.9
12.09	11.88	7.449	0	-1	2	w	5.4
	13.12	6.748	0	0	2		2.7
14.68	14.62	6.059	0	-1	3	w	6.1
20.05	19.73	4.500	0	0	3	m	15.0
	21.10	4.210	-1	0	3		12.1
	22.99	3.868	-1	-1	3		6.5
19.43	19.34	4.589	0	-1	4	m	73.7
23.93	22.48	3.955	-1	-1	4	m	61.4
	23.83	3.734	-1	0	4		11.4
	23.89	3.725	0	-2	4		21.0
	26.41	3.375	0	0	4		7.2
24.55	23.88	3.726	-1	-1	5	w – diff	9.8
30.02	29.50	3.028	0	-2	6	w	9.3
	32.95	2.718	-1	0	6		8.7
31.56	31.13	2.873	-1	-1	7	m	25.8
	31.46	2.844	-1	-2	7		9.5
33.57	34.02	2.635	0	-2	7	w	10.5

[a] 2θ is the diffraction angle using $\text{CuK}\alpha$ radiation.

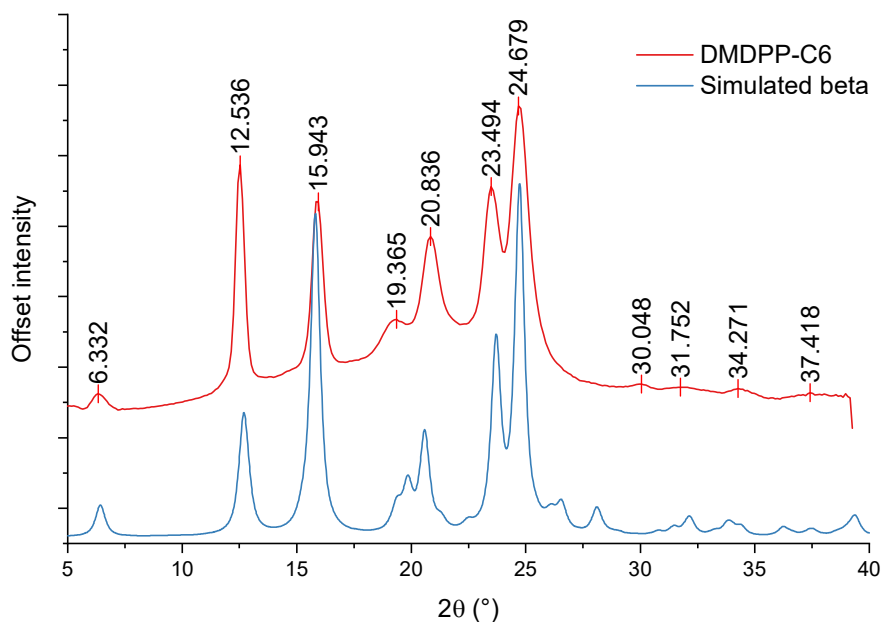


Figure 5: Simulated and measured β -polymorph powder data.

Table 3: Indexing and d-spacings for the powder data of the beta-polymorph.

#	$2\theta^{\text{obs}}$ (°)	$2\theta^{\text{calc}}$ (°)	d^{calc} (Å)	h	k	l
1	15.940	15.799	5.609	0	1	0
2	24.680	24.742	3.598	1	0	0
3	23.490	23.727	3.749	1	1	0
4	6.330	6.430	13.746	0	0	1
5	12.540	12.670	6.987	0	-1	1
6	20.840	20.530	4.326	-1	-1	1
7	20.000	19.875	4.467	0	-1	4
8	25.400	25.463	3.498	-1	-2	6

Comparing both polymorphs, several differences and similarities are observed besides the extended chain conformation and the orientation of the pyrazine ring (see **Figure 6**). Both polymers crystallize in the P-1 space group next to this the polymer chains in both polymorphs are oriented like a sheet with the pyrazine rings being in the plane of the sheet. The β -conformation of the ring forces the rings to be further apart, which results in a significantly longer c -axis shift and the tilt in the ab -plane is steeper for the β -polymorph (see **Figure 6** (A and B)). The intersheet spacing along the a -axis is very similar for both polymorphs (see **Figure 6** (C and D)). The density of both polymorphs is slightly different with the α -polymorph having a density of 1.23 g/cm³ and that of the β -polymorph being 1.17 g/cm³, suggesting that the α -polymorph is packed slightly better and should have a slightly higher melting point.

A comparison with other similar polymers for which the crystal structure has been determined reveals some interesting effects caused by the introduction of methyl groups. Most of these comparable polymers crystallize in triclinic unit cells, even when possessing higher symmetry than DMDPP-C6. Comparison to both poly(hexamethylene terephthalate)(PHT)^[16-18] and poly(octamethylene terephthalate)(POT)^[21] reveals that the *c*-axis shift in both DMDPP-C6 polymorphs is significantly higher due to the presence of methyl groups. Concerning the polymorphism found for DMDPP-C6, this type of ring flipping polymorphism is not observed in PHT^[16-18] or POT^[21] but is in naphthalate polyesters, including poly(ethylenenaphthalate) (PEN)^[20] and poly(octamethylene naphthalate)(PON).^[22] In terms of melting point most of these longer spaced polyesters are in a similar range with PON = 183 °C, PHT = 150 °C and POT = 131 °C, showing that ring stacking interactions and conjugation with the ester groups determines the melting behavior to a large extent. The fact that DMDPP-C6 lacks conjugation and the rings are spaced further apart, reiterates that this is a special case, as will be discussed later.

The fiber diffraction data show some layer-line broadening, which is indicative of crystal disorder. At first glance one may conclude that the two polymorphs cannot exist in a similar crystal lattice. However, the β -polymorph unit cell can be transformed by taking $\mathbf{b}' = -\mathbf{a} + \mathbf{b}$. This results in the following cell parameters $a = 4.73 \text{ \AA}$, $b = 7.40 \text{ \AA}$, $c = 21.70 \text{ \AA}$, $\alpha = 128.2^\circ$, $\beta = 124.5^\circ$, $\gamma = 79.9^\circ$ (unit cell II). These parameters are a lot closer to the α -polymorph with very similar angles and a similar *ab*-plane. Crystalline disorder and defects in the form of mixed phases may therefore be possible.

In a DMDPP-C6 α -lattice the polymer sheets run parallel to the *bc*-plane. In this structure a β -type defect can be formed if neighboring defect chains in the β -conformation rotate around their chain axes so that β -type sheets are formed running along the (1-10) plane of the α -lattice. This allows an $\alpha+\beta$ disorder phase in which the α -lattice enables the larger *c*-axis shift of the β -chain packing along the diagonal direction. The other way around, a β -lattice can accommodate α -conformation chains with a smaller *c*-axis shift if these are aligned along the (100) plane of β -unit cell II. So both polymorphs can have defects of the other conformation and this can be the case for both the fiber and the powder. The number of defects however, is low in both cases, since α -polymorph associated reflections are not visible in the powder data and β -polymorph reflections are not resolved in the fiber data.

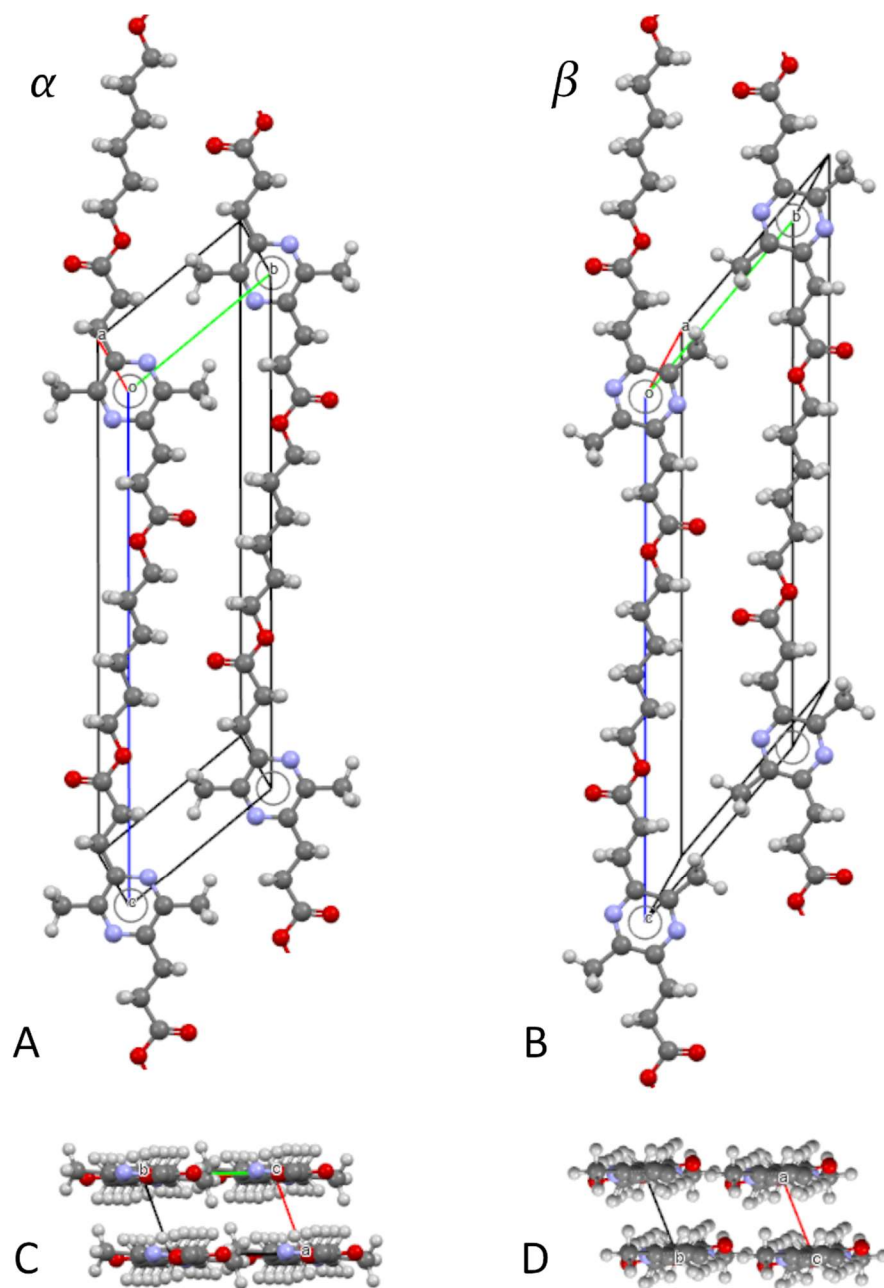


Figure 6: Crystal structure of both polymorphs viewed along the a^* -axis (A and B) and along the c -axis of unit cell I (C and D).

Short contacts are an indication of secondary interactions that have a large influence on crystal packing, such as hydrogen bonding and π -stacking. A short contact is said to be present when the distance between two atoms is smaller than the sum of their *van der Waals* radii. Contact analysis can therefore shine further light on any small differences between both polymorphs and any interactions influencing the melting point. Both polymorphs were examined for such contacts between the chains.

In the *bc*-plane (in the sheet) two short contacts were found for both polymorphs involving the ester carbonyl and a methylene proton from a neighboring chain. In the α -polymorph this distance is 2.54 Å, while in the β -polymorph it is 2.70 Å. These C=O...H interactions are probably hydrogen bonds and although their length is different they are of similar strength and influence on the melting of the polymer. In the *ac*-plane (between sheets) several proton-proton short contacts were found, these are however usually not constructive and possibly the result of the limitation of the force field. No contacts were found between any oxygen and hydrogens in this plane. Contacts were found between the pyrazine nitrogen and both methylene and methyl protons in the *ac*-plane as will be discussed further below. Overall, the short contacts for both polymorphs are similar.

DSC analysis of the DMDPP-C6 polymorphs

Upon determining the presence of polymorphism in DMDPP-C6 the melting behaviour of the polymer was studied in more detail by DSC combined with further diffraction measurements. After cooling from the melt at 10 °C/min DMDPP-C6 shows multiple endothermic events upon reheating (see **Figure 7A green**). The diffraction pattern for samples prepared in this manner was consistent with the β -polymorph. When a drawn and annealed fiber, identified via XRD to be the α -polymorph, was heated at 10 °C/min only one endothermic event was found with a similar melting point (see **Figure 7A blue**). This latter observation suggests that the multiple endothermic processes observed for the β -polymorph are likely due to a reorganization upon melting, with the higher melting point belonging to the α -polymorph.

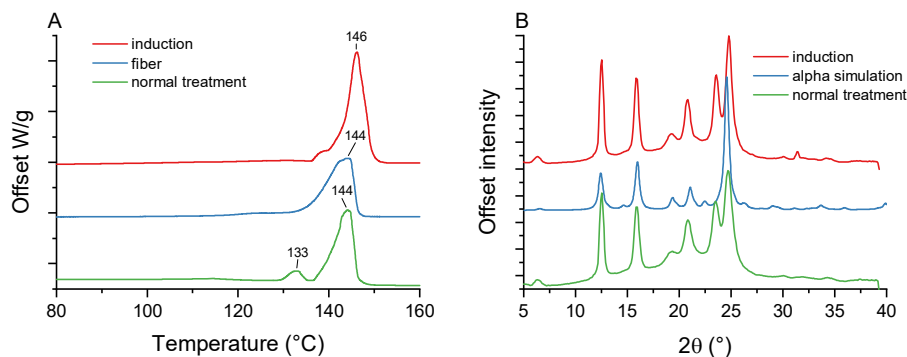


Figure 7: DSC thermograms for the induction experiment (A) and the corresponding diffraction data (B).

To test this hypothesis, we tried to thermally induce the α -polymorph. If the highest melting enthalpy belongs to α -polymorph crystals these could be induced by melting all other crystal at 140 °C and using the remaining higher melting α -crystallites as nucleation sites. Hereto a sample was heated to 140 °C kept isothermal for 1 min and cooled to 135 °C to crystallize isothermally. DSC analysis after this procedure indeed showed mostly the highest melting enthalpy at 144 °C. However, this sample did not consist of the expected α -pattern (see **Figure 7B blue**) but mostly of the β -polymorph (see **Figure 7B red**).

Since thermal induction of the α -polymorph was impossible and both the α -polymorph and the β -polymorph show similar melting points, it is clear that the α -polymorph can only be strain-induced upon drawing. The observation that both polymorphs show a similar melting temperature also indicates that the strength of the C=O...H hydrogen bonds between both polymorphs is similar.

Induction of the α -polymorph was impossible without drawing but it should be possible to induce the β -polymorph from a drawn α -polymorph fiber by thermal relaxation. A section of fiber was therefore heated to 140 °C (under the melting temperature) and kept isothermal for 60 min. X-ray analysis of this fiber before and after this thermal treatment indeed showed a splitting of the main reflection on the equator (see **Figure 8**). However, the higher order reflections remain the same indicating that no α - to β -polymorph transition took place. Due to the presence of defects and incomplete transition, the obtained diffraction data was not used to further refine the β -polymorph model.

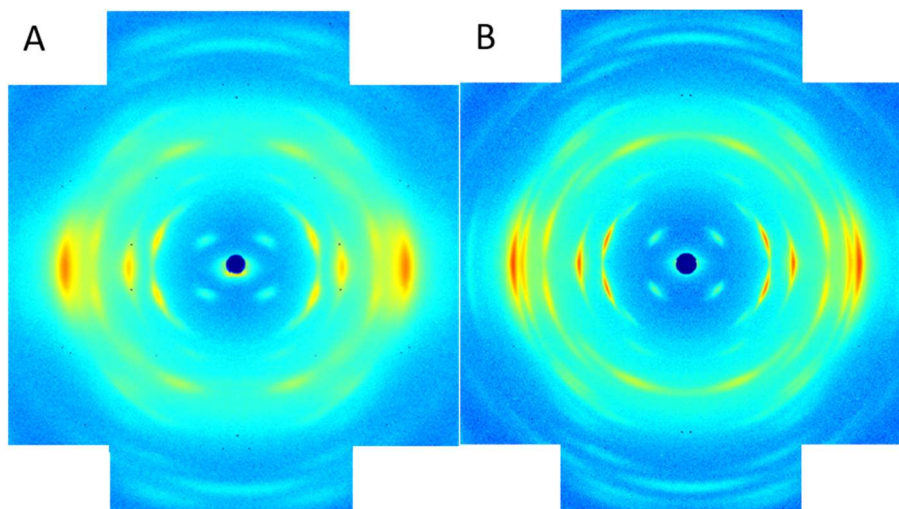


Figure 8: An α -fiber (A) and the same section thermally induced (relaxed) showing partial transition to the β -polymorph (B), with the simulated patterns below (C and D).

Hydrogen bonding

It is well known that hydrogen bonding as secondary interactions within and between unit cells can have a large effect on the melting point of crystalline solids. Water, for instance, has a much higher melting point than would be expected based on its molecular weight. A similar effect can be seen for polymers, polycaprolactone (PCL) has a melting point of around 60 °C whereas nylon 6 (polycaprolactam) has a melting point of 220 °C.^[23] These two polymers are almost identical except for the fact that the amide bonds in nylon 6 are able to form hydrogen bonds whereas the esters in PCL are not. These hydrogen bonds account for the large difference in melting point observed. Since a large difference is also seen for DPP-C6 versus DMDPP-C6, the presence of hydrogen bonds may account for this as well.

Neither DPP nor DMDPP has any hydrogen bond donors, even though they both have hydrogen bond acceptors in the form of their pyrazine lone pairs. However, a different type of hydrogen bond is possible for both these substances, i.e. non-classical hydrogen bonds involving a weak donor such as a C-H group. These types of contacts have been identified in various pyrazines when examining bond direction and proximity of the nitrogen with other groups in single crystal X-ray structures.^[24-25] Although hydrogen bonds of the C-H...N type are unreported in polymers, their presence should be theoretically possible. Especially since non-classical hydrogen bonds of the C-H...O type have been reported in poly(lactide), poly(hydroxybutyrate) polyesters and poly(glycolic acid).^[26-28]

The strength of C-H...N contacts varies significantly; sp^2 -hybridized carbons are stronger donors than sp^3 -hybridized carbons.^[29] This would mean that DPP should be able to form stronger hydrogen bonds than DMDPP. Non-classical hydrogen bonds however, like all hydrogen bonds are subject to quite limited geometries and the required overlaps between the participating orbitals are highly directional.^[30-31] Considering the similarity between DMDPP and tetramethylpyrazine, hydrogen bonds of the type found in the latter compound were expected to be present (see **Figure 9**).^[25] These specific hydrogen bonds involve the pyrazine lone pair as the acceptor with the methyl group as the donor.

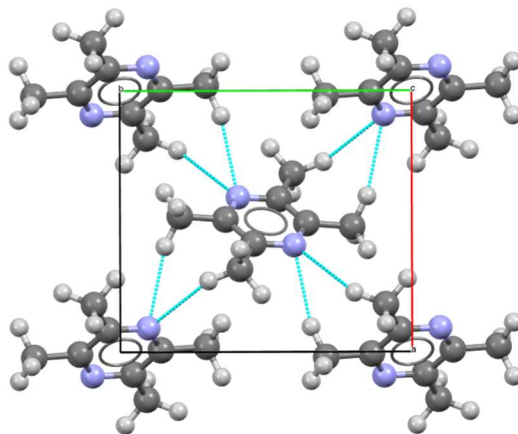


Figure 9: The non-classical hydrogen bonds involving the nitrogen electron lone pair as found in tetramethylpyrazine^[32]

Examining both polymorphs of DMDPP-C6 for short contacts adhering to the definition of non-classical hydrogen bonds showed none of the expected types of non-classical hydrogen bonds.^[33] In the plane of the ring, no hydrogens were found at a distance of ≤ 3.0 Å in either the α - or β -polymorph suggesting the nitrogen lone pairs are not involved in any hydrogen bonding. Above and below the pyrazine ring protons were found at distances ≤ 3.0 Å in both polymorphs (see **Figure 10**). These belong to the methyl-group and a methylene-group respectively.

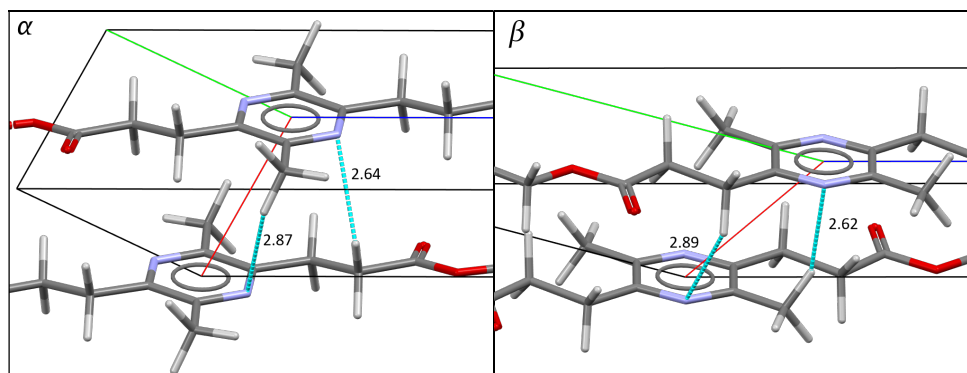


Figure 10: C-H...N interaction with the pyrazine ring in the α -polymorph (top) and β -polymorph (bottom).

The distance of these protons to the ring clearly suggests that they are involved in a constructive interaction, that is, electron density of the hydrogen is donated into the electron-poor aromatic system. This C-H... π interaction is weak but nonetheless generally considered to be a hydrogen-bonding interaction.^[33] In both polymorphs the angles and distances for the protons with the pyrazine ring fall within the required range for C-H... π bonds.^[34] Most C-H... π bonds however, are determined by their angle and distance to the center of the acceptor ring.^[35] For DMDPP-C6 this is not the case, most likely due to the electro-negative nature of the nitrogens. A similar C-H...N interaction is found in the co-crystal of 2,5-dimethylpyrazine with acetylene.^[36] Although competition between π and aliphatic nitrogen bases has been studied, no data could be found for non-hindered aromatic nitrogen bases.^[37] Further theoretical study on these interactions should reveal more about the exact nature of these interactions. Regardless of this, evidence points to these hydrogen bonds being responsible for the increased melting point of DMDPP-C6, as compared to DPP-C6.

Melting point differences

Although the exact crystal packing was not determined for the other polymers in **Table 1**, the structures and the interactions found in both polymorphs of DMDPP-C6 provide sufficient insight to explain the differences in melting points. Especially, when taking into account infrared measurements. These have shown that all polymers in **Table 1** adopt an extended chain conformation based on the lack of the typical *non-trans non-gauche* methylene rocking vibration at 917 cm^{-1} . This vibration is found in non-extended chain polyesters such as in the crumpled state of poly(butylene terephthalate) (see **Figures A10-A12**).^[16, 38-39]

Since all studied polymers adopt an extended chain conformation, the effect of differences in diol conformation are minimized. The nature of the aromatic ring thus determines the differences in crystal packing and therefore in melting point. In case of both DPP-C6 and its phenylene analog PPhen-C6 their low melting point, compared to the terephthalate polymers, is primarily due to the lack of conjugation between the ester and the ring.^[5] That no difference in melting point is observed between DPP-C6 and PPhen-C6 is likely due to the lack of hydrogen bonding in DPP-C6. The C-H...N hydrogen bonds identified in DMDPP-C6 are impossible due to the lack of methyl-groups and other hydrogen bonding interactions involving the pyrazine nitrogens, are not possible due to the conformation imposed by the polymer chain. Two DPP rings on neighboring chains cannot interact in the same manner as found for 2,5-dimethylpyrazine.^[25]

The introduction of methyl-groups on the aromatic rings has a large effect on the packing of the chains due to imposing more steric hindrance. This likely forces the polymer chains to adopt a larger *c*-axis shift causing the rings to stagger. In such a staggered formation, the methyl-groups on DMPPhen-C6 allow for a C-H... π hydrogen bonding motif similar to the C-H...N motif found in DMDPP-C6. The melting point of DMPPhen-C6 however, is still 55 °C lower than DMDPP-C6, a difference that is most likely due to the strength of the hydrogen bonds between both molecules. In case of DMDPP-C6, the interaction might be C-H... π or C-H...N, the latter of which is stronger. Next to this, the pyrazine ring in DMDPP-C6 is more electron poor causing the methyl-group to be more electron poor. This makes the protons more acidic and thus better donors. The difference in electron density for the methyl-groups between DMDPP and DMPPhen is well reflected in the proton and carbon chemical shifts of the group. For DMDPP this shift is 2.45 (¹H)/20.9 (¹³C) ppm while for DMPPhen it is 2.23 (¹H)/18.7 (¹³C) ppm (see **Figures A4** and **A6**). Considering the strength of hydrogen bonds increases significantly with proton acidity^[33], this adequately explains the higher melting point found for DMDPP-C6.

Conclusions

The remarkably large difference of 80 °C in melting point between two structurally similar biobased pyrazine containing polyesters DPP-C6 and DMDPP-C6 was investigated by synthesis and in-depth structural analysis of a series of analogs. These included the terephthalate and phenylene analogs. The structure-properties relationships for these materials revealed that both the methyl-groups and the pyrazine are responsible for the large difference in melting point.

With fiber and powder X-ray diffraction analysis both the unit cell and the crystalline packing of DMDPP-C6 was determined. Two polymorphs of the material exist depending on the conformation of the pyrazine ring in the polymer chain. One polymorph with the ring methyl-groups perpendicular to the chain is the α -polymorph with the following unit cell parameters; $a = 4.41 \text{ \AA}$, $b = 7.62 \text{ \AA}$, $c = 21.22 \text{ \AA}$, $\alpha = 129.6^\circ$, $\beta = 119.6^\circ$, $\gamma = 84.5^\circ$. While the other is the β -polymorph possessing the following unit cell parameters; $a = 4.73 \text{ \AA}$, $b = 9.46 \text{ \AA}$, $c = 21.70 \text{ \AA}$, $\alpha = 140.1^\circ$, $\beta = 124.5^\circ$, $\gamma = 50.4^\circ$ (unit cell I). Both polymorphs adopt an extended chain conformation with a single chain per unit cell. The α -polymorph exists mainly in the fiber while the β -polymorph is the main structure in bulk crystalized material. DSC analysis combined with further diffraction experiments shows that both polymorphs have similar melting behavior and that the α -polymorph could not be thermally induced in isotopically structured material. Drawing is necessary to obtain this polymorph.

The obtained crystal packing enabled us to determine any interactions influencing the melting point. Specifically, (weak) hydrogen bonds between the methyl-groups and the pyrazine system were found based on proximity. The exact nature of these hydrogen bonds, be it C-H...N or C-H...N, is unclear but C-H...N interactions are expected to be stronger. The presence of these interactions, combined with infrared data indicating that all analogs were also in an extended chain conformation, can adequately explain the observed differences in melting point. First, due to lack of ester conjugation with the aromatic core, the studied systems have lower melting temperatures than terephthalate polymers. Next, due to steric constraints, hydrogen bonds are not possible in DPP-C6, resulting in no difference with PPhen-C6. Finally the introduction of methyl-groups consequently raises the melting point by allowing either C-H... π and/or C-H...N hydrogen bonds between the aromatic systems.

This new insight in weak interactions between polymer chains will enable more directed design of new biobased polymers.

References

- [1] I. Delidovich, P. J. Hausoul, L. Deng, R. Pfitzenreuter, M. Rose, R. Palkovits, *Chem. Rev.* **2016**, *116*, 1540-1599
- [2] F. De Schouwer, L. Claes, A. Vandekerckhove, J. Verduyck, D. E. De Vos, *ChemSusChem* **2019**, *12*, 1272-1303
- [3] M. A. Würdemann, C. Nitu, S. M. A. De Wildeman, K. V. Bernaerts, R. V. A. Orru, *Chem. Eur. J.* **2020**, *26*, 8090-8100
- [4] M. A. Würdemann, K. V. Bernaerts, *ACS. Sustain. Chem. Eng.* **2020**, *8*, 12045-12052
- [5] V. V. Korshak, S. V. Vinogradova, V. M. Belyakov, *Bull. Acad. Sci. USSR, Div. Chem. Sci. (Engl. Transl.)* **1957**, *6*, 1029-1031
- [6] M. Cachia, *Annales de chimie.* **1959**, *513*, 5-41
- [7] H. Lebel, M. Davi, G. T. Stokłosa, *The Journal of Organic Chemistry* **2008**, *73*, 6828-6830
- [8] Z. Paryzek, H. Koenig, B. Tabaczka, *Synthesis* **2003**, *2003*, 2023-2026
- [9] SAXSGUI open source GNU licenced software
- [10] M. Wojdyr, *J. Appl. Crystallogr.* **2010**, *43*, 1126-1128
- [11] H. Sun, *The Journal of Physical Chemistry B* **1998**, *102*, 7338-7364
- [12] E. A. Klop, M. Lammers, *Polymer* **1998**, *39*, 5987-5998
- [13] C. F. Macrae, I. Sovago, S. J. Cottrell, P. T. A. Galek, P. McCabe, E. Pidcock, M. Platings, G. P. Shields, J. S. Stevens, M. Towler, P. A. Wood, *J. Appl. Crystallogr.* **2020**, *53*, 226-235
- [14] S. Z. D. Cheng, R. Pan, B. Wunderlich, *Die Makromolekulare Chemie* **1988**, *189*, 2443-2458
- [15] C. W. Bird, *Tetrahedron* **1986**, *42*, 89-92
- [16] A. Palmer, S. Poulin-Dandurand, J. F. Revol, F. Brisse, *Eur. Polym. J.* **1984**, *20*, 783-789
- [17] F. Brisse, A. Palmer, B. Moss, D. Dorset, W. A. Roughead, D. P. Miller, *Eur. Polym. J.* **1984**, *20*, 791-797
- [18] I. H. Hall, B. A. Ibrahim, *Polymer* **1982**, *23*, 805-816
- [19] F. Brisse, *J Electron Microsc Tech* **1989**, *11*, 272-279
- [20] C. J. M. van den Heuvel, E. A. Klop, *Polymer* **2000**, *41*, 4249-4266
- [21] Y. G. Jeong, S. C. Lee, K. Shin, *J. Polym. Sci., Part B: Polym. Phys.* **2009**, *47*, 276-283
- [22] Y. G. Jeong, K. J. Lee, W. H. Jo, S. C. Lee, *Polymer* **2008**, *49*, 1693-1700
- [23] J. Brandrup, E. H. Immergut, E. A. Grulke, *Polymer handbook, 4th edition*, Wiley, New York; Chichester, **2004**.
- [24] M. Mascal, *Chem. Commun.* **1998**, 303-304
- [25] V. R. Thalladi, A. Gehrke, R. Boese, *New J. Chem.* **2000**, *24*, 463-470
- [26] H. Sato, R. Murakami, A. Padermshoke, F. Hirose, K. Senda, I. Noda, Y. Ozaki, *Macromolecules* **2004**, *37*, 7203-7213
- [27] H. Sato, J. Dybal, R. Murakami, I. Noda, Y. Ozaki, *J. Mol. Struct.* **2005**, *744-747*, 35-46
- [28] H. Sato, M. Miyada, S. Yamamoto, K. Raghunatha Reddy, Y. Ozaki, *RSC Advances* **2016**, *6*, 16817-16823
- [29] V. R. Pedireddi, G. R. Desiraju, *J. Chem. Soc., Chem. Commun.* **1992**, 988-990
- [30] G. R. Desiraju, *Acc. Chem. Res.* **1991**, *24*, 290-296
- [31] T. Steiner, *Chem. Commun.* **1999**, 313-314
- [32] A. W. M. Braam, A. Eshuis, A. Vos, *Acta Crystallographica Section B* **1981**, *37*, 730-732
- [33] G. Desiraju, T. Steiner, *The Weak Hydrogen Bond: In Structural Chemistry and Biology*, **2001**.
- [34] M. Nishio, *PCCP* **2011**, *13*, 13873-13900
- [35] T. Osamu, K. Yuji, I. Sachiyo, S. Ko, I. Michio, T. Shuji, U. Yoji, T. Sei, N. Motohiro, *Bull. Chem. Soc. Jpn.* **2001**, *74*, 2421-2430
- [36] M. T. Kirchner, R. Boese, A. Gehrke, D. Bläser, *Crystengcomm* **2004**, *6*, 361-366
- [37] E. Marquis, J. Graton, M. Berthelot, A. Planchat, C. Laurence, *Can. J. Chem.* **2004**, *82*, 1413-1422
- [38] B. Stambaugh, J. B. Lando, J. L. Koenig, *Journal of Polymer Science: Polymer Physics Edition* **1979**, *17*, 1063-1071
- [39] I. M. Ward, M. A. Wilding, *Polymer* **1977**, *18*, 327-335

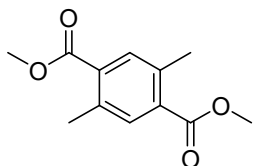
Appendix

Materials

Further chemicals used were: para-toluenesulfonic acid monohydrate (pTsOH) (>98.5% purity), sodium bicarbonate (NaHCO₃), sodium sulfate (Na₂SO₄), thionyl chloride (SOCl₂) (97%), palladium(II)acetate (97%), 1,3-bis(2,4,6-trimethylphenyl)-1,3-dihydro-2H-imidazol-2-ylidene (IMes) (97%), dry DMF, potassium carbonate, methyl acrylate (99%), Celite, palladium on carbon (10%) and ammonium formate (97%) were supplied by Sigma-Aldrich and used as received. Ethyl acetate (EtOAc) was supplied by Biosolve in analytical reagent grade. 1,4-Dibromo-2,5-dimethylbenzene (98%) was supplied by Acros organics

Data for unreported materials

Dimethyl-2,5-dimethylterephthalate

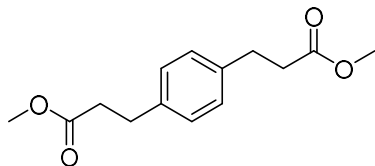


dimethyl 2,5-dimethylterephthalate

A 500 mL round-bottom flask was loaded with 2,5-dimethylterephthalic acid (2.50 g, 1 Eq, 12.87 mmol) which was suspended in methanol (125 mL) and pTsOH (49 mg, 0.02 Eq, 257 μmol) was added. The resulting mixture was heated to 65 °C. After refluxing overnight, the reaction was still a white suspension and thus extra methanol was added (100 mL) together with a few drops of sulfuric acid. After refluxing for 6 days, the reaction was complete and the reaction was concentrated *in vacuo*. The resulting crude was dissolved in 100 mL of EtOAc and extracted with 2 x 50 mL saturated NaHCO₃. The organic phase was dried over Na₂SO₄ and after concentration, the desired material was isolated in 96% yield (2.76 g, 12.42 mmol).

mp 114-116 °C; ¹H NMR (300 MHz, CDCl₃) δ (ppm) 7.69 (s, 2H), 3.84 (s, 6H), 2.50 (s, 6H); ¹³C NMR (75 MHz, CDCl₃) δ (ppm) = 167.5, 137.1, 133.5, 132.4, 52.1, 21.0; IR (ATR) $\tilde{\nu}$ (cm⁻¹) = 2957 (w), 1718 (vs), 1422 (s), 1302 (m), 1256 (vs), 1182 (s), 1099 (vs), 957 (m), 902 (m), 775 (s)

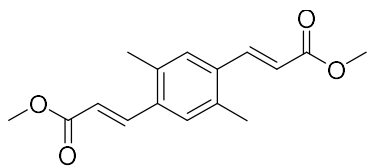
Dimethyl 1,4-phenylenedipropionate



dimethyl 3,3'-(1,4-phenylene)dipropionate

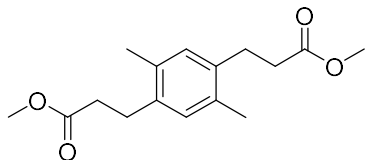
A 50 mL round-bottom flask was loaded with 1,4-phenylenedipropionic acid (2.01 g, 1 Eq, 9.03 mmol) which was suspended in methanol (20 mL) and cooled on an icebath. To the suspension was slowly added thionyl chloride (2.4 g, 1.5 mL, 2.3 Eq, 21 mmol) while stirring. Addition resulting in the colorless solid slowly dissolving, after complete addition the mixture was allowed to come to room temperature followed by heating to reflux. After refluxing overnight (19h) the reaction was allowed to cool to room temperature and a flakey solid precipitated. The reaction mixture was concentrated to dryness *in vacuo* and the crude washed with 24 mL of satd. NaHCO₃. The resulting solid was isolated by filtration, washed with 12 mL of satd. NaHCO₃ and dried *in vacuo* on the filter to obtain the desired material as shiny flakes in 98% yield (2.23 g, 8.95 mmol).

mp 119-222 °C; ¹H NMR (300 MHz, CDCl₃) δ (ppm) 7.14 (s, 4H), 3.69 (s, 6H), 2.94 (t, *J* = 7.8 Hz, 4H), 2.63 (t, *J* = 7.8 Hz, 4H); ¹³C NMR (75 MHz, CDCl₃) δ (ppm) 173.4, 138.4, 128.4, 51.6, 35.7, 30.5; IR (ATR) $\tilde{\nu}$ (cm⁻¹) = 3011 (w), 2957 (w), 1727 (vs), 1433 (s), 1301 (m), 1178 (vs), 1148 (s), 1053 (m), 976 (s), 835 (vs)

Dimethyl 2,5-dimethyl-1,4-phenylenedipropionate(2E,2'E)-dimethyl 3,3'-(2,5-dimethyl-1,4-phenylene)diprop-2-enoate (adapted from Lebel et al.)^[7]dimethyl 3,3'-(2,5-dimethyl-1,4-phenylene)
(2E,2'E)-diacrylate

Under inert conditions, a precatalyst solution was made with palladium(II) acetate (9.10 mg, 0.0041 Eq, 40.5 μmol), 1,3-bis(2,4,6-trimethylphenyl)-1,3-dihydro-2H-imidazol-2-ylidene (246 mg, 0.081 Eq, 808 μmol) and potassium carbonate (5.5 g, 4 Eq, 40 mmol) in 10 mL of dry DMF the resulting suspension was stirred for 15 min at room temperature. A solution of 1,4-dibromo-2,5-dimethylbenzene (2.64 g, 1 Eq, 10.01 mmol) in 4 mL of dry DMF was subsequently added, followed by methyl acrylate (2.81 g, 3.26 Eq, 32.64 mmol). The resulting black reaction mixture was heated to 120 °C and left to stir for 64 hours (conversion monitored by LC-MS). The mixture was cooled to room temperature followed addition of water (60 mL). The black mixture was washed with dichloromethane (3 x 40 mL) and the combined organic layers were filtered over Celite to remove palladium black. The organic phase was washed with saturated aqueous NaHCO_3 (80 mL) and dried over Na_2SO_4 . The organic phase was concentrated to dryness and dried overnight at 60 °C. The resulting dark solid was washed on a filter with 3 x 5 mL methanol resulting in isolation of the desired material as a yellow solid in 82% yield (2.25 g, 8.18 mmol).

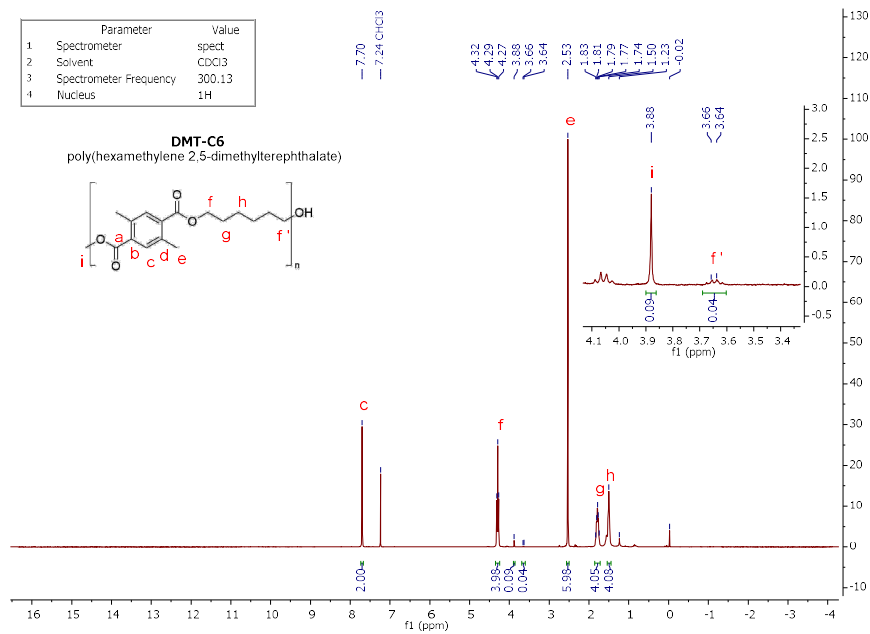
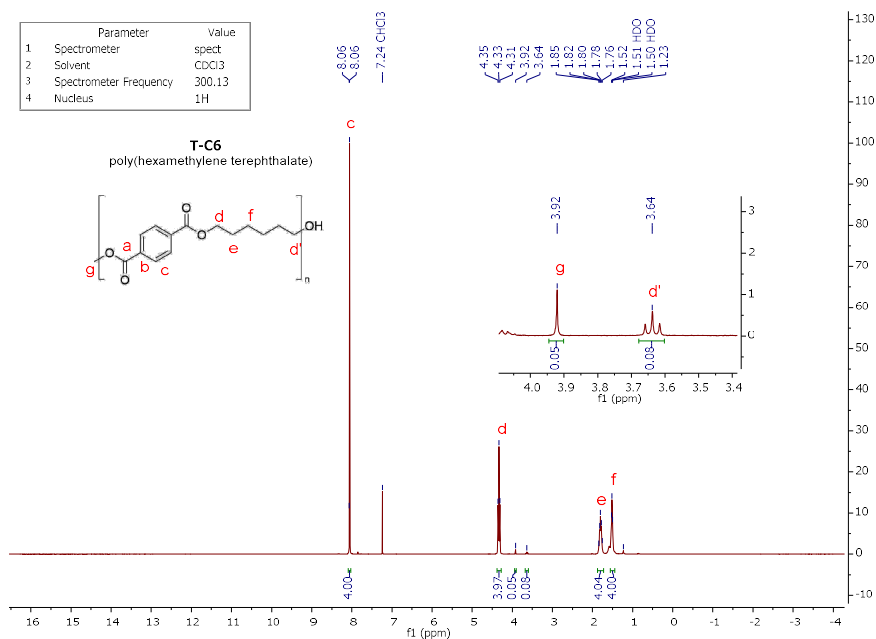
mp 176-179 °C; ^1H NMR (300 MHz, CDCl_3) δ (ppm) 7.93 (d, $J = 15.9$ Hz, 2H), 7.40 (s, 2H), 6.40 (d, $J = 15.9$ Hz, 2H), 3.83 (s, 6H), 2.43 (s, 6H); ^{13}C NMR (75 MHz, CDCl_3) δ (ppm) 167.3, 141.6, 135.5, 134.9, 128.7, 119.5, 51.7, 19.4; IR (ATR) $\tilde{\nu}$ (cm^{-1}) = 2952 (w), 1700 (vs), 1438 (m), 1274 (s), 1157 (m), 1032 (s), 979 (vs), 872 (s), 864 (s), 733 (m)

Dimethyl 2,5-dimethyl-1,4-phenylenedipropionate (adapted from Paryzek et al.)^[8]dimethyl 3,3'-(2,5-dimethyl-1,4-phenylene)
dipropionate

A 100 mL round-bottom flask was loaded with (2E,2'E)-dimethyl 3,3'-(2,5-dimethyl-1,4-phenylene)diprop-2-enoate (1.50 g, 1 Eq, 5.46 mmol), palladium on carbon 10% (300 mg, 0.52 Eq, 2.82 mmol) and ammonium formate (3.46 g, 10.0 Eq, 54.83 mmol) which were suspended in methanol (30 mL), bubble formation was observed. The resulting suspension was heated to reflux. Some formate sublimation took place, which was transferred back with some methanol resulting in renewed bubble formation. The reaction was found complete on TLC after 1 hour and 45 min. The reaction mixture was filtered over Celite and flushed with 3 x 10 mL methanol followed by concentration *in vacuo*. Concentration resulted in the desired product as a colorless solid in 83% yield (1.26 g, 4.52 mmol).

mp 74-76 °C; ^1H NMR (300 MHz, CDCl_3) δ (ppm) 6.93 (s, 2H), 3.71 (s, 6H), 2.90 (t, $J = 8.7$ Hz, 4H), 2.58 (t, $J = 8.7$ Hz, 4H), 2.27 (s, 6H); ^{13}C NMR (75 MHz, CDCl_3) δ (ppm) 136.6, 133.5, 130.6, 51.6, 34.6, 27.9, 18.7; IR (ATR) $\tilde{\nu}$ (cm^{-1}) = 2950 (w), 1722 (vs), 1437 (m), 1419 (m), 1366 (m), 1290 (s), 1166 (vs), 981 (m), 885 (s), 782 (m), 661 (w)

NMR data of polymers



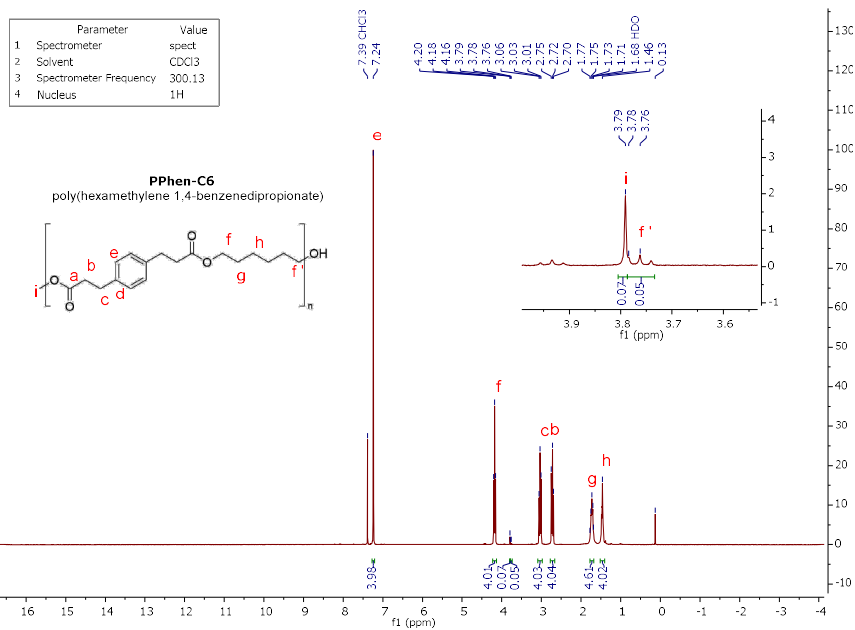


Figure A3: ¹H-NMR spectrum of PPhen-C6.

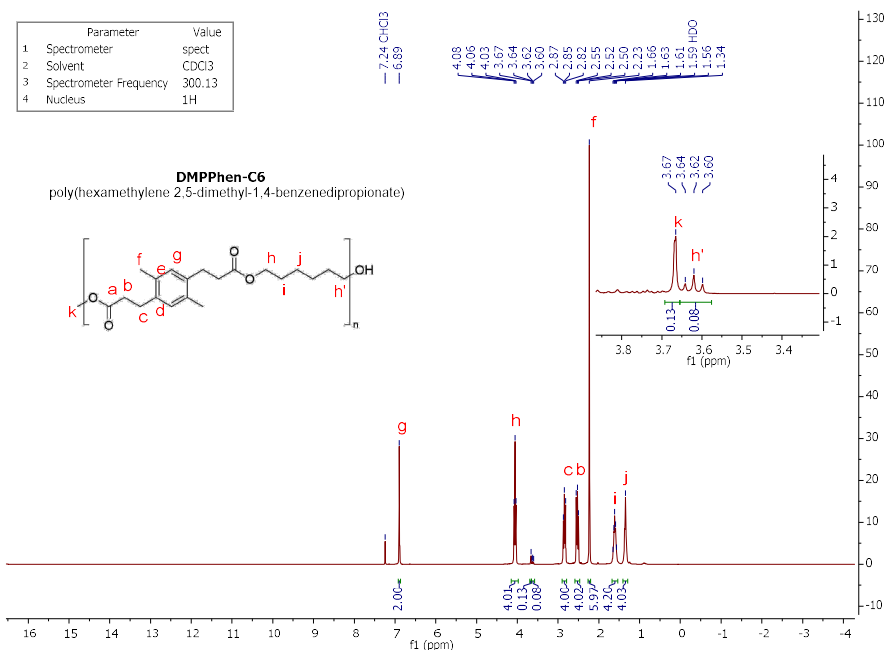


Figure A4: ¹H-NMR spectrum of DMPPhen-C6.

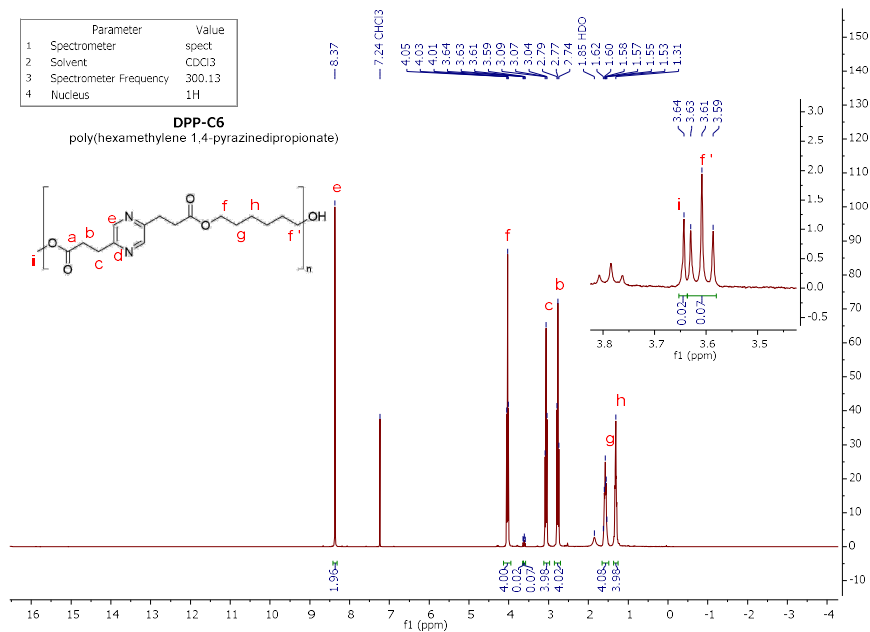


Figure A5: ¹H-NMR spectrum of DPP-C6.

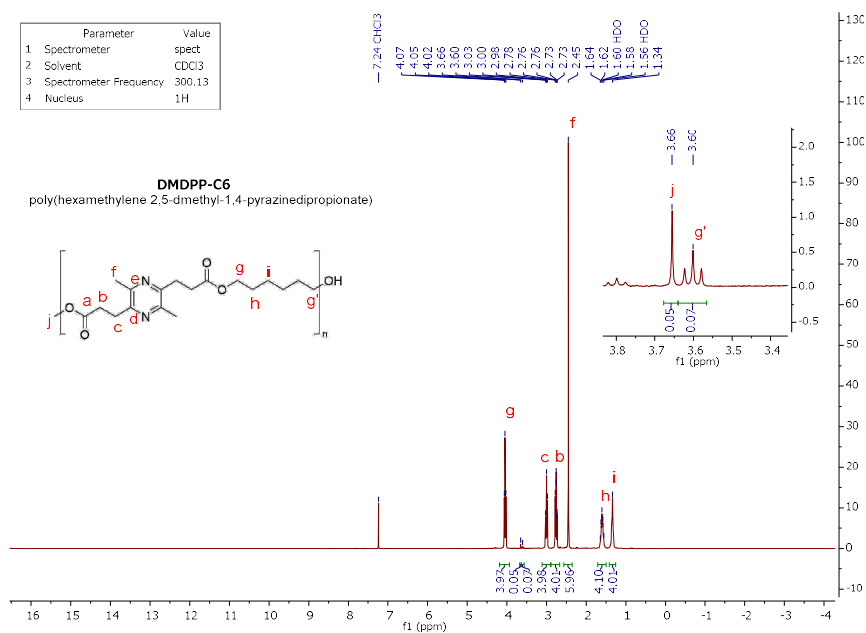
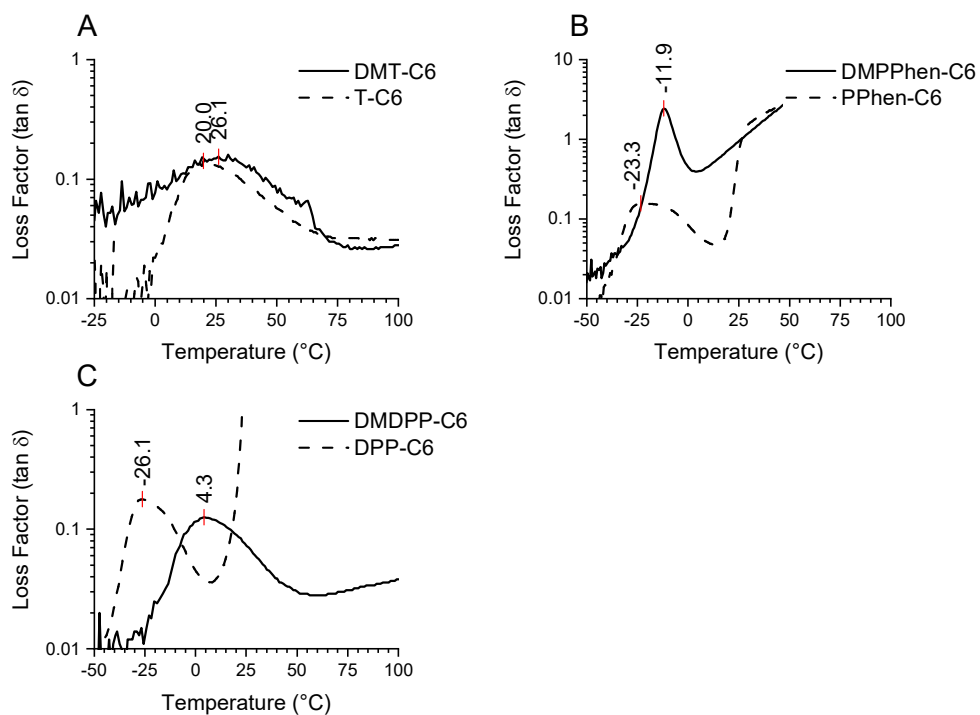


Figure A6: ¹H-NMR spectrum of DMDPP-C6.

DMA data

Figure A7: DMA data for T-C6 and DMT-C6 (panel A), PPhen-C6 and DMPPhen-C6 (panel B), DPP-C6 and DMDPP-C6 (panel C)



Cell data

Table A1: Cell parameters of both polymorphs.

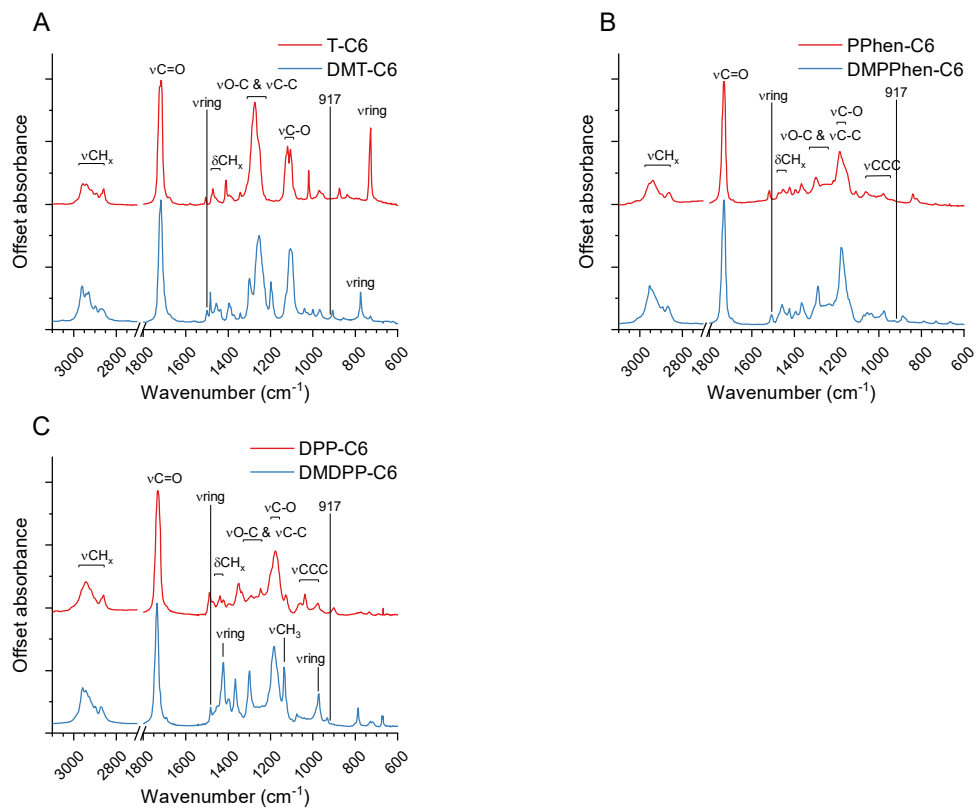
Polymorph	a (\AA)	b (\AA)	c (\AA)	α ($^{\circ}$)	β ($^{\circ}$)	γ ($^{\circ}$)	Density (g/cm^3)
α	4.41	7.62	21.22	129.6	119.6	84.5	1.231
β cell I	4.73	9.46	21.70	140.1	124.5	50.4	1.172
β cell II	4.73	7.40	21.70	128.2	124.5	79.9	1.172

Table A2: Fractional atomic coordinates of both polymorphs as obtained from XRD and COMPASS.

	alpha			beta (cell I)		
	x	y	z	x	y	z
C1	0.04893	0.79212	0.95575	0.00534	0.15953	0.01031
C2	0.01921	0.11953	0.08581	-0.02866	0.07271	0.08173
C3	0.03087	0.24281	0.17929	-0.07304	0.18131	0.17648
N4	0.05283	0.90061	0.03631	-0.02210	0.22050	0.08669
C5	0.02104	0.21501	0.29184	-0.06223	0.17294	0.29371
C6	0.01124	0.07851	0.19682	-0.00813	0.02337	0.18995
C7	0.02995	0.17466	0.39564	-0.07009	0.14661	0.39465
C8	0.08749	0.54585	0.90459	0.00897	0.34866	0.02987
H9	0.28728	0.39879	0.24367	0.11317	0.27993	0.23635
H10	0.79781	0.31353	0.17342	-0.35760	0.31955	0.19103
H11	0.75407	0.92283	0.13414	-0.20652	-0.06559	0.13837
H12	0.24612	0.00887	0.20508	0.27686	-0.11393	0.18037
O13	0.03528	0.42205	0.34603	-0.12159	0.38241	0.35948
O14	0.01102	0.06678	0.30712	-0.03478	0.03203	0.30074
C15	0.99394	0.99011	0.40253	-0.02280	-0.02777	0.39618
C16	0.02796	0.10303	0.49790	-0.02552	0.08487	0.49754
H17	0.72547	0.84561	0.33732	-0.24459	-0.09832	0.34286
H18	0.20804	0.90433	0.39820	0.24127	-0.18231	0.37066
H19	0.29366	0.25152	0.56248	0.19580	0.15617	0.54986
H20	0.80970	0.18605	0.50005	-0.28895	0.24098	0.52284
H21	0.29431	0.32255	0.46155	0.14069	0.22537	0.45090
H22	0.80969	0.25601	0.39657	-0.34265	0.29567	0.41423
H23	0.34770	0.54923	0.90941	-0.21837	0.38972	-0.01794
H24	0.08804	0.47414	0.93621	-0.02326	0.51808	0.10525
H25	0.85739	0.41725	0.82586	0.27257	0.28941	0.01722
C26	0.97926	0.23732	0.05148	-0.00488	-0.15952	0.98978
C27	0.00898	0.90992	0.92141	0.02912	-0.07270	0.91837
C28	0.99732	0.78664	0.82794	0.07350	-0.18130	0.82361
N29	0.97536	0.12884	0.97092	0.02257	-0.22049	0.91341
C30	0.00715	0.81444	0.71538	0.06269	-0.17292	0.70639
C31	0.01695	0.95094	0.81041	0.00859	-0.02336	0.81015
C32	0.99824	0.85479	0.61158	0.07054	-0.14659	0.60545
C33	0.94070	0.48359	0.10263	-0.00850	-0.34866	0.97023
H34	0.74091	0.63066	0.76356	-0.11271	-0.27992	0.76375
H35	0.23038	0.71592	0.83380	0.35807	-0.31954	0.80907
H36	0.27412	0.10662	0.87309	0.20698	0.06560	0.86172
H37	0.78207	0.02058	0.80215	-0.27640	0.11394	0.81972
O38	0.99292	0.60740	0.66120	0.12205	-0.38240	0.64062
O39	0.01718	0.96266	0.70011	0.03523	-0.03202	0.69936
C40	0.03426	0.03933	0.60469	0.02324	0.02778	0.60392
C41	0.00023	0.92642	0.50932	0.02597	-0.08486	0.50256
H42	0.30272	0.18384	0.66991	0.24504	0.09833	0.65724
H43	0.82015	0.12512	0.60903	-0.24082	0.18232	0.62944
H44	0.73454	0.77793	0.44474	-0.19535	-0.15616	0.45023
H45	0.21850	0.84339	0.50718	0.28940	-0.24097	0.47726
H46	0.73388	0.70690	0.54568	-0.14024	-0.22536	0.54920
H47	0.21850	0.77344	0.61065	0.34310	-0.29566	0.58587
H48	0.68055	0.48023	0.09785	0.21883	-0.38970	1.01804
H49	0.94003	0.55528	0.07100	0.02375	-0.51807	0.89485
H50	0.17086	0.61221	0.18135	-0.27210	-0.28942	0.98287

Infrared data

Figure A10: IR data for T-C6 and DMT-C6 (panel A), PPhen-C6 and DMPPhen-C6 (panel B), DPP-C6 and DMDPP-C6 (panel C).



Conclusions & Outlook

The main objective of this Thesis was to fill the knowledge gap regarding pyrazines in polymers by trying to answer the following initial questions:

- can we synthesize pyrazine monomers from biomass and which ones?
- can these pyrazine monomers successfully be used to synthesize polymers?
- what are the properties of pyrazine containing polymers?

Since these questions are too general several choices were made with regard to the type of biomass and the type of polymers to be investigated. Amino acids were chosen as the source of biomass and polycondensates, such as polyesters as the polymer type. This chapter highlights the most important findings in pursuit of answering these questions and will provide an outlook on future research.

Conclusions

At the start of this work, the synthesis of pyrazine monomers from amino acids was explored via the more than 90-year-old Dakin-West reaction, as reported in **Chapter 1**. A comprehensive set of functionalized proteinogenic amino acids was screened and a scalable method was developed for the transformation of six of these amino acids to their corresponding α -amino-ketones. Of special note is the general applicability of the safety measures. The classic Dakin-West reaction is exothermic and accompanied by violent carbon dioxide formation, both these risks could be minimized by our new procedure. Subsequent hydrolysis of the α -amino-ketones provided the starting materials for pyrazines. The pyrazine synthesis via dimerization and auto-oxidation in methanol showed significant side-product formation. These side-products could be minimized after mechanistic studies showed that the oxygen involved in the auto-oxidation formed superoxide radical anions. These anions in turn oxidized methanol to formaldehyde, which resulted in the formation of the side-products. Addition of hydrogen peroxide prevented the side-product formation and enabled the isolation of a toolbox of several functional dimethylpyrazines starting from amino acids.

After successfully synthesizing pyrazine monomers from biomass their use in polymerizations was explored, as reported in **Chapter 2**. This study was conducted using two of the monomers; dimethyldipropionic acid pyrazine (**DMDPP**) and dipropionic acid pyrazine (**DPP**). With these two monomers both the effect of pyrazines in polyesters as well as the effect of methyl-group introduction on the

aromatic ring could be studied. Melt polymerization of these monomers as free acids was unsuccessful due to thermal degradation. Polymerization via transesterification however, was successful and use of six diols provided a total of twelve polymers. The GPC molecular weights were between 12 300 and 47 500 g/mol with dispersities between 1.9 and 2.3. The thermal properties and the effect of methyl-groups were studied, as was the thermal stability. Six of the polymers were amorphous while the other six were semi-crystalline. The thermal degradation preventing the melt polymerization with free acids occur when the monomers were incorporated into a polymer chain. The degradation results from nucleophilic attack of the pyrazine nitrogen on the acid/ester carbonyl at elevated temperature, limiting the processing temperature of the materials to 180–190 °C. The differences in glass transition between **DMDPP** and **DPP** are determined by sterics, chain-length, and their free-volume. In terms of melting temperature, the methyl-substituted **DMDPP**-based polymers melt up to 80 °C higher than the unsubstituted **DPP**-based ones. In depth exploration of this large difference in melting temperature is reported in Chapter 5.

Some preliminary mechanical properties were determined in Chapter 2. To be able to place the new materials in a wider framework and determine an application niche the mechanical properties from one of the polyesters was investigated in detail, as reported in **Chapter 3**. The polyester chosen for this study was **DMDPP-C6**, of which the synthesis was improved by use of dibutyl tin(VI)oxide as the catalyst. Several batches of different molecular weights were synthesized but all proved under the entanglement molecular weight by rheological measurements. Attempts to obtain material above the entanglement molecular weight by use of the very active titanium butoxide catalyst or by solid-state post-condensation were unfortunately unsuccessful. Mechanical testing was nevertheless performed by compression, tensile and impact measurements. The properties of **DMDPP-C6** were found to be similar to both iPP as well as aromatic 1,6-hexanediol-based materials. Higher molecular weight material still needs to be tested to determine the dominant failure behavior (brittle vs ductile). Overall, the **DMDPP-C6** polymer can be considered a low to medium strength engineering plastic with a low T_g and high crystallinity.

Since pyrazine rings have reactive electron lone pairs these can undergo at different conditions post-modification processes. Both **DMDPP** and **DPP** diester monomers as well as polymers **DMDPP-C6** and **DPP-C6**, were used in a proof of principle study for such post-modification reactions, as reported in **Chapter 4**. Post-alkylation of **DMDPP** and its polymer was not successful as the steric demand proved too high. Also, the relatively weak nucleophilic nature of the pyrazine prevents effective post-alkylation. However, post-alkylation using trimethyloxonium tetrafluoroborate as a

reagent proved feasible for **DPP** and most likely for its 1,6-hexanediol based polymer (**DPP-C6**). However, solubility and stability issues made isolation and characterization of the modified polymer not practical. On the other hand, oxidative post-modification of both monomers and polymers is facile in the presence of *m*-chloroperbenzoic acid. The post-oxidation is accompanied with a large change in thermal properties. With increasing degree of oxidation, **DMDPP-C6** showed complete loss of crystallinity which coincided with an increase in glass transition temperature. For the dimethyl ester of **DPP** and the **DPP-C6** polymer a surprising increase in melting point was found at high degrees of oxidation. This increase is most likely caused by (weak) hydrogen bonds between the aromatic C-H and N-O groups as demonstrated by infrared spectroscopy. Selective surface oxidation was also possible and demonstrated by both infrared and XPS analysis. This modification resulted in higher wettability of the polymer surface.

The structural and physio-chemical basis for the melting point differences found in Chapter 2 was investigated by synthesis of a series of analogs of **DMDPP** and by structure elucidation using (fiber) x-ray diffraction, as reported in **Chapter 5**. These studies revealed that both the methyl-groups and the pyrazine ring are responsible for the large difference in melting point between **DMDPP-C6** and **DPP-C6**. The structure of **DMDPP-C6** was determined via fiber and powder x-ray diffraction, the polymer was found to exist in two polymorphic forms. These two polymorphs both adopted extended chain conformations with the main difference being the orientation of the pyrazine ring in the chain. The crystal packing enabled the determination of (weak) hydrogen bonds between the methyl-groups and the pyrazine system based on proximity. The exact nature of these hydrogen bonds, be it CH- π or CH-N, is still under investigation. The presence of these interaction combined with infrared data could adequately explain the observed differences in melting points for the studied analogs.

Outlook

We showed that pyrazines can be made from biomass, that they can be incorporated successfully in polyesters and that these polyesters possess interesting properties. With these results in hand several directions for future work become evident.

First of all, this work only scratches the surface in terms of which pyrazines can be made from biomass and what their properties might be. These initial results however, provide a good basis for new research. Other diols and especially diamines might result in polyester and polyamides with desired and designed properties. Polyamides have not been explored at all, as of yet, but hold great promise due to their increased

mechanical performance compared to polyesters. Further optimization of the polyester synthesis and more accurate determination of the mechanical properties might also provide insight into a suitable application for these pyrazine-containing polymers.

The biobased nature of the reported pyrazines and their ability to undergo post-modification also makes them interesting building blocks for further study as added functionality materials with tunable properties. Especially when other diols besides 1,6-hexanediol would be explored the applicability of both alkylation and oxidation might increase. The presence of N-oxides or N-alkyls can have profound effects on the reactivity and other interactions in the materials. N-Oxides for instance have been reported as electrochemical catalysts and oxidized pyrazine polymers might be interesting immobilized versions of these. The pyrazine ring, being oxidized or not, has also been reported to be a good ligand for various metals. This opens applications as anode or cathode materials in new batteries or as ligand systems for noble- or base-metal catalysis.

The reported pyrazines, although biobased are not necessarily biodegradable, although polyesters often are. Some preliminary investigations have been undertaken using Leaf Cutter Cutinase enzymes to degrade **DMDPP-C6**. These studies indicate that degradation takes place readily but further work on the (bio)degradation of pyrazine-based polyesters would be more than welcome.

The initial questions borne out of curiosity have been answered affirmatively and the effect of pyrazines on the properties of polymers have only barely been explored. These effects can be significant and were for the most part completely unforeseen at the start of this research. I hope this work is the basis for a new direction in polymers, where biobased pyrazines enable new tricks and result in the added functionality materials of the future.

Impact paragraph

As mentioned in the Introduction, this work is mostly driven by curiosity but fits well in a larger framework of sustainability efforts towards a “green” economy. However, science is not a system on its own, science is part of society in general and as such it is important to address the impact science has or might have on society. This Chapter intends to provide insight in the impact of the work described in this thesis at a scientific and at a more societal level.

The main aim of my work was to find which pyrazine containing monomers could be made from biomass and what properties these monomers might provide to corresponding polymers. Concerning the first part, it was shown that a number of functional pyrazine monomers can be easily synthesized from amino acids in a scalable fashion using the Dakin-West reaction. The developed procedure is generally applicable under safe conditions allowing scale-up to useful amounts. As a result, the Dakin-West reaction can now be considered a viable option to use in pharma and material science. Next to this, the work also showed the large potential that amino acids have as a, currently underutilized, renewable biobased starting material.

In the second part of my thesis work, a new class of pyrazine containing polymers was developed using two of these versatile building blocks. The resulting new type of polyesters show very interesting thermal behavior. One of the monomers showed melting temperatures far exceeding the other, although their structures are quite similar. By systematically changing the structure of other close analogues, I could demonstrate that the observed thermal properties are unique to this pyrazine monomer. The polymer crystal structure was determined, which showed specific interactions at the basis of the thermal properties. These non-classical or weak hydrogen bonding interactions are commonly not considered in the design of new materials. My work thus shows the importance of physical interactions in designing new materials and should provide a basis for further work in this direction using these type of biobased monomers.

Another interesting result of the work, which may deliver broader societal impact was the ability to post-modify the developed monomers and polymers. This post-modification showed that these materials have an added benefit in, that their properties can be tuned after synthesis. Next to this, the post-modification again revealed that weak physical interactions can have a large influence on material properties. In this case by showing that one fully modified material went from low

melting to high melting and by showing that the surface properties of the polymers can also be modified.

All of this work is only a first step into exploring pyrazine containing polymers and their unique chemistry. Further work will be necessary to show the overall safety profile of these materials and to find their societal added benefit. If these monomers and polymers turn out to be environmental toxins they will never be commercialized. If they are found to be benign and show great benefits, for instance biodegradability or tunable properties, these materials might be very promising in numerous applications. The initial mechanical properties indicate that the materials could be used as engineering plastics, potentially replacing poly(ethylene terephthalate), poly(butylene terephthalate) or isotactic poly(propylene) while providing extra tunability. The major challenge for any new material will remain adaptation by the market. Having published most of this work, academic-, material- and pharmaceutical-scientists can use the results in their own research and might find inspiration in the new building blocks.

Overall, the work described in this Thesis provides an insight in different materials from biomass and how little we sometimes know about physical interactions. Although not directly applicable as a replacement for fossil and unsustainable materials, the reported polymer can inspire other scientists to think more outside of the box. The work also shows how powerful a multi-disciplinary approach to new materials is. It is not only a case of synthesizing a new monomer and testing what properties the resulting polymers has but also providing a deeper understanding of those properties that provides the most scientific merit.

Next to this, I believe this work is a very good example of underappreciated blue-sky research. Work of this nature does not easily receive funding in the current funding schemes, especially since there was no earlier work in this direction. The funding provided by the Dutch Province of Limburg without any prerequisites or demands for societal impact has provided an ideal platform for the new and interesting results. Although the work has little societal impact right now, there was none at Bell laboratories or the Philips NatLab and without those institutes, we would not have cell phones, cd's or computers. I see a bright future for (biobased) pyrazines in material science.

Samenvatting

Deze Thesis is voornamelijk tot stand gekomen uit nieuwsgierigheid, het beantwoorden van de hoe, wat en waarom vragen die we ons allemaal soms stellen. Zo waren er aan het begin van dit onderzoek meerdere vragen over pyrazines, stikstofhoudende aromatische moleculen die interessante eigenschappen bezitten. Er was vrij weinig bekend over pyrazines in polymeren en het hoofddoel van deze Thesis werd dan ook het verkennen van pyrazines in deze context. Om het hiaat in onze kennis te vullen heb ik de antwoorden gezocht op de volgende vragen:

- kunnen we pyrazine monomeren maken vanuit biomassa en zo ja, welke?
- kunnen deze pyrazine monomeren worden gebruikt in de synthese van polymeren?
- wat zijn de uiteindelijke eigenschappen van pyrazine-houdende polymeren?

Om het onderzoek voldoende in te kaderen, werden deze vragen nog verder aangescherpt. Als bron van biomassa voor de synthese van pyrazines werd daarbij gekozen voor aminozuren. Polycondensaten, specifiek polyesters, werden gekozen als de te onderzoeken klasse polymeren. De belangrijkste bevindingen van het onderzoek zijn hieronder samengevat.

Voor de synthese van pyrazine monomeren vanuit aminozuren werd als eerste stap de meer dan 90 jaar oude Dakin-West reactie verkend en verder ontwikkeld zoals beschreven in **Chapter 1**. Alle functionele (zijnde niet aliphatische) proteinogene aminozuren werden getest in deze reactie. Voor de zes succesvolle substraten werd een schaalbare methode ontwikkeld naar de corresponderende α -amino-ketonen. Een van de belangrijkste bevindingen, buiten welke aminozuren getolereerd worden in de reactie, was dat de veiligheidsmaatregelen beschreven voor de reactie algemeen toepasbaar zijn. De Dakin-West reactie is normaliter exotherm en gaat gepaard met vigoureuze spontane koolstofdioxide ontwikkeling. Beide van deze proces risico's konden worden beheerst in de ontwikkelde methode. De verkregen α -amino-ketonen konden via verzeeping worden omgezet in de startmaterialen voor de daadwerkelijke pyrazines. De uiteindelijke formatie van pyrazines verloopt via dimerisatie en auto-oxidatie. In methanol als beste oplosmiddel trad daarbij echter significante vorming van zij-producten op. Deze vorming van zij-producten kon worden verminderd nadat een mechanische studie aantoonde dat de bij de auto-oxidatie betrokken zuurstof superoxide radicale anionen vormde. Deze anionen oxideerden

vervolgens de methanol naar formaldehyde, welke verantwoordelijk was voor de vorming van zij-producten. Toevoeging van waterstofperoxide voorkomt deze zij-product formatie en zodoende kon er op een schaalbare wijze een verzameling van vijf functionele dimethylpyrazine bouwstenen/monomeren uit biomassa worden gemaakt.

Na de succesvolle synthese van pyrazine monomeren uit biomassa werd hun gebruik in polymerisaties verkend zoals beschreven in **Chapter 2**. Hiervoor werden twee van de monomeren gebruikt; dimethyldipropionzuur pyrazine (**DMDPP**) en dipropionzuur pyrazine (**DPP**). Deze twee monomeren maakten het mogelijk zowel het effect van pyrazines als het effect van de introductie van methylgroepen op een aromatische ring te bestuderen. Smelt polymerisatie met de vrije zuren van deze monomeren was helaas niet mogelijk door thermische degradatie beneden de smelt temperatuur. Polymerisatie via transesterificatie was wel succesvol en met zes verschillende diolen werden uiteindelijk twaalf polymeren gemaakt. De GPC moleculairgewichten van deze polymeren waren tussen de 12300 en 47500 g/mol met dispersiteiten tussen de 1.9 en 2.3. De thermische eigenschappen en het effect van de methyl groepen werd bestudeerd alsmede de thermische stabiliteit. Zes van de polymeren bleken amorf terwijl de andere zes semi-kristallijn waren. De thermische degradatie die de directe smelt polymerisatie onmogelijk maakt bleek ook plaats te vinden wanneer de monomeren onderdeel waren van een polymeerketen. De degradatie vindt plaats door nucleofiele aanval van de pyrazine stikstof op de zuur/ester carbonyl bij verhoogde temperaturen; dit beperkt de verwerkingstemperatuur van de materialen tot 180–190 °C. De gevonden verschillen in glasovergangstemperatuur tussen **DMDPP** en **DPP** worden veroorzaakt door sterische hindering, ketenlengte en hun vrij-volume. Wat betreft het smeltpunt; de methyl-gesubstitueerde **DMDPP** gebaseerde polymeren smelten tot wel 80 °C hoger dan de ongesubstitueerde **DPP** polymeren met hetzelfde diol. Dit grote verschil is uitgebreid onderzocht zoals beschreven in **Chapter 5**.

In Chapter 2 werden enkele initiële mechanische eigenschappen bepaald. Om de pyrazine houdende polyesters in een bredere context te kunnen plaatsen en om te bepalen in welke toepassing de materialen gebruikt kunnen worden, werden de mechanische eigenschappen van een van de polyesters verder bestudeerd zoals beschreven in **Chapter 3**. Voor deze studie werd gekozen voor **DMDPP-C6**, de synthese van dit polymeer werd verder verbeterd door gebruik van dibutyl tin(VI)oxide als de katalysator. Meerdere polymeren van verschillende moleculairgewichten werden gesynthetiseerd maar deze bleken via rheologie allemaal onder het “entanglement moleculair weight” te zijn: het moleculairgewicht waarbij de mechanische eigenschappen stabiliseren. Pogingen om polymeren boven dit

“entanglement moleculair weight” te maken met gebruik van de zeer actieve titanium butoxide katalysator of via “solid-state post-condensation” waren helaas niet succesvol. Ondanks het te lage moleculairgewicht werden de mechanische eigenschappen verder bestudeerd met behulp van compressie-, trek- en botsingsmetingen. De eigenschappen van het **DMDPP-C6** materiaal zijn vergelijkbaar met zowel iPP als met andere aromatische 1,6-hexanediol gebaseerde polymeren. Materiaal met hoger moleculairgewicht zou nog getest moeten worden om het type falen van dit polymeer te bepalen (bros versus kneedbaar). Uiteindelijk kan de **DMDPP-C6** polyester worden gezien als een laag tot gemiddeld sterke “engineering plastic” met een lage glasovergangstemperatuur en hoge kristalliniteit.

Gezien pyrazines reactieve vrije elektronen paren hebben kunnen ze verschillende post-modificatie processen ondergaan. Zowel de **DMDPP** en **DPP** diester monomeren als de **DMDPP-C6** en **DPP-C6** polyesters zijn gebruikt in een studie om het principe van deze post-modificaties aan te tonen. Dit is beschreven in **Chapter 4**. Post-alkylatie van **DMDPP** en **DMDPP-C6** bleek niet mogelijk door zowel de sterische hindering rond de stikstoffen als door de zwakke nucleofieliciteit van dit pyrazine. Post-alkylatie was wel mogelijk met het **DPP**-monomeer door middel van trimethyloxonium tetrafluoroboraat. Modificatie van het **DPP-C6** polymeer resulteerde in onoplosbaar materiaal; verder bewijst voor modificatie door middel van alkylatie moet nog worden geleverd. Oxidatieve modificatie daarentegen bleek erg makkelijk en succesvol voor alle pyrazines met behulp van meta-chloorperbenzoëzuur. Post-oxidatie gaat gepaard met grote veranderingen in de thermische eigenschappen van de materialen. Hogere mate van oxidatie veroorzaakte volledig verlies van kristalliniteit in **DMDPP-C6** (op DSC-tijdschalen), terwijl de glasovergangstemperatuur toenam. Voor zowel de dimethylester van **DPP** als **DPP-C6** werd een onverwachte toename van de smelttemperatuur gevonden bij toenemende mate van oxidatie. Deze toename in smelttemperatuur wordt waarschijnlijk veroorzaakt door (zwakke) waterstofbruggen tussen de aromatische C-H bindingen en de N-oxides, zoals aangetoond met infraroodspectroscopie. Selectieve modificatie van het oppervlak bleek ook mogelijk, zoals aangetoond met zowel infraroodspectroscopie als met röntgen foton spectroscopie (XPS). De oppervlakte modificatie zorgde voor een toename in adhesie.

Als laatste werd de fysio-chemische basis voor het smelttemperatuur verschil tussen **DMDPP-C6** en **DPP-C6** zoals gevonden in Chapter 2 verder onderzocht. Dit is beschreven in **Chapter 5**. Hiervoor werd een serie van analoge verbindingen gemaakt waarvan de thermische eigenschappen werden bepaald en werd de structuur van **DMDPP-C6** opgehelderd via röntgen (vezel) diffractie. Uit deze studie bleek dat zowel de methyl-groepen als de pyrazine ring verantwoordelijk zijn voor de hogere smelttemperatuur van **DMDPP-C6**. De structuur van **DMDPP-C6** werd bepaald met

behulp van vezel- en poederdiffractie gevolgd door krachtveld berekeningen. Hieruit kwam naar voren dat dit polymeer in twee polymorphen kristalliseert welke beide een gestrekte keten conformatie hebben. Het verschil tussen beide polymorphen ligt voornamelijk in de oriëntatie van de pyrazine ring ten opzichte van de keten-as. Op basis van een contact analyse in de structuur en kristalpakking kon het hoge smeltpunt van DMDPP-C6 worden toegeschreven aan waterstofbruggen tussen de methyl-groepen en de pyrazine ring. De precieze aard van deze waterstofbruggen, zij het CH- π of CH-N wordt nog onderzocht. De aanwezigheid van deze interacties gecombineerd met infrarood data voor de structuur analogen waren voldoende om de waargenomen verschillen in smeltemperatuur te verklaren.

Terugkomende op de belangrijkste onderzoeksvragen aan het begin van dit onderzoek kan het volgende geconcludeerd worden. De synthese van pyrazine monomeren uit biomassa is mogelijk en geeft een aantal zeer interessante verbindingen. De synthese van polymeren van deze monomeren is inderdaad mogelijk en maakt het mogelijk om naast het effect van pyrazines ook het effect van methyl-groepen te bestuderen. De eigenschappen van pyrazine-houdende polyesters zijn zeer uiteenlopend en zwakke interacties zoals waterstofbruggen spelen hier een grote rol. Dit onderzoek naar pyrazines in polymeren is slechts het begin van een nieuw onderzoeksveld maar ik zie de toekomst van pyrazines uit biomassa rooskleurig in.

Acknowledgements

It took some time but it is finally finished. The research described in this Thesis would never have been possible if I did not have support from others and I would hereby like to take the opportunity to thank a number of people.

First of all, I would like to thank my promotion team. Romano, Andrij and Katrien thank you very much for helping me on my academic journey and your supervision. Five years ago I came to Maastricht with some idea of how to do research but lacking some of the necessary skills. Without your feedback, my work would have never made it to paper. Katrien I would especially like to thank you for showing me the way in polymer science and teaching me the first fundamentals. I would also like to thank Stefaan for providing me with the opportunity to start such an open-ended project. I really enjoyed the freedom this gave me to become an independent researcher in many ways. Romano and Andrij I would like to thank the both of you for the trust you placed in me to finish this work and to stand behind the choices in direction I had already made before you joined the institute. I would also like to thank Romano for letting me help setup and continue in his new research group on campus.

A Thesis, of course, also needs to be assessed and I would therefor like to thank my assessment committee, Maarten, Matthew, Gert-Jan and Thomas for the time and effort to read my Thesis and be present at the defense. I hope this work inspired you to look at pyrazines more often.

Next to this, I would like to thank my other collaborators. Jules thank you very much for the interesting talks about polymer physics and your willingness to help find the answers to the melting temperature problem. You triggered a strong desire in me to find the physical reasons behind properties and the importance of hydrogen bonds. Which brings me to thank Junyu and Sven for helping me learn how x-ray diffraction works in practice. This, together with the invaluable help of Enno, has enabled the structure of the pyrazine polymers to be uncovered. Also Yvonne, thank you very much for your support and our chats over the years, I hope your research group will do great things at AMIBM. Thank you Ermo for managing the institute and making sure we can do our research.

Besides collaborators, there were students who helped me with the work and who I enjoyed teaching the tricks of the trade. Thank you Antonis, Cristina, Teresa, Chevonne and Peter for your willingness to be subjected to my endless questions.

A lab is more than just a workplace; it is also colleagues, who make it a nice place to be. I would thus like to thank my AMIBM/UM colleagues over the years, Jules, Milo, Carlos, Pouya, Ola, Christiaan, Christian, Monika, Cristina, Stefan, Naveen, Vahid, Ramiro, Manta, Hai, Jurrie, Joe and Renato. Of course, there was a recent addition of the Amsterdam crew Jay, Daniel and Prabhat thank you for drinks and chats around the office/lab. Special thanks to Jordy, who would have thought that we would be working together again 8 years after our time at SOC.

The campus is more than AMIBM/UM, I would therefore like to thank the people of the Young Professional Board; Astrid, Dannie, Isabel, Carlo, Ryan, Kevin, Maud and Lizzy for the networking opportunities we built together and opening the campus to more people, for me it really worked. On the way to campus, you also run into people for instance, in the train. Thank you Viny and Laurent for the chats in the train or over coffee, the little sparring sessions on research problems and the occasional beer.

Considering beers, thank you Tate, Margaux, Evelien, Carey, Mike, Timme and Inês for all the great parties, drinks and quiznight meetings we have had as part of the PhD social committee, they were a lot of fun. Via the PhD academy, other people have also joined in social events and beyond. Frank, Julia, Giulio and Martha, thanks for the joy of dice and pretending to be somebody else for an evening.

Besides colleagues at work there are also colleagues who share evenings and drinks together so thank you Gijs, Varun and Andrea for the distractions on the work floor and fun evenings at in Maastricht and in Sittard. In addition, special thanks to Marie for letting me be her paranymp and for the good talks at and next to work, I always enjoyed them.

Verhuizen naar Maastricht was niet zomaar wat, dus Ime en Luc indirect bedankt voor het beste appartement in de stad en natuurlijk voor het zijn van soort van ouders weg van de ouders. Via jullie ben ik bij de Brouwerij terecht gekomen en ik wil ook graag alle vrijwilligers bedanken die hebben geholpen met mijn integratie in de stad, met name, Jean en Mieke hartelijke bedankt. Ik woonde hier natuurlijk niet alleen maar had ook onderburen die vrienden werden, Joost en Soetkin bedankt voor de spelletjes avonden, fietsritjes, renrondjes en gezamenlijk gezeur over de academie.

Zonder training, vooral ook de fysieke, blijft de geest niet scherp dus wil ik graag de Dutch Mountains bedanken omdat ik daardoor meer fiets. Vooral, Peter, Floor en Mark bedankt voor het vaak gaan fietsen en het prettige gezelschap. Daarnaast ook Frank en Phil bedankt voor de mooie ritten, weer of geen weer, de biertjes en de leuke vakanties op de fiets.

Ook Geke wil ik graag bedanken voor het helpen integreren in Maastricht, van Kafé België tot een café in België, ik vond het altijd leuk om over Saurus, geneeskunde en politiek met je te praten en soms ook een feestje mee te mogen pakken.

Over training gesproken, het Silenus Cycling Team: Joris, Joris, Pieter, Kees en Ruben wil ik ook graag bedanken voor de leuke tijden. Of het nou 265 km van Diekrich naar Valkenswaard is, de verkeerde afslag in de Eifel, een weekend Mallorca of een week naar Parijs, het zijn altijd mooie ritten samen en een mooi avontuur.

Lang geleden begon het scheikunde avontuur in Utrecht waar ik onder begeleiding van mijn scheikunde ouders werd ingeleid in het studenten leven. Jan-Peke en Sara bedankt voor alle leuke dingen en de goede tijd in Utrecht die mijn uiteindelijk hier gebracht heeft. Buiten scheikunde was er natuurlijk ook Orca in Utrecht, hier was enkele overlap met de Scheikunde-Orca crew, Bart en Anne bedankt voor het delen van deze rare combi. Van alleen Orca zijn er natuurlijk ook mensen, Ingeborg bedankt voor de gekke feestjes, de mooie fiets ritjes en de koffies op Chemelot. Daarnaast Jens, Shaun, Laura en Laura bedankt voor ritjes, avondjes, oud en nieuw feestjes en het Orca gevoel.

Van Orca zijn er ook Marius, Michiel, Marcel en Frans, de CHZ+. Hoewel we Orca wel zijn ontgroeid is het altijd leuk om in Utrecht of Haarlem te komen en een spelletje te spelen, biertje te drinken, herinnering op te halen en nieuwe te maken. We kennen elkaar erg goed en ik ben altijd blij om jullie te zien en hoewel Frans altijd wint hoop ik dat we dit nog lang kunnen blijven doen en ook onze weekendjes weg blijven hebben.

Wageningen kan ook niet vergeten worden en met sommige mensen verlies je nooit contact. Arne dankjewel voor de logeerplek in Amsterdam, de nostalgische avondjes en de goede gespreken, al 27 jaar en counting. Ook Merel bedankt voor het helpen met het ontwerp van mijn cover, zonder jou zou het toch een beetje een saai boekje zijn. Daarbij wil ik je bedanken voor onze lange vriendschap en de mooie tijden.

Zonder zijn paranimfen is een promovendus nergens tijdens zijn verdediging. Dus Geert, dankjewel dat je collega's kwam opzoeken op de eerste werkdag, dat je wel vrienden met ze wilde worden en dat je me meegesleurd hebt naar de PhD sociaal committee. Zonder jou zou leven in Maastricht een hoop saaier zijn geweest. Laat ons biertjes blijven drinken, spelletjes spelen en soms ook maar een rondje rennen. Ook Camiel bedankt, je zorgt er altijd voor dat ik meer van leven en de kleine dingen geniet en bedankt voor het overdragen van je *joie de vivre* op mij. Onze fietstrips en entetjes zijn hoogtepunten van het jaar en ik hoop dat, dat nog jaren zo blijft.

Ik wil ook graag mijn familie bedanken, hoewel scheikunde niet makkelijk is waren jullie altijd geïnteresseerd in wat ik deed en probeerde ik het zo goed en zo kwaad als het ging uit te leggen. Het gezin kan niet vergeten worden, Papa, Mama en Franka bedankt voor alle steun door de jaren heen en het helpen bij al mijn keuzes, ik kan altijd op jullie aan.

Por último, mas não menos importante, Bruna, meu amor, obrigado por ter estado ao meu lado. Obrigado por sempre ter me apoiado em minhas decisões, e espero muito poder continuar fazendo o mesmo por você. Espero ainda termos muitos bons momentos juntos como doutores.

Curriculum Vitae



Martien Adriaan Würdemann was born on the 1st of June 1989 in Wageningen. In 2008 he graduated from “het Pantarijn” in Wageningen with a VWO diploma and started his bachelors in Chemistry at Utrecht University. While there he was a full-time board member of the student rowing club A.U.S.R. Orca in the academic year 2010-2011. He obtained his BSc diploma with a thesis in early 2012 on semi-synthetic metalloenzymes at the group of prof. dr. Klein-Gebbink. He continued his studies with a Masters in Chemistry at both the University of Amsterdam and the Vrije Universiteit Amsterdam where he finished his MSc degree in 2015, with a thesis on chiral phosphoric acid catalyzed Pictet-Spengler

reactions in the group of prof. dr. Hiemstra. During this time, he also did an internship at then AkzoNobel Industrial Chemicals in Deventer (now Nouryon). After a self-supported bike trip through Europe, he started working at then Mercachem Process Research in 2015 (now Symeres). This sort stint in industry was followed in 2016 by further academic training when he started his PhD research on pyrazines from biomass and their application in polymers at Maastricht University in the Aachen Maastricht Institute for Biobased Materials (AMIBM), initially under the supervision of prof. dr. De Wildeman and dr. Bernaerts. Supervision was eventually shared between prof. dr. Orrù, prof. dr. Pich and dr. Bernaerts and resulted in the work described in this dissertation. In 2020 he joined the group of prof. dr. Orrù full-time on a post-doc project for Chemelot InSciTe on a biobased drop-in.

As of 2022 Martien is looking to use his knowledge and expertise in a connecting role, helping to drive innovation and contribute to a more sustainable planet.

Publication list

From this thesis:

M.A. Würdemann, T. Faber, J.A.W. Harings, K.V. Bernaerts, R.V.A. Orrù and A. Pich.
Post-Modification of Biobased Pyrazines and Their Polyesters
Macromolecules, **2021**, *54*(23), 10850-10859

M.A. Würdemann and K.V. Bernaerts.
Biobased Pyrazine-Containing Polyesters
ACS Sustainable Chemistry & Engineering, **2020**, *8*(32), 12045-52

M.A. Würdemann, C. Nitu, S.M.A. de Wildeman, K.V. Bernaerts and R.V.A. Orrù.
The Forgotten Pyrazines: Exploring the Dakin-West Reaction
Chemistry: a European Journal, **2020**, *26*(36), 8090-8100

M.A. Würdemann, E.A. Klop, J. Li, R. Graf, K.V. Bernaerts, R.V.A. Orrù, J.A.W. Harings.
Structure and melting of biobased polyesters
Manuscript submitted

Previous publications:

A. Ruiz-Olalla, M.A. Würdemann, M.J. Wanner, S. Ingemann, J.H. van Maarseveen and H. Hiemstra.
Organocatalytic Enantioselective Pictet-Spengler Approach to Biologically Relevant 1-Benzyl-1,2,3,4-Tetrahydroisoquinoline Alkaloids
The Journal of Organic Chemistry, **2015**, *80*(10), 5125-5132

M. Basauri-Molina, C.F. Riemersma, M.A. Würdemann, H. Kleijn and R.J.M. Klein-Gebbink.
Lipase active site covalent anchoring of Rh(NHC) catalysts: towards chemoselective artificial metalloenzymes
Chemical Communication, **2015**, *51*, 6792-6795

